

Seismic response of post-installed anchors in concrete

Dissertation

Vorgelegt von

Dipl.-Ing. Anton Rieder

Universität für Bodenkultur Wien
Department für Bautechnik und Naturgefahren
Institut für Konstruktiven Ingenieurbau

Begutachter:

O. Univ. Prof. Dipl.-Ing. DDr. Konrad Bergmeister, M.Sc.
Privatdozent Dipl.-Ing. Dr. Alfred Strauss

Wien, 2009

Vorwort

Willst du dich am Ganzen erquicken,
So musst du das Ganze im Kleinsten erblicken.

Johann Wolfgang v. Goethe

Goethe meinte mit dem Ganzen die Naturwissenschaft und mit dem Kleinsten das Wort, das zur Beschreibung und Erklärung der Natur für den Dichter und Naturwissenschaftler unentbehrlich ist. Übertragen auf die Bautechnik verhält es sich ähnlich mit all den kleinen Details wie zum Beispiel Befestigungselementen, die notwendig sind um ein Bauwerk als Ganzes erst zu ermöglichen.

In dieser Dissertation werden Verfahren und Möglichkeiten aufgezeigt, wie die Sicherheit von Befestigungselementen im Erdbebenfall erhöht werden kann. Prof. Konrad Bergmeister hat hierzu nicht nur die Idee geliefert, sondern auch die Betreuung und Erstbegutachtung der Dissertation übernommen und die Forschungsaufenthalte an der University of Canterbury in Neuseeland ermöglicht. Vor allem für diese Erfahrung von unschätzbarem Wert bin ich Prof. Konrad Bergmeister zu besonderem Dank verpflichtet.

Grundlegend für das Gelingen dieser Dissertation war das gute Arbeitsklima am Institut für Konstruktiven Ingenieurbau. Dies äußerte sich nicht nur im Aufbau und in der Pflege der Kochgemeinschaft, sondern vor allem in den unzähligen fachlichen und nichtfachlichen Diskussionen mit den Kollegen und in der gegenseitigen Unterstützung bei den unterschiedlichsten Problemen. Genannt seien hier Ulrich Santa, Ronald Mihala, Panagiotis Spyridis, Raimund Hilber, Jürgen Suda, Roman Wendner, Roman Smutny, Ulla Ertl, Michael Dell'Antonio, Theodor Guggenberger, Duro Petricevic und Andreas Unterweger. Für die Übernahme der Zweitbegutachtung der Dissertation geht besonderer Dank an Alfred Strauss.

An der University of Canterbury sind in zahlreichen Diskussionen mit Prof. Athol Carr, Prof. Stefano Pampanin und Masoud Moghaddasi wesentliche Beiträge aus dem Erdbebeningenieurwesen in die Dissertation eingeflossen. Besonderer Dank gilt Stuart Toase und John Maley, ohne deren Unterstützung und praktischen Ideen im Labor der Versuchsaufbau wohl nicht so gut gelungen wäre. Interessante Menschen aus verschiedenen Ländern der Erde haben meinen persönlichen Horizont während des Aufenthaltes in Neuseeland nachhaltig erweitert.

Die Zusammenarbeit mit der Fa. fischer und deren finanzielle Unterstützung waren sehr bedeutend für das Zustandekommen der vorliegenden Arbeit. Dank hierfür gebührt Dr. Hannes Spieth und Marc Schäffer, die als Ansprechpartner die nötigen Informationen und Kontakte lieferten.

Für das entgegengebrachte Verständnis und die Geduld vor allem in der Schlussphase der Dissertation bin ich meiner Verlobten Renate zu tiefstem Dank verpflichtet.

Diese Dissertation ist meinen lieben Eltern Martha und Rudolf gewidmet.

Wien, im August 2009

Abstract

Post-installed metal anchors for use in concrete have gained high importance in construction technology due to their flexible application, large variety of types and products and economic design. Anchors are used to connect structural and non-structural elements to reinforced concrete structures, but also for seismic retrofitting in seismic hazard zones. While our understanding of the behavior of fasteners, as well as the methods used for their qualification, have advanced significantly over the past 30 years, relatively little information exists about the behaviour of fasteners under earthquake conditions. No specific provisions are available concerning the response to seismic shear loading for the case that a hole clearance between base plate and anchor and hence a system with slackness exists. Additionally, most design codes do not take into account the mitigating effect of damping devices applied on a post-installed anchor connection.

This dissertation attempts to provide a basis and solutions for the enhancement of the safety of post-installed anchors used in seismic regions. An overview of research related to the behavior of fastenings under seismic conditions with special emphasis on shear loading is presented and existing seismic qualification methods for fasteners are examined.

Experimental data is provided by quasi-static reversed cyclic shear loading and uniaxial shake table testing and completed by numerical investigations concerning the seismic action on shear loaded anchors with slackness. Specifically, the inherent damping properties and the plastic deformation capacity are determined for different anchor types. The influence of the anchor type on the behaviour under realistic seismic conditions is simulated by triaxial shake table tests with increasing amplitude up to failure.

This dissertation is accomplished by a feasibility study concerning the effect and application of various damping devices in order to mitigate the seismic action on post-installed anchors. This is done by means of transfer of knowledge from other branches of earthquake engineering, numerical investigations and experimental validation.

Based on the results of the investigations, recommendations are given for the modification of the calculation of seismic forces taking into account the slackness between base plate and anchor due to hole clearance in case of shear loading and due to plastic deformation in case of axial loading. Additionally, a more efficient use of the behaviour factor is proposed in calculating the seismic load on non-structural elements. For the mitigation of seismic shear forces a promising damper resulting from the feasibility study is suggested which has to be optimized and proven in future research work.

Kurzfassung

Nachträglich installierte Dübeln in Beton haben aufgrund der hohen Flexibilität beim Einbau, des breiten Spektrums an erhältlichen Produkten und der wirtschaftlichen Bemessung eine große Bedeutung in der Bautechnik erlangt. Sie verbinden tragende und nichttragende Elemente mit Stahlbetonstrukturen und werden auch vielfach zur Ertüchtigung von Bauwerken in seismisch aktiven Zonen eingesetzt. Während unser Wissen über das Verhalten von Dübeln, aber auch die Methoden zur Prüfung der Eignung unter vorwiegend ruhender Belastung in den letzten 30 Jahren bedeutend erweitert wurden, gibt es relativ wenig Informationen über das Verhalten unter Erdbebenbelastung. Die Ein- und Auswirkung von seismischen Querlasten im Fall eines in der Praxis häufig auftretenden Lochspiels zwischen Dübel und Ankerplatte wird in Leitlinien nicht behandelt. Außerdem berücksichtigen die meisten Vorschriften keine mögliche Reduktion der seismischen Lasten falls Isolations- oder Dämpfersysteme in die Dübelverbindung eingebaut werden.

Im Rahmen dieser Dissertation werden sowohl die Grundlagen geschaffen als auch Lösungen präsentiert und diskutiert, um die Sicherheit von nachträglich installierten Dübeln in seismischen Zonen zu erhöhen. Ein einführender Überblick betreffend Forschung zum Erdbebenverhalten von Dübeln ist begleitet von einer Zusammenfassung bestehender und im Entwurf befindlicher Prüfrichtlinien.

Ergebnisse von quasi-statischen Querkzugversuchen mit alternierendem Vorzeichen und von einaxialen Rütteltischversuchen liefern ein besseres Verständnis der Auswirkung eines Lochspiels zwischen Dübel und Ankerplatte. Im speziellen werden wichtige Parameter wie die inhärente Dämpfung und das plastische Verformungsvermögen für verschiedene Ankertypen bestimmt. Aus dreiaxialen Rütteltischversuchen können das Verhalten und die Versagensmechanismen unter realistischen Erdbebenbedingungen für unterschiedliche Dübeltypen abgeleitet werden.

Diese Dissertation schließt mit einer Machbarkeitsstudie über die Auswirkung und Anwendung von verschiedenen Dämpfersystemen auf nachträglich installierte Dübeln. Hierbei kommen mehrere Instrumente und Methoden zum Einsatz: Wissenstransfer von anderen Zweigen des Erdbebeningenieurwesens, numerische Untersuchungen und experimentelle Überprüfungen.

Auf der Grundlage der Untersuchungen werden Empfehlungen zur Modifizierung von bestehenden Erdbebenvorschriften abgegeben, um den Einfluss des Lochspiels zwischen Dübel und Ankerplatte unter seismischer Querbelastung einerseits und die Wirkung von plastischen Verformungen unter seismischer Zugbelastung andererseits erfassen zu können. Außerdem wird ein dübel-spezifischer Verhaltensfaktor unter Querlast bei der Berechnung der seismischen Einwirkung vorgeschlagen. Für die Reduktion von seismischen Querlasten wird auf der Grundlage der Machbarkeitsstudie ein Dämpfer empfohlen, der durch zukünftige Forschungsarbeiten noch optimiert und beurteilt werden muss.

Content

1	INTRODUCTION	9
2	STATE OF THE ART.....	12
2.1	Types of post-installed anchors	12
2.1.1	Undercut anchors	12
2.1.2	Expansion anchors	13
2.1.3	Bonded anchors	14
2.2	Design by testing.....	14
2.2.1	General.....	14
2.2.2	Non-seismic qualification.....	15
2.2.2.1	Test program	15
2.2.2.2	Failure modes	15
2.2.2.3	Influence of cracks.....	17
2.2.3	Seismic qualification	18
2.2.3.1	General	18
2.2.3.2	Testing protocols in the U.S.	19
2.2.3.3	Testing protocols in Canada.....	20
2.2.3.4	Draft for testing protocols in Europe	21
2.3	Seismic action on fasteners	23
2.3.1	General.....	23
2.3.2	Design models for seismic loads.....	24
2.4	Seismic applications of fasteners	26
3	RESPONSE OF FASTENERS UNDER MONOTONIC AND CYCLIC SHEAR LOADING	28
3.1	General	28
3.2	Monotonic loading.....	28
3.2.1	General.....	28
3.2.2	Prediction models	29
3.2.2.1	Beam on foundation	29
3.2.2.2	Numerical models.....	31
3.2.2.3	Geometrical models.....	33
3.2.3	Ductility	35
3.2.3.1	General.....	35

3.2.3.2	Influence of concrete stress.....	35
3.2.3.3	Influence of anchor material	36
3.3	Cyclic loading	38
3.3.1	General.....	38
3.3.2	Stiffness and strength.....	40
3.3.3	Combined axial and shear loading	42
3.4	Summary	44
4	EXPERIMENTAL SIMULATION OF SEISMIC ACTION	45
4.1	General	45
4.2	Quasi-static cyclic shear loading	46
4.2.1	General.....	46
4.2.2	Increasing amplitude	48
4.2.2.1	Influence of anchor type	48
4.2.2.2	Influence of friction and anchor material	52
4.2.2.3	Influence of cracked concrete.....	53
4.2.3	Decreasing amplitude.....	55
4.3	Uniaxial shake table tests.....	58
4.3.1	Experimental test setup.....	58
4.3.1.1	Shake table.....	60
4.3.1.2	Driving mass	60
4.3.1.3	Concrete mass.....	62
4.3.1.4	Instrumentation and data logging	63
4.3.2	Testing procedure.....	63
4.3.2.1	Input motion	64
4.3.2.2	Shake table tracking	64
4.3.2.3	Data filtering.....	64
4.3.3	Test results	65
4.3.3.1	Amplification effects.....	65
4.3.3.2	Loading rate.....	68
4.4	Triaxial shake table tests	69
4.4.1	Experimental test setup and testing procedure.....	69
4.4.2	Test results and analysis	72
4.4.2.1	Sine sweep tests.....	73
4.4.2.2	Undercut anchor	73
4.4.2.3	Expansion anchor	76
4.4.2.4	Bonded anchor	77

4.4.2.5	Influence of anchor type	79
4.5	Summary	80
5	MODELLING OF ANCHORS FOR SEISMIC SHEAR LOADING	82
5.1	General	82
5.2	Analytical model	83
5.3	Semi-empirical model	85
5.3.1	Static loading	85
5.3.2	Cyclic loading.....	89
5.3.2.1	Hysteresis with concrete degradation	90
5.3.2.2	Hysteresis with steel degradation.....	92
5.3.2.3	Hysteresis at variable amplitude.....	94
5.4	Comparison of the two models	95
5.5	Time history analysis	95
5.5.1	General	95
5.5.2	Calibration of the model.....	98
5.5.3	Influence of hole clearance.....	99
5.5.4	Design proposal for hammer effect	102
5.5.4.1	Single anchors	102
5.5.4.2	Anchor groups	102
5.5.5	Conclusions for seismic tension loading	104
5.6	Real behaviour versus experimental and numerical studies.....	106
5.7	Summary	107
6	MITIGATION OF SEISMIC INDUCED SHEAR LOADS	108
6.1	Introduction.....	108
6.2	Numerical feasibility study	112
6.2.1	Viscous fluid damper	112
6.2.2	Friction damper.....	117
6.2.3	Hysteretic damper	120
6.2.4	Comparison of different dampers	125
6.3	Experimental validation	126
6.3.1	General	126
6.3.2	Quasi-static cycling pre-tests.....	126

- 6.3.3 Uniaxial shake table tests..... 128
 - 6.3.3.1 Sinusoidal input 129
 - 6.3.3.2 Seismic input 132

- 6.4 Summary 134

- 7 SUMMARY AND OUTLOOK..... 135

- 8 LITERATURE 141

1 Introduction

In the past decade, an area of increased interest has been dynamic and reverse cyclic loading. This is attributed to the fact that more catastrophic failures occur during dynamic loading associated with natural disasters than due to gravity loads. The Loma Prieta earthquake (San Francisco) in 1989, the Northridge earthquake (Los Angeles) in 1994, quakes in Turkey (1999), Iran (2003) China (2008) and Italy (l'Acquila 2009) have raised the public's interest and the awareness of improving the engineering and reliability of structures. As a direct result of world population growth and migration, today, more people than ever live in densely populated areas with enhanced risk to be shaken by earthquakes (Figure 1.1 and Figure 1.2).

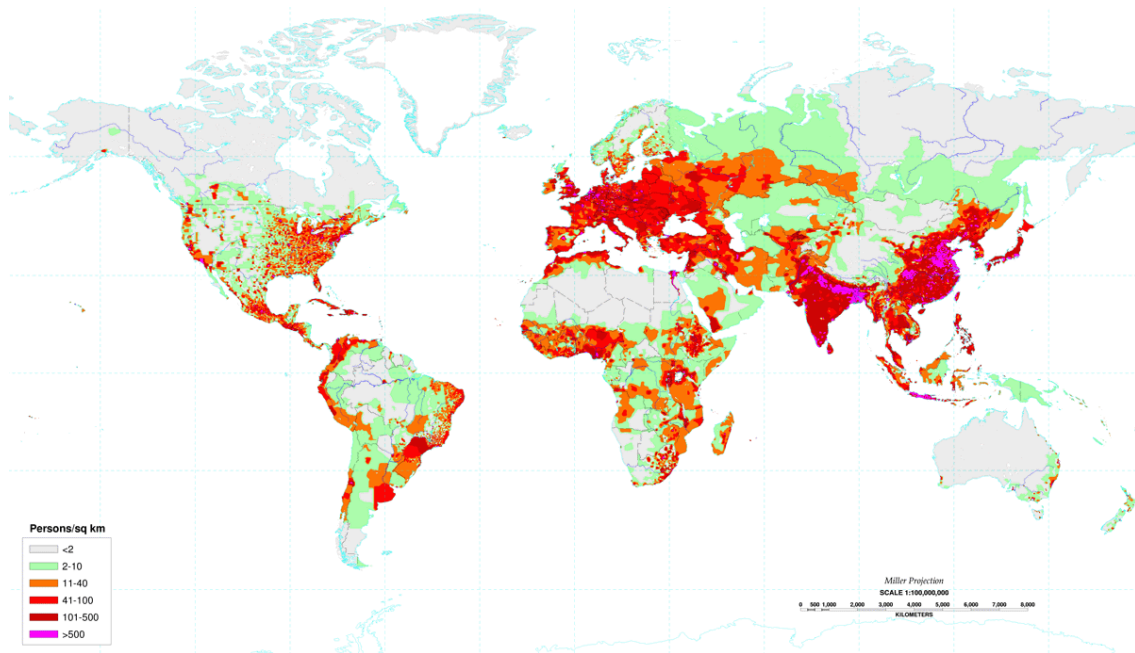


Figure 1.1: World population density as of 1994 (source: U.S. Department of Agriculture)

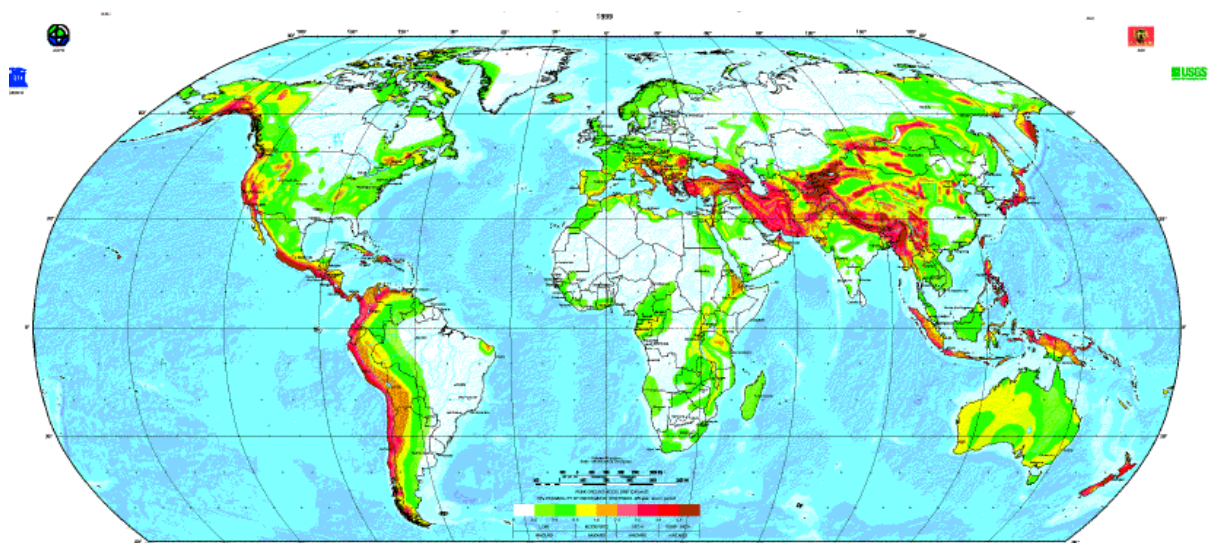


Figure 1.2: Global seismic hazard map (from: <http://www.seismo.ethz.ch/GSHAP/global/>)

Population density and building construction methods are the two main factors determining earthquake risk. Advances in seismic codes and their application in structural engineering have increased the safety of structures today. This issue is well demonstrated by the Loma Prieta earthquake (1989) with a magnitude of $M = 7.1$ leading to 67 casualties, 2435 injured and 7362 homeless persons. The earthquake of Armenia in 1988 with a magnitude $M = 6.9$, similar topography and population density was the cause for more than 25,000 casualties, 31,000 injured and 514,000 homeless persons. The main difference were the very poor seismic design provisions adopted in Armenia at this time (*Bachmann 1995*).

When dealing with seismic risk the effect of failure of non-structural elements is often neglected or underestimated. Such failure may cause break-out of fire through liquid gas leakage from tubes or tanks, shut-down of telecommunication systems by failure of electrical equipment or server stations, non-operability of life-saving equipment in hospitals etc. Since all these non-structural elements are fixed to the main structure usually by means of post-installed anchors, failure of the anchor leads to failure of the attached element with huge potential of secondary damage.

Since today and in future the major earthquake threat to human life and property loss comes from the existing buildings, retrofitting measures represent the most challenging emphasis of earthquake engineering and of code-writing (*Fardis 2008*). In the large field of seismic retrofitting of existing structures post-installed anchors play a decisive role in connecting old elements with new ones. For retrofitting purposes fasteners are expected to transfer cyclic seismic actions between existing and new elements in a reliable way.

Although the majority of fasteners on the market today are designed and tested for use in non-seismic environments, they are commonly used for applications in structures located in earthquake regions. This is especially true for Europe where currently no standardized (pre-)qualification of fasteners for seismic applications is available. Inadequately tested or inappropriately used fasteners can lead to unanticipated behavior that can negatively affect structural or non-structural performance during an earthquake and endanger human life. While our understanding of the behavior of fasteners, as well as the methods used for their qualification, have advanced significantly over the past 30 years, relatively little information exists about the behaviour of fasteners under earthquake conditions. Especially the response to seismic shear loading is difficult to predict since during construction it is a good practice to use a hole clearance between base plate and anchor which leads to a slack system.

In the case of non-structural elements, it is evident that a properly designed primary structure constitutes the fundamental prerequisite for the application of adequately tested and designed fasteners, i.e. if the primary structure collapses the secondary structure is obsolete. In the future this situation may change since the proportion of new structures with good seismic performance and retrofitted structures with enhanced seismic performance will increase. Basically, two options and/or a combination of them may be adopted in order to enhance the safety of post-installed anchors under seismic conditions:

1. To provide a simplified but realistic seismic testing protocol with corresponding acceptance criteria for anchor approval and thus filtering off anchors not suitable for seismic regions;

2. To mitigate the seismic action by means of dampers and /or energy dissipation devices and therefore avoiding seismic overloading and potential catastrophic failure.

An attempt to provide solutions for the first option is made by *Hoehler (2006)* and details are currently discussed within the members of the European Organization for Technical Approvals (EOTA). To the knowledge of the author no research is available which focuses on the second option.

The primary goals of this dissertation are:

1. To present an overview of research related to the behavior of fastenings under seismic shear loading and existing seismic qualification methods for fasteners.
2. To provide experimental data completed by numerical investigations for the seismic action on shear loaded anchors with slackness. Specifically, the inherent damping properties and the plastic deformation capacity under reversed cyclic shear loading are determined for different anchor types.
3. To investigate the influence of the anchor type on the behaviour under realistic seismic conditions. This goal is fulfilled by triaxial shake table testing with increasing amplitude up to failure.
4. To establish a feasibility study for the application and effect of various damping devices in order to mitigate the seismic action on anchors. This is done by means of transfer of knowledge from other branches of earthquake engineering and numerical investigations.

Based on the results of the investigations, recommendations are given for the modification of the calculation of seismic forces taking into account the slackness between base plate and anchor due to hole clearance in case of shear loading and due to plastic deformation in case of axial loading. Additionally, a more efficient use of the behaviour factor is proposed in calculating the seismic load on non-structural elements. For the mitigation of seismic shear forces a promising damper resulting from the feasibility study is suggested which has to be optimized and proven in future research work.

2 State-of-the-Art of fasteners in concrete for seismic applications

2.1 Types of post-installed anchors

Today, various systems of post-installed anchors are available to connect both structural and non-structural elements to concrete as base material. According to *EOTA (1997)* they can be classified in compliance with the different load transfer mechanisms mechanical interlock, friction and bond (Figure 2.1).

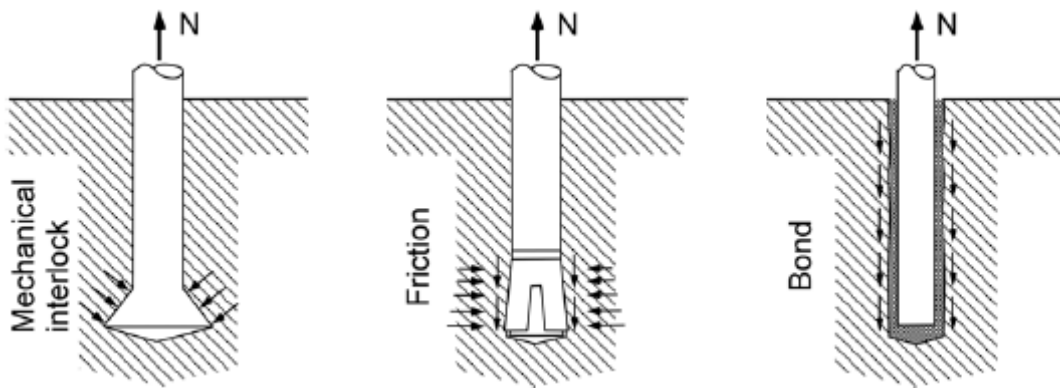


Figure 2.1: Tension load transfer mechanisms for post-installed anchors (after *Elgehausen 2000*)

2.1.1 Undercut anchors

The mechanical interlock of undercut anchors is achieved by a cone-shaped borehole at the end of the anchor where the sleeve is able to expand and to form a bearing area (Figure 2.2). The characteristic borehole can be realized through special drills or through self-drilling anchors.

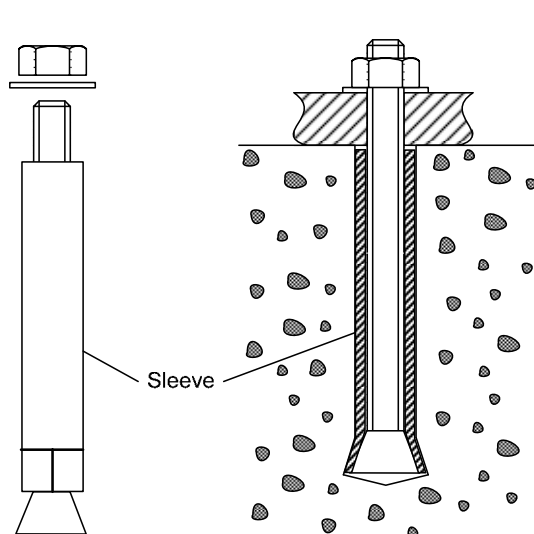


Figure 2.2: Undercut anchor (after *EOTA 1997*)

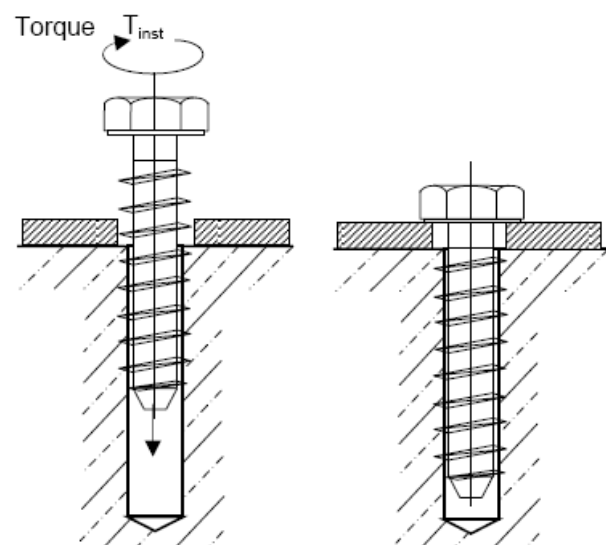


Figure 2.3: Concrete screw (*DIBt 2003*)

Screw anchors according to Figure 2.3 are screwed into a pre-drilled cylindrical hole. The special thread of the anchor cuts an internal thread into the concrete member while setting. The installation is typically performed by an electrical or pneumatic impact screw driver. The anchorage is characterised by mechanical interlock in the concrete thread.

2.1.2 Expansion anchors

Anchors that transfer load by friction have a geometry that generates an expansion force, which in turn gives rise to a friction force between the anchor and the sides of the borehole. This friction force resists the applied tensile force. Mechanical expansion anchors can be divided into two groups:

- force-controlled, which generate friction resistance by drawing an expansion cone into an expansion sleeve or expansion segments through the application of a defined torque moment with a calibrated torque wrench, thereby expanding the expansion element(s) against the sides of the drilled hole (Figure 2.4a),
- displacement-controlled, where friction resistance is generated by driving an expansion plug into a sleeve with a setting tool and a hammer as shown in Figure 2.4b or, alternatively, by driving the sleeve over the cone.

Force-controlled expansion anchors may be further classified as either sleeve-type or bolt-type. Sleeve-type anchors generally consist of a bolt or threaded rod with nut, washer, spacer and expansion sleeve and one or more expansion cones. Bolt-type anchors typically consist of a bolt, the end of which has been machined into a conical shape, expansion segments nested in the recessed conical end of the bolt and a nut and washer.

Combination anchors such as bonded-expansion anchors and bonded-undercut anchors also exist. Detailed descriptions of the various fastener types and their load transfer mechanisms are provided in *EOTA (1997)*.

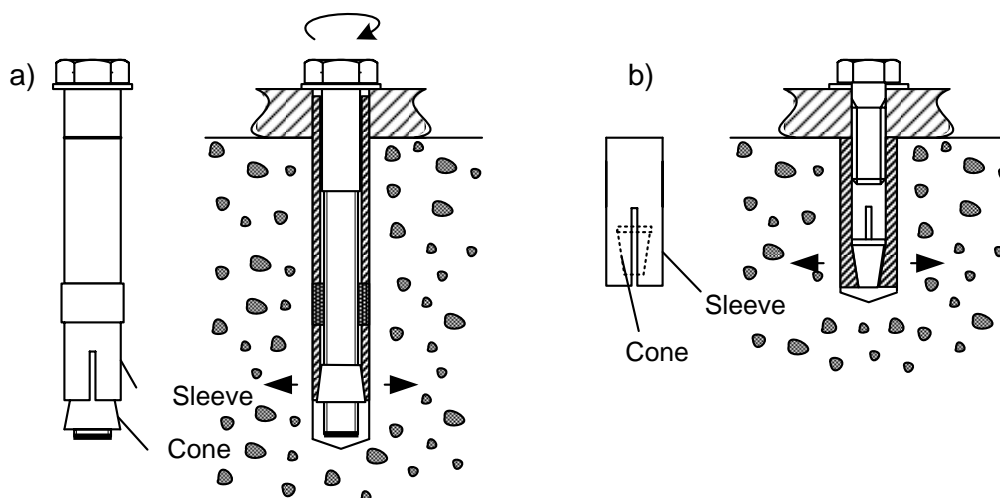


Figure 2.4: Expansion anchors; a) force controlled, b) displacement controlled (after *EOTA 1997*)

2.1.3 Bonded anchors

In the case of bonded anchors, the tension load is transferred to the anchorage material by means of chemical interlock, i.e. some combination of adhesion and micro-keying provided by a binding material with aggregates. Commonly used binding materials are resins (e.g. polyester, vinylester, epoxyde), cement or a mixture of both. Capsule-type bonded anchors as shown in Figure 2.5a are installed by insertion of the capsule in the cleaned borehole and driving in the anchor with the hammer drill. Injection-type bonded anchors according to Figure 2.5b can be set by hand after injecting the mortar in the borehole with a special cartridge. After the prescribed curing time the recommended torque moment is applied and the anchor can be loaded.

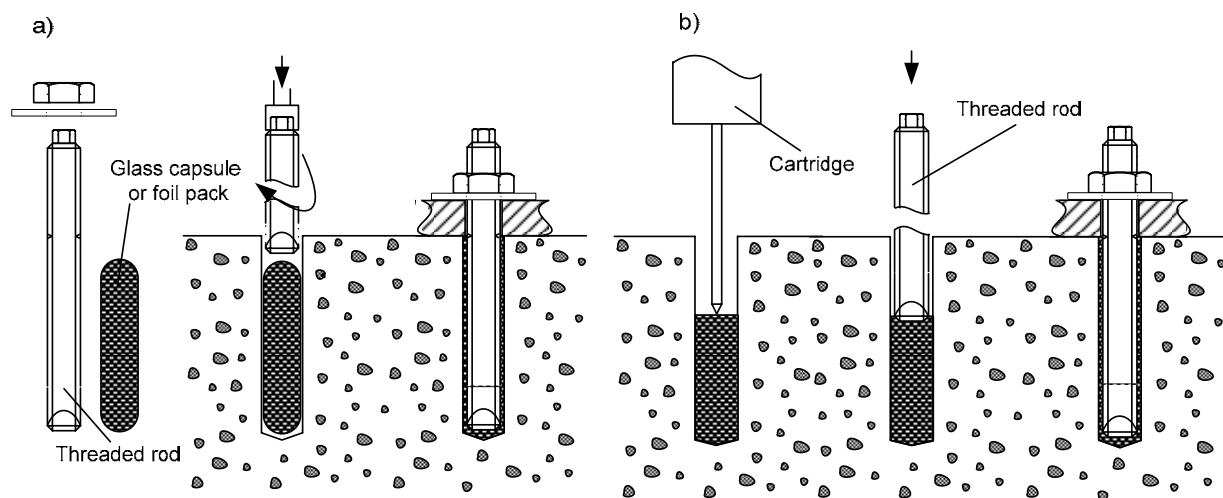


Figure 2.5: Bonded anchors; a) capsule type, b) injection type (after EOTA 1997)

2.2 Design by testing

2.2.1 General

Safety and reliability during service life of post-installed anchors represent the basic criteria for producers, engineers and construction industry. Since the single and mutual influence of different factors e.g. base material, installation quality, corrosive environment, type of loading etc. is not known sufficiently in order to derive the properties in a theoretic way, tests are necessary for the assessment and design of post-installed anchors. Systematic research during the past 30 years and close cooperation between universities, anchor producers and public authorities enabled the formulation of the first international testing and design guideline for metal anchors in concrete ETAG 001 which has been endorsed by EOTA (1997). With some modifications, it has been introduced in the U.S. by application in an earlier version of ACI 355.2 (2004) for mechanical anchors and in AC308 for bonded anchors (ICC-ES 2009). Both testing guidelines are based on the combination of testing and current experience. Thus, the test program may be reduced if current experience is available for a specific product. Technical Approvals released on the base of these guidelines are recognized in many countries over the world and hence they give a decisive contribution for the facilitation of trade.

2.2.2 Non-seismic qualification

2.2.2.1 Test program

The testing guidelines ETAG 001, ACI 355.2 and AC308 are valid for undercut anchors, expansion anchor and bonded anchors and require three different types of tests:

- Suitability tests
- Reference tests
- Tests for admissible service conditions

Aim of the suitability tests is to check the sensitivity of anchors to deviations from the manufacturer's installation instructions (e.g. too low or too high torque moment, reduced cleaning of the borehole) and to unfavourable base material conditions (e.g. large static cracks, cycling cracks, borehole diameter) and combinations of both. By comparison of the results of the suitability tests with those of the reference tests (anchors are installed according to the manufacturer's installation instructions) characteristic resistances and partial safety factors are derived. The tests for admissible service conditions are optional and serve for the determination of minimum spacing and edge distance. Since the characteristic resistance is determined dependent on loading direction (Figure 2.6) and failure mode (following figures), the presented testing guidelines enable an economic design.

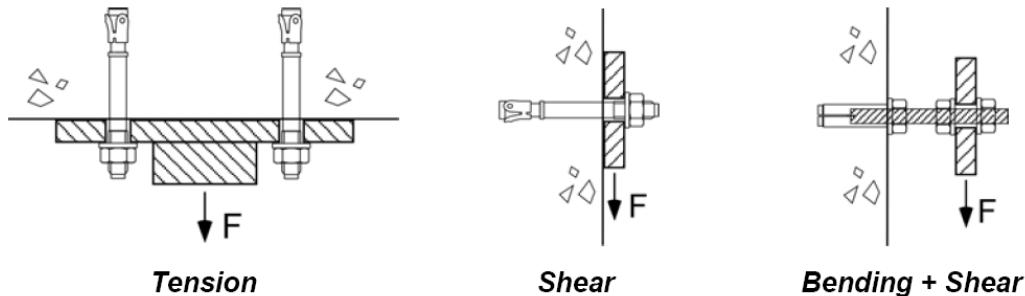


Figure 2.6: Loadings on anchors (after *Eligehausen 2000*)

2.2.2.2 Failure modes

The load-displacement behavior and the failure mode of post-installed anchors are product dependent and influenced by numerous geometrical, material and environmental parameters. A comprehensive discussion of fastener load-bearing behavior can be found for example in *Eligehausen (2000)*. A brief overview of behavior relevant for this dissertation is presented below.

For loading in tension, five general failure modes can be distinguished: pull-out, pull-through, concrete cone failure, splitting and steel failure (Figure 2.7). Pull-out failure is characterized by the anchor being pulled out of the drilled hole completely, whereby the concrete in the immediate vicinity of the anchor may or may not be damaged (Figure 2.7a₁). This (unfavourable) failure mode can occur with expansion anchors, if the friction between cone and sleeve is higher than that between sleeve and concrete. For

bonded anchors the pull-pot failure can be classified in failure between the threaded rod and the mortar (Figure 2.9a), failure between the mortar and the concrete (Figure 2.9b) and mixed failure (Figure 2.9c). In all three cases a concrete cone with a depth of $2-d$ to $3-d$ (d = threaded rod diameter) forms close the concrete surface and bond failure occurs along the rest of the embedment depth.

Pull-through failure is unique to force-controlled expansion anchors and is characterized by the expansion cone being pulled through the expansion elements, i.e. the expansion elements remain in the drilled hole (Figure 2.7a₂).

Concrete cone failure is characterized by a cone-shaped concrete breakout (Figure 2.7b). The individual concrete cones for a group of anchors may overlap or the cone may be truncated if it is located close to an edge.

Failure due to splitting of the concrete typically occurs when the dimensions of the concrete component are limited (Figure 2.7c₁), the anchor is installed too close to an edge (Figure 2.7c₂) or a line of anchors are installed in close proximity to each other (Figure 2.7c₃).

Steel failure of the anchor bolt or sleeve represents the upper limit of the load carrying capacity of a fastener. Fastenings with large edge distances and embedment depths loaded in shear will fail by local concrete spalling in front of the anchor followed by steel failure (Figure 2.8a). In chapter 3.2 a more detailed analysis will be provided.

If the fastening is located close to an edge (Figure 2.8b_{1,2}) or in a corner (Figure 2.8b₃) and loaded in shear towards the edge, concrete edge breakout will occur. For thin (Figure 2.8b₄) or narrow (Figure 2.8b₅) members, the concrete breakout body will be truncated.

Stiff fastenings with relatively shallow embedment depths may fail by pryout of the concrete on the side of the anchor opposite to the direction of the applied shear load (Figure 2.8c_{1,2}).

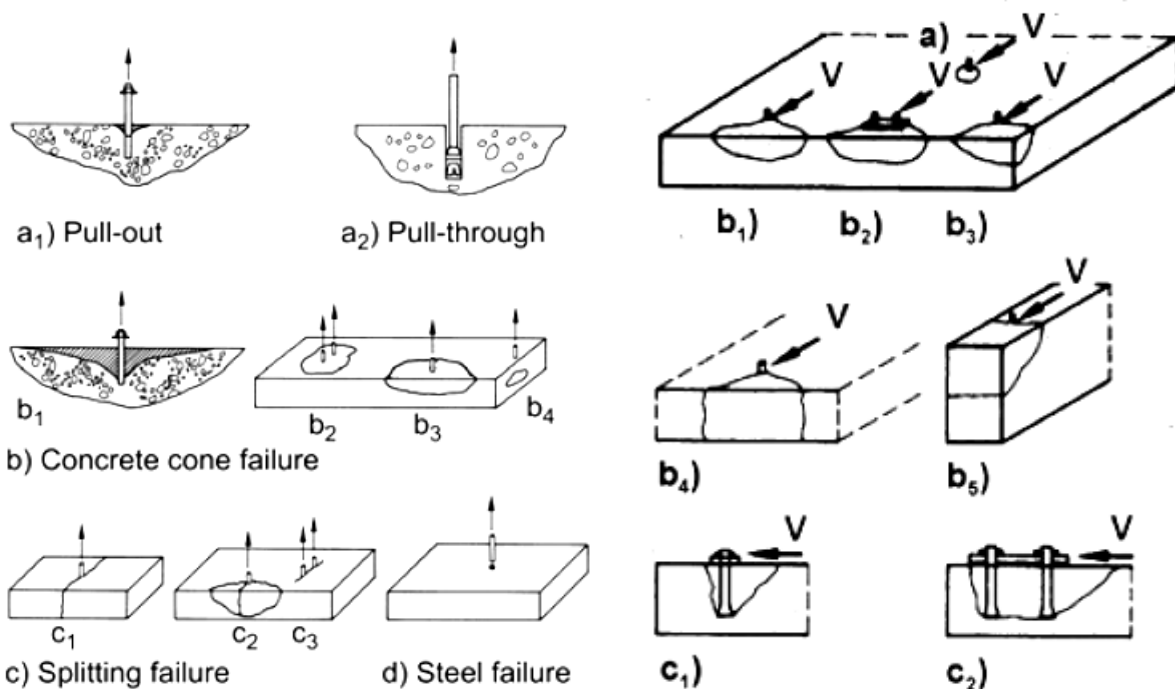


Figure 2.7: Tension failure modes (after Eligehausen 2000)

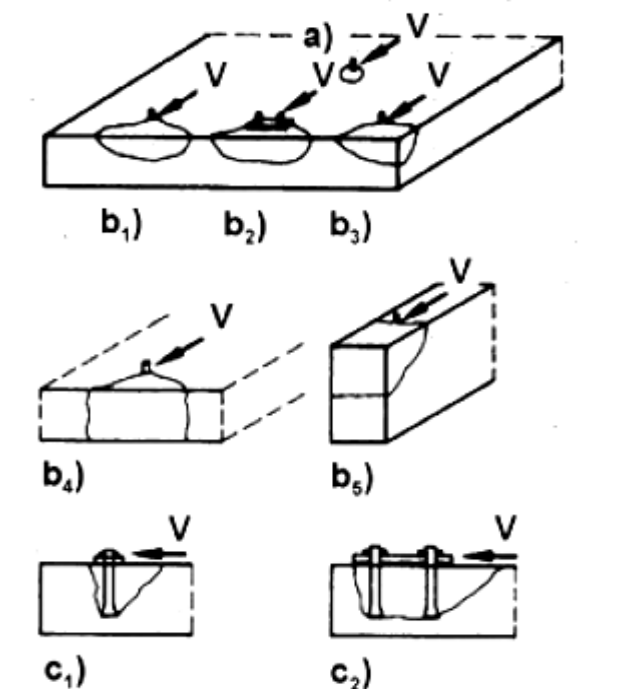


Figure 2.8: Shear failure modes (after Eligehausen 2000)

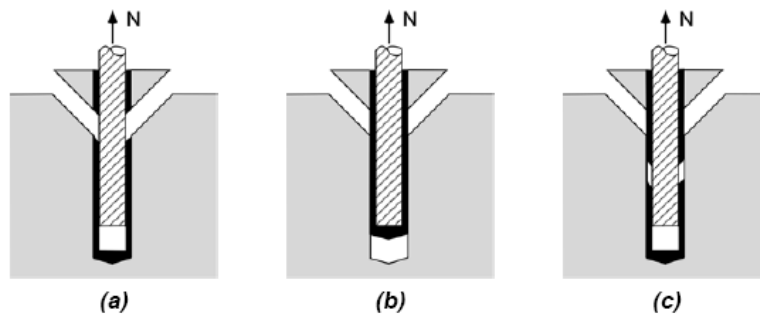


Figure 2.9: Pull-out failure modes of bonded anchors: (a) threaded rod / mortar; (b) mortar / concrete; (c) mixed failure (after Cook 1998)

Analytic methods to determine the ultimate loads of fasteners failing in the various failure modes discussed above under monotonic loading can be found in *Eligehausen (2000)*. Different approaches for the development of a resistance model applicable to post-installed anchors are compared and discussed in *Bergmeister (2004)*.

2.2.2.3 Influence of cracks

Numerous investigations have shown that the load-bearing behavior of post-installed anchors in cracked concrete can differ significantly from that in uncracked concrete, e.g. *Eligehausen (2000)*. The difference in behavior is expressed as a change in stiffness, ultimate load capacity, and possibly, in the failure mode of the fastener (Figure 2.10). The friction between cone and sleeve of torque-controlled expansion anchors plays a decisive role regarding the displacement behaviour under constant loading in opening and closing cracks (Figure 2.11, slip versus crack openings).

Many fasteners designed for use in uncracked concrete are not suitable for use in cracked concrete. Critical factors hereby are the fastener type and design and the crack width. Tests on a variety of anchors loaded in tension in static cracks, show reductions of the resistance of 30% and more even at relatively small crack widths ($\Delta w = 0.3$ mm). Figure 2.12 shows experimentally obtained ratios of the resistance in cracked and uncracked concrete and the trends for reduction of resistance due to cracking for undercut, expansion and bonded anchors.

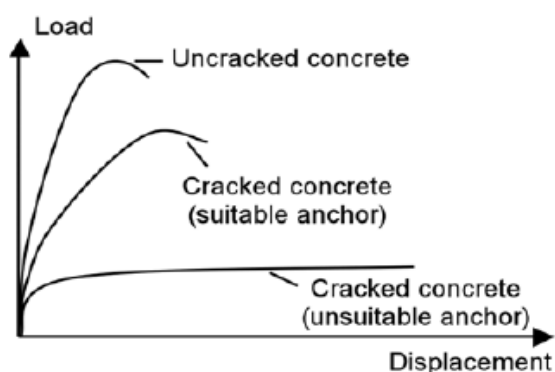


Figure 2.10: Effect of cracking on the tension load-displacement curves for a torque-controlled expansion anchor (after *Eligehausen 2000*)

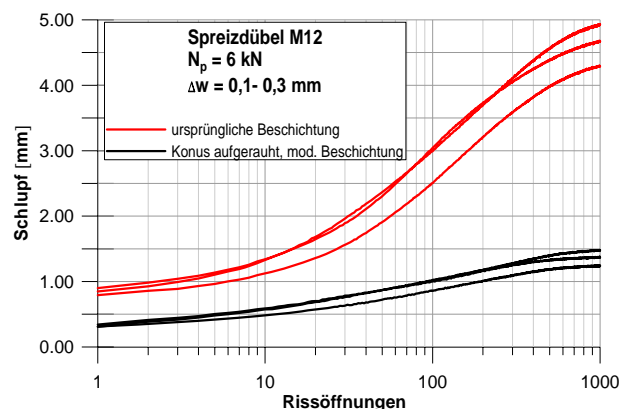


Figure 2.11: Effect of crack cycling on the tension displacement for a torque-controlled expansion anchor (*Rieder 2001*)

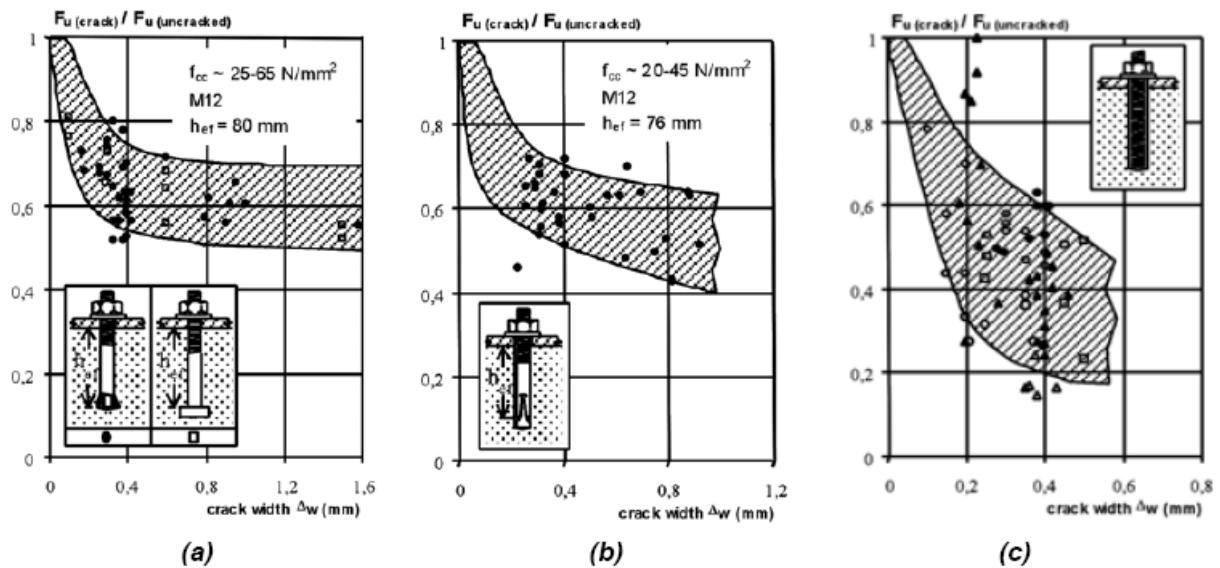


Figure 2.12: Resistance of fasteners in cracks under tension loading: (a) undercut anchors and headed studs; (b) torque-controlled expansion anchors designed for use in cracked concrete; (c) bonded anchors not designed for use in cracked concrete (after *Eligehausen 1995*)

2.2.3 Seismic qualification

2.2.3.1 General

During an earthquake a post-installed anchor may be subjected to a combination of cyclic tension and shear forces. Furthermore, the fastener may be located in a crack that either forms during the earthquake or already exists before. Since according to *Bergmeister (1988)* the formation of cracks close to anchors occurs with high probability also during non-seismic action, uncracked concrete may be excluded at least for medium seismicity. The crack width will typically vary over the duration of the earthquake, e.g. the crack will open and close several times, as a result of deformation of the structure in which the fastener is located. Consequently, the seismic behavior of anchorages depends on numerous parameters, including (*Hoehler 2006*):

- the amplitude, rate, sequence and number of cycles of the imposed actions,
- the direction of application of the actions (axial, shear, combined),
- the state of the surrounding concrete (uncracked or cracked, crack cycling, crack width),
- quantity and orientation of reinforcement in the vicinity of the anchorage, and
- the characteristics of the anchor, including load transfer mechanism, material properties, diameter and embedment depth

In the following various existing and still developing seismic testing protocols and assessment criteria for post-installed anchors are shortly presented and compared.

2.2.3.2 Testing protocols in the U.S.

The simulated seismic tests according to *ACI 355.2 (2004)* subject a series of 5 fasteners situated in cracked concrete ($\Delta w = 0.5$ mm) to stepwise decreasing, pulsating tension (Figure 2.13a) or alternating shear (Figure 2.13b) load controlled cycles. The load steps are determined based on the mean ultimate strength from the reference tests in cracked concrete ($\Delta w = 0.3$ mm). The load cycling frequency can be chosen between 0.1 and 2 Hz and the total number of cycles is 140. After completion of the load cycles, the fastener is loaded monotonically to failure using an initial crack width not less than the crack width at the end of the load cycling. Qualification of the fastener is based on the exclusion of failure during load cycling and attainment of a mean residual capacity after load cycling of at least 80% of the mean capacity from the corresponding static reference tests. If an anchor fails during load cycling, the amplitude shall be reduced and the seismic resistance will be diminished by the same amount.

Some remarks and comments regarding the testing protocol prescribed by *ACI 355.2 (2004)* are given in chapter 4.2.

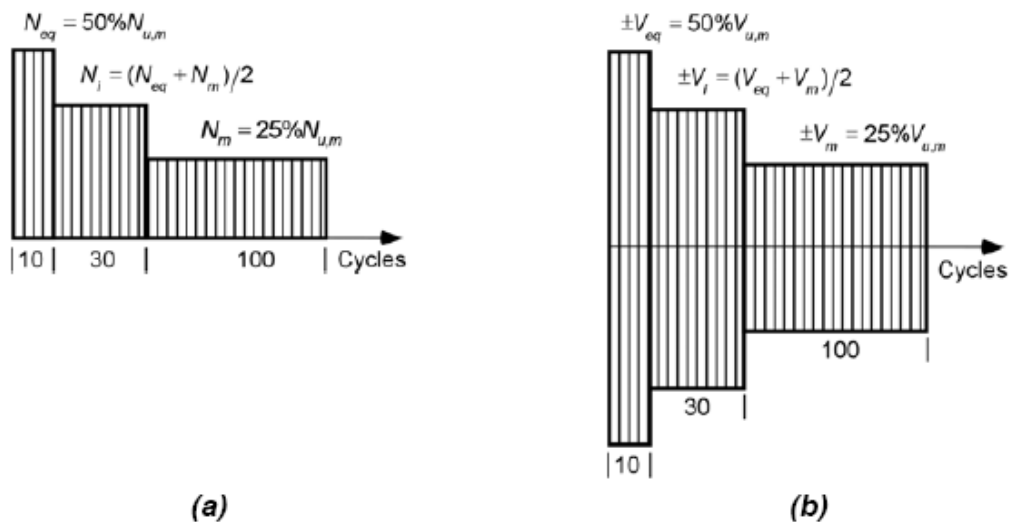


Figure 2.13: Loading patterns for simulated seismic tests in *ACI 355.2 (2004)*: (a) tension; (b) shear

The Structural Engineers Association of Southern California (SEAOSC) proposed a seismic test for fasteners based on the assumption that historical provisions for cast-in anchors in the Uniform Building Code (*UBC 1997*) had proven adequate in past earthquakes. Accordingly, the SEAOSC Standard Method of Cyclic Load Test for Anchors in Concrete or Grouted Masonry (*SEAOSC 1997*) requires side-by-side testing of post-installed anchors with code cast-in anchors (standard hex A307 bolts) of like diameter. It is not specified whether the tests are to be performed in uncracked or cracked concrete. The anchors are loaded cyclically in steps of five cycles each up to failure. The load steps are determined by first identifying (from static test data) the First Major Event (FME), which is the load level at which the load-displacement curve undergoes a significant change. The load steps are then established as 25% increments of the FME, i.e. 25%FME, 50%FME, 75%FME, 100%FME, 125%FME, etc. to failure (Figure B.3). The resulting load-displacement curves and ultimate loads of the post-installed and cast-in anchors are compared. Qualification of the post-installed anchor is based on performance equal to or exceeding that of the cast-in anchor.

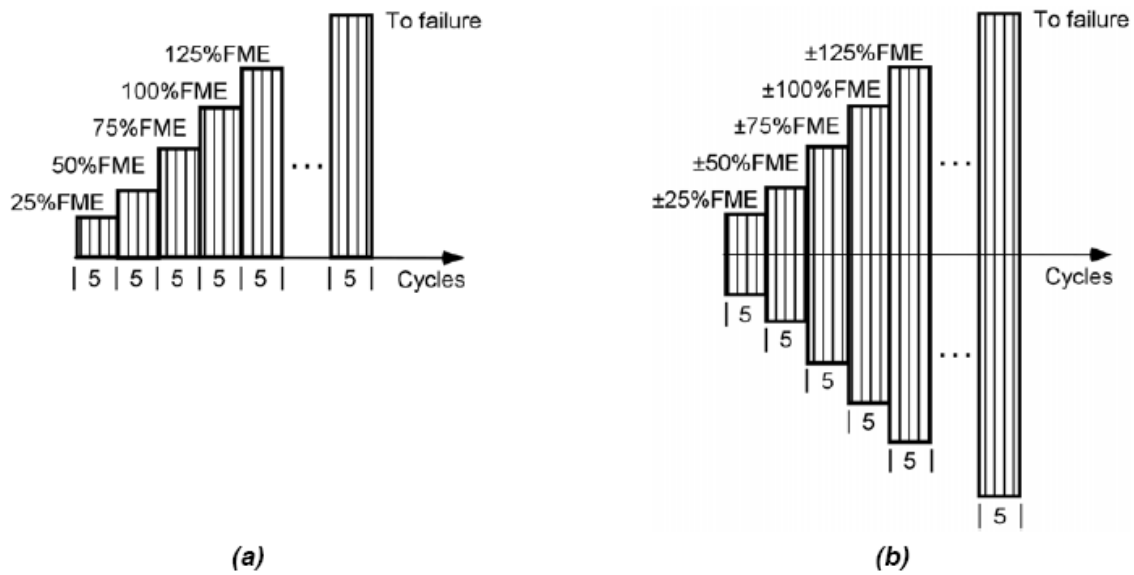


Figure 2.14: Loading patterns for simulated seismic tests in *SEAOSC (1997)*: (a) tension; (b) shear

2.2.3.3 Testing protocol in Canada

Seismic testing requirements for fastenings used in Canadian nuclear power plants are specified in *CSA-N287.2 (2003)*. All tests are performed in uncracked, unreinforced concrete (20 MPa). Monotonic tension tests in which concrete cone failure occurs, e.g. by selecting a bolt strength large enough to prevent yielding of the steel, are to be performed to establish the concrete cone failure strength. Monotonic shear tests are to be performed using an anchor bolt material identical to that used in the actual application to establish the steel failure load in the case of shear. Simulated seismic tests subject fasteners to stepwise decreasing, pulsating tension (Figure 2.15a) or alternating shear (Figure 2.15b) load cycles with a frequency of 5 Hz. The load steps are determined based on the specified minimum yield strength of the fastener steel. After completion of the load cycles, the fastener is loaded monotonically to failure. Qualification of the fastener is based on the exclusion of failure during load cycling and attainment of the steel yield load after load cycling.

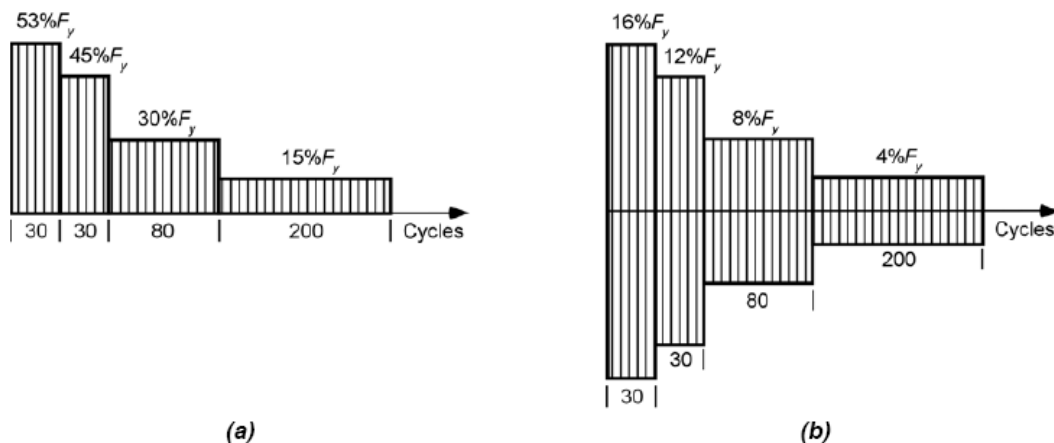


Figure 2.15: Loading patterns for simulated seismic tests in *CSA-N287.2 (2003)*: (a) tension; (b) shear (F_y = calculated fastener yield load)

The presented seismic testing protocols agree in pulsating tension and alternating shear loading. However, considerable differences can be observed with regard to amplitude, loading sequence, number of cycles, concrete conditions and loading frequency. This may be due to the different seismic design philosophy in the various countries based on specific experience, construction technology and public awareness. Thus it is evident that the results obtained by the specific testing protocols cannot be compared with each other, e.g. the same anchor may be suitable for the use in Canada but not in California.

2.2.3.4 Draft for testing protocol in Europe

Up to now no testing guidelines for the qualification of post-installed anchors in seismic regions are available in Europe. Within the members of EOTA a new concept for seismic qualification tests is discussed currently. It is based on two anchor seismic performance categories (ASPC) dependent on the seismicity at the location where the anchor will be applied. For very low and low seismicity as defined in Eurocode 8 the ASPC1 with low demand on testing conditions is decisive. For the application of an anchor in a region exhibiting medium seismicity, tests according to ASPC2 are necessary where the testing conditions are more severe (Table 2.1). The decisive parameter defining the seismic performance class is represented by the peak ground acceleration in the various member states which varies between 0.10g and 0.15g (with the gravity acceleration g).

A proposal for the testing conditions related to ASPC2 is based on the research done by *Hoehler (2006)* which is summarized in the following.

Table 2.1: EOTA-draft for seismic anchor testing

Seismicity	Anchor seismic performance category	Testing conditions
Very low and low	ASPC1	soft
Medium	ASPC2	severe

Crack cycling tests were conducted to determine the performance of various fastener types when loaded by a constant tension load of $N_w \sim 0.4 \cdot N_{u,m}$ (with the mean ultimate load $N_{u,m}$) and subjected to 10 crack cycles between $w_1 = 0.8$ mm and $w_2 = 0.0$ mm. Full crack closure simulates the (cyclic) compression zone of e.g. a column close to the beam joint and may be achieved by subjecting the test specimen to a compressive force of 15% of f_c . The upper crack width w_1 indicates a mean expectable value for various RC member geometries and reinforcement ratios at yielding outside of plastic hinges. The investigated fasteners were headed studs ($d_{nom} = 19$ mm), bolt-type (M16) and sleeve-type (M12) torque-controlled expansion anchors, undercut anchors (M10) and screw anchors ($d_{nom} = 20$ mm). The investigated headed studs, undercut anchors and sleeve-type expansion anchors failed by concrete cone breakout in pull-out tests performed in an open crack ($\Delta w = 0.8$ mm) subsequent to the crack cycling. The bolt-type expansion anchors failed by pull-through and the screw anchors failed by pull-out after crack cycling. For anchors failing by concrete cone breakout the following conclusions are drawn:

1. If the displacement during crack cycling is less than the displacement at ultimate load in comparable monotonic pull-out tests in a static crack, the crack cycling appears to have little influence on the residual strength;
2. If the displacement during crack cycling is equal to or greater than the displacement at ultimate load in comparable monotonic pullout tests in a static crack, the residual strength is reduced as a function of the lost embedment depth according to $(h_{ef} - \delta)^{1.5}$;
3. Concrete cone failure during crack cycling can occur if the embedment depth is reduced sufficiently to cause failure at the applied fastener tension load;
4. splitting of the member may occur for large fastener displacements and/or high compressive member loads before one of the above-stated failure cases occurs.

For anchors failing by pull-through (see Figure 2.7):

1. In the case of pull-through failure during crack cycling or in pullout tests performed subsequent to the crack cycling where the anchor expansion elements do not slip relative to the wall of the drilled hole, the load-displacement behavior is bounded by the monotonic envelope curve;
2. This failure mode is typically associated with large fastener displacements;
3. If the displacement during crack cycling is less than the displacement at ultimate load in comparable monotonic pullout tests in a static crack, the fastener behavior during subsequent pull-out becomes stiffer;
4. If the displacement during crack cycling is equal to or greater than the displacement at ultimate load in comparable monotonic pull-out tests in a static crack, the residual strength is reduced following the descending branch of the monotonic curve and often exhibits a large amount of scatter.

For screw anchors failing by pull-out:

1. If the screw anchors fail in pure pull-out failure in both monotonic and crack cycling tests, the load-displacement behavior is expected to be similar to that for pull-through failure, i.e. the load-displacement curve for the crack cycling test would be bounded by the monotonic load-displacement curve;
2. The amount of fastener displacement that can occur during crack cycling is less than the anchor thread spacing.

Hoehler (2006) concludes that the most important factors influencing the displacement behaviour are the type of anchor and failure mode, the crack opening and closing widths (w_1 , w_2), the number of crack cycles (n) and the fastener bearing pressure (Figure 2.16). Additionally, further research is necessary to establish displacement assessment criteria for anchor prequalification.

Tension load cycling tests at near ultimate load levels with post-installed fasteners in cracked concrete ($\Delta w = 0.8$ mm) showed robust performance of fasteners failing by concrete cone breakout (sleeve-type expansion anchor), pull-through (bolt-type expansion anchor) and pull-out (screw anchor). For seismic

qualification *Hoehler (2006)* proposes additional test series with pulsating tension and alternating shear cycling with stepwise increasing amplitude up to failure similar to the procedure adopted in *SEAOSC (1997)*.

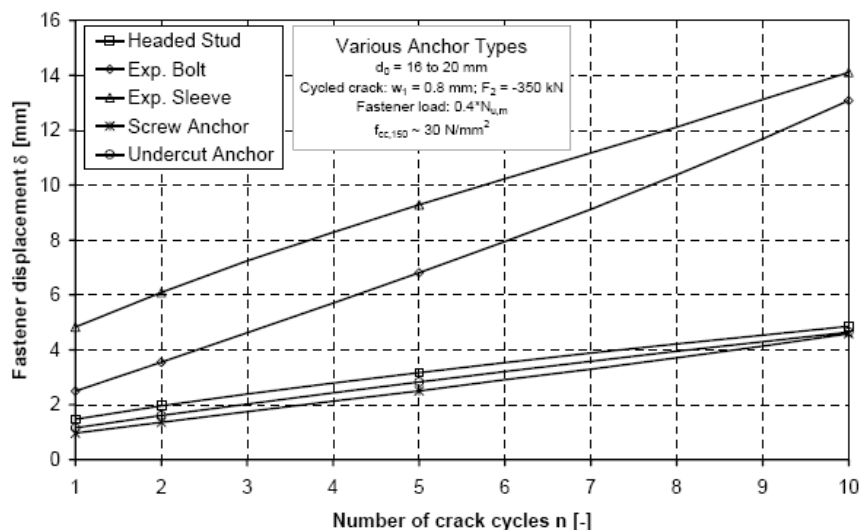


Figure 2.16: Fastener displacement as a function of the number of crack cycles for various fastener types (*Hoehler 2006*)

2.3 Seismic action on fasteners

2.3.1 General

Earthquakes generate actions (forces and displacements) on a structure in a variety of ways including ground acceleration, differential settlement of the foundations and lateral and vertical displacement across a fault trace. From a design perspective, induced structure acceleration represents the most obvious and prevalent loading case to be considered.

Typically, ground accelerations are translated through a structure via the foundations, which interact with the surrounding and supporting soil and rock via a complex interplay of frictional and bearing forces. The input motions from the ground generate varying responses in the structure depending on the magnitude, frequency content and duration of the ground motion, the efficiency of the soil-structure interface and the dynamic characteristics of the structure. In reinforced concrete structures earthquake induced degradation is mainly expressed through cracking in the structural elements. Additionally, the motion of the primary structure will generate actions on secondary structures. If the secondary structure is connected to the primary structure by fasteners, the motion of the primary structure generates tension and shear forces on the fasteners (Figure 2.17).

Earthquake induced forces vary with time and are designated as dynamic forces. The presence of inertial and damping forces, which arise as a result of strong ground motion, is the critical distinction between dynamic and static or quasi-static loading.

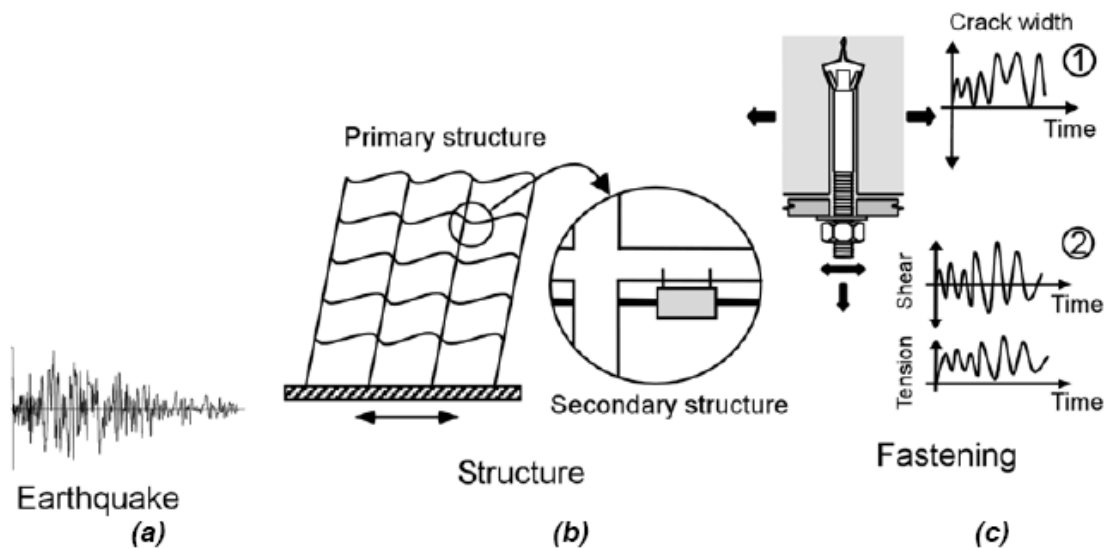


Figure 2.17: Load path and actions under earthquake loading (Hoehler 2006)

2.3.2 Design models for seismic loads

The complex interaction between soil, primary structure and secondary structure attached by means of post-installed anchors cannot be determined accurately. In fact, different formulas attempting to calculate the seismic forces acting on a fastener may be considered only as a rough estimation of the real situation. In most cases earthquake induced forces F_{eq} consist of the following parameters (Bachmann 1993):

$$F_{eq} = \alpha_1 \cdot \alpha_2 \cdot \alpha_3 \cdot \alpha_4 \cdot \alpha_5 \cdot \alpha_6 \cdot \alpha_7 \cdot a_g \cdot m \quad (2.1)$$

With

- α_1 factor related to the seismic zone
- α_2 dynamic factor
- α_3 soil factor
- α_4 damping factor
- α_5 structural factor depending on ductility (behaviour factor)
- α_6 risk factor
- α_7 importance factor
- a_g ground acceleration
- m dead load

The value of the ground acceleration on a specific site is taken from seismic hazard maps and can be calculated by probabilistic seismic hazard assessment. Herein the usual expression relating earthquake magnitudes with their rates of occurrence is the "magnitude-frequency formula" (Gutenberg 1944) which states that in a certain region and in a given period of time given an earthquake event:

$$\log N(M) = a - b \cdot M \quad (2.2)$$

Where $N(M)$ is the mean number of earthquakes per unit volume and per unit time having magnitude greater than M and a and b are zone dependent constants.

It follows that the Magnitude M in a region has a truncated exponential distribution, i.e. for $M_1 \leq M \leq M_2$ the cumulative probability distribution is given by:

$$F(M) = \frac{1 - \exp[-\beta(M - M_1)]}{1 - \exp[-\beta(M_2 - M_1)]} \quad (2.3)$$

In which

$\beta \quad \sim 2.3$

$M_1 \quad$ smallest magnitude of engineering interest considered in the model (here $M_1 = 4.0$)

$M_2 \quad$ largest magnitude event which can be expected in the region (here $M_2 = 8.0$)

In a good approximation, earthquakes occur according to a poisson process with mean occurrence rate ν . The exceedance probability $P[A \geq a]$ in a reference period T per unit area can be estimated by (*JCSS 2001*):

$$P[A \geq a] = 1 - \exp(-\nu \cdot T \cdot P'[A \geq a]) \quad (2.4)$$

With

$\nu \quad$ number of earthquakes with $M > M_1$ per unit of time (occurrence rate)

$T \quad$ period of time

$P'[A \geq a] \quad$ probability of $A > a$ given an earthquake with $M > M_1$ in one source area

Recommendations for modelling the statistical uncertainty of ν are given in *JCSS (2001)*. For engineering purposes a 10% probability of exceedance in 50 years for the ground acceleration a_g is used. However, in real earthquakes this value may be exceeded considerably, e.g. in the l'Acquila event 2009 about the double of the design value was measured (*Franchi 2009*).

Many codes attempt to describe the seismic action on the basis of geological observations and experience. Therefore different values for the various α -factors may be expected in specific countries. The design loads for fasteners are generally higher than the forces specified for the design of the structure for the following reasons (*Bergmeister 2000*):

1. Motions of upper floors exceed ground acceleration
2. additional amplification may be induced by the attached system
3. fasteners usually exhibit limited ductility

Bergmeister (2000) made a comparison of various codes adopted in the U.S. and in Europe and found differences for the seismic force F_{eq} of a factor 2 in case of a rigidly fixed non-structural element and a

factor 4.5 (!) in case of a vibration isolated non-structural element. Thus, the uncertainties in calculating seismic loads are reflected by the various codes. Especially the possibility of taking into account an isolating or damping system is not covered in the different codes. In chapter 4 the design according to *CEN/TS (2004)* will be presented more detailed.

2.4 Seismic applications of fasteners

When discussing fastenings for seismic applications it is useful to distinguish between structural and nonstructural applications. This distinction is important since different loadings exist for the two types of applications and different factors of safety may need to be considered in the design of the fastening. For seismic applications *Eurocode 8 (2003)* provides the following definitions:

Nonstructural elements	Architectural, mechanical or electrical elements, systems and components which, whether due to lack of strength or to the way they are connected to the structure, are not considered in the seismic design as load carrying elements.
Structural elements	Members considered as part of the structural system that resists the seismic action, modelled in the analysis for the seismic design situation and fully designed and detailed for earthquake resistance according to the rules of <i>Eurocode 8 (2003)</i> .

In the following table and figures some examples for standard applications and for retrofitting purposes are given. Applications for claddings can be found in *Spieth (2009)*. Detailed informations and examples for seismic retrofitting are available e.g. in *CEB (1995)*.

Table 2.2: Application of fastenings

Standard fastening applications (seismic and non-seismic)	Fastening applications for retrofitting
<ul style="list-style-type: none"> • Facades • Suspended ceilings new and existing structures • Heating, ventilation, air conditioning • Pipelines reinforced polymer meshes • Mechanical equipment • Structural connections 	<ul style="list-style-type: none"> • Structural connections between new and existing structures • Restraint of wire and fiber reinforced polymer meshes



Figure 2.18: Connection of claddings (*fischer 2007*)



Figure 2.19: Connection of prefabricated elements (*fischer 2007*)

3 Response of fasteners under monotonic and cyclic shear loading

3.1 General

Single anchors and group of post-installed anchors in concrete under monotonic shear loading with and without the influence of free edges have attracted much attention in the past and the subject is well researched (*Fuchs 1992, Hofmann 2004, Unterweger 2008*). Numerical and geometrical models, especially for single anchors, have come to a high level of complexity and versatility being able to describe the influence of various parameters such as concrete strength, loading direction, member thickness and anchor geometry.

In contrast to monotonic loading, little research has been done on post-installed anchors using a reversed cyclic loading scheme which is essential when analyzing seismic performance. This lack may be due to the fact that in many countries this type of anchors are designed and applied only for predominantly monotonic loading conditions and hence no information or provision is given for cyclic loading. The necessity of research in this subject seems to be a crucial issue since many documented anchor failures during seismic events can be related to excessive shear loading (*Silva 2001*). Since the hysteretic characteristics for the primary connection of a subassembly govern its cyclic behaviour, the determination of the hysteretic response of anchors enables the characterisation of non-structural and structural elements attached to the supporting structure by these anchors.

This chapter attempts to compile and summarize past findings and inductions that have contributed to the current understanding of the performance of single anchors under monotonic and cyclic shear loading without the influence of free edges.

3.2 Monotonic loading

3.2.1 General

Fasteners without influence of free edges develop high stresses in the surrounding concrete. After reaching a critical load the concrete fails locally close to the anchor. This mechanism may be defined as service limit state with the corresponding resistance and (partial) safety factor. However, the ultimate load is achieved when steel rupture occurs at large displacements.

Threedimensional finite element analysis on the base of linear elastic material properties performed by *Utescher (1983)* show that a significant influence of the anchorage depth h_{ef} on the magnitude and distribution of stresses and displacements can be observed only for ratios $h_{ef}/d \leq 5$. The majority of available post-installed anchors exhibit a ratio $h_{ef}/d \geq 5$. On the concrete surface the stress distribution is akin to a cut through a shell, therefore the failure pattern develops correspondingly.

3.2.2 Prediction models

There is an abundance of connection models reported in the literature. It is not the purpose of this study to provide a complete description of all formulations attempting to predict anchor behaviour, but to give an overview of the various methods and whose combinations.

3.2.2.1 Beam on foundation

A fastener embedded in concrete and laterally loaded (see Figure 3.3) can be described as a beam on an elastic foundation. Studies of beams on elastic foundations have been reported in the literature for more than a century. General analyses have focussed on a linear elastic foundation where the reaction forces are proportional to the beam deflection at any point (Winkler foundation). It is assumed that the foundation is not capable of transferring shear loads. Thus, it can be modelled as an infinite number of independent springs supporting the beam. In addition, the Winkler hypothesis assumes that the foundation acts both in tension and compression. Hence, the beam is always in contact with the foundation and does not lift off.

According to Hetényi (1946), the deflection curve of a beam on this foundation between concentrated transverse loading forces can be described by the differential equation

$$E \cdot I \cdot \frac{d^4 y}{dx^4} = \frac{d^2 M}{dy^2} = \frac{dQ}{dx} = -k \cdot y \quad (3.1)$$

With the general solution

$$y = e^{\lambda \cdot x} (C_1 \cdot \cos(\lambda x) + C_2 \cdot \sin(\lambda x)) + e^{-\lambda \cdot x} (C_3 \cdot \cos(\lambda x) + C_4 \cdot \sin(\lambda x)) \quad (3.2)$$

Where

$$\lambda = \left(\frac{k}{4EI} \right)^{\frac{1}{4}} \quad (3.3)$$

The integration constants are determined based on boundary conditions. The decisive parameters are:

E	modulus of elasticity beam material	N/m ²
I	moment of inertia	m ⁴
k	modulus of foundation per beam width	N/m ²
x	distance from origin of coordinates	m
y	beam deflection (orthogonal to x)	m
C _i	integration constants	
λ	characteristic of the system	1/m

The application of the theory of beams on elastic foundation to anchors in concrete has been frequently reported in the literature. *Timoshenko (1951)* adopted it to determine in a simple way the internal stresses of the concrete, the bending moment in the bolt, its bending resistance and the interaction with the concrete. The crucial issue consists in choosing the proper modulus of foundation since it depends upon type of loading (monotonic or cyclic), stiffness, diameter and anchorage depth of the fastener and material properties of concrete under compression. For the ratio k/d where d is the diameter of the bolt values between 400 and 500 N/mm^3 are recommended (*Fuchs 1992*). Though extreme values of 40 N/mm^3 (*Dei Poli 1987*) and 2400 N/mm^3 (*Paschen 1983*) have been reported.

Friberg (1940) and *Basler (1967)* continued the research of *Timoshenko (1951)* and published an equation for the determination of a critical load F_{uR} :

$$F_{uR} = \frac{d}{k} \cdot \frac{2 \cdot \lambda^3 \cdot EI \cdot f_{c,edge}}{1 + \lambda \cdot e} \quad (3.4)$$

With

- F_{uR} critical load [N]
- d diameter of bolt [mm]
- $f_{c,edge}$ maximum stress on concrete edge [N/mm^2]
- e eccentricity [mm]

Friberg (1940) determined the latter from test results with $h_{ef}/d = 8$ by a regression analysis and found

$$f_{c,edge} = \frac{25 \cdot (f_c - 4.8) + 13.5 \cdot d}{0.9 \cdot d + 24} \quad (3.5)$$

With

- f_c concrete compressive strength [N/mm^2]

Basler (1967) assumed for the maximum stress on the concrete edge $f_{c,edge} = 2 \cdot f_c$. The critical load F_{uR} obtained by this approach is 2.5 times higher compared to the results of equation (3.5). These results show clearly the uncertainties involved in the use of an elastic foundation.

Concrete is not linear elastic when stressed to capacity and the analysis of anchors requires a look beyond the elastic limit. *Foschi (1974)* exploited a non-elastic foundation for laterally loaded nails in wood which accounts for crushing of the wood underneath the nails. This situation is very similar to a fastener in concrete and therefore it is presented shortly. The characteristics of the foundations are expressed as

$$p = (P_0 + P_1 x) \cdot \left(1 - e^{\frac{-kx}{P_0}} \right) \quad (3.6)$$

With

P	reaction force of foundation	N
k	initial stiffness	N/mm
P ₁	slope of the asymptote	N/mm
P ₀	y-intercept	N
x	displacement	mm

The constants k , P_1 and P_0 can be acquired from nonlinear least square fitting of experimental data obtained through embedment tests (Figure 3.1).

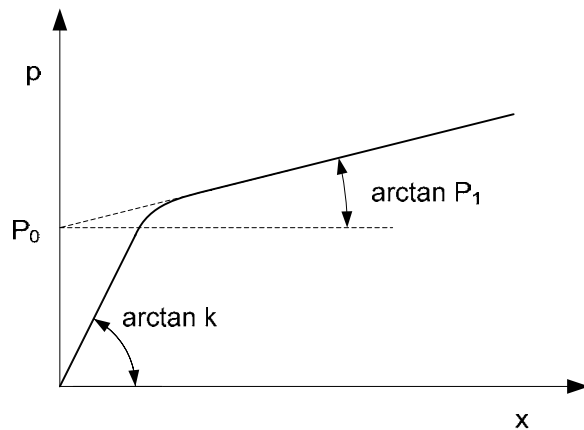


Figure 3.1: Foundation model (Foschi 1974)

3.2.2.2 Numerical models

In light of ever-increasing computing power, the capabilities of structural analysis today have become enormous. Numerical modelling has become powerful enough to provide approximated solutions with great accuracy of the most complex problems. Yet, the accuracy of numerical models rises and falls with the ability to quantify the material properties and their interaction by means of a proper material model. Encouraging results are obtained with the microplane model formulation of *Bazant (1990)* implemented in a finite element code by *Ožbolt (2005)*.

Earlier research made by *Cziesielski (1983)* on the base of a linear elastic behaviour of concrete and taking into account the results of beam theory on foundation provides an equation to determine the critical load F_{uR} :

$$F_{uR} = f_c \cdot \frac{d^2}{333 + 12.2 \cdot e} \quad (3.7)$$

It is restricted to $h_{ef}/d \geq 5$ and distance to the free edge $c \geq 6d$.

The influence of the ratio h_{ef}/d on the crack pattern is shown in the following figures. A small embedment depth leads to failure of the concrete on the surface and pronounced crack formation at the end of the anchor inside the concrete. Increased h_{ef} reduces the amount of cracks at the same load which is an indication for reduced stress. On the base of additional simulations *Fuchs (1992)* found that the maximum failure load is achieved for $h_{ef}/d = 5$. The anchor is deformed mainly between the loading

point and $2.5d$ inside the concrete. Failure occurs in all cases through concrete spalling at the loading point.

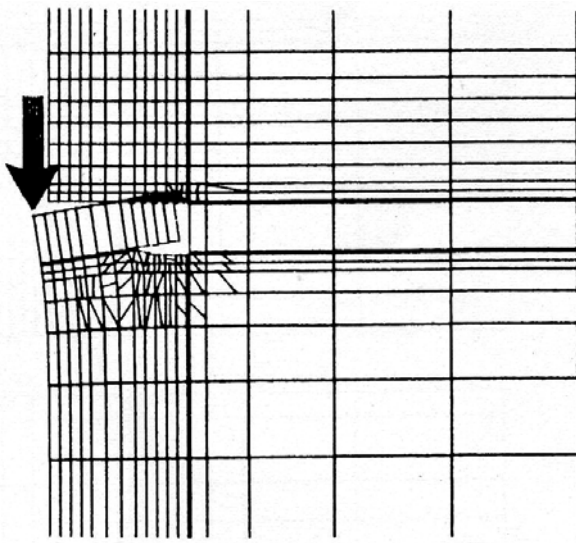


Figure 3.2: Crack pattern for $h_{ef}/d=3$ (Fuchs 1992)

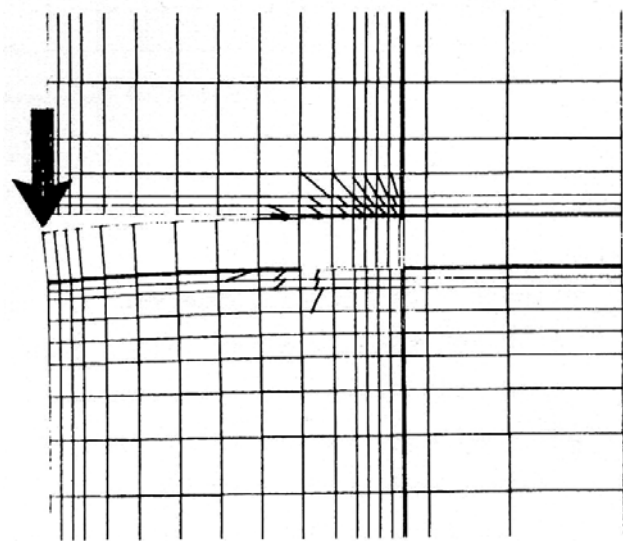


Figure 3.3: Crack pattern for $h_{ef}/d = 7$ (Fuchs 1992)

In the following figure the stress trajectories are shown for different ratios h_{ef}/d . A variation of the embedment depth has almost no influence on the stress distribution close to the loading point. Only the zero stress line changes with increase h_{ef}/d (the dot and dash line marks $h_{ef}/d = 7$). As already mentioned the stress distribution close to the concrete surface is akin to a cut through a shell.

An anchor loaded in shear suffers also bending deformations which induce a tensile force F_z in the fastener. This force increases rapidly for small shear loads and remains almost constant when 50% of the ultimate shear load is reached. The influence of the embedment depth is small at low shear loads and negligible at higher shear loads.

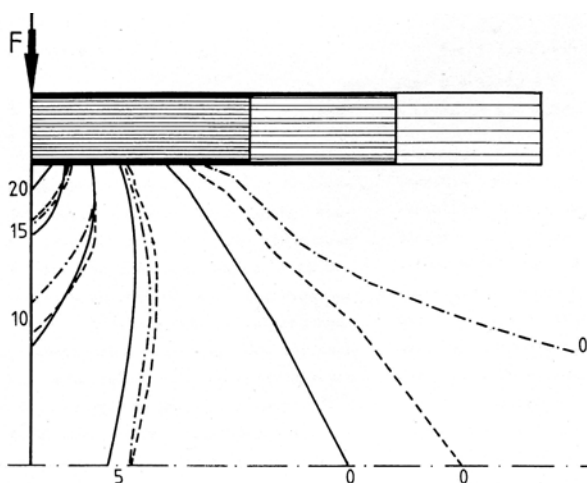


Figure 3.4: Stress trajectories (Fuchs 1992)

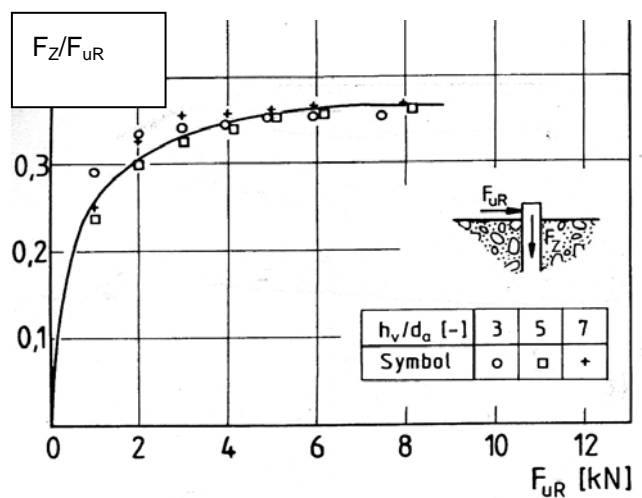


Figure 3.5: Tension vs. shear load (Fuchs 1992)

3.2.2.3 Geometrical models

Vintzéleou (1987) assumes a rectangular stress distribution between concrete surface and formation of a plastic hinge in the anchor bolt which takes place in a depth equal to $2.5 \cdot d$. On the base of a maximum concrete resistance of $5 \cdot f_c$ and equilibrium of moments following equation for the critical load F_{uR} and small eccentricity e is derived:

$$F_{uR} = \sqrt{\frac{(10 \cdot f_c \cdot e \cdot d)^2}{4} + 1.7 \cdot d^4 \cdot f_c \cdot f_y} - 10 \cdot f_c \cdot e \cdot d / 2 \quad (3.8)$$

With

f_y yielding of steel [N/mm²]

A similar equation derived by *Rasmussen (1963)* is restricted to low values for steel yielding f_y and hence it is not applicable for typical anchor materials used nowadays.

On the base of numerical stress analysis *Fuchs (1992)* developed a model to predict the critical load F_{uR} . He assumes a rectangular and a triangular stress distribution in the cross section and a parabolic spread on the concrete surface with the maximum value $\max p$ equal to $3.5 \cdot f_c$ and the formation of a plastic hinge at $2d$ below the surface (see Figure 3.6). Equilibrium of moments yields:

$$0.17 \cdot d^3 \cdot f_y = F_{uR} \cdot (2 \cdot d + e) - 1.26 \cdot \max p \cdot d^3 \quad (3.9)$$

And with $\max p = 3.5 \cdot f_c$

$$F_{uR} = \frac{d^3}{2 \cdot d + e} \cdot (0.17 \cdot f_y + 4.5 \cdot f_c) [N] \quad (3.10)$$

According to the results of the numerical analysis this formula is valid for $h_{ef}/d \geq 5$ and for anchors with constant stiffness over the whole length.

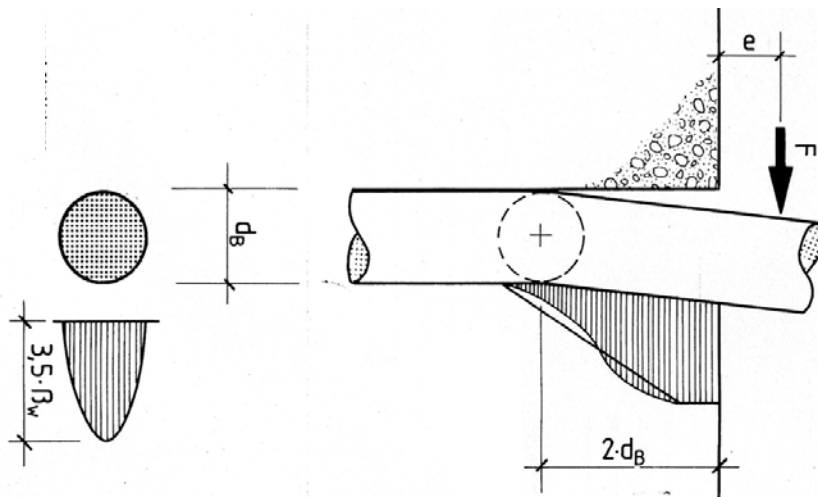


Figure 3.6: Idealized distribution of stresses (*Fuchs 1992*)

Characteristic resistance in case of steel failure is calculated by the following formula (Fuchs 1992):

$$V_{Rk,s} = 0.5 \cdot A_s \cdot f_{uk} \quad [N] \quad (3.11)$$

With

$V_{Rk,s}$ Characteristic resistance for steel failure [N]

A_s cross section of anchor bolt [mm²]

f_{uk} Ultimate strength of steel [N/mm²]

Therefore the load for local concrete failure according to equation (3.10) is only 40% compared to the steel failure load.

Hofmann (2004) investigated the influence of the boundary condition at the loading point on the stress distribution in the concrete. If the anchor is rigidly restrained at the loading point the stresses in the concrete decrease and the ultimate load increases dependent on the stiffness h_{ef}/d as shown in Figure 3.7. Experimental results lie between the extreme situations rigid restraint and no restraint.

Hofmann (2004) evaluated the stress in the concrete in front of the anchor at ultimate shear load for various anchor sizes assuming a stressed area equal to d^2 . The large scatter of test data reflects the local inhomogeneity due to aggregates but also the experimental uncertainty in determining the load F_{UR} when the concrete crushes. The maximum stress reaches up to 180 N/mm².

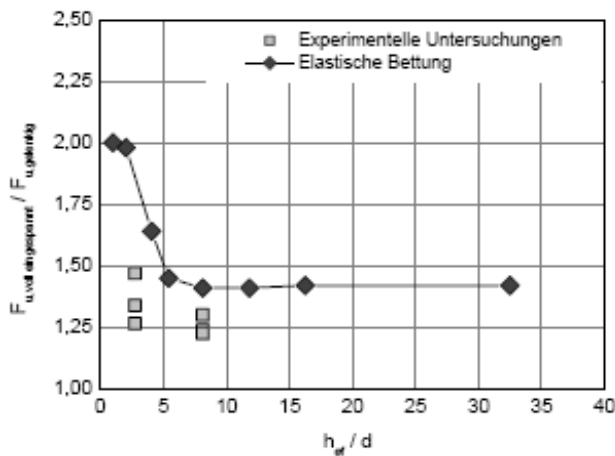


Figure 3.7: Theoretical and experimental ultimate load for different anchor stiffness and boundary condition (Hofmann 2004)

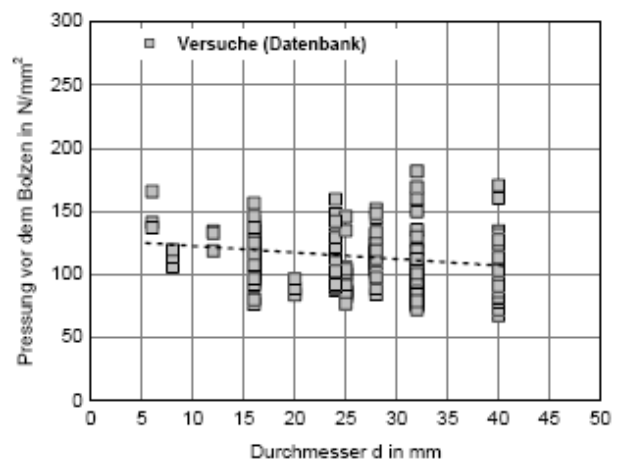


Figure 3.8: Maximum concrete stress (Hofmann 2004)

Unterweger (2008) developed a geometrical model for groups of anchors subjected to shear load close to the free edge taking into account a hole clearance between anchor and base plate. Thus, after (unfavourable) failure of the anchors close to the edge the resistance of the residual anchors is reduced.

3.2.3 Ductility

3.2.3.1 General

Since seismic design of anchors is performed by means of a static horizontal load, the elastic load can be reduced in dependence of the ductility. Within *CEN/TS (2004)* this reduction is described by the behavior factor q_a which varies between 1.0 and 2.0 dependent on type of nonstructural element fixed to the main structure. Hence, it is assumed that post-installed anchors exhibit limited ductility. No provision is made whether the behavior factor q_a depends upon type of anchor.

The ductility μ of an anchor under shear load can be defined as following:

$$\mu = \frac{\Delta_u}{\Delta_y} \quad (3.12)$$

With

- μ Ductility factor [-]
- Δ_u Displacement at ultimate load [mm]
- Δ_y Displacement at first nonlinearity [mm]

Taking into account the principle of the same energy of deformation of a linear-elastic and an elastic-plastic material the elastic force is reduced by the factor α_μ (*Bachmann 1995*):

$$\alpha_\mu = \frac{1}{\sqrt{2\mu - 1}} \quad (3.13)$$

The reduction factor α_μ is equivalent to $1/q_a$ defined in *CEN/TS (2004)*. Equation (3.13) is valid in the medium frequency range between 2 and 10 Hz which is typical for seismic waves in stiff and moderate stiff soils. For lower frequencies α_μ is slightly reduced, whereas in the high frequency regime (> 33 Hz) the material has no time to develop plastic deformations and therefore α_μ gets equal to 1 (*Bachmann 1995*).

3.2.3.2 Influence of concrete stress

Since the displacement at ultimate load is similar for monotonic and cyclic loading (see chapter 4.2), monotonic shear tests performed in cracked concrete C20/25 (*Rieder 2003*) may be used for the following evaluation. By referring the ultimate shear loads to the area d^2 a measure for the maximum concrete stress can be determined. *Hofmann (2004)* adopted the same procedure in calculating the concrete stress in front of the anchor. In the case of bolt type anchors d means the diameter of the bolt and for sleeve type anchors it describes the diameter of the sleeve. The anchor parameters are listed in Table 3.1. For the sleeve anchor a pre-setting variant is used, i.e. the sleeve does not penetrate the base plate. In Figure 3.9 the results of expansion anchors (bolt type M8 – M24) and undercut anchors (sleeve type M6 – M16) are plotted versus the maximum concrete stress. A significant increase of the

ductility factor μ occurs at approximately 200 N/mm² and the reduction factor α_{μ} decreases correspondingly. The enhanced plastic deformation capacity is observed only for the small and medium sizes M8 – M16 of the bolt type anchor whereas the size M16 marks the transition zone.

Table 3.1: Anchor properties

Type	Sleeve anchor						Bolt anchor						
Material	unalloyed					A4	unalloyed						A4
Thread	M6	M8	M10	M12	M16	M12	M8	M10	M12	M16	M20	M24	M12
d [mm]	10	12	14	18	22	18	8	10	12	16	20	24	12
f_{uk} [Mpa]	800					700	700				600	540	625
ϵ_u [%]	~ 15					37	~ 15						23

As already shown in Figure 3.8 the maximum stress corresponding to concrete crushing takes place at 180 N/mm². Therefore the enhanced ductility beyond 200 N/mm² might be interpreted as extended concrete damage. For concrete stresses below 200 N/mm² the source for plastic deformation stems partly from the anchor steel material and partly from the concrete. The exact distribution cannot be determined from these tests.

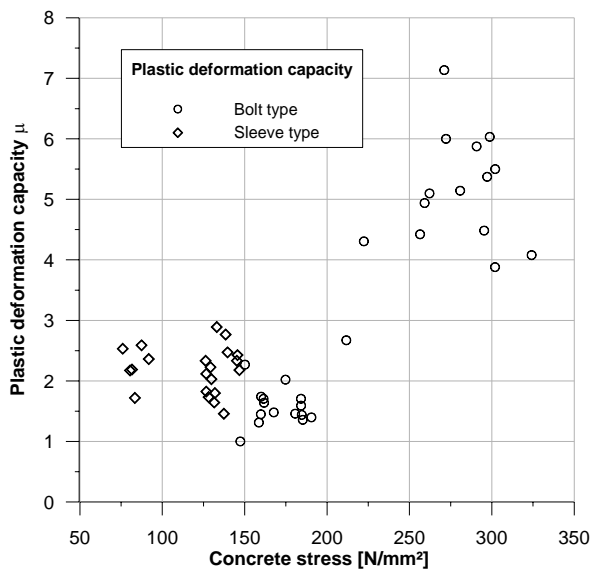


Figure 3.9: Plastic deformation capacity vs. maximum concrete stress (Rieder 2003)

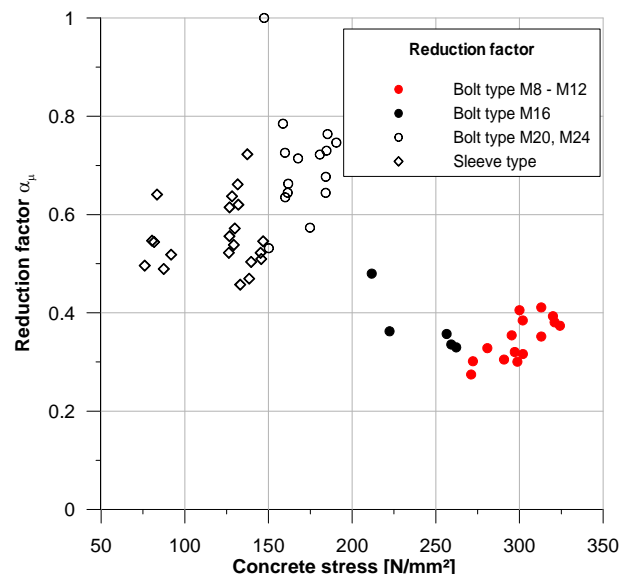


Figure 3.10: Reduction factor vs. maximum concrete stress (Rieder 2003)

3.2.3.3 Influence of anchor material

In order to study the effect of a more ductile anchor material tests with bolt and sleeve anchors M12 made of stainless steel (A4) are considered in the evaluation. As shown in the following figures for the bolt anchor practically no influence and for the sleeve anchor only a very small increase of plastic deformation capacity respectively decrease of α_{μ} can be observed. These results indicate that the main source for plastic deformations is due to the concrete where a much larger volume compared to the steel bolt is activated for the formation of micro- and macro-cracks.

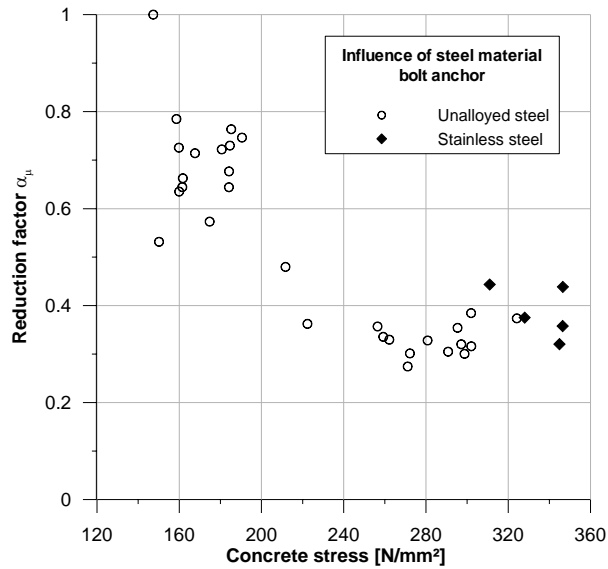


Figure 3.11: Influence of steel material, bolt anchor (Rieder 2003)

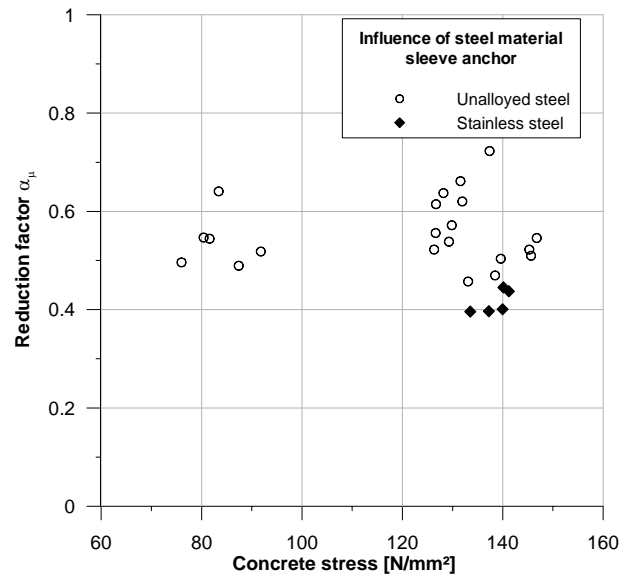


Figure 3.12: Influence of steel material, sleeve anchor (Rieder 2003)

According to Figure 3.13 and Figure 3.14 the reduction factor can be evaluated separately for anchors with low and higher plastic deformation capacity. In both cases the distribution is well approximated by a Gauss curve. The corresponding statistical evaluation is summarized assuming a confidence level of 90% and unknown standard deviation. It is valid for cracked concrete C20/25 and anchor material (ultimate) strength between 600 and 800 N/mm². For higher steel strength or for through-setting sleeve anchor variants the values given in Table 3.2 are more conservative.

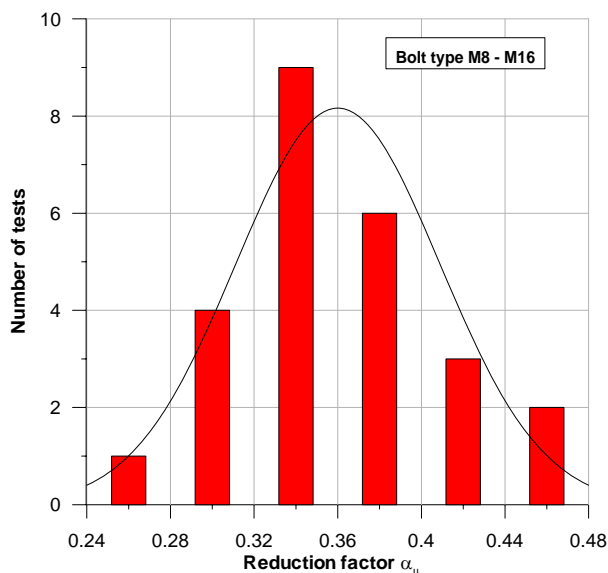


Figure 3.13: Distribution of α_{μ} for bolt type M8 – M16

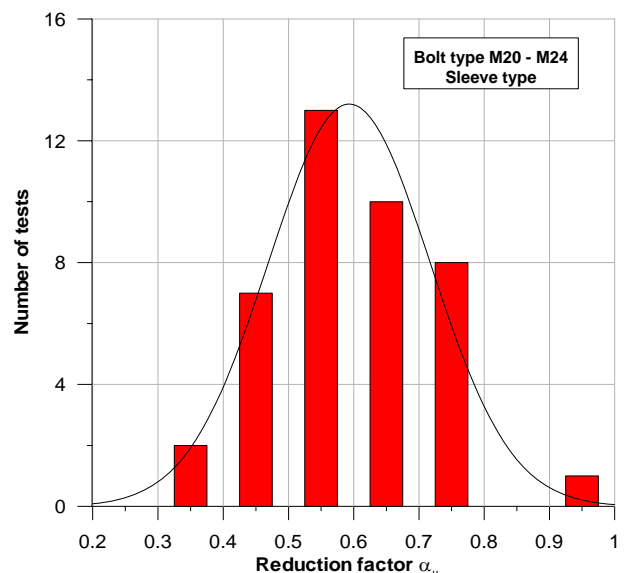


Figure 3.14: Distribution of α_{μ} for bolt type M20 – M24 and sleeve type

Assuming a similar behavior for cyclic loading, on the base of this evaluation it seems more efficient to relate the behaviour factor q_a to the type of anchor rather than to the type of non-structural element as proposed in *CEN/TS (2004)*. A proposal is given in the last column of Table 3.2. The properties of the non-structural element itself may be considered by the importance factor γ_a . For non-structural elements

deemed of high importance *CEN/TS (2004)* prescribes $\gamma_a = 1.5$ and $\gamma_a = 1.0$ otherwise. Thus, additional importance classes in compliance with *Eurocode 8 (2003)* may be defined.

In order to get a comprehensive understanding of the behaviour factor, for future research a similar procedure is necessary concerning axial loading for various post-installed anchors and failure modes.

Table 3.2: Anchor type dependent behavior factor for shear load and steel failure

Anchor	Mean α_{μ}	St. dev. α_{μ}	COV [%]	n	k- factor ¹⁾	95%- fractile	$q_a =$ $1/\alpha_{\mu}$	Proposed q_a
Bolt type M8 – M16	0.36	0.05	14	25	2.15	0.47	2.1	2
Bolt type M20, M24 Sleeve type M6 – M16	0.59	0.12	21	41	2.0	0.84	1.2	1

¹⁾ according to *Owen (1963)*

3.3 Cyclic loading

3.3.1 General

In contrast to monotonic loading, little research has been done on post-installed anchors using a reversed cyclic loading scheme, although cyclic loading provides important information about energy absorption through plastic deformations and damping properties, which is essential when analyzing seismic performance. A reason for this lack could be the common design philosophy that the primary objective of ductile element requirements is load redistribution, not energy dissipation or accommodation of imposed displacements (*Silva 2007*). However, regarding a major task of this thesis consisting in the development of a damper for mitigation of seismic action, it is essential to have a closer look on the inherent dissipative mechanisms by analyzing the cyclic behavior of fasteners.

Excitation loads that produce inelastic deformations associated with dissipation of energy, generate a load-displacement response which is referred to as hysteresis. Fasteners under shear load exhibit pinched load-slip hysteresis loops due to a progressive degradation of lateral stiffness for each successive loading cycle (Figure 3.15). The displacement increases between two successive cycles at the same load level. Cyclic stiffness degradation is a result of the fastener crushing the concrete surrounding it at each progressive load phase beyond the elastic limit. A cavity is formed around the bolt, leaving the anchor unsupported during successive cycles until the displacement increases and the fastener again becomes supported by the previously crushed concrete. But, until the shank contacts the crushed concrete, only bending resistance of the bolt shank within the cavity and friction counteracts the external force. This is reflected in the pinched part of the hysteresis loops. As displacements increases, more concrete crushes around the bolt and the cavity enlarges. The part where the external force is resisted by bolt bending increases and consequently the pinched sections of the hysteresis loops become longer and the moment increases (Figure 3.16).

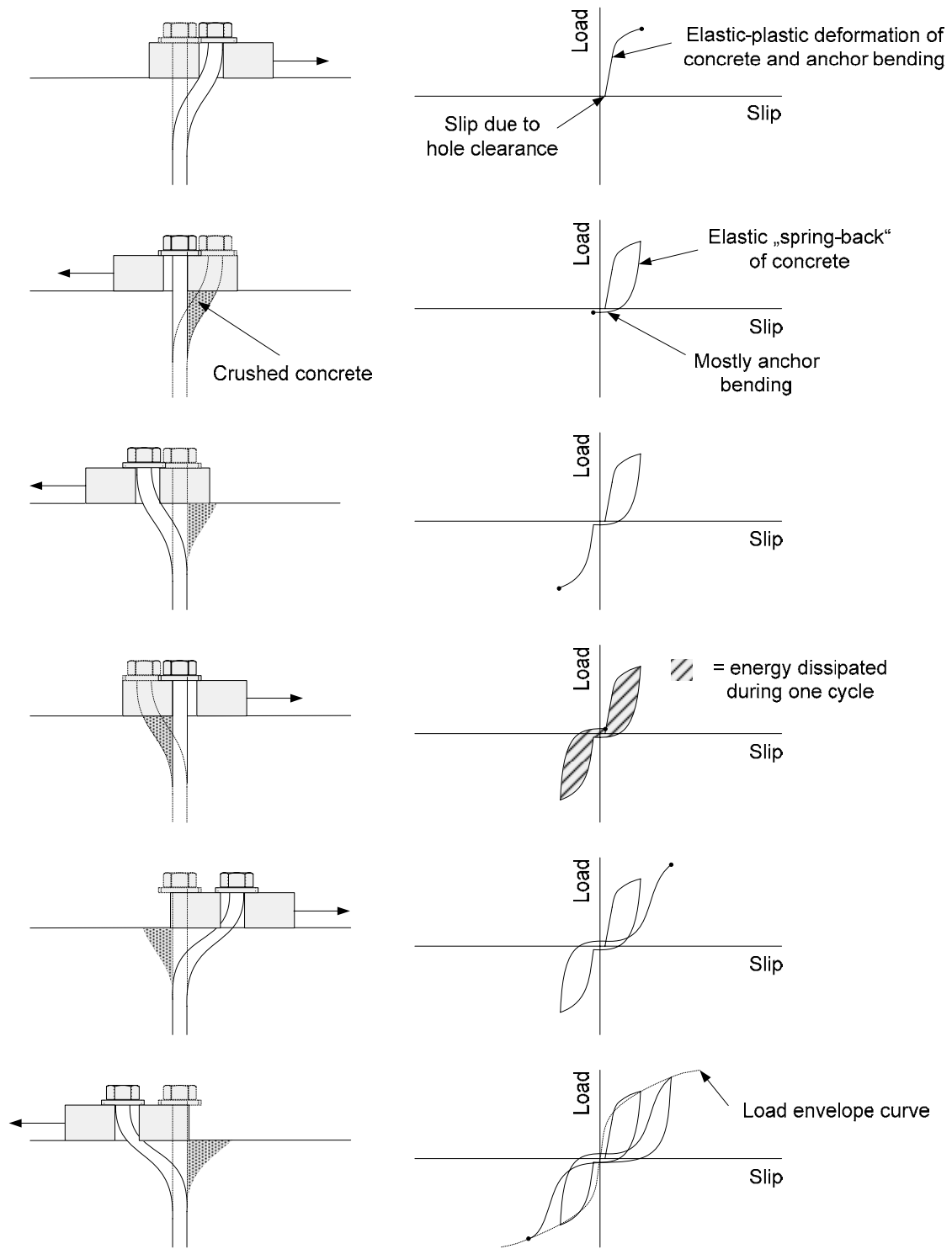


Figure 3.15: Hysteretic performance of an anchor in shear stressed beyond the elastic limit. Left side shows anchor at various deformation states, corresponding load-slip curves are depicted on the right

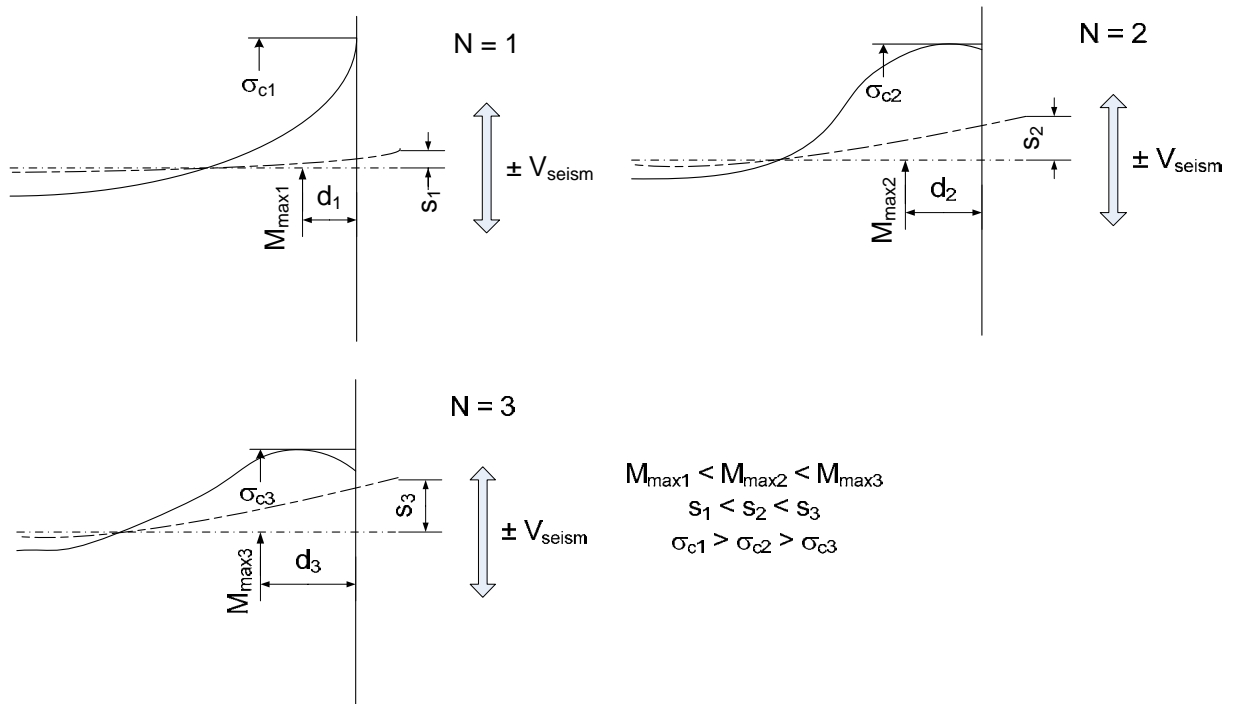


Figure 3.16: Qualitative evolution of maximum moment, displacement and concrete stress during a load controlled cyclic shear test

3.3.2 Stiffness and strength

Vintzéleou (1991) investigated the stiffness degradation dependent on number of cycles for undercut anchors, expansion anchors and bonded anchors with and without influence of a free edge. For this purpose displacement controlled cyclic tests in cracked concrete C20/25 were performed. In the following only the test results without influence of a free edge are summarized. Figure 3.17 shows the force degradation (V_n/V_1) in the nth cycle as a function of the number of cycles. Since no failure occurred during the load cycling, the authors concluded that the stiffness degradation was due to the local deterioration of the concrete on the loaded side of the anchor.

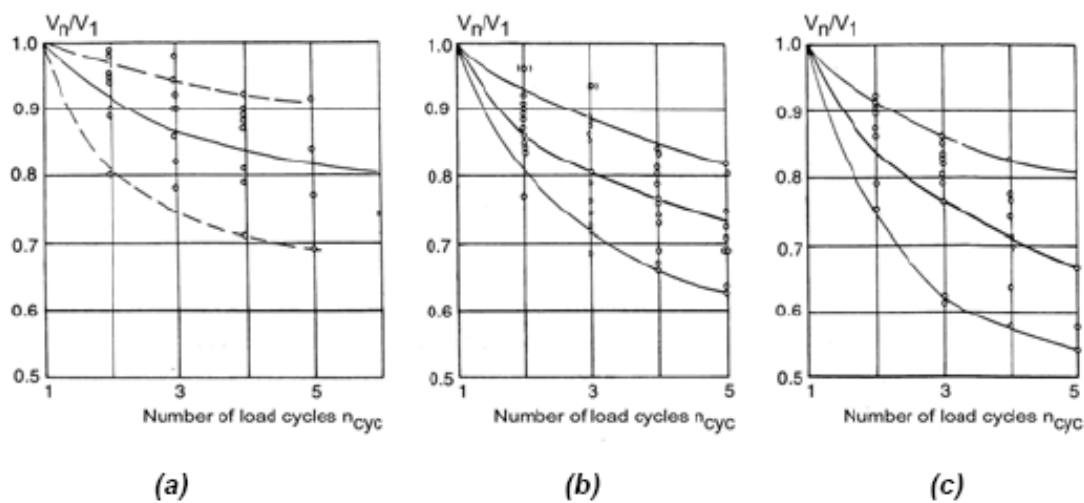


Figure 3.17: Stiffness degradation under cyclic shear loading for different anchors: a) undercut anchor, b) expansion anchor (sleeve type), c) bonded anchor (Vintzéleou 1991)

Although the scatter of the measured V_n/V_1 values was quite large, the following empirical equation was given to estimate the expected force response during the n th displacement reversal ($n < 10$):

$$V_n = V_1 \cdot [1 - a(n-1)^{0.5}] \quad (3.14)$$

With

- a = 0.11 for undercut anchors
- = 0.13 for expansion anchors
- = 0.17 for bonded anchors

Vintzéléou (1991) reached the following conclusions:

- All of the investigated anchors behaved similarly under monotonic and cyclic shear loading in spite of the fact that their behavior under tension loading is rather different, especially in cracked concrete.
- The load-displacement curve after ultimate load was almost vertical. Therefore, reliable cycling behavior can only be obtained for imposed displacements smaller than the value corresponding to ultimate load under monotonic loading Δ_u .
- Stiffness degradation was pronounced for all investigated anchor types during symmetric alternating shear cycling between displacement values $\Delta_{\max} \leq 0.75 \cdot \Delta_u$. Torque-controlled expansion anchors and especially bonded anchors seemed to be more sensitive to the cyclic actions than the undercut anchors.
- For displacement values larger than the maximum value during cycling, the monotonic envelope was reached and then followed. Alternating cyclic displacement for $\Delta_{\max} \leq 0.75 \cdot \Delta_u$ therefore has no significant influence on the shear capacity and the displacement at peak load. This is valid for steel failure when low-cycle fatigue does not occur.

Usami (1980) performed cyclic shear tests on groups of headed studs ($d = 19$ mm; $f_u = 480$ MPa) cast in uncracked concrete C20/25 with large edge distances. The embedment depth ($h_{ef} = 5.3 \cdot d$ and $8.4 \cdot d$), the number of anchors ($n = 2$ and 4) and the anchor spacing (150 and 200 mm) were varied, as was the type of loading (pulsating and alternating shear loading). Specimens with both one and two shear planes were tested. The results can be summarized as follows:

- Failure was generally caused by fracture of the anchor steel during cycling (low-cycle fatigue).
- The failure load obtained with the two-plane specimen was significantly higher than that obtained with the one-plane specimen under the same conditions. The conditions in practice are better represented by the one-plane specimen,
- The displacement under pulsating shear loading at failure (~ 45 mm) was much larger than under alternating shear (~ 15 mm) (Figure 3.18).
- With alternating shear loading the shear strength was only about 70% to 80% of the value for pulsating loading (Figure 3.18). In two of the three tests used to determine these values, a change of failure mode from concrete breakout (pulsating shear) to steel failure (alternate

shear) occurred. Monotonic reference tests to determine the influence of the pulsating shear loads were not reported.

- During alternating shear loading, considerable pinching and degradation of the force response was observed.

The similar displacement at failure for monotonic and reversed cyclic shear loading as observed for single anchors (see chapter 4.2) is therefore not confirmed for groups of anchors. Load redistribution effects might be responsible for this effect. However, additional research is necessary to clarify this issue.

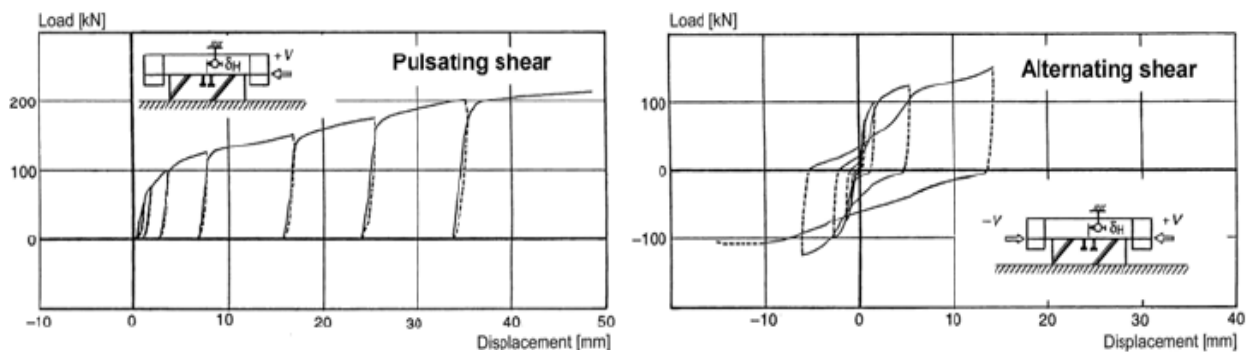


Figure 3.18: Cyclic shear tests with a group of anchors (*Usami 1980*)

Klingner (1982) found that under alternating cyclic shear loading, bolts typically failed at loads approximately 50% lower than those resisted by monotonically loaded bolts owing to the effects of low-cycle fatigue.

3.3.3 Combined axial and shear loading

A general design model for combined static axial and shear loading has the following form (*EOTA 1997*):

$$\left(\frac{N_{Sd}}{N_{Rd}}\right)^{\alpha} + \left(\frac{V_{Sd}}{V_{Rd}}\right)^{\alpha} \leq 1.0 \quad (3.15)$$

With

N_{Sd} (N_{Rd}) Design action (design resistance) for tension [kN]

V_{Sd} (V_{Rd}) Design action (design resistance) for shear [kN]

α = 2.0 if steel failure governs

= 1.5 for other failure modes

In the literature numerous tests with combined cyclic axial and shear loading are reported. However, due to the different parameters (e.g. crack width, number of cycles) the results are not directly comparable. This is illustrated in the following examples.

Meszaros (1994) subjected displacement-controlled expansion anchors M12 and bonded anchors M12 located in cracked concrete $w = 0.3$ mm C20/25 to constant tension load N and simultaneously to alternating cyclic shear load V . Approximately 1000 shear load cycles were performed at service load levels. The ratio between N and V was varied to obtain different resultant load inclination angles. If no failure occurred during load cycling, the fasteners were tested monotonically to failure with the respective load inclination angle. On the base of the ultimate strengths obtained from the subsequent anchor pullout tests *Meszaros (1994)* concluded that:

- A constant axial load in combination with an alternating shear load may negatively influence fastener behavior.
- The ultimate strength of the displacement-controlled expansion anchors that did not fail during the load cycling was not affected by the inclined load cycling.
- The bonded anchors did not fail during load cycling. During the subsequent tests to failure, rupture of the steel was observed. The ultimate load was slightly lower than that for comparable anchors without previous load cycling.

Mesureur (2004) used torque-controlled expansion anchors (sleeve and bolt type), undercut anchors and bonded anchors located far from edges in cracked concrete ($w = 0.5$ mm) were subjected to a constant tension or shear load and simultaneously to cycled load in the orthogonal direction, i.e. in shear or tension, respectively, to investigate cyclic interaction up to failure. The load cycles were applied using a stepwise-increasing pattern with 10 cycles per step resulting in 70 – 80 cycles to failure for cyclic shear loading and 100 – 140 cycles to failure for cyclic tension loading. The ratio of the magnitude of the tension and shear loads was kept constant throughout the test, i.e. as the cyclic load increased, the constant load in the orthogonal direction increased proportionally.

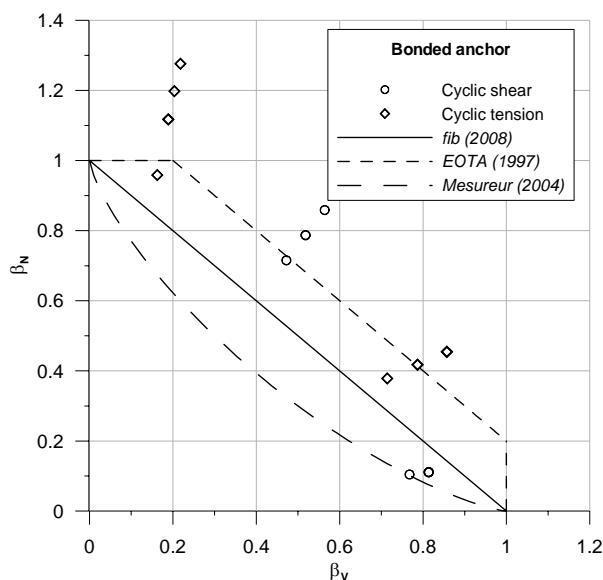


Figure 3.19: Interaction bonded anchor

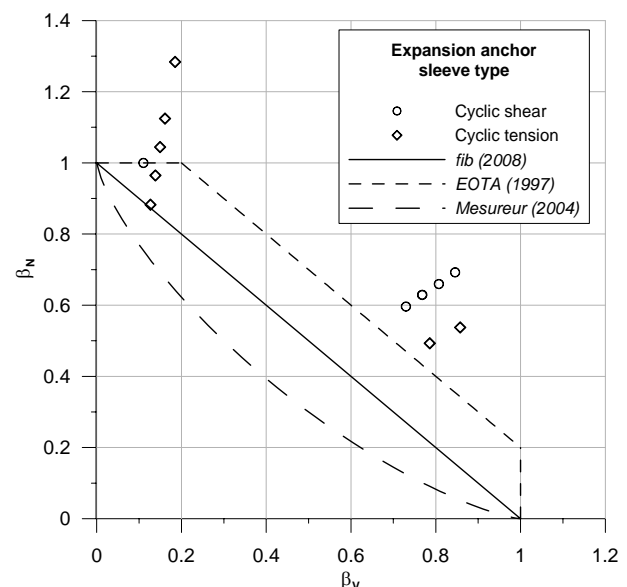


Figure 3.20: Interaction sleeve expansion anchor

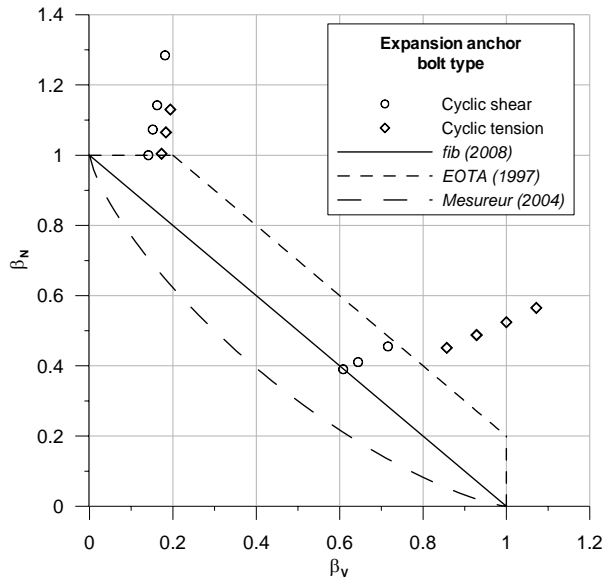


Figure 3.21: Interaction bolt anchor

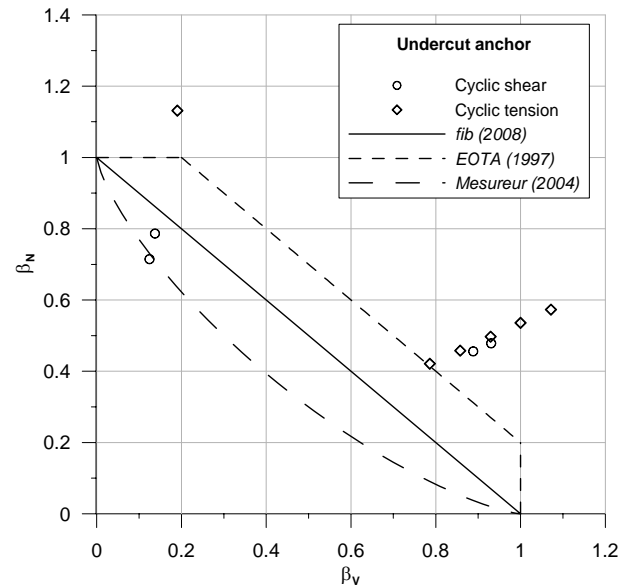


Figure 3.22: Interaction undercut anchor

The test results shown in Figure 3.19 to Figure 3.22 indicate that in many cases a quadratic interaction might be unconservative. An exponent $\alpha = 0.75$ or at least a linear interaction is recommended for seismic applications. Both proposals are plotted in the diagrams. Also in *CEN/TS (2004)* a linear interaction is proposed.

It should be noted that the testing conditions applied by *Mesureur (2004)* with approximately 100 cycles seem to be more representative for seismic loading than the 1000 cycles imposed by *Meszaros (1994)*. The interaction diagram used for static design definitively represents an unconservative approach.

3.4 Summary

Various models attempting to predict the shear load where concrete damage occurs are presented. Loading beyond this level leads to plastic deformations whose main source is due to concrete crushing where a much larger volume compared to the steel bolt is activated for the formation of micro- and macro-cracks. The influence of a more ductile anchor material (e.g. stainless steel) is negligible. Since the plastic deformation capacity under shear loads for steel failure depends upon type and diameter of anchor, it is more efficient to relate the behaviour factor q_a to the type of fastener rather than to the type of non-structural element as proposed in *CEN/TS (2004)*. A proposal is given for various anchor types and diameters under seismic shear loading. In future research case a similar procedure for axial loading and various failure modes (steel failure, pull-through, pull-out) may be established.

4 Experimental simulation of seismic action

4.1 General

Experimentation has been a cornerstone to the advancement of our knowledge of the behaviour of post-installed anchors for use in concrete (*Eligehausen 2000*). Simulation integrated with experimentation has provided researchers with the ability to extend those experimental results to a broad range of applications (*Ozbolt 2005*). Nevertheless, the suitability and the admissible service conditions have to be checked within numerous test series for new products in order to guarantee the admissible probability of failure during service life. The qualification is given in Technical Approvals released by public Approval bodies (e.g. members of EOTA in Europe, ICC in USA) which facilitate the free trade and use within a specific region.

Unfortunately this is not true for the qualification of post-installed anchors to be used in seismic regions, a fact which might reflect the lack of research available nowadays. Since the testing guideline in accordance with *ACI 355.2 (2004)* does not take into account cycling cracks it seems that the conditions in a real reinforced concrete structure are not captured properly. On the other hand, full scale shake table tests show that the number of load cycles applied on the anchor is not representative for a typical seismic event (*Hoehler 2007*). Within the EOTA currently new testing guidelines for the seismic qualification of post-installed anchors are prepared which should consider these issues.

Basically, three different testing methods simulating seismic action are possible: cyclic quasi-static testing, pseudo-dynamic testing and shake table testing. The first is characterized by load or displacement controlled typically sinusoidal input with a specific amplitude and frequency. Such tests are easy and useful in determining the hysteretic damping of a specific component. By variation of the frequency within the velocity limit of the actuator potential viscous and hence velocity dependent damping may be identified. Since the velocity limit of standard actuators is very low (typically in the range between 50 and 100 mm/s), the resulting frequency lies in the magnitude of 1 Hz. The advantage is the simple test procedure which can be reproduced by means of a servo-hydraulic actuator with a closed loop control. As already addressed in the previous paragraph the crucial issue consists in determining a proper sequence of cycles representative for an earthquake event.

In pseudo-dynamic testing the structure is idealized as a lumped mass system with an effective stiffness or a bilinear stiffness on which the deformations are imposed via an actuator solving the equation of motion for a specific time history and assumed damping forces. To the knowledge of the author the only available pseudo-dynamic tests with post-installed anchors are reported in *Zhang (2001)*. The advantage of this test procedure consists in simulating quite realistic seismic conditions; disadvantages are the high sophisticated control algorithm and the high demand on velocity of the hydraulic system. Furthermore, for specific components an effective or bilinear stiffness might not be representative.

In a shake table test a model is fixed to a platform and subjected to a specific ground acceleration history. Due to capacity limitations of most shake tables, test structures are typically reduced scaled models, a fact which has to be considered in detailing the test specimen. For the tests performed within this thesis no scaling effects have to be dealt with since anchors exhibiting full size are used. Seismic ground motion occurs simultaneously in all directions in a random fashion. According to *ICBO (2000)*

uniaxial, biaxial or triaxial tests are allowed. If a uniaxial test is performed, the test shall be performed in three steps, with the specimen rotated after each step, such that all three principal axes of the specimen have been tested. In the case of a biaxial test the specimen shall be rotated 90 degrees about the vertical axis for the second step. Triaxial tests represent the most realistic input motion, but at the same time they can be considered as the most cost consuming one. As a main output shake table testing yields basic information regarding amplification and damping forces which enable the formulation and calibration of suitable damping models for extended numeric simulation. The high costs usually are the main limiting factor when dealing with shake table testing.

Within this thesis a combination of different testing methods is chosen in order to get a more comprehensive understanding of the seismic behaviour of post-installed anchors in concrete. An overview of the test program with the corresponding methods, parameter and purpose is given in the following chart. The link to the numerical simulations will be presented in chapter 5.

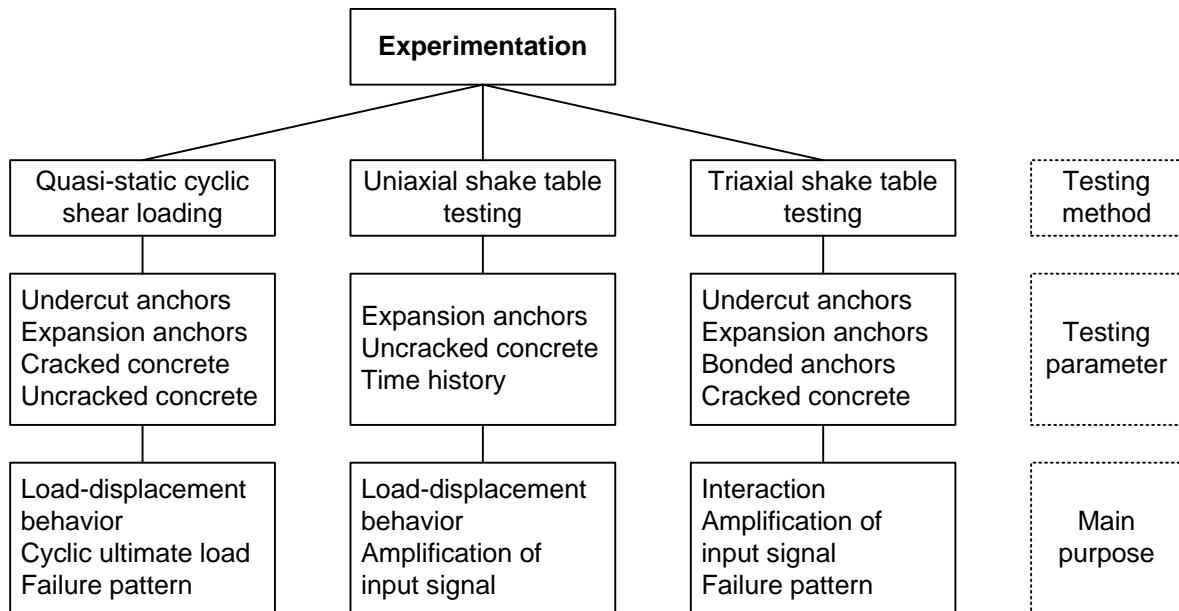


Figure 4.1: Experimental testing program

4.2 Quasi-static cyclic shear loading

4.2.1 General

Cyclic shear tests can be used for the determination of the equivalent viscous damping of a post-installed anchor. In equation (4.1), the area within the inelastic force-displacement response curve, E_D , is a measure of the hysteretic damping or energy dissipation capacity of the member, and E_S depicts the recoverable elastic strain energy stored in an equivalent linear elastic system. The hysteretic damping in terms of equivalent viscous damping ξ_{eq} can be expressed according to *fib (2003)*:

$$\xi_{eq} = \frac{1}{4\pi} \cdot \frac{E_D}{E_S} \quad (4.1)$$

Where E_D corresponds to the area in the shaded parallelogram of Figure 4.2:

$$E_D = 4 \cdot (S_{ay} \cdot S_{dm} - S_{am} \cdot S_{dy}) \quad (4.2)$$

And E_S corresponds to the area of the shaded triangle in Figure 4.2:

$$E_S = \frac{1}{2} \cdot (S_{am} \cdot S_{dm}) \quad (4.3)$$

K_{initial} means the stiffness during the first cycle before yielding and K_{eff} denominates the effective stiffness at peak load after yielding (see Figure 4.2). Since the load-displacement behaviour of anchors under cyclic shear loading cannot be described by a simple bilinear curve, the values for E_D are calculated numerically from the experimental data. E_S is taken as the average between positive and negative strain energy.

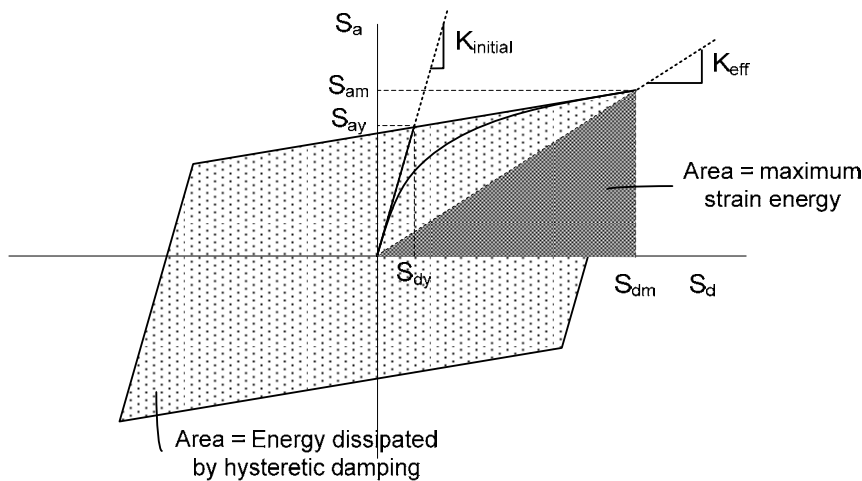


Figure 4.2: Energy dissipated (after *fib* 2003)

Finally, the effective damping ξ_{eff} is viewed as a combination of inherent damping ξ_{inh} and hysteretic damping from equation (4.1):

$$\xi_{\text{eff}} = \xi_{\text{inh}} + \lambda \cdot \xi_{\text{eq}} \quad (4.4)$$

where λ is a modification factor to account for the approximation involved in describing the hysteretic response of the system by a bilinear representation. It ranges from 0.3 for systems with poor and unreliable hysteretic behaviour, to a value of 1.0 for well-detailed elements with stable hysteresis loops. ξ_{inh} can be interpreted as inherent damping in the system from sources different from inelastic response (e.g. friction, ambient air, etc.). For many systems (e.g. reinforced concrete structures, wood structures) this value is based on experience, for specific systems it has to be assumed.

It should be noted that equation (4.1) is derived for steady state response under harmonic excitation, and at resonance condition. Therefore the validity of equation (4.1) for random excitations like

earthquakes is limited. However, it can be used as a base for the assessment of the dissipative mechanism of fasteners with and without any additional damping devices. This will be discussed in the next chapters.

4.2.2 Increasing amplitude

4.2.2.1 Influence of anchor type

According to the issues discussed in chapter 3 the most critical case is represented by cyclic shear loading with alternating sign. However, all available tests focus on ultimate load during cyclic loading and no evaluation and/or assessment about hysteretic damping and potential influencing factors is provided. The latter seems to be of major interest for modelling and numeric simulation of the seismic behaviour of post-installed anchors in concrete. Therefore it is the aim of this chapter is to get data concerning hysteretic damping and stiffness starting at service load and stepwise increasing amplitude up to failure. This procedure enables the definition of a safety margin in case of seismic overloading and the corresponding hysteretic damping which limits the seismic induced accelerations and hence the seismic forces.

The initial amplitude V of the sine-shaped alternating shear load is determined by the static service load:

$$V = \frac{V_{Rk,S}}{\gamma_{Ms} \cdot \gamma_F} [kN] \quad (4.5)$$

with

$V_{Rk,S}$	characteristic resistance for steel failure under shear loads (taken from approval)
γ_{Ms}	partial safety factor for steel failure (taken from approval)
γ_F	partial safety factor for action = 1.4 (mean value of permanent and variable actions)

For the tests undercut anchors and expansion anchors of the bolt type both size M12 with an approval according to *EOTA (1997)* are used. The anchors are installed in uncracked concrete of the strength class C20/25 according to the manufacturer's installation instruction and after 10 minutes the torque moment is reduced to 50% of T_{inst} simulating the long-time loss of pre-stressing force (*Eligehausen 2000*). After 5 load-controlled cycles with a frequency of 0.1 Hz the amplitude is increased by 10% and 5 cycles are imposed again. This procedure is repeated keeping constant the load step until failure occurs (*Rieder 2003*).

Typical load-displacement diagrams for alternating and monotonic shear load are shown in the following figures for both types of anchors. Due to the hole clearance between anchor and fixture the axis of symmetry is shifted to the left side. A stable hysteretic performance can be observed up to 30kN for the undercut anchor respectively up to 20 kN for the expansion anchor. Up to this level the monotonic curve represents a good approximation of the envelop for cyclic loading. Further load increase leads to an abrupt enlargement of displacements and thus a decrease of stiffness and increased dissipated energy per cycle. Displacement at rupture is similar for cyclic and monotonic loading.

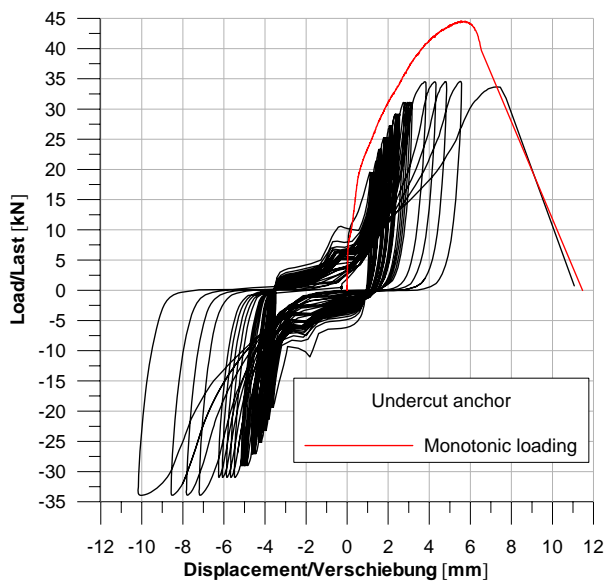


Figure 4.3: Cyclic and monotonic load-displacement of undercut anchor

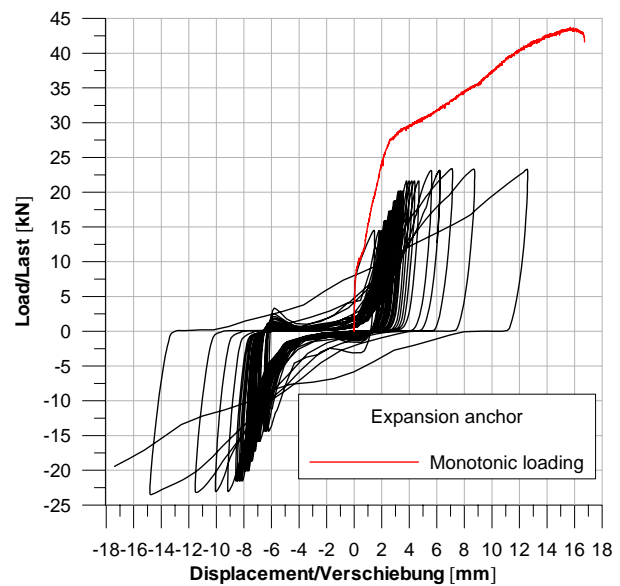


Figure 4.4: Cyclic and monotonic load-displacement of expansion anchor

For design purposes the ultimate load $V_{u,cycl}$ achieved in the cyclic tests may be an indication for the seismic performance of the specific anchor type. The undercut anchor reaches 82% of the static capacity $V_{u,m}$, whereas the expansion anchor exhibits only 54% of the ultimate load determined in monotonic tests. The explanation for this difference could be the cumulative spalling of concrete in front of the anchor in both loading directions due to the higher stress compared to the undercut anchor. The latter incorporates a sleeve between anchor rod and concrete and therefore local damage of concrete is prevented (except some minor crushing) and no additional bending moment arises (s. the following figures and Table 4.1). Steel failure of both expansion and undercut anchors occurs in the thread between base plate and concrete surface, whereas the fracture surface exhibits a very rough pattern similar to that observed in monotonic tests up to failure.



Figure 4.5: Damage pattern expansion anchor



Figure 4.6: Damage pattern undercut anchor

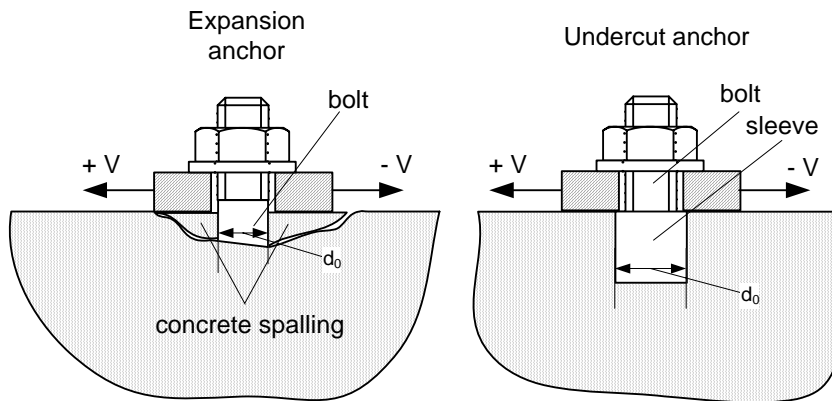


Figure 4.7: Anchor geometry dependent cumulative damage of concrete (Rieder 2004)

Table 4.1: Parameter and results for cyclic tests

Anchor	d_0 [mm]	T_{inst} [Nm]	$V_{u,m}$ [kN]	γ_{Ms}	V_{Rk} [kN]	V_{Rd} [kN]	V [kN]	$V_{u,cycl}$ [kN]	n	$V_{u,cycl}/V_{u,m}$	$V_{u,cycl}/V_{R,d}$	$M_{u,cycl}/M_{R,d}$
Undercut	18	60	42.5	1.25	33.8	27	19.3	34.8	39	0.82	1.29	-
Expansion	12	60	42.4	1.5	30	20	14.3	22.9	34	0.54	1.14	1.3

The hysteretic damping in terms of equivalent viscous damping determined in accordance with equation (4.1) and the stiffness are plotted in the next figures for the two anchor types as a function of the ultimate cyclic load $V_{u,cycl}$. In all the diagrams the average of three test replicates is taken. With increasing amplitude and number of cycles the damping diminishes continuously, which may be explained by the decreasing friction due to loss of pre-stressing force between base plate and concrete due to axial (plastic) slip of the anchors. In the load-displacement plots in Figure 4.10 and Figure 4.11 the decreasing damping can be clearly seen in terms of increased pinching.

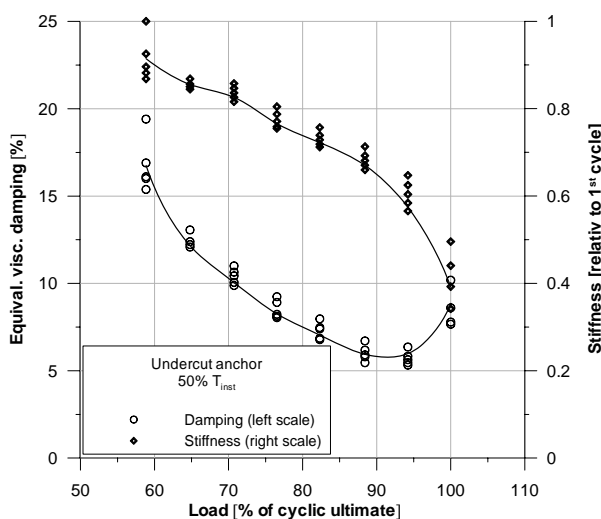


Figure 4.8: Damping & stiffness (undercut anch.)

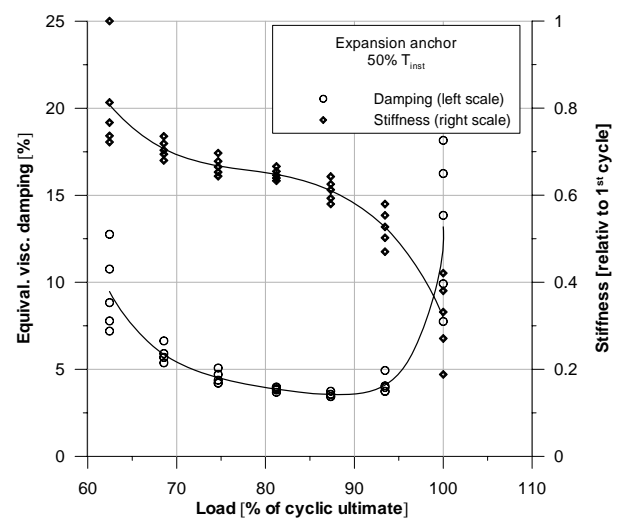


Figure 4.9: Damping & stiffness (expansion anch.)

The undercut anchor exhibits slightly increased hysteretic damping compared to the expansion anchor at low and medium amplitudes. Especially the decreasing rate of damping with increasing amplitude is less pronounced for the undercut anchor. This is shown in Figure 4.12 where the hysteretic damping is plotted versus the number of cycles. Since the applied torque moment is the same and the

corresponding pre-stressing forces do not differ significantly for the two anchor types according to *Bergmeister (1998, 2005)*, this effect could be explained by the higher axial stiffness of the undercut anchor which prevents axial displacement and thus a loss of pre-stressing force (s. also Figure 3.5). Just before rupture the damping increases rapidly which indicates damage of steel and/or concrete. The high value of the expansion anchor can be related to the pronounced concrete spalling discussed in the previous paragraph.

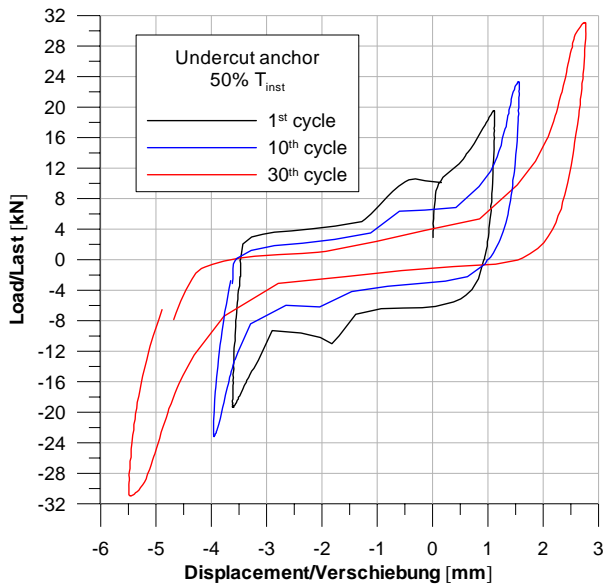


Figure 4.10: Load-displacement of undercut anchor at different cycles

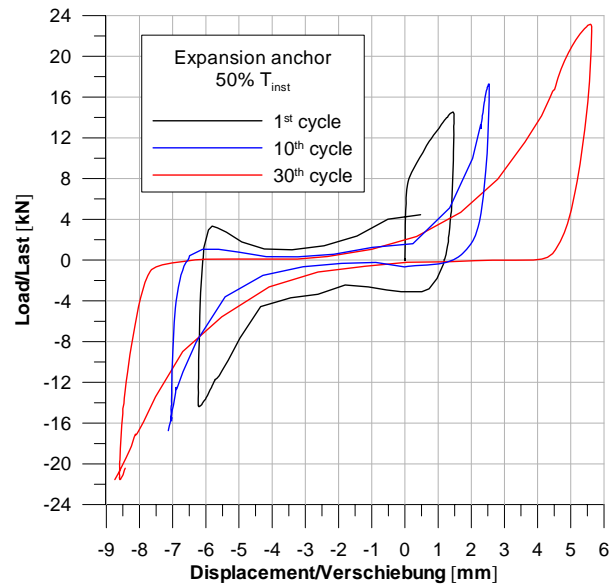


Figure 4.11: Load-displacement of expansion anchor at different cycles

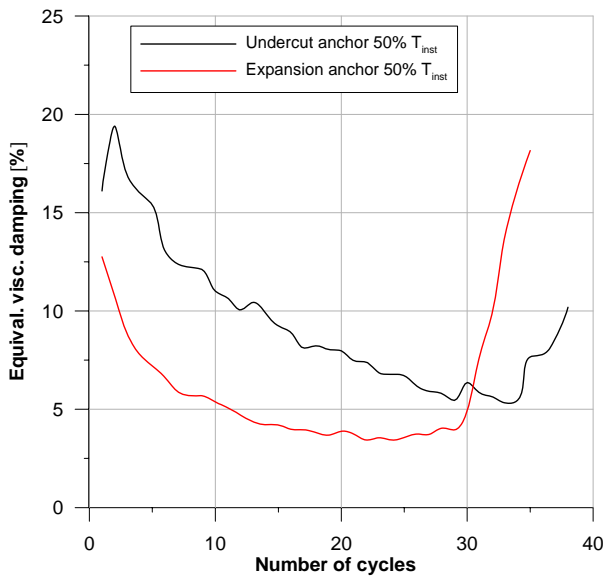


Figure 4.12: Comparison of damping undercut and expansion anchor

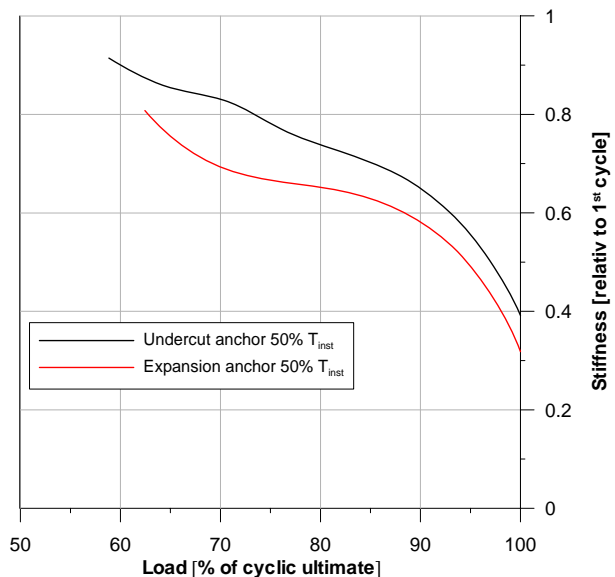


Figure 4.13: Comparison of stiffness undercut and expansion anchor

The more pronounced loss of stiffness of the expansion anchor during the first 5 cycles reported by *Vintzéleou (1991)* is confirmed by the tests. Stiffness of the anchors decreases almost linearly with increasing amplitude and number of cycles up to 90% of cyclic ultimate load. At this level about 60% of

the stiffness obtained during the first cycle is measured. Shortly before rupture the stiffness drops to 30 and 40% for the expansion respectively the undercut anchor.

4.2.2.2 Influence of friction and anchor material

In order to simulate to complete loss of pre-stressing force between base plate and concrete (which might be the case in cracked concrete) cyclic shear tests are performed with a torque moment reduced to zero after correct installation of the expansion anchor. Figure 4.14 indicates a pronounced reduction of hysteretic damping and increased pinching beginning already from the first cycle. Consequently, hysteretic damping is reduced at low and medium amplitudes compared to the tests performed with 50% of T_{inst} . Close to cyclic ultimate load the difference is negligible (s. Figure 4.18).

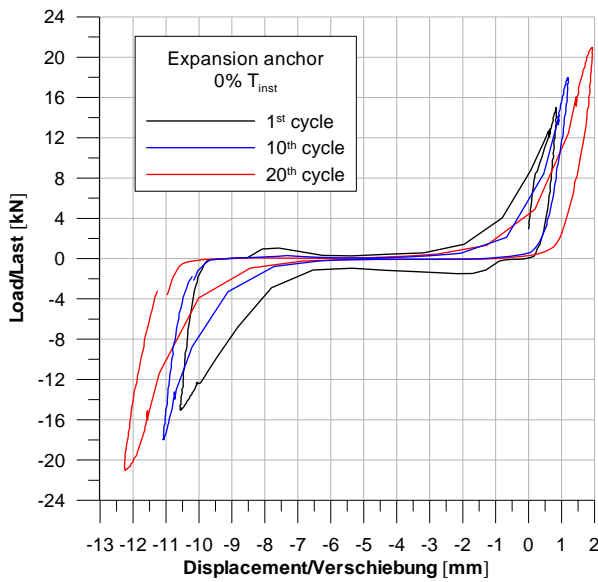


Figure 4.14: Load-displacement of expansion anchor without friction at different cycles

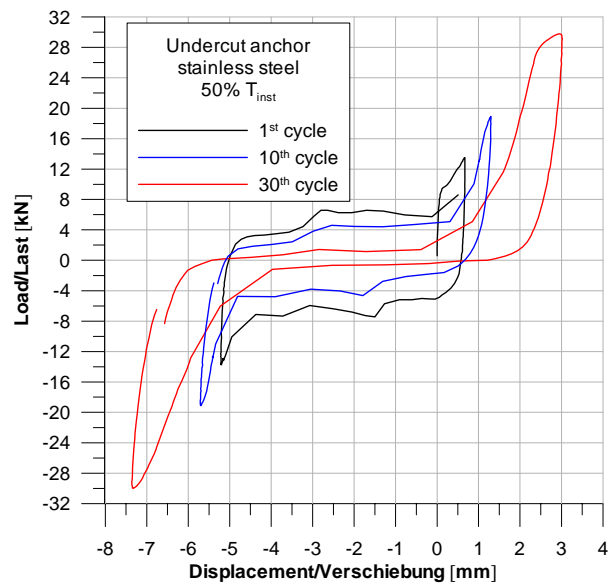


Figure 4.15: Load-displacement of undercut anchor (stainless steel) at different cycles

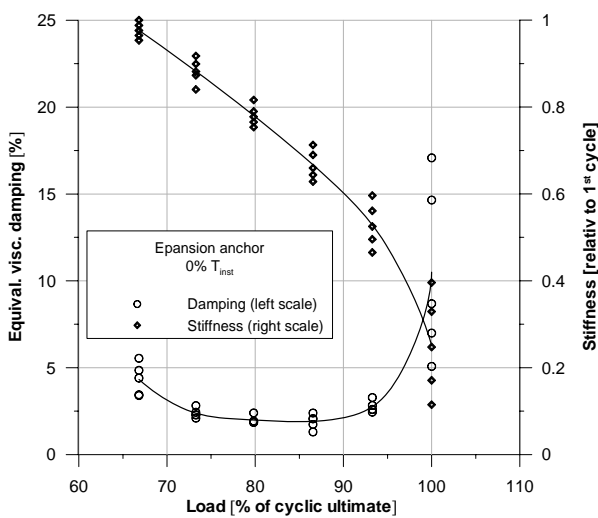


Figure 4.16: Damping and stiffness of expansion anchor without friction

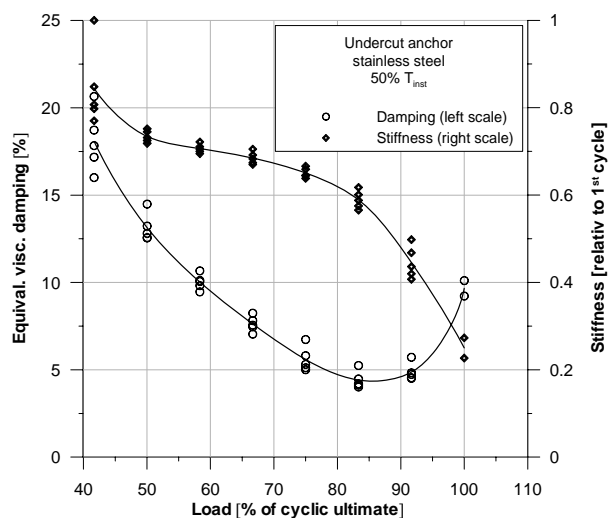


Figure 4.17: Damping and stiffness of undercut anchor (stainless steel)

The influence of a more ductile anchor material can be neglected according to the example shown in Figure 4.19 for an undercut anchor made of stainless steel. For these tests the same material is used as for the monotonic one discussed in chapter 3.2.3. All the cyclic tests are performed in the same concrete batch. This result indicates that the main source for hysteretic damping is provided by friction between base plate and concrete for low and medium amplitudes and by damage of concrete at high amplitudes. Thus, increasing the friction e.g. by a spring an enhanced damping could be achieved, a possibility which will be focussed on in one of the next chapters.

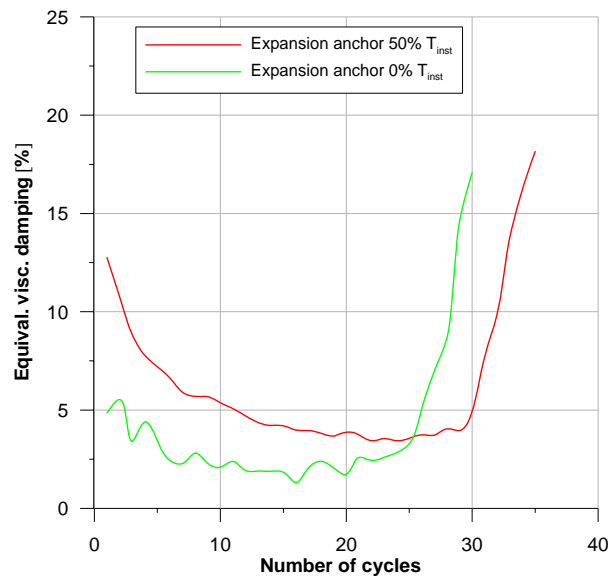


Figure 4.18: Influence of friction (expansion anchor)

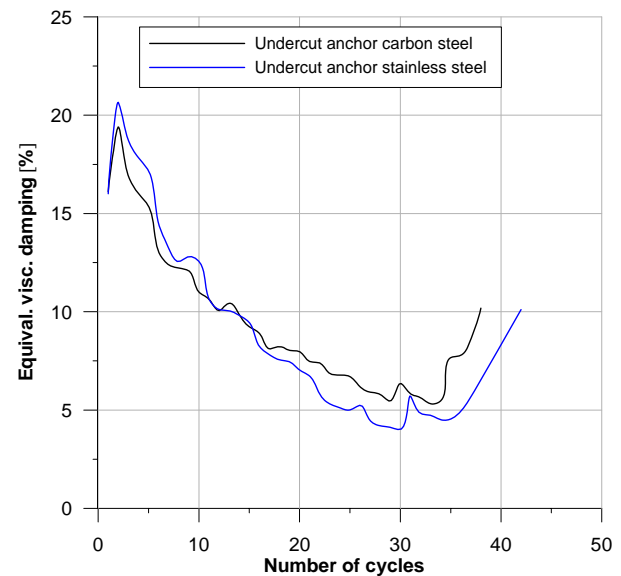


Figure 4.19: Influence of material (undercut anchor)

4.2.2.3 Influence of cracked concrete

All the tests presented up to now are performed in uncracked concrete. In seismic hazardous zones the probability of cracked concrete may be assessed as very high, an assumption which is reflected also in existing seismic testing protocols for post-installed anchors in concrete (*ACI 355.2 2004*). Within the test program of the present chapter it has to be clarified whether cracked concrete changes the damping properties of a fastener subjected to cyclic shear loading and if yes, to which extend. The same expansion anchor from the previous chapter is used for tests in cracked concrete of the strength class C20/25. 10 minutes after installing the anchor in fine hair cracks in accordance with the manufacturer's installation instruction the torque moment is reduced to 50% of T_{inst} and then the crack is opened to 0.5 mm. The direction of loading is parallel to the crack.

As shown in Figure 4.21, at low amplitudes no significant difference between cracked concrete (50% T_{inst}) and uncracked concrete (0% T_{inst}) can be observed. Thus the opening of the crack has the same effect as the reduction of the torque moment to zero. At higher amplitudes the hysteretic damping increases compared to uncracked concrete and 0% T_{inst} . This might be attributed to a reduced local strength and stiffness of cracked concrete referred to uncracked concrete and therefore leading to microcracks and spalling at lower shear loads. Cyclic ultimate load is not affected by the crack.

In order to get an idea about scatter of test results, the average damping calculated from three tests and the average value \pm standard deviation are plotted versus the number of cycles in Figure 4.20. Increasing number of cycles tends to larger coefficient of variation (s. Figure 4.22). Similar results are obtained in uncracked concrete. The degree of local concrete damage for a specific strength class depends upon strength, size and distribution of aggregates close to the edge of the bore hole. This inhomogeneity might explain the large scatter of test data.

However, cyclic ultimate load is not affected by the variation of hysteretic damping since all anchors exhibit the same failure load within the test series. Only the total number of cycles varies between 30 and 34. The failure pattern is similar to that obtained in uncracked concrete (s. Figure 4.23 and Figure 4.5).

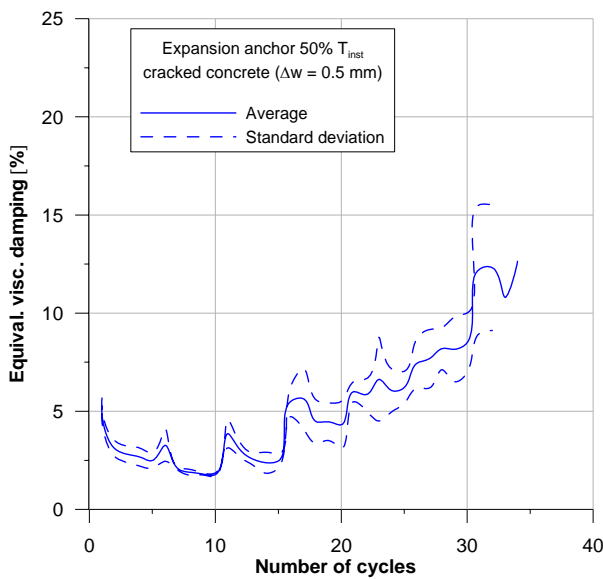


Figure 4.20: Damping in cracked concrete (expansion anchor)

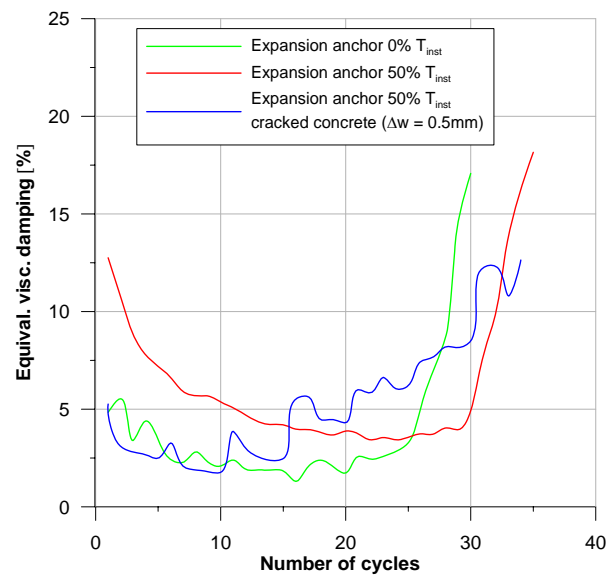


Figure 4.21: Influence of cracked concrete (expansion anchor)

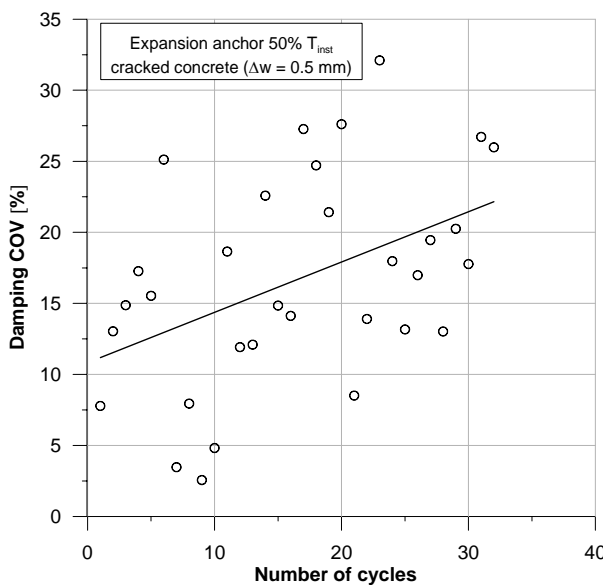


Figure 4.22: Scatter of test results in cracked concrete (expansion anchor)



Figure 4.23: Damage pattern in cracked concrete (expansion anchor)

Trial tests are performed in cracked concrete starting with 5 cycles and an amplitude corresponding to 10% of static ultimate load. This amplitude is approximately 1/3 of that used in the previous tests. Then the amplitude is increased to 20% of static ultimate etc. No significant difference concerning hysteretic damping and cyclic ultimate load is observed. Thus, the results may be extrapolated to very low load levels (< 5 kN).

4.2.3 Decreasing amplitude

Since an earthquake represents a random action the loading sequence consists of increasing and decreasing amplitudes. The latter is addressed by evaluation of tests performed according to *ACI 355.2 (2004)* with the same expansion anchor used in the previous section. Thus, cracked concrete ($\Delta w = 0.5$ mm) according to the strength class C20/25 is used. Additionally, in order to extend the results to larger sizes, an expansion anchor of the diameter M16 is tested.

In the following figures the hysteretic damping in terms of equivalent viscous damping and the stiffness related to the first cycle are plotted versus the load amplitude for both sizes. No significant difference can be observed between the diameter M12 and M16. The damping remains almost constant between 4 and 5% and the stiffness drops to 45 – 50% of the value obtained during the first cycle. Due to irreversible mechanisms (micro-cracks, compaction as a consequence of hydrostatic stress in the concrete) a reduction of amplitude does not lead to smaller displacements as it would be the case for a linear system. This memory effect is strongly pronounced between the 10th and the 40th cycle as shown in Figure 4.27.

Compared to increasing amplitudes the memory effect causes slightly enhanced energy dissipation at low amplitudes as shown in Figure 4.26. Thus, the concrete “remembers” that damage has occurred at previous higher amplitudes. However, this effect is compensated at higher amplitudes and consequently the average hysteretic damping for increasing and decreasing amplitude may be regarded as equivalent.

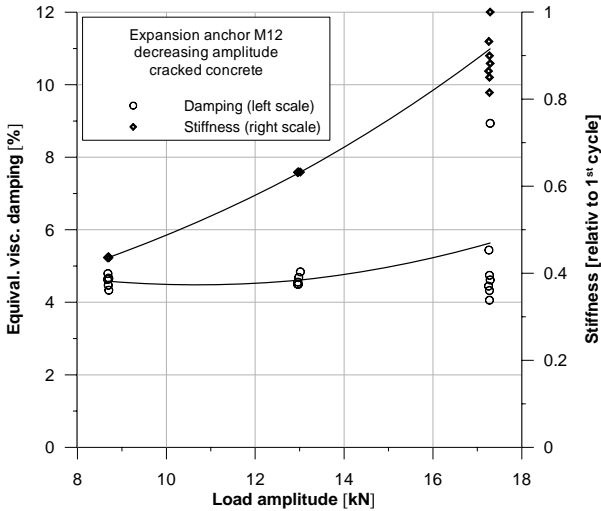


Figure 4.24: Damping and stiffness of expansion anchor M12 (decreasing amplitude)

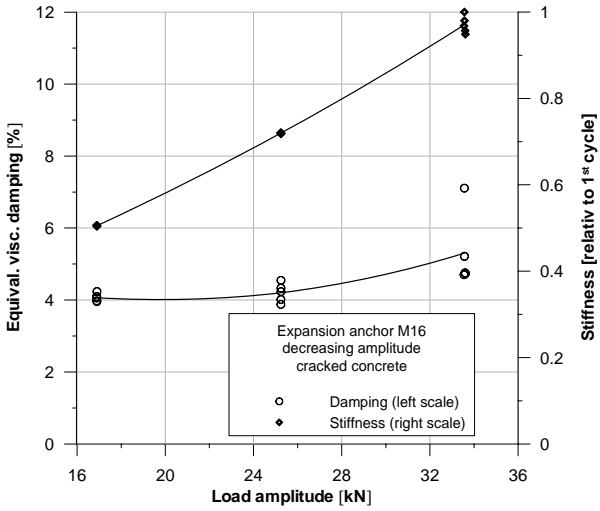


Figure 4.25: Damping and stiffness of expansion anchor M16 (decreasing amplitude)

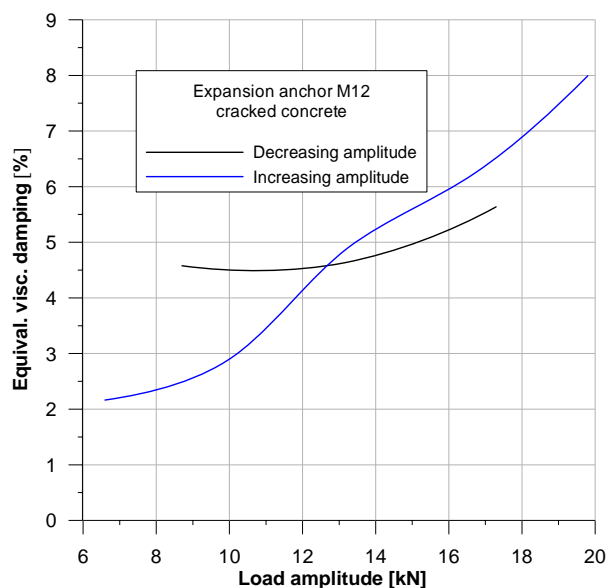


Figure 4.26: Damping for decreasing and increasing amplitude

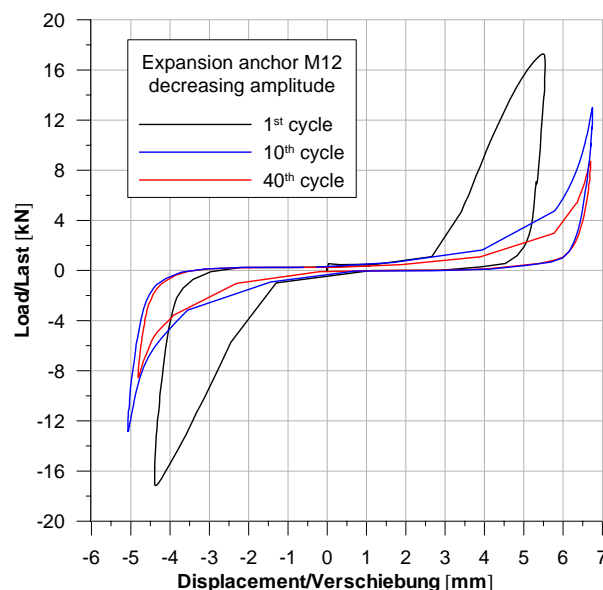


Figure 4.27: Load-displacement of expansion anchor for decreasing amplitude

In case of failure during tests with decreasing amplitudes, rupture of the anchor bolt usually occurs in the shaft approximately $2d_s$ below the concrete surface (s. Figure 4.28) or in the reduced neck section (s. Figure 4.29). These failure patterns result from superposition of shear, bending and axial stresses in the anchor rod. The fracture surface is very smooth which indicates low-cycle fatigue failure typical for 100 cycles and more. Since a seismic event usually is not comparable to low cycle fatigue action, it is a legitimate question whether the testing protocol according to *ACI 355.2 (2004)* simulates an earthquake in a proper way. It should be mentioned that failure in the neck section can be problematic for large anchor sizes because premature fracture cannot be identified nor during the cyclic tests either when determining the residual strength in the subsequent monotonic test.



Figure 4.28: Steel failure in the shaft



Figure 4.29: Steel failure in the neck

Also *Hoehler (2007)* concludes on the base of full size shake table tests with a reinforced concrete structure and by application of the rainflow method that the typical number of cycles which can be

related with high probability to seismic action is not more than 30. A potential change of load amplitude should be a focus of future investigations.

On the basis of all the results an average damping can be defined for very low, low and medium amplitudes up to the load level F_{lim} where strong damage and abrupt increase of hysteretic damping occur and the hysteresis loops become unstable. Excluding the high values before rupture means that the factor λ in equation (4.4) can be set equal to 1.0. The average values for hysteretic damping dependent on anchor type, concrete condition and anchor material listed in Table 4.2 are valid for increasing and decreasing amplitudes. Thus, they may be used as a basis for numerical simulation of post-installed anchors under seismic action. This issue will be treated in chapter 5.

Table 4.2: Average hysteretic damping

Anchor	Expansion anchor		Undercut anchor
T/T_{inst}	0.5	0	0.5
F_{lim} [kN]	20	20	30
concrete	Cracked and uncracked	uncracked	uncracked
steel material	unalloyed	unalloyed	Unalloyed and stainless
Average ξ_{eq} [%]	5	2.5	9

Based on the results of cyclic shear tests with increasing and decreasing amplitude in cracked and uncracked concrete the stiffness within the range of stable hysteretic loops is reduced to 50 – 70% referred to monotonic loading. Therefore an effective stiffness K_{eff} under seismic shear loading is proposed which may be assumed equal to 60% of the stiffness determined in monotonic tests. For sensitive applications (e.g. fastening of pipes containing inflammable liquids, life-saving electrical equipment) this issue has to be considered.

The combination of increased scatter of stiffness under cyclic shear loading and the scatter of number of cycles where failure occurs may have an impact on the ultimate load of groups of anchors. Thus, dependent on the ductility of the steel a reduced resistance of the group is possible. This might be more pronounced in case of concrete edge failure due to brittle behaviour (*Unterweger 2008, Spyridis 2008*). However, additional tests are necessary in order to provide a statistical significant basis for analysis and assessment of this issue.

4.3 Uniaxial shake table tests

Shake table tests on a full-scale single-degree-of-freedom (SDOF) system representing an attached non-structural component to a floor level of a 5-story monolithic concrete frame building, are carried out at the Structural Engineering Laboratory of the University of Canterbury (NZ). The aim of the tests is to examine the behaviour of the anchor rods under real simulation of the earthquake motion. These tests provide a unique opportunity to take a closer look at the available design methods for anchors under seismic shear loads and also to study the effect of anchors on the acceleration and displacement transferred to the attached non-structural component. The provided input motions to the shaking table include ground motion at the base of the building as well as numerical simulated floor motions.

4.3.1 Experimental test setup

The setup is composed of three main parts which are: a concrete block representing the floor slab, a driving mass representing the attached non-structural component, and the anchorage system. The excitation imposing to the system is generated through the motion of the shaking table. The ground motion is transmitted to the floor level concrete mass and passes the attachment and excites the attached non-structural component. The whole test setup is presented in Figure 4.34 and the detailed specification about each part is explained in the following section.

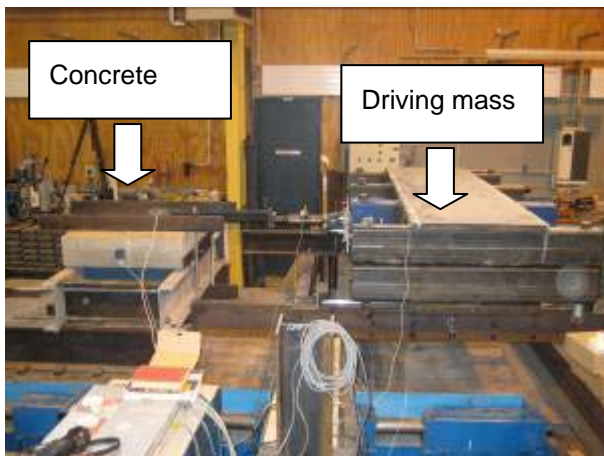


Figure 4.30: Experimental test setup



Figure 4.31: Low friction rollers



Figure 4.32: Anchor connection

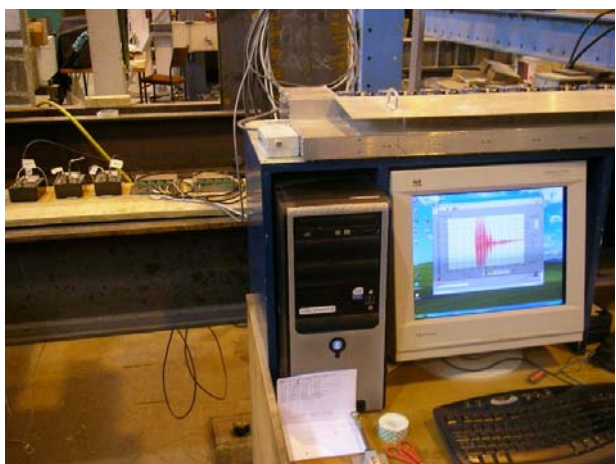


Figure 4.33: Data logging

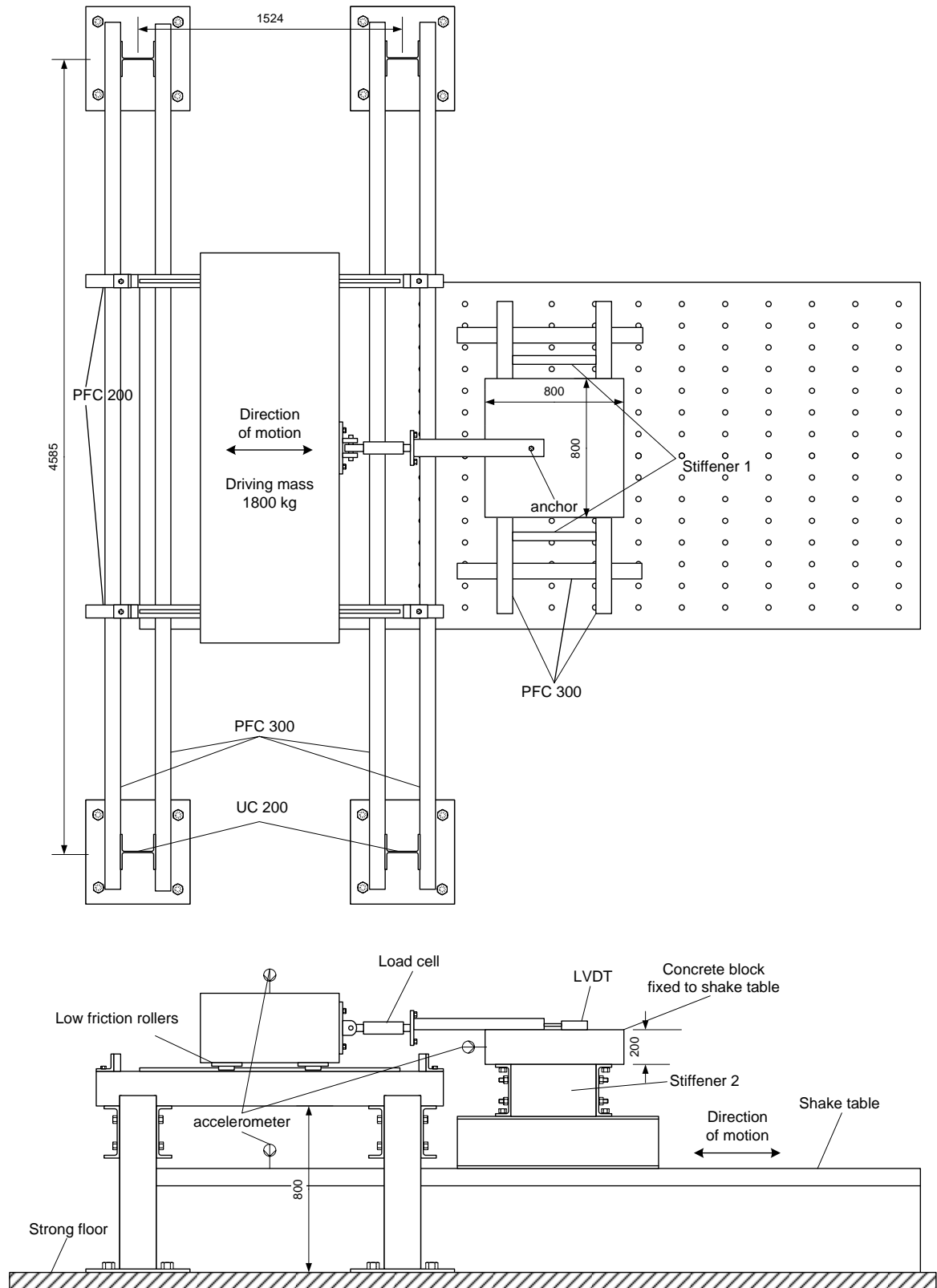


Figure 4.34: Schematic test setup (all measures in mm)

4.3.1.1 Shake table

The shake-table at the University of Canterbury is a uni-axis earthquake ground motion simulator. The table has a plan area of 2 m wide by 4.5 m in length an unloaded mass of 2500 kg. Details of the construction can be found in *Rieder (2008b)*. The MTS control is a closed servo loop using proportional, integral and derivative feed forward adjustment. A table command is given to the system via a displacement time history double integrated from the desired acceleration time history.

The shake-table has a payload capacity of 20 tonnes with a displacement amplitude of 130 mm (total stroke of 260 mm). The capacity of the servo valves limits the velocity of the table to approximately 242 mm/s. This is defined as the saturation velocity of the table and in all cases should be avoided. Within this context it should be noted that the maximum velocity arising from typical near field events is about 1500 mm/s. Thus, the experimental possibilities are limited.

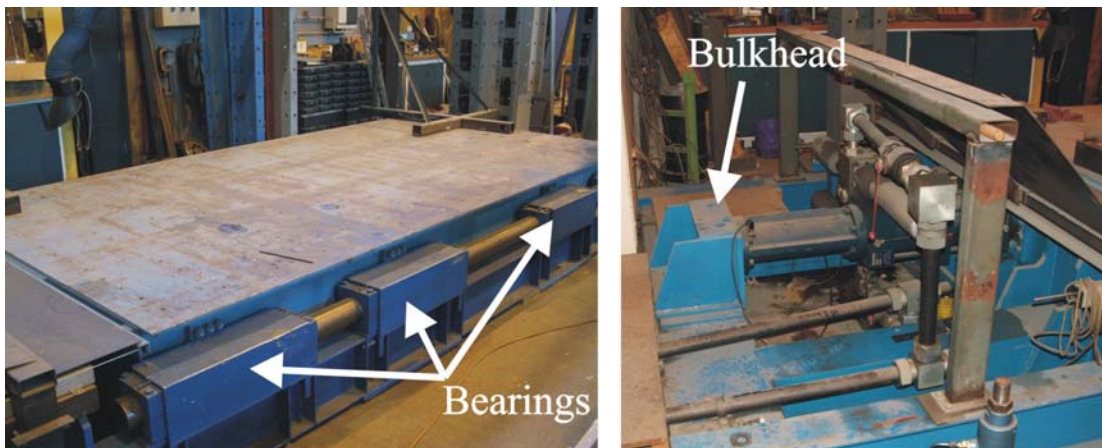


Figure 4.35: University of Canterbury Uni-Axis Shake-table

4.3.1.2 Driving mass

The driving mass is represented by two rigidly connected steel weights which are supported by low friction linear guideways shown in the next figures. Their special design (ball re-circulation, high rigidity-4-row angular) prevents potential uplifting of the driving mass which is movable parallel to the direction of shaking of the table. The rails have to be adjusted on the bridge with an accuracy of 0.1 mm over their entire length of 1.5 m. This results in a maximum driving mass displacement of 700 mm and several anchors can be tested in a straight line without moving the concrete block. In order to prevent damage of the rollers in case of anchor failure rubber elements are fixed at each end of the rails.

The experimentally determined friction force with the moving driving mass lies between 70 and 90 N and thus a dynamic coefficient of friction of the whole system of approximately 0.5 % may be assumed.



Figure 4.36: Linear guideways

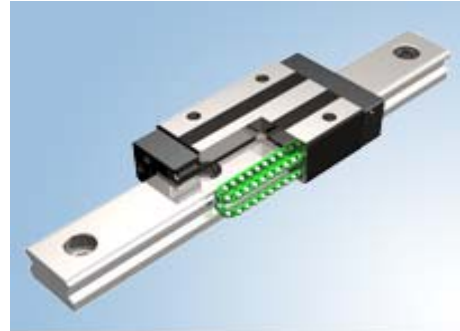


Figure 4.37: Rollers with ball re-circulation system

A set of four steel columns bolted to the strong floor and beams connected with the columns form the bridge over the shake table and enables the decoupling of the driving mass and the shake table. The bridge is designed for a maximum deflection of 1 mm under service load.

The amount of the driving mass is calculated according to the provisions in *CEN/TS (2004)* by substitution of the acting seismic force F_a with the seismic resistance of the anchor under shear loads

$V_{Rd,seis}$:

$$W_a = \frac{V_{Rd,seis} \cdot q_a}{S_a \cdot \gamma_a} [kN] \quad (4.6)$$

W_a Driving mass in kN

$V_{Rd,seis} = 0.75 \cdot V_{Rd}$ according to *ACI 318 (2005)* Appendix D

$V_{Rd} = 23.6$ kN according to *DIBt (2007b)*

$q_a = 2.0$ (assumed anchor ductility)

$\gamma_a = 2.0$ (assumed importance factor)

$$S_a = \alpha \cdot S \cdot \left[\left(1 + \frac{z}{h} \right) \cdot A_a - 0.5 \right]$$

$\alpha = 0.35$ g (peak ground acceleration)

$S = 1.0$ (assumed soil actor)

$A_a = 3$ (assumed amplification factor for mechanical equipment)

$z/h = 0$ (position of the anchor)

All these parameters lead to a total mass W_a equal to 2000 kg for the non-structural element represented by the driving mass. The slightly reduced weight of the available steel mass (1800 kg) may be acceptable. A steel tube constitutes the link between anchor and load cell whereas the inertia force acts in the centre of the attached element, i. e. at a distance of 10 mm above the concrete surface (see the following figure). The attached element exhibits no slack within the push and pull element. The connection between load cell and driving mass is performed by a universal hinge without any slackness.

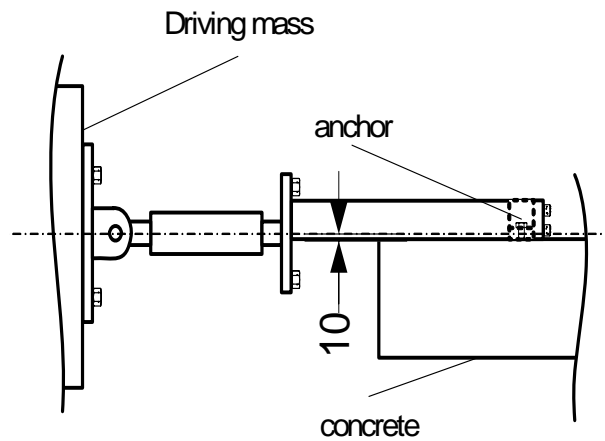


Figure 4.38: Anchor connection (schematic)



Figure 4.39: Anchor connection with load cell

4.3.1.3 Concrete mass

The supporting structure of the uncracked concrete block consists of 2 PFC 300 fixed on the shake table in the shaking direction and two PFC 300 fixed on the top in transverse direction with additional stiffener. The concrete block is bolted down with 4 threaded rods M24 and each of them pre-stressed with a torque moment of 150 Nm. A free vibration test yields a natural frequency of 35 Hz which may be acceptable for seismic experiments.



Figure 4.40: Concrete block connection

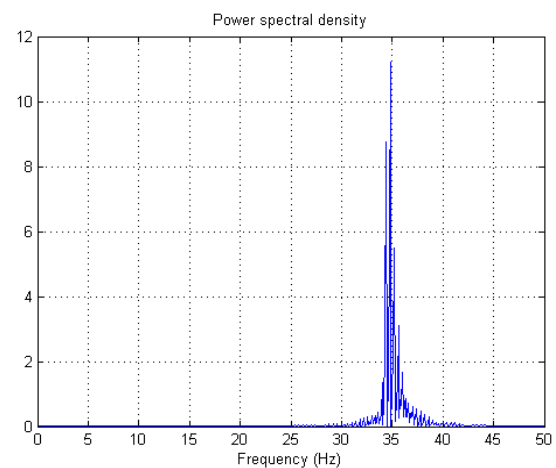


Figure 4.41: Resonance frequency of concrete block

With the resonance frequency of the supporting structure and the concrete mass (350 kg) the relative displacement between concrete and shake table can be estimated in the following way:

$$f_{res} = \frac{1}{2 \cdot \pi} \cdot \sqrt{\frac{K}{m}} \text{ [Hz]} \quad (4.7)$$

With $K = 17 \text{ kN/mm}$ and

$$s_{max} = F_{max}/K$$

The maximum expectable load $F_{\max} = 17$ kN results in a relative displacement between concrete block and shake table $s_{\max} = 1$ mm. This value may be acceptable by the following reasons:

1. It is very small compared to the absolute displacement of the shake table at the highest seismic level (130 mm).
2. It corresponds to the slackness between anchor and attached element and therefore it may be neglected.

Consequently, the connection between shake table and concrete block may be regarded as stiff and the difference in response between these two elements is negligible. The compressive strength of the concrete at time of testing lies between 25 and 30 MPa.

4.3.1.4 Instrumentation and data logging

A load cell with a nominal capacity of 100 kN is installed between the driving mass and the link to measure the load transferring to the anchor rod. This load is a function of stiffness of the anchor, damage in the concrete, and also transferred acceleration to the driving mass.

Measurement of the acceleration in the system is conducted by three LIVM accelerometers, attached to the concrete block, driving mass, and the shaking table. The acceleration of the table is measured as a mean to compare the input record's acceleration and the driving acceleration (the control parameters of the shaking table has the main role to do this matching). Acceleration for the case of concrete block is measured to be sure that concrete block and the table has the same motion (the rigid attachment to the table should make these two acceleration to be the same). Finally, acceleration in the driving mass represents the transferred acceleration to the non-structural component. Measuring the acceleration in the driving mass gives the ability to evaluate the effect of attachment type in the transferred acceleration to the non-structural component.

The relative displacement between the driving mass and concrete block is measured by the use of a potentiometer which is attached to the concrete block and also connected to the link.

Data acquisition for the shake-table is collected via a high speed logger and computer arrangement. The logger unit has an in-built analogue low-pass filter with a cut-off frequency of 200Hz – that is, at 200Hz the normalised voltage is equal to 0.707.

Data is sampled at 1000 Hz for release and during all the tests. Although the full effect of sampling at 1000 Hz would not be felt due to the analogue filter, it was retained in order to have a sufficient sample size for filter options during post-processing.

4.3.2 Testing procedure

For all tests post-installed expansion anchors of the bolt type size M12 and M16 according to the classification in ETAG 001 part 2 (*EOTA 1997*) are used. The anchors are installed according to the manufacturer's installation instruction and after 10 minutes the torque is reduced to zero (i. e. hand tightened) in order to simulate the total loss of prestressing force in cracked concrete. This procedure lies on the safe side and is also in compliance with *CEN/TS (2004)* where no friction between base

plate and concrete can be taken into account for seismic design. The hole in the adapter fixed at the end of the link between anchor and driving mass corresponds to the anchor diameter plus 2 mm. Therefore a gap of ± 1 mm is achieved.

4.3.2.1 Input motion

Sinusoidal tests are performed at 1 Hz and 3 Hz for different amplitudes. For the seismic input various earthquake records according to Table 4.3 are scaled to reach different levels of peak ground acceleration (PGA) within the (velocity) limit of the shake table. The various time histories can be found in *Pampanin (2008)*.

Table 4.3: Earthquake records for seismic input

Earthquake event	M	Year	Station	R [km]	Soil Type (NEHRP)	PGA [g]	Duration [s]
Cape Mendocino	7.1	1992	Rio Dell Overpass-FF	18.5	C	0.38	36
Loma Prieta	6.9	1989	Gilroy Array #7	24.2	D	0.23	40
Northridge	6.7	1994	LA-N Faring Rd	23.9	D	0.27	30
Landers	7.3	1992	Yermo fire station	24.9	D	0.15	44

M: Magnitude, R: Epicentral distance, PGA: Peak ground acceleration

4.3.2.2 Shake table tracking

For sinusoidal input the bare table shows perfect tracking at 5 Hz and 5 mm amplitude. However, a strong interaction between shake table and attached driving mass can be observed limiting the acceptable frequency to 3 Hz (*Rieder 2008b*).

Chase (2005) reports that shake table control in testing large near-field seismic events is often a trade-off between accurate tracking and nonlinear velocity saturation of the hydraulic valves that can result in severe acceleration spikes. In order to avoid these irregularities the shake table input is chosen in such a way that the maximum velocity does not exceed 95% of the system capability. According to *Rieder (2008b)* the shake table with attached driving mass shows a good tracking for the Cape Mendocino record up to a peak ground acceleration of 0.3g.

4.3.2.3 Data filtering

Choosing the proper filter for post-processing seems to be a crucial issue since disturbing frequencies have to be filtered off and interesting frequencies should be kept in the signal. The following figures show the power spectral density of an unfiltered acceleration signal measured on the shake table for a 1 Hz sinusoidal excitation with an amplitude of 0.08 g. The numerous peaks between 15 and 30 Hz represent noise from various sources (hydraulic pump, etc.) and consequently should be filtered off.

This goal is met by a Butterworth low pass filter of 6th order with a cut-off frequency of 10 Hz. It can be seen in Figure 4.44 that there are still some irregularities in the filtered signal (bottom), though the applied filter seems to represent an acceptable compromise since the nominal amplitude of 0.08 g can be clearly identified.

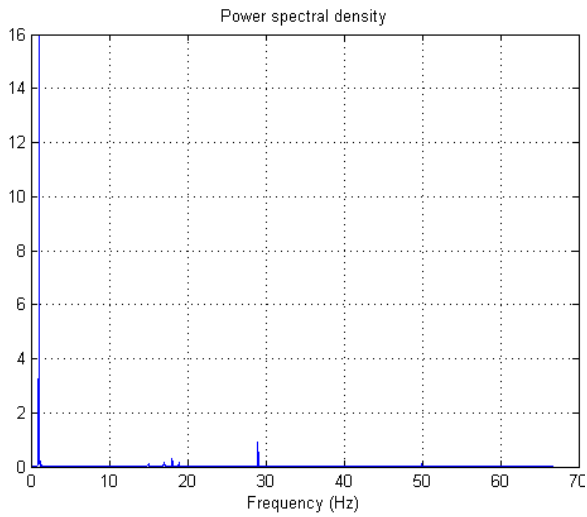


Figure 4.42: Noise at 1 Hz excitation

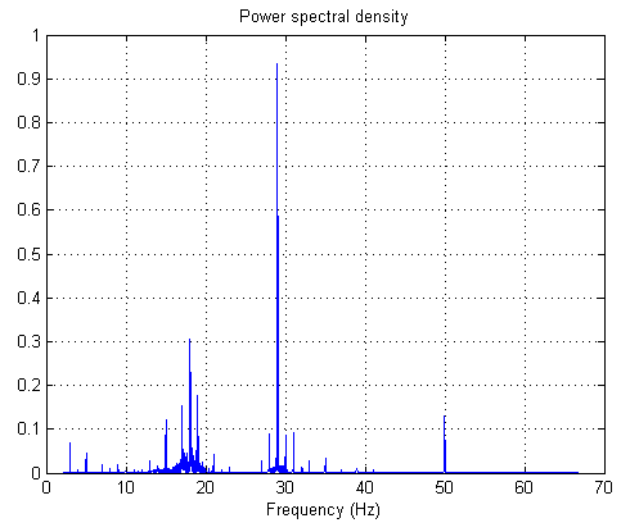


Figure 4.43: Noise at 1 Hz excitation (without input peak)

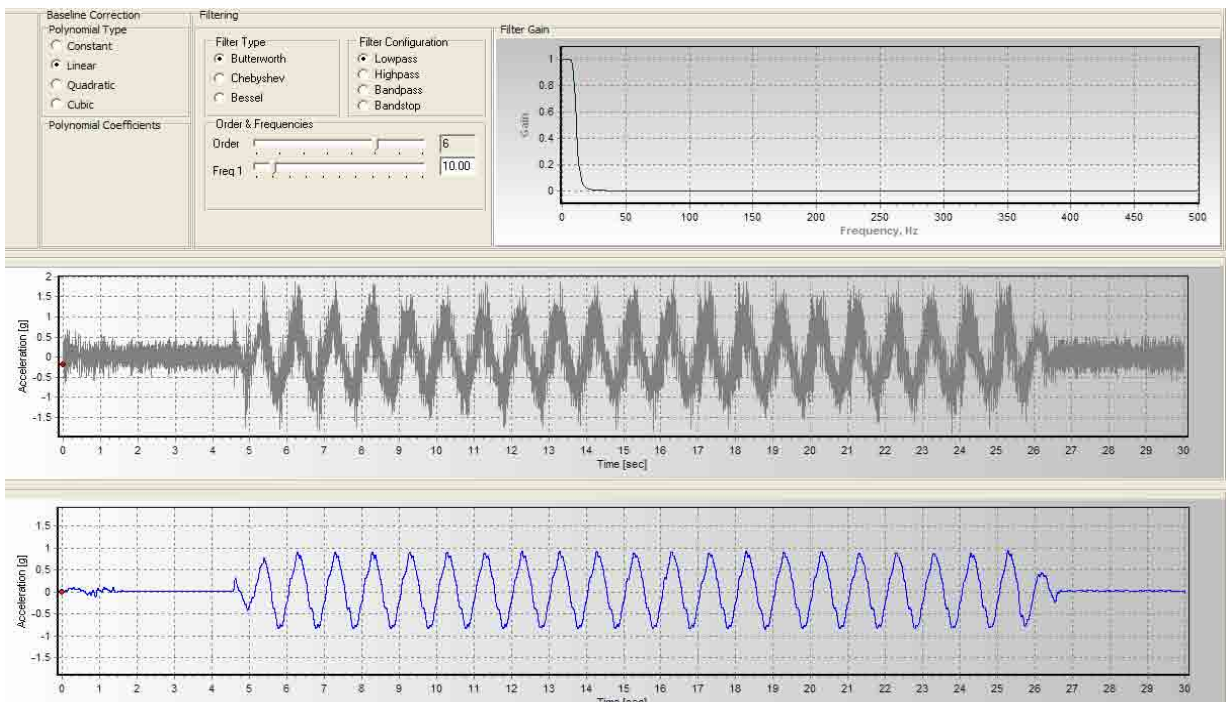


Figure 4.44: Filter design

4.3.3 Test results

All the detailed results can be found in *Pampanin (2008)* and *Rieder (2008b)*. In this section the basic evaluation with the corresponding conclusions are presented.

4.3.3.1 Amplification effects

The following figures show the (filtered) acceleration measured on the shake table, on the concrete block and on the driving mass for sinusoidal and seismic input signal. The most interesting phenomenon is the considerable amplification of the acceleration on the driving mass with respect to

ground motion for both sinusoidal and seismic excitation. This issue will be discussed more detailed in the next section.

The acceleration on the concrete block is increased only by a very small amount which might be due to the feedback from the driving mass. However, the acceleration of the concrete is representative for the shake table input simulating the floor acceleration.

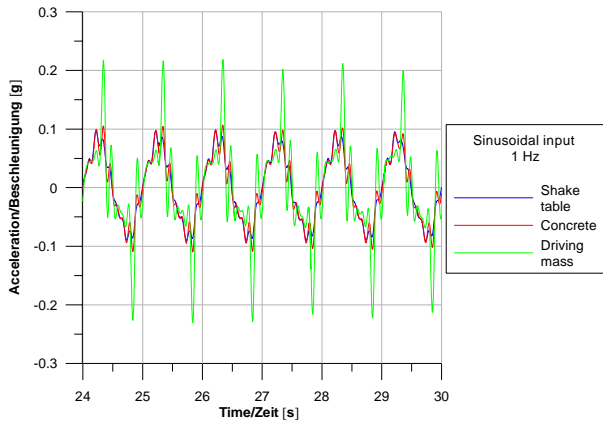


Figure 4.45: Various accelerations, sinusoidal input

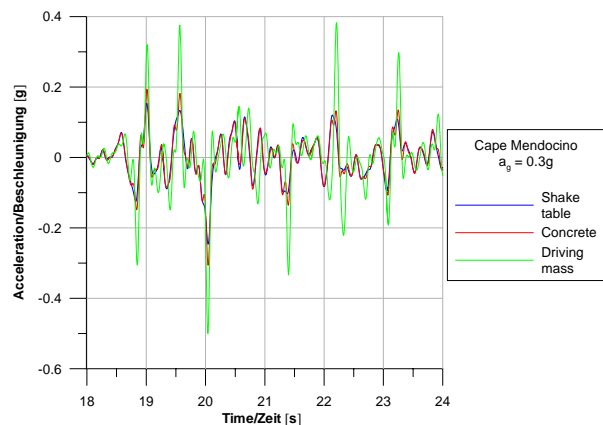


Figure 4.46: Various accelerations, seismic input

The gap between anchor and attached element leads to a small phase shift between concrete and driving mass movement. This can be seen clearly in Figure 4.47 for sinusoidal input. Therefore anchor and driving mass exhibit a velocity with opposite sign at the time of contact. This enhanced relative velocity is the cause for increased change of velocity in terms of acceleration. The theoretical upper limit for the relative velocity is represented by the double velocity of the shake table. More complex is the resulting maximum acceleration because it depends upon anchor stiffness, hole clearance and concrete damage. A comprehensive analysis of these effects constitutes the focus of chapter 5.5.

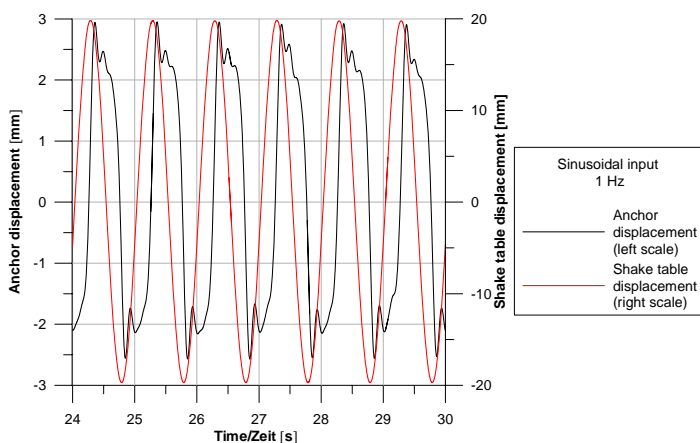


Figure 4.47: Anchor and shake table displacement

The force measured with the load cell corresponds well to the load calculated via the acceleration and weight of the driving mass. In the next figures the load displacement behaviour of the anchor is plotted. It should be noted that the displacement is not set to zero at the beginning of each test and therefore

the curves are not symmetric with respect to the displacement. The additional loops close to zero load arise from the slackness of the anchor within the adapter. The pronounced pinching, i.e. the narrow load-displacement curve close to zero load observed in case of quasi-static cyclic loading in chapter 4.2 is confirmed by the shake table tests.

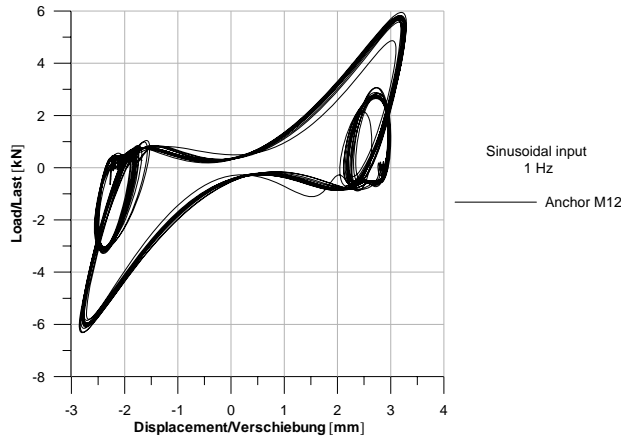


Figure 4.48: Load-displacement, sinusoidal input

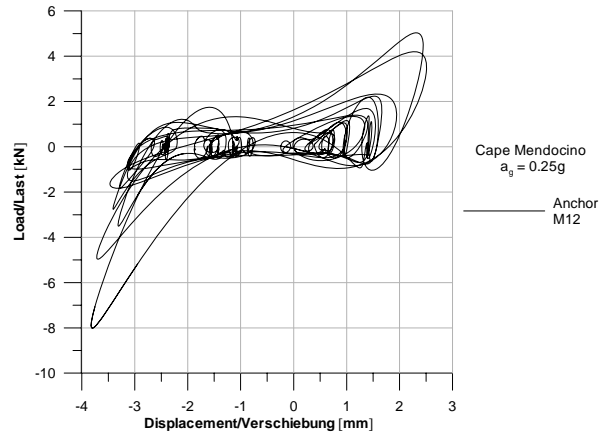


Figure 4.49: Load-displacement, seismic input

Figure 4.50 shows the maximum amplification of the input signal for the different earthquake records. Legend without any indication means the size M12. The high value obtained for the Landers input at 0.06g may be regarded as an outlier. With increasing peak ground acceleration the amplification increases up to an average factor of 2.5 and then a slight decrease occurs. The latter may be due to the first micro-cracks in the concrete leading to plastic deformations and energy dissipation (see also chapter 5.5).

The results of the size M16 lie within the same band of scatter as the size M12. However, more tests and also larger sizes up to M24 may be necessary in order to get a comprehensive understanding of the gap-induced amplification effect. The experimental results are completed by numerical investigations in chapter 5.

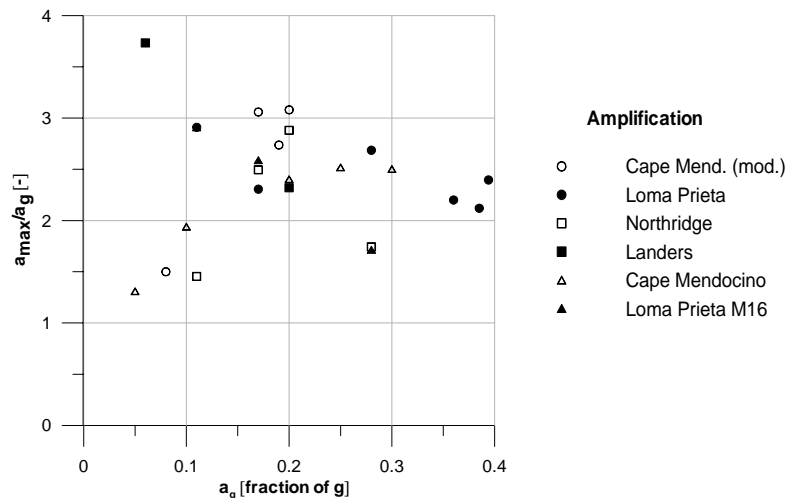


Figure 4.50: Amplification of acceleration

4.3.3.2 Loading rate

In Figure 4.51 the force measured by the load cell and the loading rate over time during the strong motion part of the Cape Mendocino record is plotted exemplarily for a peak ground acceleration of 0.3 g. The order of magnitude confirms the considerations of *Hoehler (2006)* who proposes loading rates for fasteners arising from seismic actions up to 2000 kN/s. It should be noted that the loading rate dF/dt as the first derivative of the load is equal to zero at peak load and therefore the maximum value of dF/dt is always reached at a lower load for each local peak. For the presented example approximately 50% of peak load is measured at maximum loading rate. Since experimental investigations with high loading rate usually are performed with a constant loading rate up to failure their validity for seismic conditions is limited. Thus, a potential increase of resistance obtained from (simplified) tests with high loading rate might be taken into account only partially for seismic design. The characteristic seismic loading pattern consisting of variable loading rate with alternating sign can be simulated in the most realistic way only by means of shake table testing.

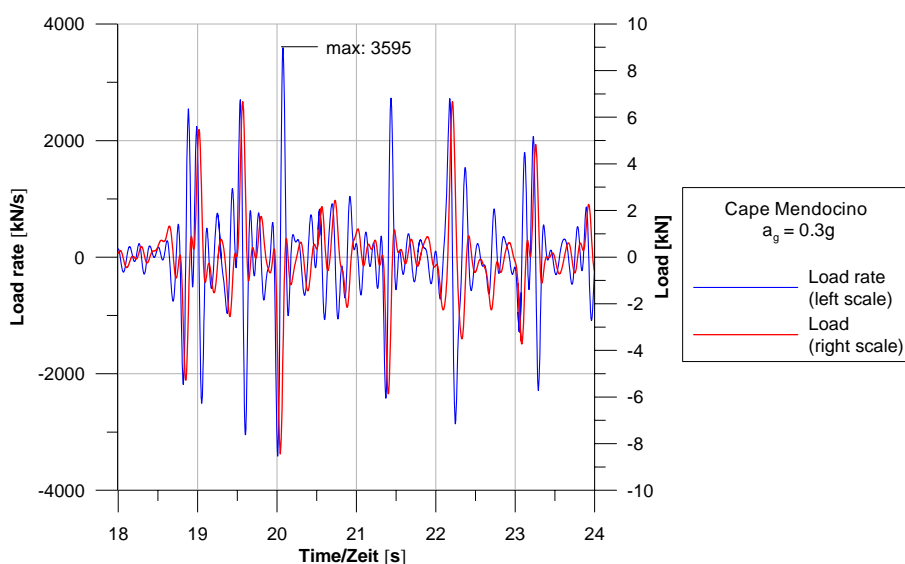


Figure 4.51: Loading rate for Cape Mendocino, PGA = 0.3g

According to different authors (*Eibl 1989a, Eibl 1989b, Klingner 1998, Fujikake 2003, Hoehler 2006*) the increase of resistance under high rate axial loading depends upon anchor type, mode of failure and crack width. A loading rate of 4000 kN/s increases the concrete cone failure load up to 30% but the resistance in case of pull through is lowered by approximately 5%.

Within the presented testing procedure of this chapter the shake table capacity is not sufficient to achieve anchor failure. Up to date to the knowledge of the author no simplified experimental testing addressing shear loads with high loading rate up to failure is available. The influence of high rate shear loading might depend upon the possible failure modes steel failure, pry-out failure and concrete edge failure. However, the resistance under earthquake relevant shear loading rates will probably be at least as large as that obtained under quasi-static loading. As a conservative approach the latter may be acceptable also for seismic design.

4.4 Triaxial shake table tests

Since the capacity of the shake table used in the previous chapter is limited especially in terms of velocity, additional tests are carried out with the high performance testing facility of the research center ISMES located in Seriate (I). Aim is the investigation of the influence of triaxial seismic action on the response of different types of anchors and the determination of the failure pattern under realistic seismic conditions. Together with the previous results, the findings of this chapter should yield a more comprehensive knowledge of the seismic behaviour of post-installed fastener with respect to interaction between axial and shear loads. Details of the tests can be found in *Rieder (2005a)*.

4.4.1 Experimental test setup and testing procedure

For the seismic tests a concrete specimen with a compressive strength $f_c = 29$ MPa is bolted to the shake table as a wall. As already discussed in chapter 2 the pull-out resistance of post-installed anchors strongly depends upon crack width. The probability that an anchor will be located in a crack during an earthquake may be regarded as very high. In order to meet this goal the concrete specimen is equipped with cast in place metal tubes and sheets according to Figure 4.53. Hardened cones are inserted from the back side and by gentle hammer blows fine hair cracks are opened, whereby the sheet acts as a “crack controller”. Then the anchors are installed in the fine cracks according to the manufacturer’s instruction, loaded with the steel weights and prestressed with the prescribed torque moment. In order to simulate the long time loss of prestressing force, after 10 minutes the torque moment is reduced to 50% of the nominal value and the cracks are opened until a width of 1.5 mm. This large crack width represents the maximum expectable damage to reinforced concrete structures outside of plastic hinges (*DIBt 1998a*). Crack width is monitored by dial indicator gauges. The chosen crack width represents severe damage of the concrete which might occur close to a plastic hinge in the case of strong ground motion. The concrete specimen is designed in the way that two anchors can be tested simultaneously for each seismic event.

Three different anchor types of the size M12 are object of the investigation: undercut anchor, expansion anchor and bonded anchor according to their functioning principle mechanical interlock, friction and bonding, respectively (see Figure 4.52). The technical data listed in Table 4.4 are taken from the corresponding European Technical Approvals (*DIBt 1998b, DIBt 2005, DIBt 2007b*).

Table 4.4: Technical data of used anchors

Anchor	h_{ef} [mm]	d_0 [mm]	N_{Rd} [kN]	V_{Rd} [kN]	M_{Rd} [Nm]
Undercut	80	18	11,8	27	84
Expansion	80	18	12,2	26,4	84
Bonded	75	14	11,8	20,8	84

h_{ef}	Anchorage depth
N_{Rd}	Design resistance in tension
V_{Rd}	Design resistance in shear
M_{Rd}	Design resistance bending moment

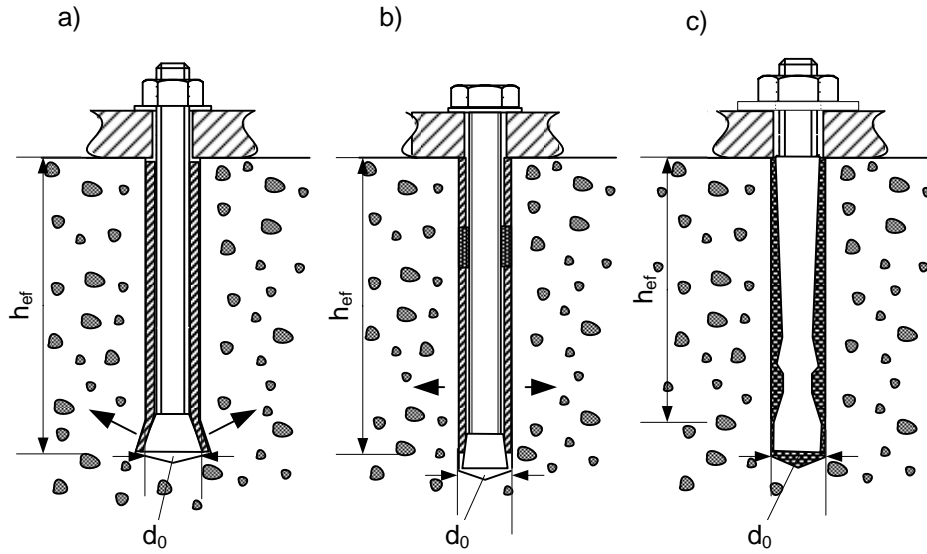


Figure 4.52: Tested anchors: a) undercut anchor, b) expansion anchor, c) bonded anchor

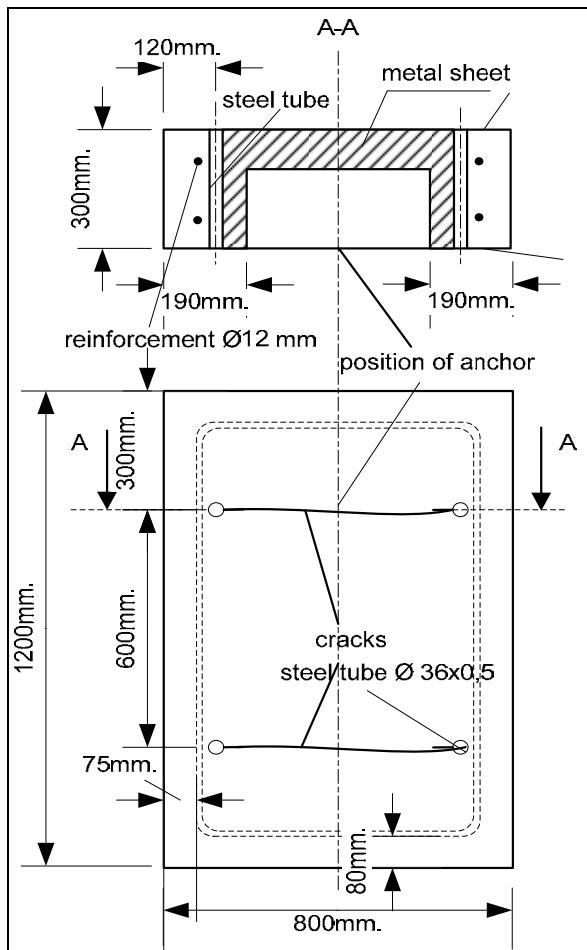


Figure 4.53: Details of concrete specimen

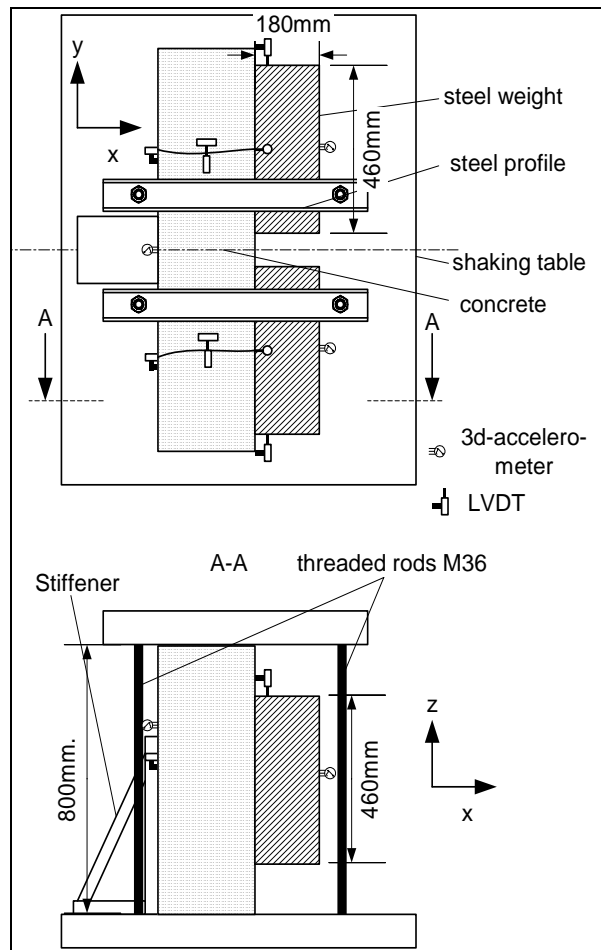


Figure 4.54: Test setup and instrumentation

Following data are monitored during the test: acceleration in all three directions on the steel masses and on the concrete specimen, displacement of the steel masses in y- and z- direction, crack widths and axial displacement of the anchors through a hole from the back side of the specimen.

The weight of the steel masses is determined by calculation according to *CEN/TS (2004)* Annex E and using the static resistance of the anchors from Table 4.4. The interaction is verified according to the loading conditions shown in Figure 4.55 and using the formula proposed by *Mesureur (2004)*:

$$\left(\frac{N_{Sd}}{N_{Rd}} \right)^{0.75} + \left(\frac{V_{Sd}}{V_{Rd}} \right)^{0.75} \leq 1.0 \quad (4.8)$$

As already mentioned in chapter 3.3.3 the exponent 0.75 in equation (4.8) represents a conservative value since the reference load for pure shear resp. axial loading is taken from monotonic tests up to failure. According to the results of chapter 4.2 the ultimate load under pure cyclic shear loading depends on anchor type and can be much lower than that for monotonic loading. Thus, using the reference load obtained in cyclic shear tests leads, a larger exponent in equation (4.8) is achieved. The proposal of *Mesureur (2004)* is used in order to get data also at very low seismic levels.

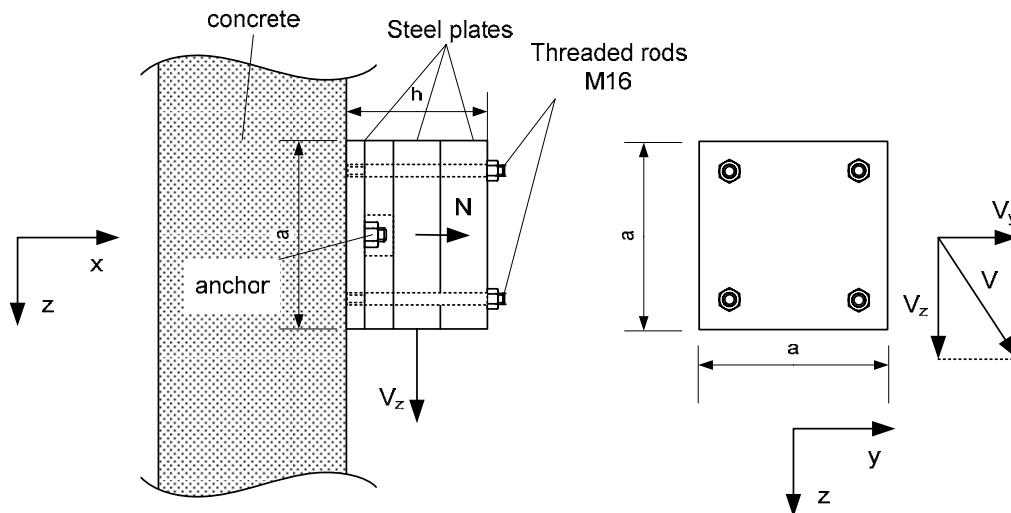


Figure 4.55: Loads acting on the anchor



Figure 4.56: Test setup (front side)



Figure 4.57: Test setup (back side)

For the dimension of the steel plates the values $a = 460$ mm and $h = 180$ mm are obtained resulting in a mass of 300 kg. The whole test setup is illustrated in Figure 4.56 and Figure 4.57.

The input signal for the ground acceleration is in accordance with the *IEEE 693 (1997)* standard (Figure 4.58) which is commonly used for seismic qualification tests of electrical equipment. It consists of three incoherent synthesized signals with a (horizontal) peak acceleration in x- and y- direction of 0.5 g and in (vertical) z-direction of 0.4 g, a frequency content between 1.2 Hz and 37 Hz and a duration of 32 seconds. The required response spectrum is determined for 2% damping. The high demand of the used record in terms of width and height of the acceleration spectrum is illustrated in Figure 4.59. Thus, the maximum amplification is 3.25 between 1 and 7 Hz.

The shake table tests are started at 1/8 of the nominal seismic level and then the amplitude is increased successively for the same test specimen. This procedure is repeated until large deformations or failure of the anchors occurs. Data are sampled at 200 Hz and a 60 Hz low-pass filter is applied.

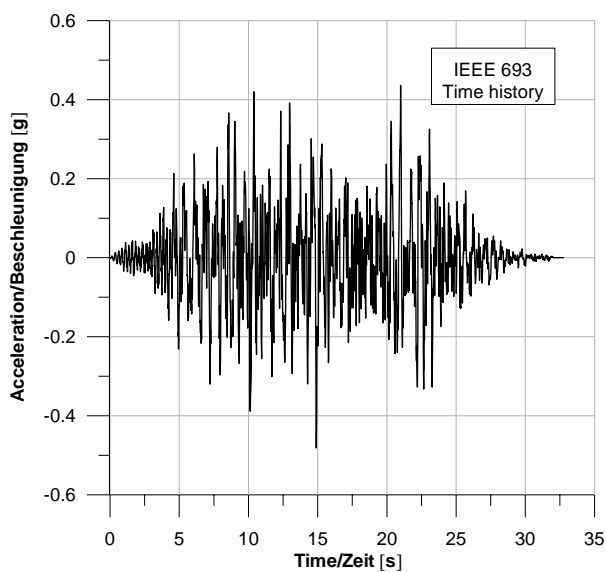


Figure 4.58: Time history (x-direction)

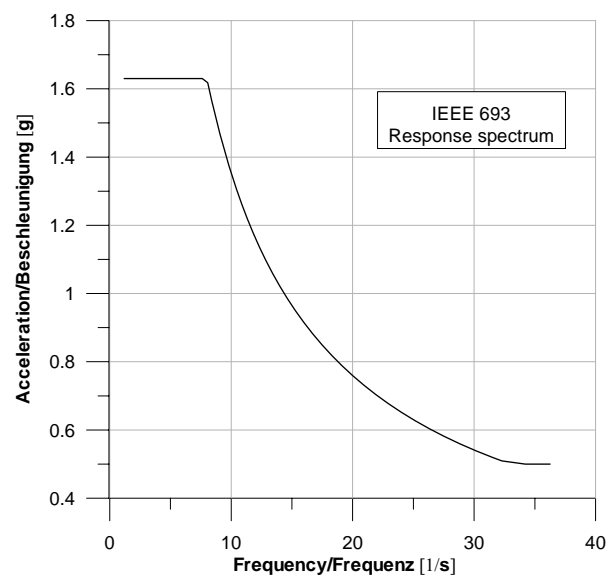


Figure 4.59: Design response spectrum

4.4.2 Test results and analysis

Axial load N and shear load V acting on the anchor as indicated in Figure 4.55 are calculated for each time step via measured accelerations on the steel masses multiplied by their weight according to the following formulas.

$$V_z = m \cdot g + m \cdot a_z \quad (4.9)$$

$$V_y = m \cdot a_y \quad (4.10)$$

$$V = \sqrt{V_y^2 + V_z^2} \quad (4.11)$$

$$N = \frac{h}{a} \cdot V + m \cdot a_x, a_x \geq 0 \quad (4.12)$$

With

a_x, a_y, a_z measured acceleration in the corresponding direction in m/s^2

V_y, V_z shear load in the corresponding direction in N

m mass of steel plates
= 300 kg

a length of steel plates
= 460 mm

h height of steel weights
= 180 mm

V resulting shear load in N

N resulting axial load in N

4.4.2.1 Sine sweep tests

Before starting with the seismic tests the stiffness of the test setup is checked in a sine sweep test in the weak (x) -axis with frequencies between 1 and 50 Hz. In Table 4.5 the resonance frequency f_{res} and the frequency f_2 where an amplification factor of 2 is achieved. For frequencies up to f_2 any amplification effects may be neglected. Therefore the relevant frequencies are outside of the seismic range for all anchor types and the system may be considered as stiff.

Table 4.5: Results of the sine sweep tests

	Undercut anchor			Expansion anchor			Bonded anchor		
	concrete	Anchor 1	Anchor 2	concrete	Anchor 1	Anchor 2	concrete	Anchor 1	Anchor 2
f_2 [Hz]	41	37	42	40	33	41	40	37	42
f_{res} [Hz]	> 50	> 50	> 50	43	43	43	> 50	> 50	> 50

4.4.2.2 Undercut anchor

The crack width remains constant during all the tests. In Figure 4.60 the maximum displacements in axial and shear (vertical) direction of one undercut anchor for each seismic level are plotted versus the maximum acceleration of the shake table referred to the nominal level α_{nom} . The displacement consists of the sum of elastic and plastic deformations. Both axial and vertical displacements increase almost linearly up to a seismic level which corresponds to 800% of the nominal level. Further increase of the seismic input leads to a sudden increment of both axial and shear displacements which can be referred to superficial concrete crushing and bending of the anchor bolt (Figure 4.62). The acting bending moment depends upon axial anchor slip and extent of concrete damage. Since the latter cannot be determined during the tests it is not possible to calculate the moment in a reliable way.

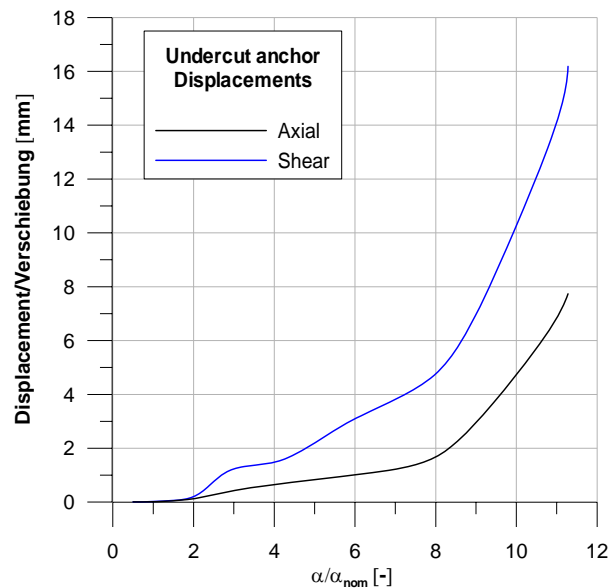


Figure 4.60: Maximum displacements undercut anchor

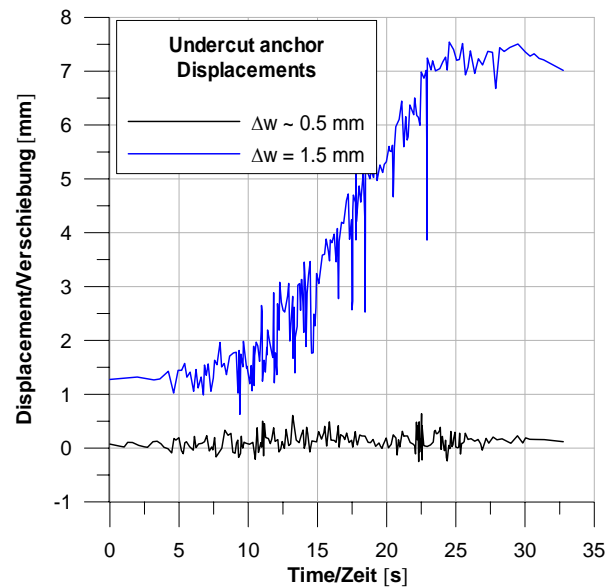


Figure 4.61: Crack width dependent axial displacement at $\alpha/\alpha_{nom} = 11$

According to Figure 4.61 the other anchor suffers practically no damage during the whole tests. This significant difference can be related to crack branching shown in Figure 4.63 so that at the position of the anchor the crack width reaches only about 0.5 mm on the concrete surface. Inside the concrete the crack width might differ from this value. However, this result is a clear indication that the seismic performance of post-installed anchors is crucially influenced by the degree of damage of the concrete.



Figure 4.62: Damage pattern ($\Delta w = 1.5$ mm)



Figure 4.63: Crack branching ($\Delta w \sim 0.5$ mm)

In the next figure the interaction calculated in compliance with equations (4.8) - (4.12) is plotted for the different seismic levels. The design level for interaction according to *Mesureur (2004)* is reached at $\alpha/\alpha_{nom} = 4.5$ and according to *EOTA (1997)* at $\alpha/\alpha_{nom} = 5.5$. Since failure in terms of excessive deformation occurs at approximately $\alpha/\alpha_{nom} = 11$ a “safety margin” $\gamma_{Mesureur}$ and γ_{EOTA} of 2.5 and 2 respectively can be deduced. The proposal given in the draft design guideline of the *fib (2007)* yields a

value between these two. Peak axial load reaches up to a factor 2 and peak shear load up to a factor 3 related to the static resistance. The latter may be due to high frequency oscillations which are not filtered off by the used 60 Hz low-pass filter.

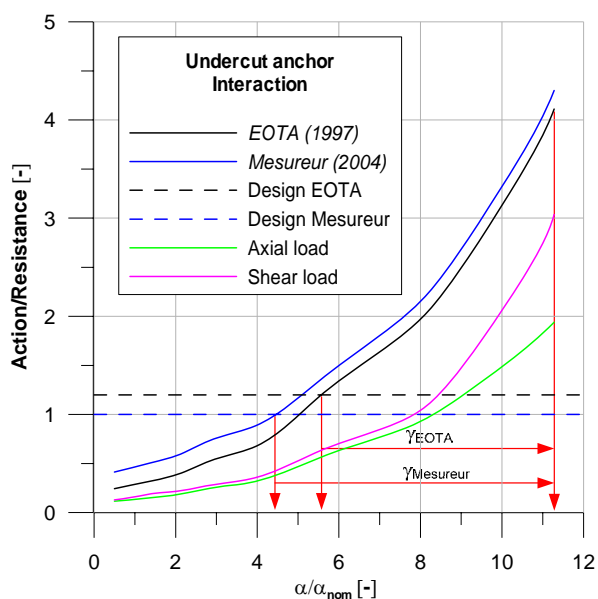


Figure 4.64: Interaction for undercut anchor

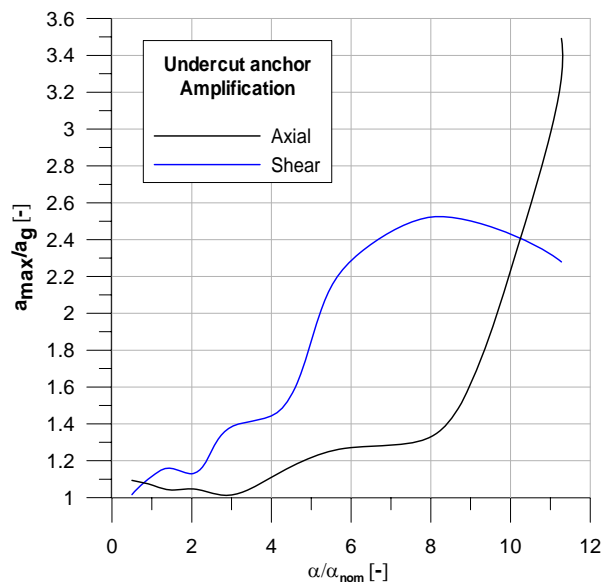


Figure 4.65: Axial and shear Amplification

The non-linear increase of the interaction forces beyond $\alpha/\alpha_{nom} = 4$ can directly be related to the increasing amplification of both axial and shear acceleration. According to Figure 4.65 the amplification in shear (y)-direction due to the gap between anchor and base plate confirms the results of the uni-axial shake table tests presented in chapter 4.3. At the highest seismic level the large axial displacement leads to an enhanced amplification factor of 3.5. The effect of increased gap will be investigated in chapter 5.

In the following table the maximum loads and displacements of the anchor placed in the crack with the nominal width are summarized for each seismic level. Since the results of only one anchor are usable the statistical significance is limited. But due to the small difference between anchor 1 and 2 for the other anchor types (see next sections) one may assume low scatter of test data also in case of the undercut anchor.

Table 4.6: Test results for undercut anchor

α/α_{nom}	Axial displ [mm]	Vertical displ. [mm]	V/V_{Rd}	N/N_{Rd}
0.50	0.01	0.01	0.13	0.12
1.00	0.01	0.02	0.16	0.13
1.40	0.04	0.05	0.19	0.15
2.00	0.12	0.20	0.22	0.18
2.82	0.37	1.12	0.28	0.25
4.00	0.65	1.48	0.36	0.32
5.64	0.95	2.80	0.65	0.58
8.00	1.67	4.76	1.04	0.93
11.28	7.74	16.18	3.04	1.94

4.4.2.3 Expansion anchor

Maximum displacements and loads with corresponding interaction models are plotted in the next figures for the expansion anchors. Due to a data acquisition failure only one shear (vertical) displacement is shown. As already mentioned the difference in axial displacement between the two anchors is very low. The results of the second test at the seismic level $\alpha/\alpha_{nom} = 8$ are shown only in Table 4.7. The design level for interaction according to *Mesureur (2004)* is reached at $\alpha/\alpha_{nom} = 3.7$ and according to *EOTA (1997)* at $\alpha/\alpha_{nom} = 5.2$. Failure in terms of excessive deformation occurs at $\alpha/\alpha_{nom} = 8$, thus in compliance with the undercut anchor a “safety margin” $\gamma_{Mesureur}$ and γ_{EOTA} of 2.2 and 1.5 respectively can be deduced.

Since the anchor sleeve consists of two parts separated by a plastic ring the shear stiffness is reduced with increasing concrete damage which leads to very high shear deformations. According to Figure 4.68 the concrete is crushed and the position of the joint between the two parts of the sleeve can be seen. Axial displacement is only due to relative slip between sleeve and cone of the anchor. This behaviour is typical for expansion anchors in large cracks (*Eligehausen 2000*).

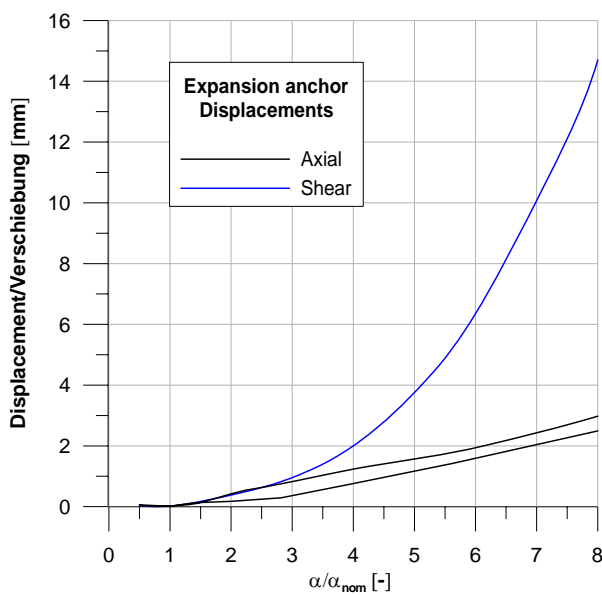


Figure 4.66: Max. displacements expansion anchor

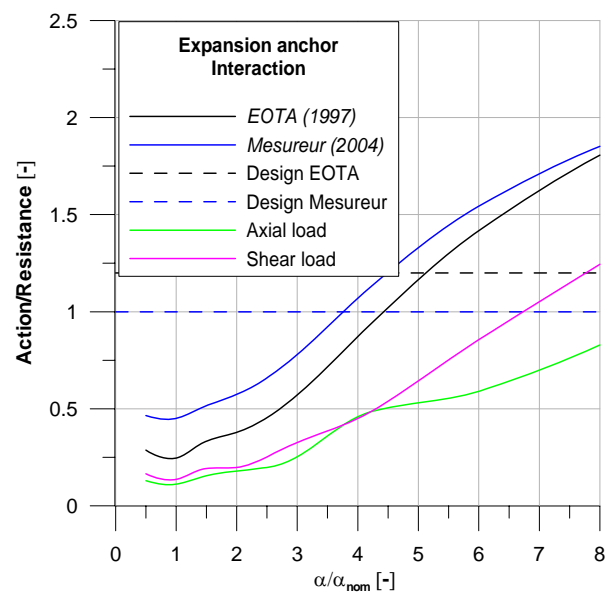


Figure 4.67: : Interaction for expansion anchor



Figure 4.68: Damage pattern of expansion anchor

Table 4.7: Test results for expansion anchor

α/α_{nom}	Axial displ. [mm]		Vert. Displ. [mm]	V/V_{Rd}		N/N_{Rd}	
	Anchor 1	Anchor 2		Anchor 1	Anchor 2	Anchor 1	Anchor 2
0.50	0.04	0.06	0.04	0.16	0.17	0.13	0.13
1.00	0.02	0.01	0.02	0.13	0.14	0.11	0.11
1.40	0.10	0.13	0.13	0.18	0.19	0.14	0.15
2.00	0.42	0.17	0.38	0.22	0.20	0.17	0.18
2.82	0.75	0.29	0.82	0.27	0.30	0.25	0.23
4.00	1.24	0.76	1.99	0.54	0.45	0.34	0.46
5.64	1.79	1.43	5.26	0.82	0.78	0.66	0.56
8.00	2.98	2.50	14.70	0.98	1.24	0.83	0.83
8.00	4.58	3.17	27.34	1.24	1.22	1.03	1.05

4.4.2.4 Bonded anchor

As shown in Figure 4.71 and Figure 4.72 the bonded anchors fail by complete pull-out and local concrete crushing at $\alpha/\alpha_{nom} = 8$. Since the design level for interaction according to *Mesureur (2004)* is reached at $\alpha/\alpha_{nom} = 3.5$ and according to *EOTA (1997)* at $\alpha/\alpha_{nom} = 5$, a “safety margin” $\gamma_{Mesureur}$ and γ_{EOTA} of 2.3 and 1.6 respectively can be deduced. This safety margin means safety against failure.

Thus, seismic loading leads to damage of bonding between adhesive and concrete and hence to a significant reduction of bond strength. This issue is also investigated in detail by *Simons (2008)* for post-installed rebars under cyclic axial tensile and compression loading. Dependent on the type of investigated adhesive, 10 cycles performed with displacement controlled amplitude of 2 mm reduce the bond strength to 20 – 30% referred to the static strength in cracked concrete.

Cyclic tensile loading without any compression (which is the case for post-installed bonded anchors) seems to be less critical, since according to Table 4.8 failure occurs at 78% of the static design resistance (average value). With $\gamma_{Mp} = 1.5$ and $N_{Rk} = 0.75 \cdot N_{Ru}$ the axial failure load in the seismic test corresponds to 40% of the static resistance. Without any interaction the ultimate axial load would be higher. Separate tests are necessary to get reliable information for pure axial loading.

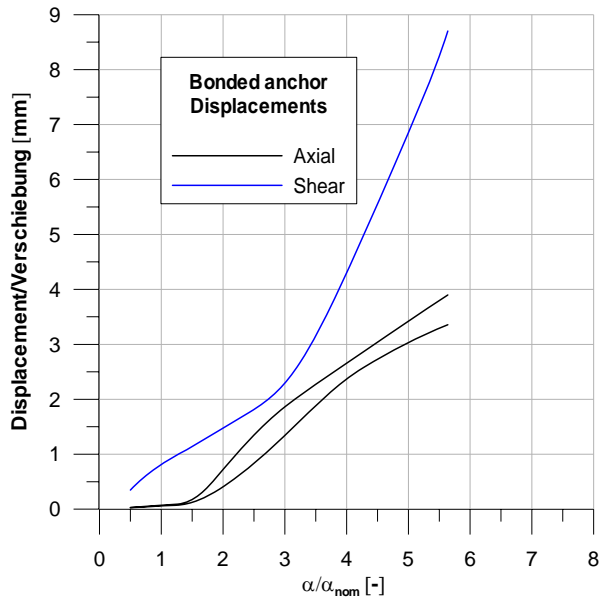


Figure 4.69: Maximum displacements bonded anchor

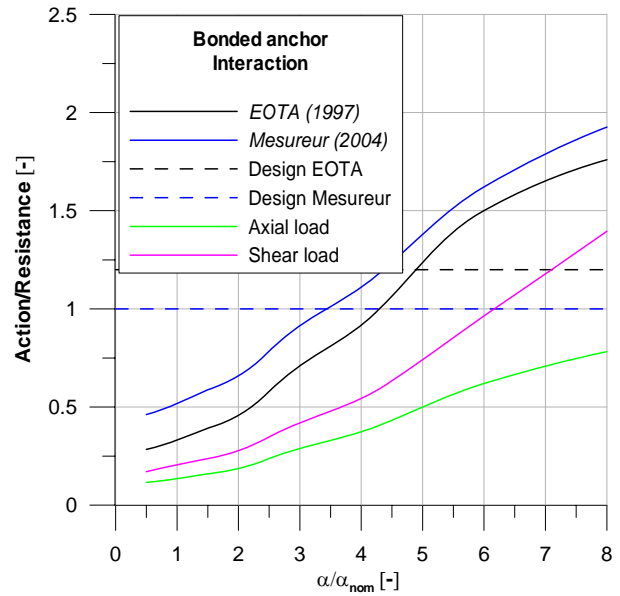


Figure 4.70: : Interaction for bonded anchor



Figure 4.71: Deformed bonded anchor



Figure 4.72: : Concrete damage, bonded anchor

Table 4.8: Test results for bonded anchor

α/α_{nom}	Axial displ. [mm]		Vert. Displ. [mm]	V/V_{Rd}		N/N_{Rd}	
	Anchor 1	Anchor 2		Anchor 1	Anchor 2	Anchor 1	Anchor 2
0.50	0.03	0.02	0.35	0.17	0.17	0.12	0.12
1.00	0.07	0.06	0.82	0.21	0.20	0.13	0.14
1.40	0.12	0.09	1.07	0.23	0.23	0.16	0.15
2.00	0.72	0.41	1.48	0.29	0.26	0.20	0.17
2.82	1.69	1.15	2.08	0.47	0.32	0.32	0.22
4.00	2.66	2.37	4.30	0.58	0.51	0.40	0.35
5.64	3.90	3.36	8.70	0.90	0.87	0.62	0.54
8.00	Pull-out	Pull-out	-	1.67	1.12	0.94	0.63

On the base of the triaxial shake table tests it may be concluded that the investigated bonded anchor is more prone to simultaneous axial and shear loading. This issue is also confirmed by *Mesureur (2004)* who used a similar bonded anchor for the quasi-static cycling interaction tests (s. chapter 3.3.3). It should be noted that the horizontal and vertical accelerations usually are not coherent in a real seismic event. This fact is also reflected by the time histories used within the IEEE standard. Therefore additional safety is provided by the fact that the different acceleration components don't reach peak level simultaneously. In some cases the opposite may happen and as a consequence leading to disastrous damage and loss of lives like during the earthquake with the epicentre close to L'Aquila in Italy in April 2009 (*Franchi 2009*).

4.4.2.5 Influence of anchor type

In the following figures the maximum displacements of the three anchor types are compared with each other. The undercut anchor exhibits the smallest displacements in axial and shear direction. The first might be due to the functioning principle (mechanical interlock) and the latter results from the monolithic design of the anchor sleeve. A reduced crack width (0.5 mm) has the decisive effect that no plastic deformations occur.

Expansion anchors tend to pull through failure in cracked concrete with reduced capacity and increased displacements compared to concrete cone breakout. Up to $\alpha/\alpha_{nom} = 3$ the shear displacement of the undercut anchor does not differ from that of the expansion anchor. This might be an indication that damage of the concrete starts from that level. The successively enhanced shear deformation of the expansion anchor compared to the undercut anchor may be explained by the non-monolithic design of the sleeve. For seismic applications an extension of the first segment of the anchor sleeve into the bore hole might be advantageous.

Due to de-bonding of the injection mortar from the bore hole the bonded anchor exhibits the largest axial displacements. The missing sleeve leads to enhanced pressure on the bore hole, an effect which is observed also for cycling tests presented in chapter 4.2. Therefore the bonded anchor undergoes the largest shear displacement.

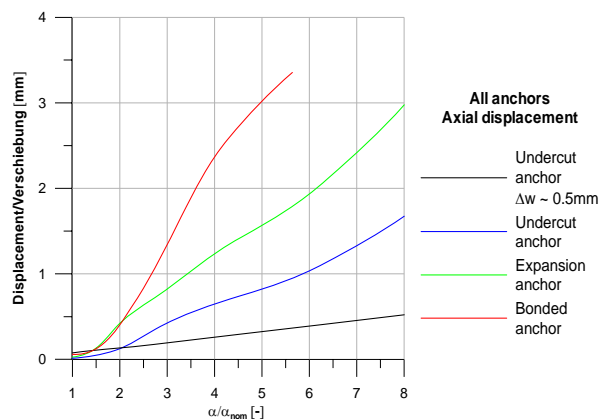


Figure 4.73: Comparison of axial displacements

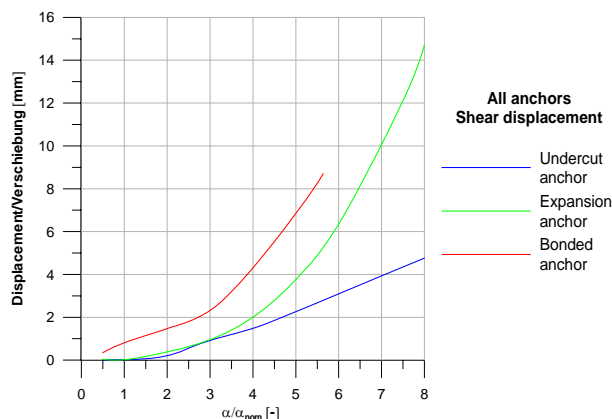


Figure 4.74: Comparison of shear displacements

A possible consideration of the anchor type dependent response for seismic design of post-installed fasteners will be presented in the next chapter. On the base of the results of triaxial shake table testing in *Rieder (2008c)* a practical application of post-installed anchors for seismic retrofitting is analysed and discussed.

4.5 Summary

Cyclic shear loading with increasing amplitude show that the cyclic ultimate load and hysteretic damping depend on anchor type. Undercut anchors confined by a sleeve reach 82% of the static capacity and the investigated bolt-type expansion anchor exhibits only 54% of the ultimate load determined in monotonic tests. Different stresses in the concrete in front of the anchor lead to different cumulative damage of concrete and superposition of shear and bending stresses of the anchor bolt. The rough fracture surface of the steel bolt is similar to that observed in monotonic tests up to failure.

Friction between base plate and concrete increases the average hysteretic damping from 2.5% for no pre-stressing to 5% in case of 50% of nominal torque moment for the expansion anchor in uncracked concrete. The loss of pre-stressing force in cracked concrete is compensated by enhanced probability of micro-cracks resulting in the same damping ratio as in uncracked concrete. Compared to the expansion anchor, the undercut anchor exhibits approximately the double average hysteretic damping ratio in uncracked concrete.

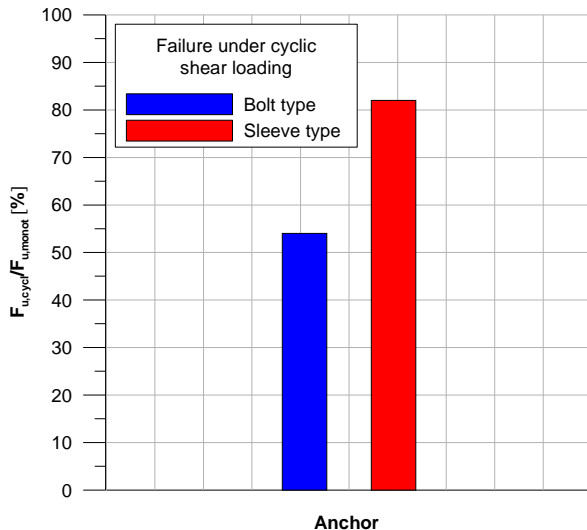


Figure 4.75: Influence of anchor type on cyclic ultimate load

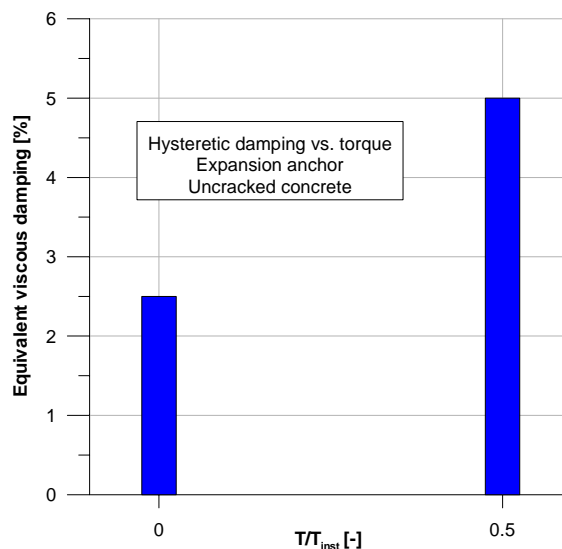


Figure 4.76: Hysteretic damping versus torque moment (expansion anchor)

Since the influence of a more ductile anchor material can be neglected it can be concluded that the main source for hysteretic damping is provided by friction between base plate and concrete for low and medium amplitudes and by damage of concrete at high amplitudes. The inhomogeneous distribution of aggregates might explain the large scatter of test data for hysteretic damping.

Due to irreversible mechanisms, at decreasing amplitudes the memory effect causes slightly enhanced energy dissipation and reduced stiffness. An effective stiffness under seismic shear loading is proposed

which may be assumed equal to 60% of the stiffness determined in monotonic tests. The smooth fracture surface indicating low-cycle fatigue failure legitimates a critical review of current seismic testing protocols.

Uniaxial shake table tests with sinusoidal and various seismic inputs yield a first basis for the assessment of the amplification of acceleration in case of a gap between anchor under shear loading and base plate. While the theoretical upper limit for their relative velocity is represented by the double floor velocity, the resulting maximum acceleration is more complex because it depends upon anchor stiffness, hole clearance and concrete damage. With increasing peak ground acceleration the amplification increases up to an average factor of 2.5 and then a slight decrease occurs which may be due to the first micro-cracks in the concrete leading to plastic deformations and energy dissipation. In order to get a comprehensive understanding of the gap-induced amplification effect, more tests and also with larger sizes up to M24 are necessary.

Triaxial shake table tests with increasing amplitude show that the failure mode of post-installed metal anchors depends on the anchor type. Undercut and expansion anchors fail by excessive axial and shear deformations resulting in steel bolt bending and concrete crushing, whereas the investigated bonded expansion anchor exhibits complete pullout failure. On the base of design limits for interaction a safety margin for each anchor type can be defined for various models.

The undercut anchor shows the smallest deformations for all seismic levels which can be attributed to the working principle in case of axial loads and to the monolithic design of the sleeve in case of shear loads. A positive influence of small axial displacements can be observed in terms of reduced amplification of acceleration. Damage of the concrete in terms of large cracks strongly influences the seismic anchor performance.

The main conclusion from triaxial shake table testing is the identification of anchors which are sensitive to combined axial and shear loading under realistic seismic excitation. This issue cannot be determined by uniaxial shake table testing. It is evident that for economic reasons in future seismic testing protocols not every new product can be tested by this procedure, but in combination with the tests and proposals of *Mesureur (2004)* the results may serve as an additional basis for the establishment of simplified testing guidelines.

5 Modelling of anchors for seismic shear loading

5.1 General

All concrete and steel parts and the interaction of those parts dictate the static strength of a connection. All the factors that affect static connection performance presumably affect the cyclic performance as well, but the reverse is not true. Not all factors that influence cyclic behaviour have an effect on static performance. For this reason the study of cyclic/dynamic loading is of basic interest. Under reversed cyclic loading strength and stiffness are related to load history, i. e. the load-displacement relation of each loading cycle is influenced by the load magnitude of the preceding cycle. Due to this load history (or memory) effect the modelling of anchors subjected to cyclic loading is much more complex than the formulation of a unidirectional load-slip model. Conventional models used to approximate the elastic-plastic behaviour of steel and concrete are not directly applicable for fasteners under shear load, as they do not allow for incorporation of slackness or pinching.

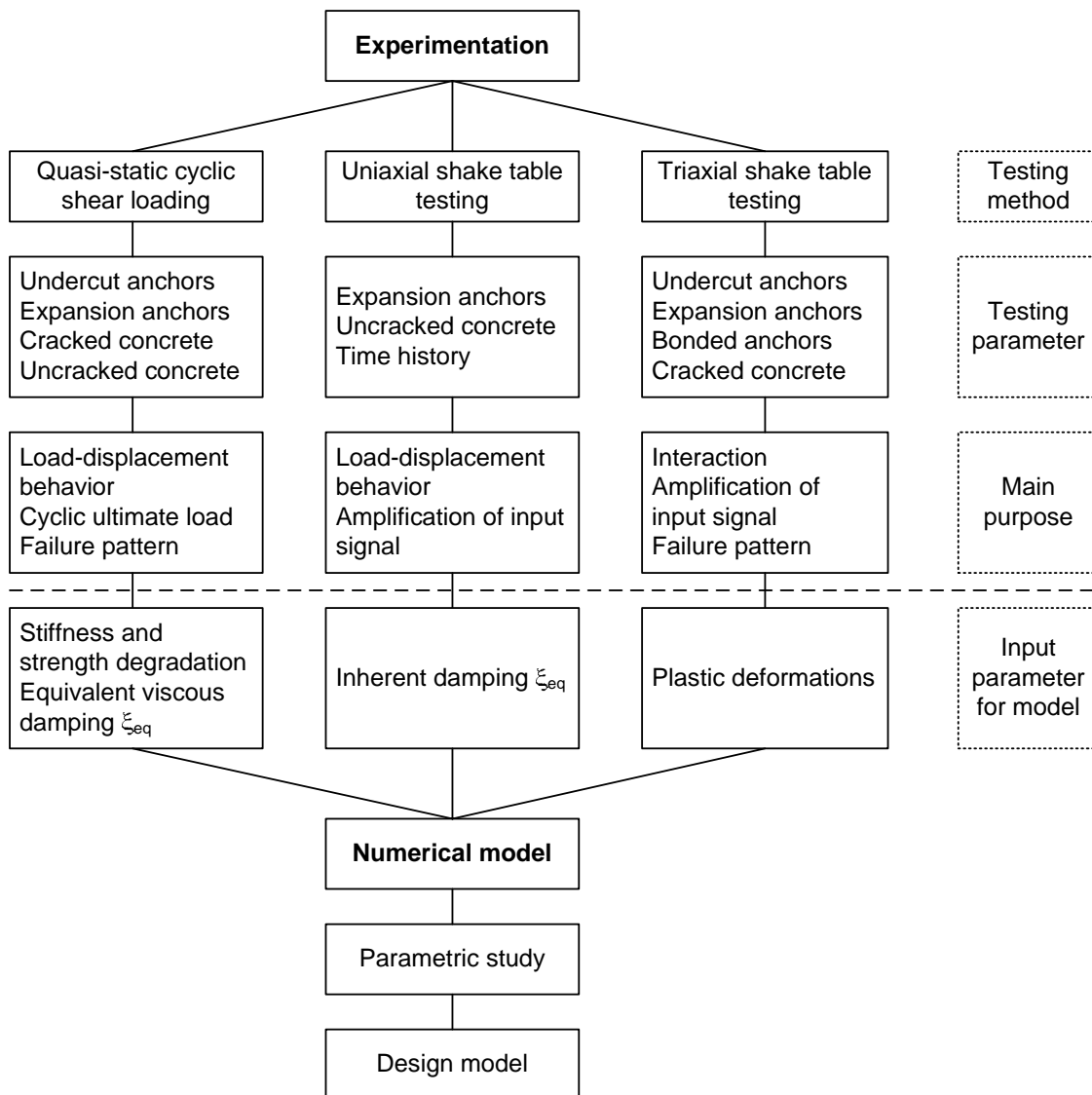


Figure 5.1: Correlation between experimentation and numerical modelling

For this purpose it is the aim to develop a model capable to describe the load-displacement behaviour for cyclic shear loading involving strength/stiffness degradation, plastic deformation and slackness due to hole clearance between anchor and base plate. The link to the experimental investigations from chapter 4 providing the basic parameters is illustrated in Figure 5.1.

5.2 Analytical model

The core of any analytical model attempting to describe the response of cyclically loaded fasteners is the formulation or method that describes the hysteresis. There are many hysteresis formulations that have been advanced by several researchers for specific structural elements and/or structural materials (e.g. column beam connections of reinforced concrete, infill walls, etc.) and for entire structures. The most widely used hysteresis formulations are those that follow a set of rules that specify stiffness functions and transition points for various cases such as loading, unloading, loading after previous loading, etc. The system identification problem consists in estimating parameters that determine a mathematical description of a hysteretic system. Dependent on the number of parameters, the minimization of the difference between experimental results and model output requires high sophisticated numerical tools. An example is a genetic algorithm which was used by *Heine (2001)* to estimate 11 parameters describing the hysteretic behaviour of timber joints.

A less sophisticated model represents a formulation of *Stewart (1987)* who developed a general rule for the representation of timber framed structural walls sheathed in plywood nailed to the framework. The model allows for initial slackness as well as subsequent degradation of the stiffness as the anchor enlarges the holes and withdraws itself from the plywood. An anchor installed in concrete and subjected to cyclic shear load represents the analogue system. The model is shown in the following figures.

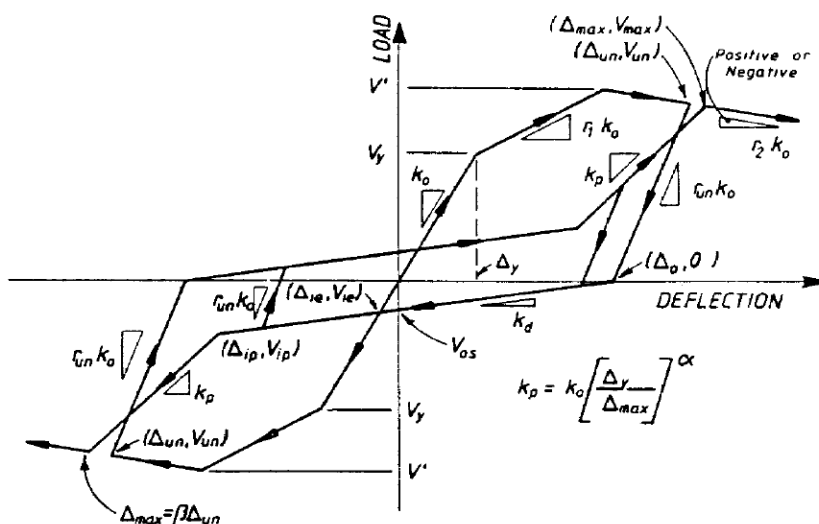


Figure 5.2: Hysteresis model without slackness as utilized by *Stewart (1987)*

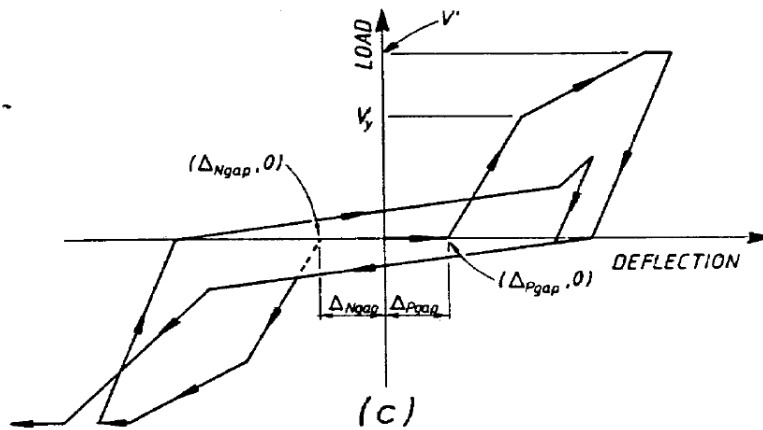


Figure 5.3: Hysteresis model with slackness as utilized by Stewart (1987)

The hysteretic approximation consists of a series of straight-line segments with initial stiffness k_0 until a predefined yield point Δ_y is reached. Stiffness is reduced by a bilinear and tri-linear factor r_1 and then r_2 depending on when unloading occurs. The “pinching stiffness” k_p is expressed in terms of the initial stiffness according to

$$k_p = k_0 \left(\frac{\Delta_y}{\Delta_{un}} \right)^\alpha \quad (5.1)$$

where

$$\Delta_{max} = \beta \cdot \Delta_{un} \quad (5.2)$$

k_0	initial stiffness	[N/m]
k_p	pinching stiffness	[N/m]
k_d	degrading stiffness	[N/m]
r_1, r_2, r_{un}	stiffness parameters	
V'	ultimate force	[N]
Δ_y	yield displacement	[m]
Δ_{un}	displacement where unloading occurs	[m]
Δ_{max}	successive maximum displacement in the respective loading direction	[m]
α	parameter controlling rate of stiffness degradation	
β	softening parameter	
Δ_{Pgap}	initial positive slackness	[m]
Δ_{Ngap}	initial negative slackness	[m]

For a practical application the various parameters are adapted to test data discussed in chapter 4.2 and implemented in the RUAOMOKO finite-element code which has been developed at the University of Canterbury (Carr 2004). The results for increasing amplitude are shown in the following figures. The

shape of the hysteresis and peak load and displacement during the first cycle at the same amplitude match quite well the experiments. However, stiffness degradation stops after the second cycle which may be explained by load controlled cycling instead of displacement controlled cycling. The latter is typically used for numeric analysis of the hysteretic behaviour of structures and/or structural elements. Another lack of the model consists in overestimating the initial stiffness and consequently the hysteretic energy dissipation exceeds the experimental value.

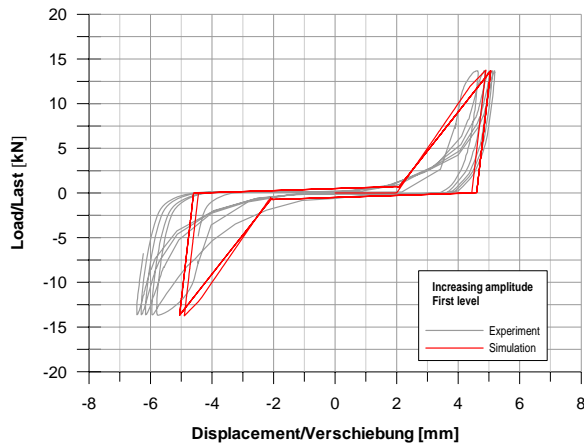


Figure 5.4: 1st sequence at increasing amplitude

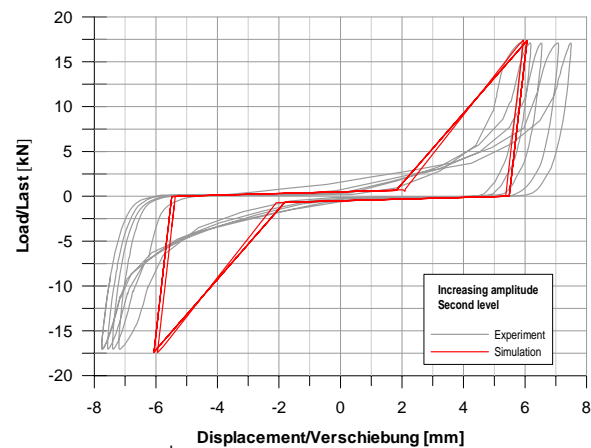


Figure 5.5: 2nd sequence at increasing amplitude

The presented model replicates the response of the entire connection and thus making it case dependent, which means that each new anchor configuration has to be tested first to obtain the necessary input parameters. In contrast to statically stressed connections, very little research has been conducted to determine the cyclic response of the individual components, i.e. steel anchor, concrete and interaction of both. To close the discrepancies between the knowledge of static and cyclic behaviour, a component approach is proposed and developed in terms of a semi-empirical model in the next chapter, where ultimately input variables constitute basic material properties and geometry.

5.3 Semi-empirical model

Objective is the modelling of a post-installed anchor in concrete subjected to static and cyclic shear loads by means of a 2D system of nonlinear springs and beams. The model is calibrated on test data discussed in chapter 4.2 and implemented in the RUAOMOKO finite-element code which has been developed at the University of Canterbury (*Carr 2004*). In a second step it will be used to capture the influence of additional dampers applied on various positions of the system. Time history analysis will provide possibilities for mitigation of seismic induced acceleration. This issue will be developed and discussed in a separate chapter.

5.3.1 Static loading

The concrete is modelled by springs and the anchor by a beam (Figure 5.7). The latter consists of two members in parallel where one member is elastic and the second is elastic or has a perfect hinge at one or both ends of the member (Figure 5.6). Due to the stress concentration at the upper part of the anchor

the distance between the springs is reduced close to the surface of the concrete. By connecting the springs to the beam it is sufficient to model only one side. The hole clearance in the base plate is simulated with parallel springs with specific properties which will be discussed later. In order to enhance the clearness the various springs have the same colour as the load-displacement curve in Figure 5.7.

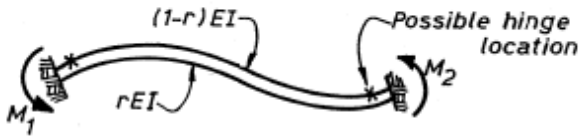


Figure 5.6: Two component beam model (Carr 2004)

Since no specific material model for concrete is implemented and the accurate stress distribution is neglected, the magnitude of the spring stiffness may be estimated according to the following formula:

$$K = \frac{EA}{L} \quad [N/m] \quad (5.3)$$

With

E Modulus of elasticity of concrete
= 30GPa for concrete class C20/25

A cross section of considered part of concrete
= $a \cdot d_s$

Whereas a is the distance between the springs and d_s the bolt diameter

L distance from the anchor where the stress drops to zero
= $20 \cdot d_s$ (assumed value)

These parameters yield a stiffness $k_{01} = 4.5 \cdot 10^6$ N/m for the first spring (representing the concrete edge).

The anchor steel is assumed to behave ideal elastic-plastic with the plastic bending moment M_y calculated according to *Eligehausen (2000)*:

$$M_y = 0.17 \cdot d_s^3 \cdot f_y \quad [Nm] \quad (5.4)$$

With

M_y Plastic bending moment
= 200 Nm

f_y yield strength of bolt material
= 700 MPa (from manufacturer)

d_s bolt diameter

Shear deformations are not suppressed whereby the effective shear area is assumed to 50% of the cross section of the anchor. The rotation at the loading point seems to be a crucial issue because in practice it depends on the hole clearance and thickness of the base plate and hence it may be somewhere between free rotation and fixed rotation. Both extreme cases are analysed in the simulations. For the experiments presented in chapter 4.2 a 10 mm thick base plate is used and hence the eccentricity between concrete surface and loading point amounts to 5 mm. In the simulations a load of 30 kN is applied on the anchor.

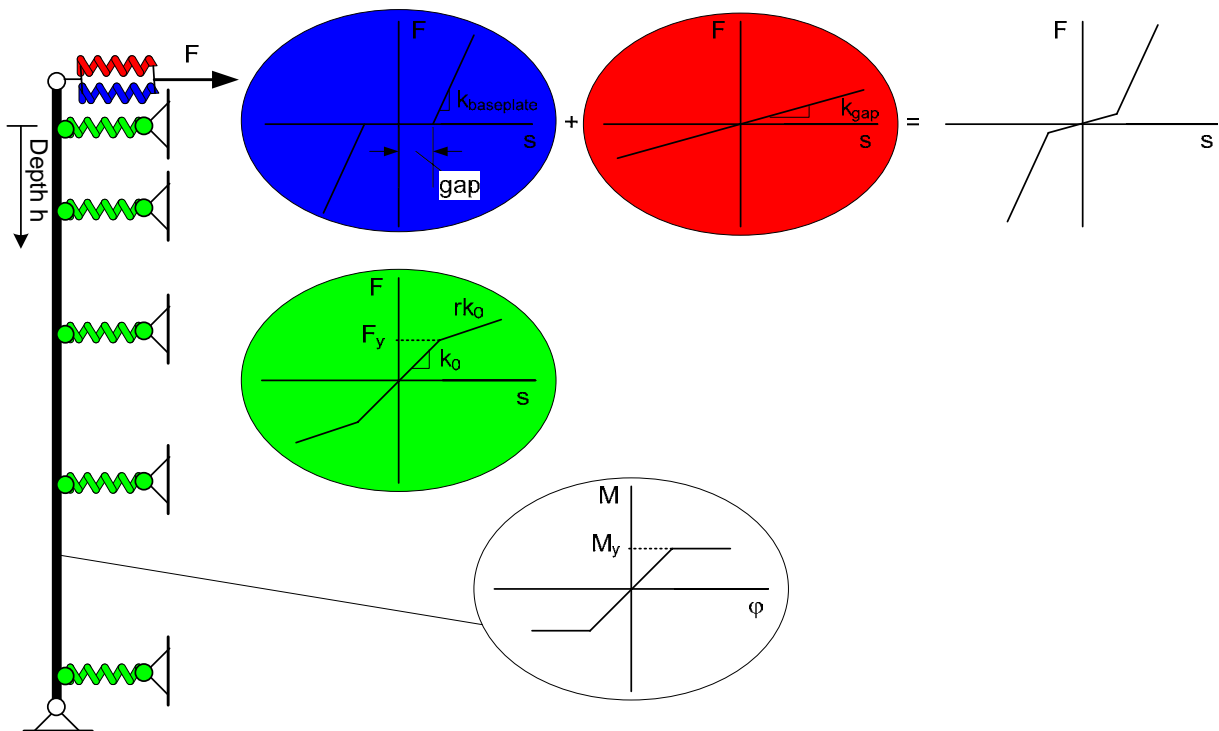


Figure 5.7: RUAUMOKO-model of the anchor under shear load

According to Figure 5.8 the stiffness of the anchor under shear load is too high compared to test results in cracked concrete ($\Delta w = 0.5$ mm). This may be due to the following reasons:

1. The high local stress in front of the anchor lead to enhanced deformation
2. Cracked concrete exhibits reduced stiffness (loading parallel to the crack)

These issues are considered by a reduced area A (8 mm instead of 12 mm) and increased length L ($25 \cdot d_s$ instead of $20 \cdot d_s$) in equation (5.3) leading to better results as it can be seen in Figure 5.9. The initial stiffness of the anchor is captured very well if free rotation at the loading point is assumed. According to chapter 3.2.3 the real behaviour lies between the extremes free and fixed rotation. For reasons of simplicity all following simulations are performed with free rotation boundary condition.

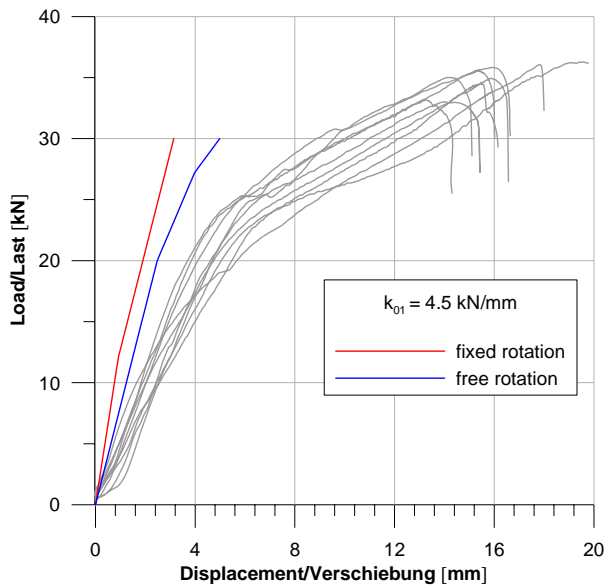


Figure 5.8: Trial stiffness without base plate

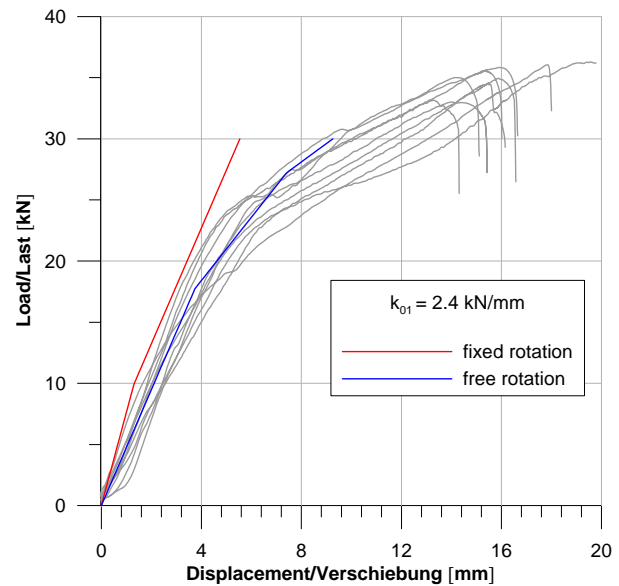


Figure 5.9: Modified stiffness without base plate

The first nonlinearity in Figure 5.9 at 18 kN stems from steel yielding at the position of the third concrete spring (32 mm depth) and agrees very well with the formula proposed by *Fuchs (1992)* given in equation (3.10).

The second nonlinearity at 28 kN is due to yielding of the steel at the position of the first spring (concrete surface) which is not interesting for future analysis. However, it can be clearly seen that yielding starts from a specific depth inside the concrete and moves to the surface.

The missing parameter F_y for yielding of the springs representing the concrete can be estimated from *Fuchs (1992)* who assumes that the concrete compressive strength due to the triaxial stress condition in front of the anchor is equal to $3.5 f_c$. For the model it is assumed that F_y represents the load where the first micro-cracks appear. The results of the simulation with the obtained value $F_y = 5800$ N for different slopes r after yielding are plotted in Figure 5.10. The parameter r describes the plastic stiffness as a fraction of the elastic one and is explain in Figure 5.7. Yielding of the concrete (defined as micro-cracks) takes place at 12 kN and hence before yielding of the steel, a behaviour which is proofed by *Unterweger (2008)* through measurements with an optical interferometer in the sub-micro region. This issue is not relevant for monotonic loading but essential for the analysis of anchors subjected to cyclic shear loads. The latter loading conditions lead to cumulative damage of the concrete with subsequent increasing bending moment of the steel anchor. Therefore the developed model seems to be suitable to describe the seismic behaviour of fasteners under shear loads.

The influence of the slope r after yielding of the concrete is studied in Figure 5.10, whereby decreasing slope leads to slightly decreasing yielding of the steel. By applying $r = 0.5$ the parabolic stress-strain curve of concrete proposed in *EC 2 (2005)* is fitted in a proper way although the system gets a little bit too soft at high loads. For seismic analysis this inaccuracy may be accepted.

Although *CEN/TS (2008)* proposes to avoid hole clearances for seismic applications, in practice usually the diameter of the hole in the base plate is larger than the diameter of the anchor and hence a slack arises between base plate and anchor. The hole clearance is implemented in the model according to Figure 5.7 with two springs in parallel whereas one exhibits very high stiffness indicated as $k_{\text{baseplate}}$ and

a gap in the hysteresis curve and the other one a rather low stiffness k_{gap} . A zero gap stiffness would lead to a singular stiffness matrix. *Zhang (2001)* used a similar model for time history analysis of multiple anchor connections. The stiffness of the baseplate can be estimated with equation (5.3) assuming an area $A = 240 \text{ mm}^2$ and $L = 10 \text{ mm}$, which yields $k_{\text{baseplate}} = 3 \cdot 10^9 \text{ N/m}$. For k_{gap} a stiffness of $7 \cdot 10^5 \text{ N/m}$ is assumed.

The sensitivity of the system with respect to these two stiffness parameters has to be proofed by time history analysis. This issue will be analyzed in one of the next chapters.

The results for static loading are shown in Figure 5.11 for different gaps. In the experimental plots the hole clearance is not visible because a small pre-load is applied before starting the tests.

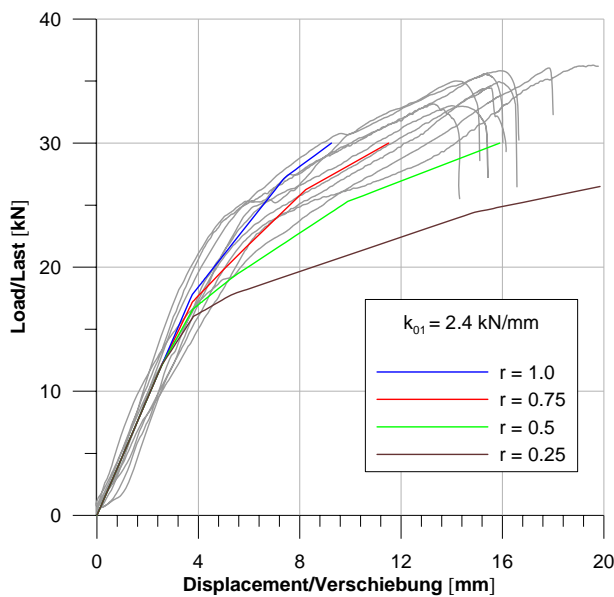


Figure 5.10: Concrete post-yield parameter study

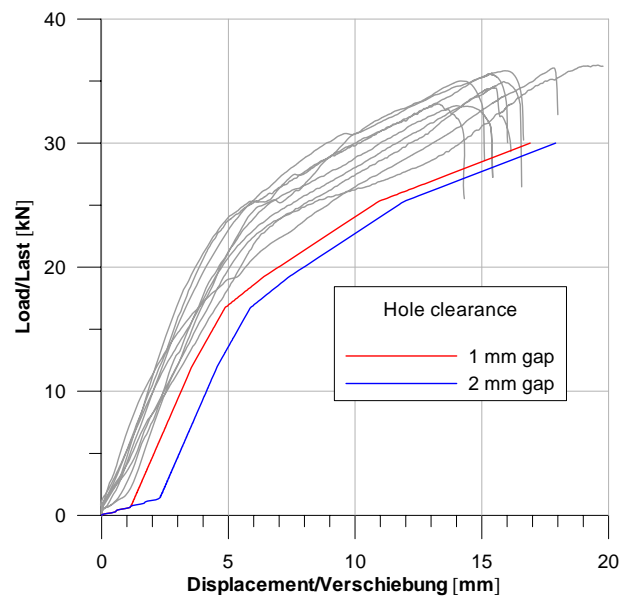


Figure 5.11: Final model with different gaps

5.3.2 Cyclic loading

Cyclic reversed shear loading leads to stiffness or strength degradation whose extent depends upon number of cycles and type of anchor (see Figure 3.17). The formulation of the hysteresis in terms of strength and/or stiffness degradation and pinching is the core of any model attempting to describe the response of cyclically loaded anchors. The simplest way to describe degradation effects is the assumption of a decrease of strength (at yielding) with increasing number of cycles as shown in Figure 5.12. For the application of this general model available in Ruaumoko (*Carr 2004*) the parameters n_1 , n_2 and $F_{y,\text{red}}$ have to be estimated for concrete and possibly also for steel.

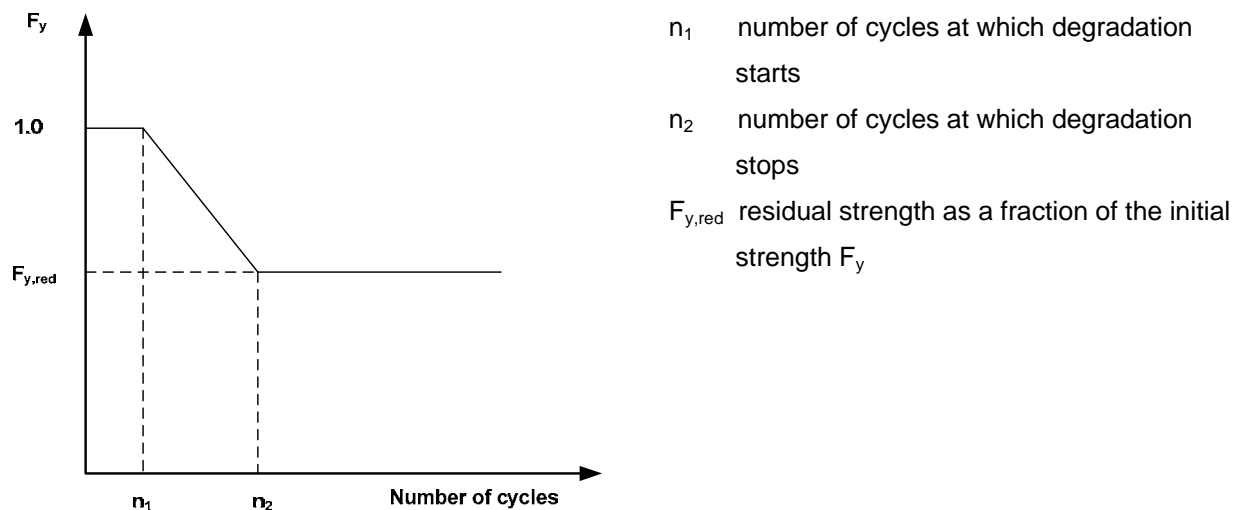


Figure 5.12: Degrading strength model (Carr 2004)

5.3.2.1 Hysteresis with concrete degradation at constant amplitude

The results of a force simulation with the trial values $n_1 = 1$, $n_2 = 10$ and $F_{y,red} = 0.8$ for concrete and no degradation for steel are presented in the Figure 5.13 to Figure 5.16 and compared with test data. The load amplitude is chosen in the way that the steel is close to yielding at the first cycle and consequently the effect of degrading concrete on the behaviour of the steel can be analysed in detail. Unfortunately a very limited data base of cyclic shear tests with all relevant material and testing parameters like concrete and steel strength, thickness of base plate and hole clearance is available. The present test results are taken from tests according to *ACI 2004* which prescribes load-controlled cyclic shear tests with different amplitudes and number of cycles. In order to get yielding in the model the sequence with the highest load is investigated. It corresponds also roughly to the seismic design resistance.

The displacement at peak load is captured very well for each cycle, but at lower loads the model yields too high stiffness during loading and too low stiffness during unloading. The first might be explained by the additional gap between borehole and anchor which varies from 0.5 to 0.8 mm dependent on the diameter of the drill bit. The latter is a weakness of the model and could be solved with a modified hysteresis, i.e. increasing the unloading stiffness after yielding of the springs representing the concrete.

The discussed deviations lead to an inverse evolution of the energy dissipation: with increasing number of cycles the model implicates increasing energy dissipation per cycle but according to the test data the dissipated energy decreases. This behaviour might be explained by an increasing gap due to cumulative damage of the concrete and hence leading to enhanced pinching.

However, due to reduced hysteretic damping (at least during the first three cycles, see Figure 5.13 to Figure 5.15) the model should yield larger accelerations compared to the real behavior and hence more conservative results for seismic analysis. This issue will be discussed in the next chapter.

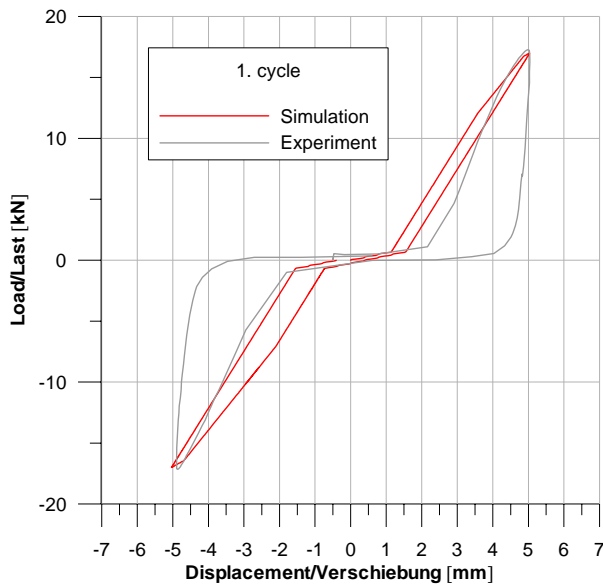


Figure 5.13: Hysteresis at first cycle

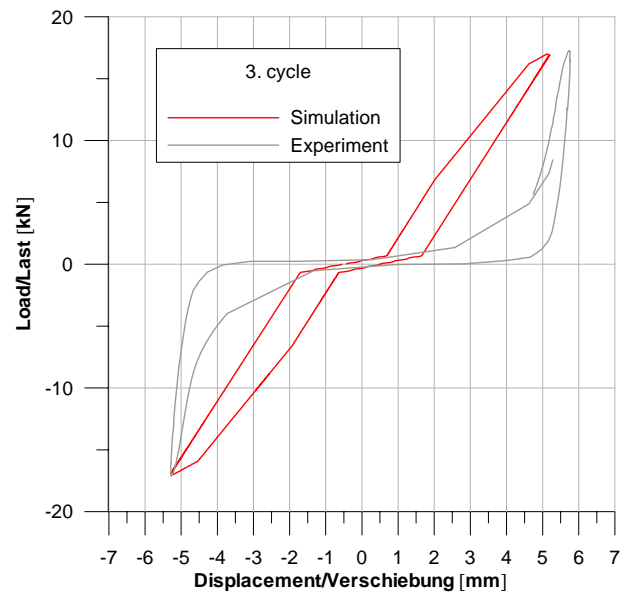


Figure 5.14: Hysteresis at third cycle

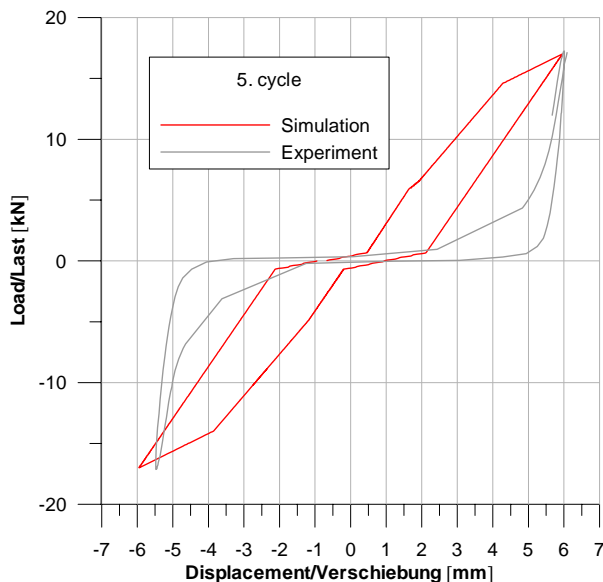


Figure 5.15: Hysteresis at fifth cycle

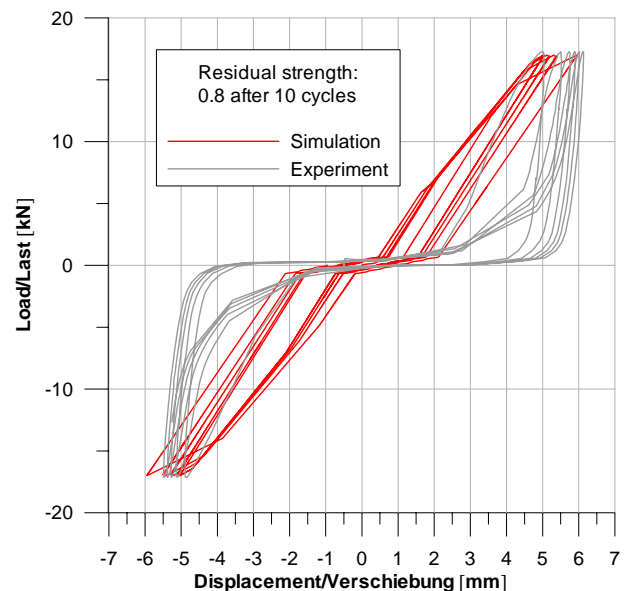


Figure 5.16: Hysteresis at first 5 cycles

In Figure 5.17 and Figure 5.18 the distribution of the acting moment and the curvature are plotted as a function of the distance h to the concrete surface for different cycles. The maximum moment (curvature) and therefore the plastic hinge take place at about $2.5 \cdot d_s$ inside the concrete, a value which corresponds quite well with various models proposed in the literature (*Fuchs 1992*). Outside the plastic hinge there is only a small increase of the moment between the first and fifth cycle, but inside the plastic hinge the curvature increases with growing number of cycles. According to the load-displacement curves this issue reduces the shear load where steel yields, starting from 17.5 kN in the first cycle and finishing at 15 kN in the fifth cycle. This effect is the basis for the plastic strain dependent on number of cycles and hence the cumulative damage of the steel leading to low-fatigue failure of the anchor at higher load amplitudes.

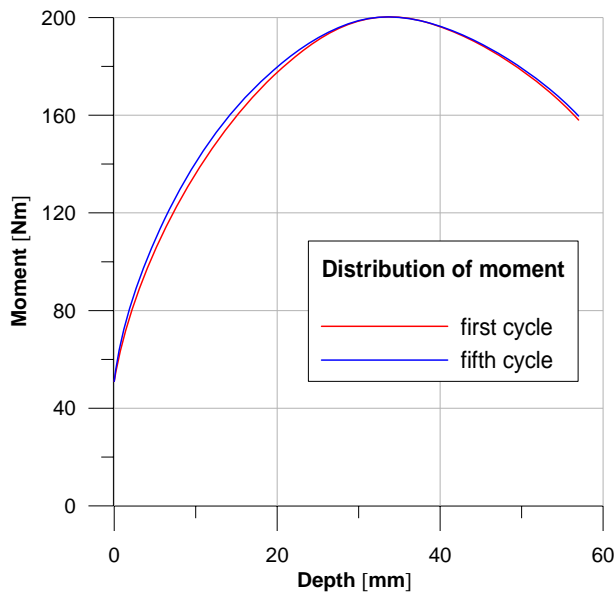


Figure 5.17: Moment acting on anchor

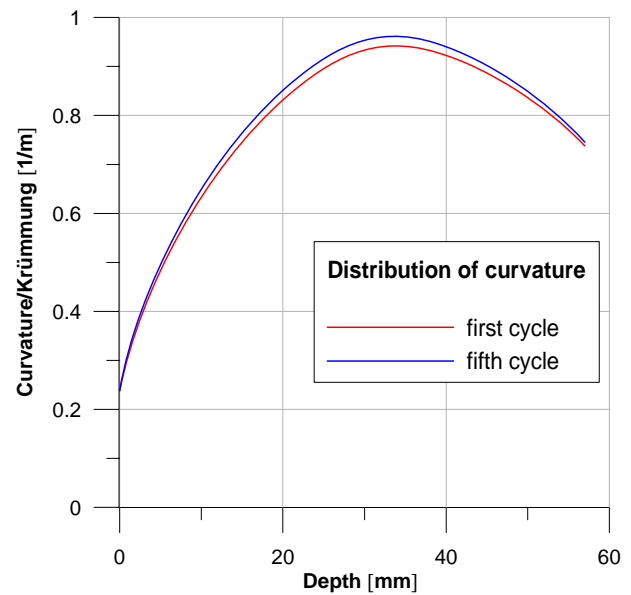


Figure 5.18: Curvature of anchor

5.3.2.2 Hysteresis with steel degradation

Due to the objective of modelling the hysteresis and not the ultimate load of the system it does not seem to be a crucial issue to consider steel degradation which might occur by initiation and growth of cracks. The only possibility of degrading strength during the first cycles is represented by the Bauschinger effect which is shown schematically in Figure 5.19 for an ideal elastic-plastic material and symmetric behaviour, i.e. the strength degradation $\Delta\sigma_y$ is identical for compression and tension. In a technical material the strength degradation parameter depend strongly upon chemical composition, heat treatment and load history. Time dependent strain aging effects may influence the behaviour after a strong earthquake which causes steel yielding (*Momtahan 2009*).

The additional strain demand in case of the simple model may be estimated by the following formula:

$$\Delta\varepsilon = \frac{\Delta\sigma_y}{\tan \alpha} = \frac{\Delta\sigma_y}{E} \quad (5.5)$$

With

E Modulus of elasticity [MPa]
 = 210000 MPa

$\Delta\sigma_y$ = 150 MPa (equivalent to a reduction of 20% for the material used in the model)

The additional strain per cycle is the double of $\Delta\varepsilon$ and amounts to 0.15% on the basis of the assumed values. This lies in the same range as the elastic strain and therefore the additional damage may be neglected in the case of low number of cycles ($n < 10$). More interesting is the effect on the hysteresis of the whole system which is analysed for two different steel degradation factors, whereas no concrete degradation is assumed.

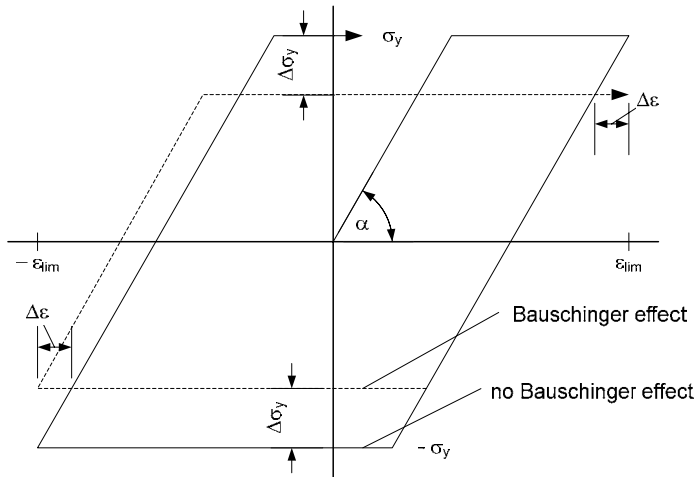


Figure 5.19: Idealised Bauschinger effect

It is not possible to implement the Bauschinger effect (i.e. degradation starting in the compression branch) in the steel hysteresis model; therefore the same strength degradation model as for concrete is used but with different parameters. Steel degradation starts after the first cycle and stops after the second one at 90% resp. 80% of the initial strength. According to Figure 5.20 and Figure 5.21 increasing steel degradation lead to slightly enhanced peak displacement and to considerable increased energy dissipation. The latter seems to be overestimated since the model without steel degradation matches the test results properly. Therefore the Bauschinger effect is neglected for future analysis.

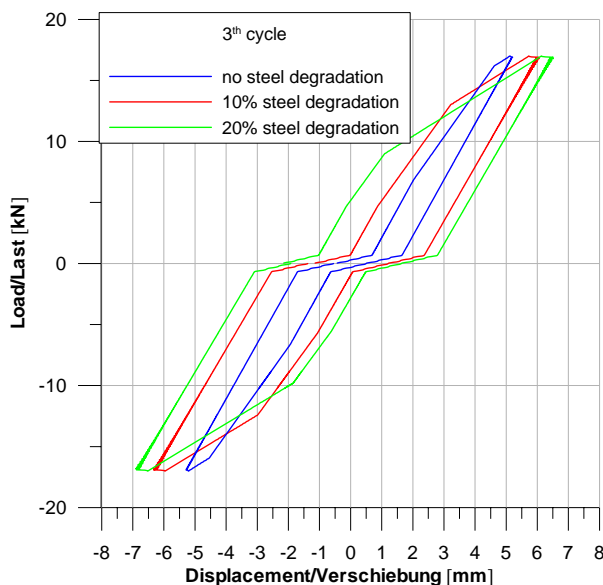


Figure 5.20: Third cycle with steel degradation

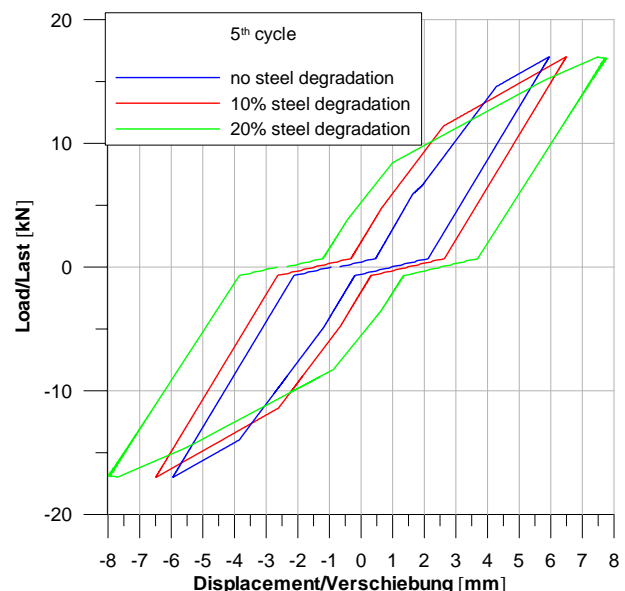


Figure 5.21: Fifth cycle with steel degradation

For a detailed analysis of the Bauschinger effect specific tests would be necessary which enable the investigation of the steel behaviour separated from the concrete (e.g. cyclic bending test without concrete block). Focussing of future research work on this issue could explore innovative, even though sophisticated possibilities to enhance the hysteretic damping by modification of the steel properties and consequently to mitigate seismic induced acceleration on non-structural elements.

5.3.2.3 Hysteresis with concrete degradation at variable amplitude

All the simulations up to now are performed with constant load amplitude. Since a typical seismic action consists of various amplitudes with arbitrary sequence the influence of increasing and decreasing loads is investigated using the model with concrete degradation. According to the available experimental data each sequence for both increasing and decreasing amplitude consists of 5 cycles with constant amplitude. In order to improve the clearness only one sequence is illustrated in the following figures.

Peak displacements are captured with sufficient accuracy by the model in case of increasing amplitude, but energy dissipation is underestimated for low loads and overestimated at higher loads. In case of decreasing amplitude the already mentioned memory effect can be observed, i.e. after load reduction the displacement does not decrease proportionally by the expected amount. The system “remembers” the deformation which occurred at higher loads and consequently the model predicts too small displacements and also too small hysteretic damping after load reduction.

The main weakness of the model is therefore represented by the missing memory effect arising from decreasing load amplitudes.

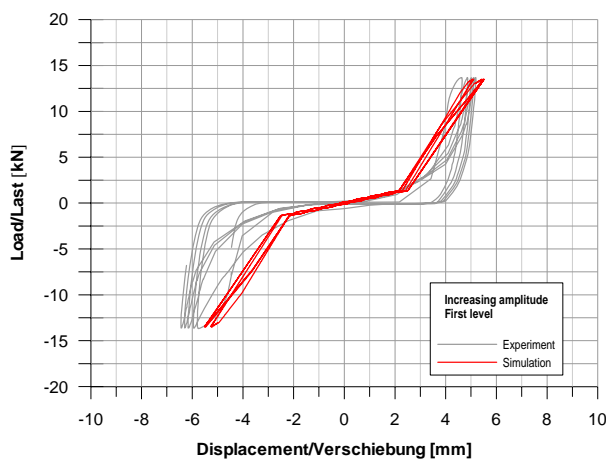


Figure 5.22: 1st sequence at increasing amplitude

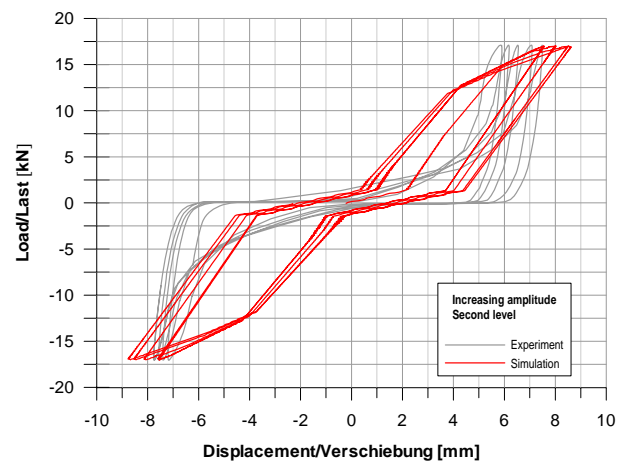


Figure 5.23: 2nd sequence at increasing amplitude

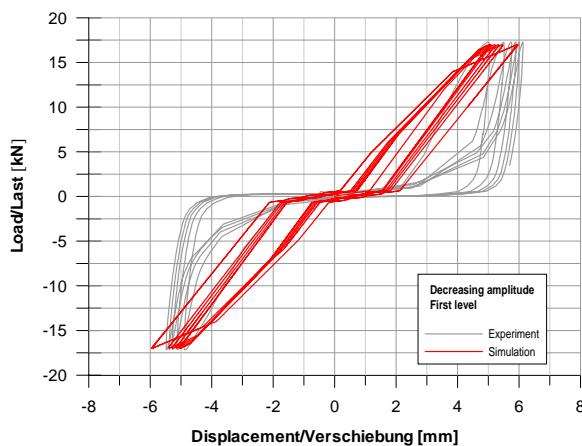


Figure 5.24: 1st sequence at decreasing ampl.

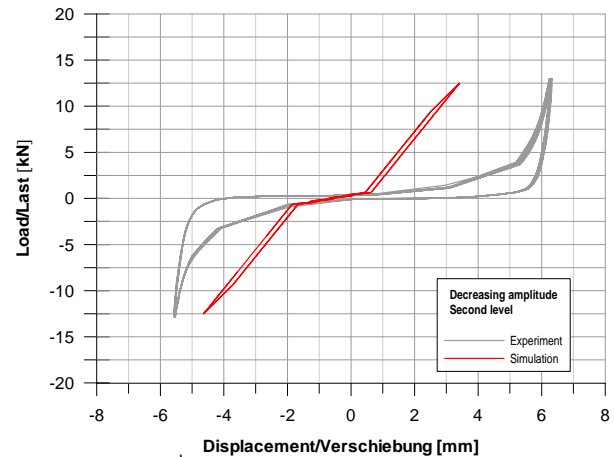


Figure 5.25: 2nd sequence at decreasing amplitude

5.4 Comparison of the two models

Various analytical hysteresis models for structures and/ or materials are available today which can be easily implemented in a software program. However, the behaviour of specific elements or combination of elements like a fastening system cannot be captured in a satisfactory way because the properties of the different parts and materials (steel and concrete) must be addressed and modelled specifically. Therefore the “component” approach in terms of a semi-empirical model is much more efficient to simulate the hysteretic energy dissipation, strength and stiffness degradation.

The proposed model has to be calibrated for the following parameter:

- Type of anchor (bolt or sleeve)
- Concrete condition (cracked/uncracked)
- Concrete strength

A variation of these three parameters for fixed anchor size and steel strength enables all possible combinations of these parameters including also steel strength and anchor size. For the analytical model presented in chapter 5.2 each new configuration has to be tested first to obtain the necessary input parameters. Due to the large variety of combinations this is not practicable either economic.

The main advantage of the proposed model consists in the easy implementation of additional damping elements at specific locations of the fastening system. This issue will be treated in detail in chapter 6 for different damping systems.

5.5 Time history analysis

5.5.1 General

On the basis of the developed semi-empirical hysteresis of the anchor subjected to cyclic shear loading, within this chapter time history analysis is performed with various accelerograms. The system as configured in Figure 5.7 has one degree of freedom (DOF). For the integration of the dynamic equation of equilibrium the unconditionally stable Newmark constant average acceleration method is used (Carr 2004). During the time step Δt from time t to $t + \Delta t$ the acceleration is assumed to be constant

$$\ddot{u} = \frac{\ddot{u}(t) + \ddot{u}(t + \Delta t)}{2} \quad (5.6)$$

Integrating with respect to time over the time step Δt to get the velocity and displacement and rearranging to use the increment in the displacement Δu as the variable gives the increment in the acceleration

$$\Delta \ddot{u} = \ddot{u}(t + \Delta t) - \ddot{u}(t) = \frac{4\Delta u}{(\Delta t)^2} - \frac{4\dot{u}(t)}{\Delta t} - 2\ddot{u}(t) \quad (5.7)$$

and the increment in the velocity as

$$\Delta \dot{u} = \dot{u}(t + \Delta t) - \dot{u}(t) = \frac{2\Delta u}{\Delta t} - 2\dot{u}(t) \quad (5.8)$$

Substitution into the equation of equilibrium at time $t + \Delta t$ gives

$$[M]\{\ddot{u}(t) + \Delta \ddot{u}\} + [C]\{\dot{u}(t) + \Delta \dot{u}\} + [K]\{u(t) + \Delta u\} = \{P(t + \Delta t)\} \quad (5.9)$$

Noting that the stiffness term may be rewritten as

$$[K(t + \Delta t)]\{u(t) + \Delta u\} = [K(t)]\{u(t)\} + [K_T]\{\Delta u\} = \{F_{Elastic}(t)\} + [K_T]\{\Delta u\} \quad (5.10)$$

with

$[K(t)]$	secant stiffness matrix at time t
$\{F_{Elastic}(t)\}$	nodal equivalent of the member forces at time t
$[K_T]$	current tangent stiffness matrix

Similarly the damping term may be rewritten

$$[C(t + \Delta t)]\{\dot{u}(t) + \Delta \dot{u}\} = [C(t)]\{\dot{u}(t)\} + [C_T]\{\Delta \dot{u}\} = \{F_{Damping}(t)\} + [C_T]\{\Delta \dot{u}\} \quad (5.11)$$

With

$\{F_{Damping}(t)\}$	nodal damping forces at time t
$[C_T]$	current tangent damping matrix

Therefore the equation of equilibrium may be rewritten in the form

$$[M]\{\Delta \ddot{u}\} + [C_T]\{\Delta \dot{u}\} + [K_T]\{\Delta u\} = \{P(t + \Delta t)\} - [M]\{\ddot{u}(t)\} - \{F_{Damping}(t)\} - \{F_{Elastic}(t)\} \quad (5.12)$$

Substitution for the increments of acceleration and increments of velocity in terms of the increments leads to the equation

$$\begin{aligned} \frac{4}{(\Delta t)^2} [M] + \frac{2}{\Delta t} [C_T] + [K_T]\{\Delta u\} &= \{P(t + \Delta t)\} + [M]\left\{\ddot{u}(t) + \frac{4}{\Delta t}\dot{u}(t)\right\} \\ + 2[C_T]\{\dot{u}(t)\} - \{F_{Damping}\} - \{F_{Elastic}\} & \end{aligned} \quad (5.13)$$

If the damping matrix is constant, i.e. does not change with time, this equation may be simplified to give the following equation

$$\frac{4}{(\Delta t)^2} [M] + \frac{2}{\Delta t} [C_T] + [K_T] \{\Delta u\} = \{P(t + \Delta t)\} + [M] \left\{ \ddot{u}(t) + \frac{4}{\Delta t} \dot{u}(t) \right\} + \{F_{Damping}\} - \{F_{Elastic}\} \quad (5.14)$$

This equation may be solved for the incremental displacements. The displacement, velocity and acceleration vectors can now be updated and the member forces at time $t + \Delta t$ computed giving the elastic force vector and the damping force vector at the new time step can also be computed. After updating the damping and stiffness matrices the above sequence is repeated for the next time step.

The crucial issue hereby consists in finding the proper time step Δt so that an adequate accuracy is achieved for reasonable computing time. According to Carr (2005) it should be less than 0.1 of the period of the highest mode of free vibration that contributes significantly to the response of the structure. Additionally, the time step should not be larger than the time step at which the earthquake accelerogram is digitized.

For time history analysis the Rayleigh or Proportional damping model is used where the structure damping matrix C is given by

$$[C] = \alpha[M] + \beta[K] \quad (5.15)$$

with

[M] mass matrix

[K] stiffness matrix

The coefficients α and β are computed to give the required levels of viscous damping at two different frequencies, most commonly those of the first and second modes of free vibration. For the analysis of the anchor subjected to seismic shear loads only the first mode is relevant. According to Figure 5.26 the natural frequency increases the amount of damping almost linearly with frequency.

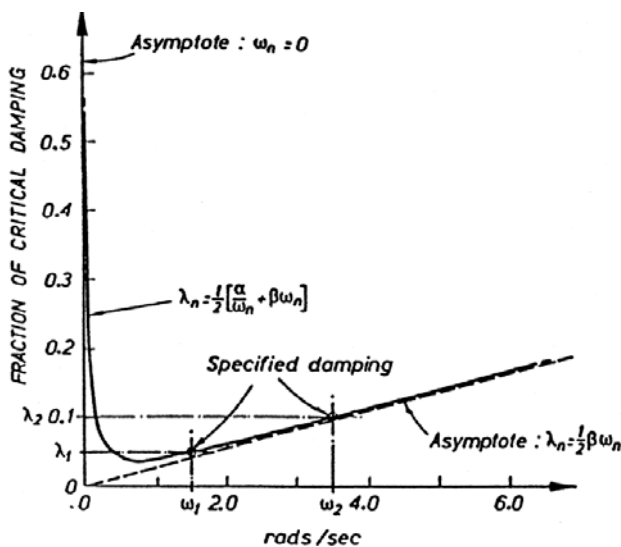


Figure 5.26: Rayleigh or Proportional damping model (Carr 2005)

For the calculation of the damping matrix the initial elastic stiffness matrix and hence a constant damping is used. As the structure yields resulting in a decrease in the stiffness, then the fractions of critical damping in the structure increase. In case of large plastic deformations extra damping is provided by member hysteresis. These two effects may lead to an overestimation of damping forces, but since only small inelastic deformations are expected and the assumed viscous damping is rather low (see next chapter) this issue does not seem to have a significant impact on the final results.

5.5.2 Calibration of the model

The main task of time history analysis is the calibration of the damping factors in terms of fraction of critical damping on the basis of the uniaxial shake table test results discussed in chapter 4.3 and the implementation in the final model. In Figure 5.27 the results of a damping parameter study are compared with test data for the Cape Mendocino record scaled to different peak ground acceleration, whereas the ordinate represents the maximum amplification of the attached mass. A trial simulation with 3% and 10% of critical viscous damping yields too high values for low peak ground acceleration. This indicates that the friction cannot be neglected although it is very small. The total friction force $F_{Friction}$ may be estimated according to the tests from chapter 4.3:

$$F_{Friction} = F_{Friction,baseplate} + F_{Friction,rollers} [N] \quad (5.16)$$

With

$F_{Friction,baseplate}$ friction between concrete and base plate
= 100 N (from tests)

$F_{Friction,rollers}$ friction between attached mass and substructure
= 100 N (from tests)

Friction is modelled by an ideal elastic-plastic spring between base plate and concrete (see Figure 6.12) with high stiffness (about double the overall anchor stiffness) that yields at a force of 200 N. For reasons of simplicity the static friction is assumed to be equal to the dynamic friction which is independent on the velocity. Good agreement with the test results is achieved assuming 3% of critical viscous damping. This value agrees also with the test results presented in chapter 4.2 where it is shown that the average hysteretic damping for load amplitudes up to 20 kN in uncracked concrete and no torque moment amounts to 2.5% of critical equivalent viscous damping (s. Table 4.2). The inherent damping ξ_{inh} from equation (4.4) may be interpreted as the sum of 0.5% viscous damping and friction damping between base plate and concrete addressed in equation (5.16). Thus, the present model represents a helpful tool to predict the seismic response if specific conditions (e.g. hole clearance, additional damping elements, accelerogram) are changed.

Time history analysis with varying $k_{baseplate}$ shows that the system is not sensitive with respect to this parameter, e.g. reducing $k_{baseplate}$ to 1% of the initial value changes the acceleration only about 10%. A variation of k_{gap} between $0.7 \cdot 10^5$ and $9 \cdot 10^5$ N/m leads to a change of the simulated acceleration of the

baseplate by about $\pm 15\%$. In light of the expectable large scatter of seismic data these deviations may be acceptable.

In Figure 5.28 the simulated response for the Cape Mendocino record is compared with the whole set of experimental data from chapter 4.3 where also higher accelerations are measured. Base plate accelerations beyond 0.7 g (corresponding to an anchor load of approximately 12 kN, see chapter 5.3.1) lead to yielding of the surrounding concrete. On this base the yielding curve within the Cartesian coordinate system used in Figure 5.28 is defined by $x \cdot y = 0.7$ which describes a hyperbola.

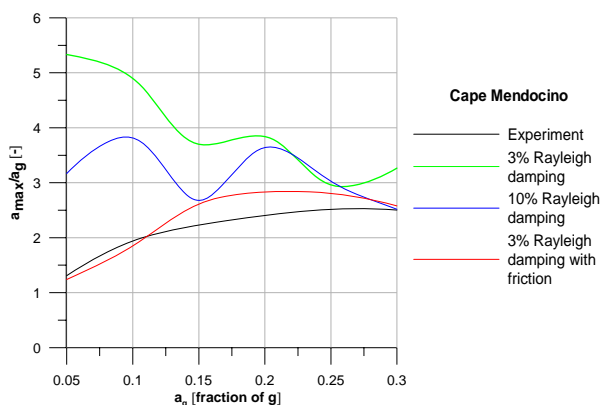


Figure 5.27: Calibration of damping parameter

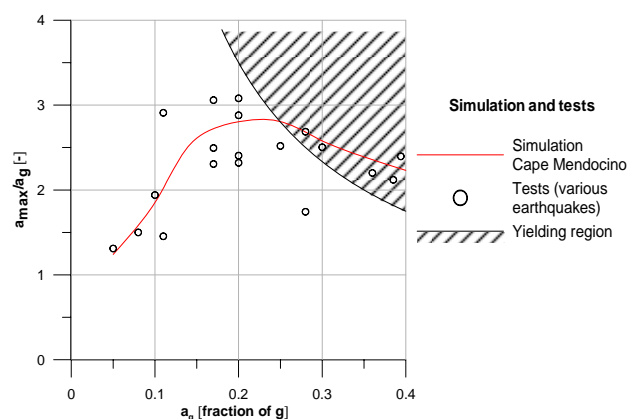


Figure 5.28: Simulation and test results

The shaded region indicates yielding in case of no inherent or added damping. Any additional damping shifts the yielding region towards higher values. The effect of reduced maximum amplification when plastic deformations occur will be discussed more detailed in the next chapter. The simulated response for the Cape Mendocino record represents an acceptable average curve of all the experimental values obtained from different earthquakes.

5.5.3 Influence of hole clearance

Although it is proposed in *CEN (2004)* to avoid gaps between anchor and base plate for seismic applications, it does not seem to be possible without special measures (e.g. filling the gap with mortar). For practical applications the typical hole clearance depends on anchor diameter and lies between 1 mm and 3 mm if an economic design according to *EOTA (1997)* is performed. However, in many cases it may be beyond these limits due to enhanced convenience during installation. Taking into account this issue simulations are carried out with hole clearance between zero and 5 mm. Larger values do not seem to be relevant for practical applications. The results are plotted in Figure 5.29 for different peak ground accelerations, whereby the hole clearance is defined according to equation (5.20). In all simulations a symmetric hole clearance (i.e. the same gap on both sides) is assumed. For zero gap no friction is considered and thus simulating the worst case in practical applications.

The lowest earthquake level does not seem to be representative because the inertia forces are not much larger than the friction force and hence it will be neglected for further analysis. For zero gap the amplification is independent of seismic level and equivalent to the spectral amplification γ_{spec} which will be discussed later. With increasing hole clearance the curves show a clear trend towards a maximum

amplification at a gap of 1.5 mm and a subsequent stabilisation. However, for larger gaps the scatter increases.

The positive influence of yielding is shown in Figure 5.30 where the maximum amplification decreases when the yielding point is reached. The maximum ductility at the various seismic levels and corresponding gaps is listed in Table 5.1.

Table 5.1: Maximum ductility

gap [mm]	2.5	2	1.5	1	2.5	2	1.5	2	1.5
a_g	0.35	0.35	0.35	0.35	0.3	0.3	0.3	0.25	0.25
ductility	1.5	1.22	1.3	1.17	1.26	1.37	1.16	1.13	1.04

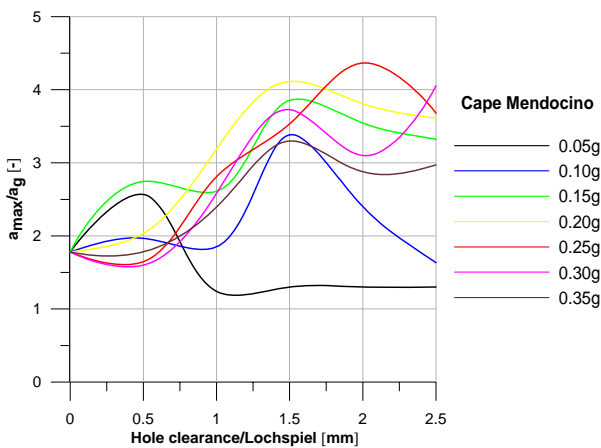


Figure 5.29: Influence of hole clearance

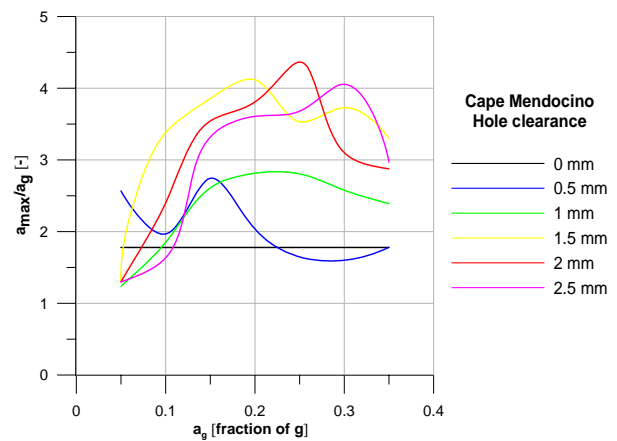


Figure 5.30: Influence of PGA

According to the experimental results from chapter 4.3 different earthquakes lead to different acceleration on the base plate. In order to provide a more comprehensive basis for the assessment of a fastening system with slackness additional simulations are performed with the artificial time history according to *IEEE 693 (1997)* and with the Friulli earthquake record (1976). The response (see next figures) shows a similar trend as for the Cape Mendocino record, i. e. increasing hole clearance implicates enhanced acceleration. However, the Friulli record exhibits more scatter.

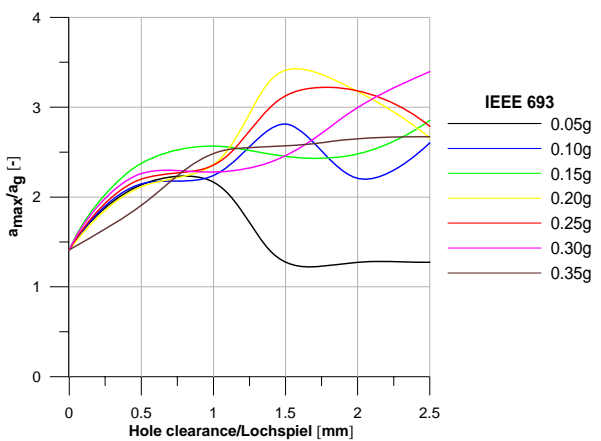


Figure 5.31: Hole clearance for IEEE record

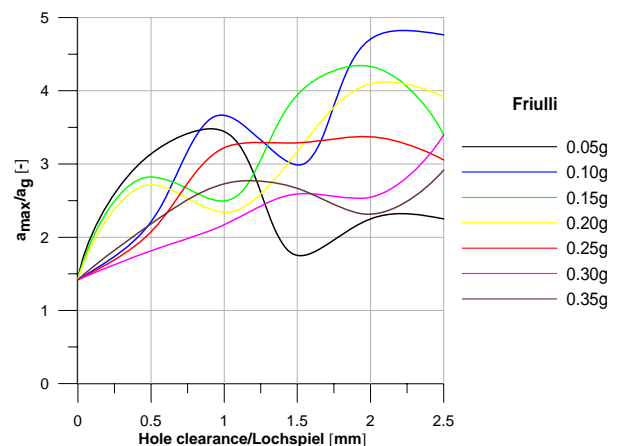


Figure 5.32: Hole clearance for Friulli record

The effect of asymmetric gap, i.e. presence of gap only in one direction is also investigated for a few representative parameters. The results suggest that the most critical case is represented by a symmetric gap.

Simulations with a smaller mass indicate a reduced amplification. An increase of the mass of the attached element could also influence the hammer effect. But since the used mass represents the design situation for pure seismic shear loading a further increase is not allowed and hence the investigated system yields the most conservative values. The trial tests with a larger anchor size (M16) and the same mass presented in chapter 4.3 indicate that increased anchor stiffness does not influence significantly the maximum amplification. However, additional tests and simulations may be necessary in order to ensure the results for the available range of anchors from M8 to M24.

In order to be able to compare the different earthquakes it is necessary to separate the spectral response factor γ_{spec} and the hammer effect factor γ_{gap} in case of a hole clearance between anchor and base plate. The spectral response factor γ_{spec} can be taken directly from the diagrams for hole clearance equal to zero. The total amplification γ_{tot} is known and can be calculated as

$$\gamma_{tot} = \gamma_{spec} \cdot \gamma_{gap} \quad (5.17)$$

From this equation the hammer effect factor γ_{gap} can be determined for each time history and hole clearance. The results are plotted in Figure 5.33 including all three time histories and all corresponding seismic levels. This evaluation should guarantee a comprehensive analysis of the seismic induced hammer effect. The mean value increases linearly until a gap of 1.5 mm and then remains constant. The coefficient of variation between 13% and 25% reflects the large variety of input parameters and should enable the formulation of a statistical representative design proposal.

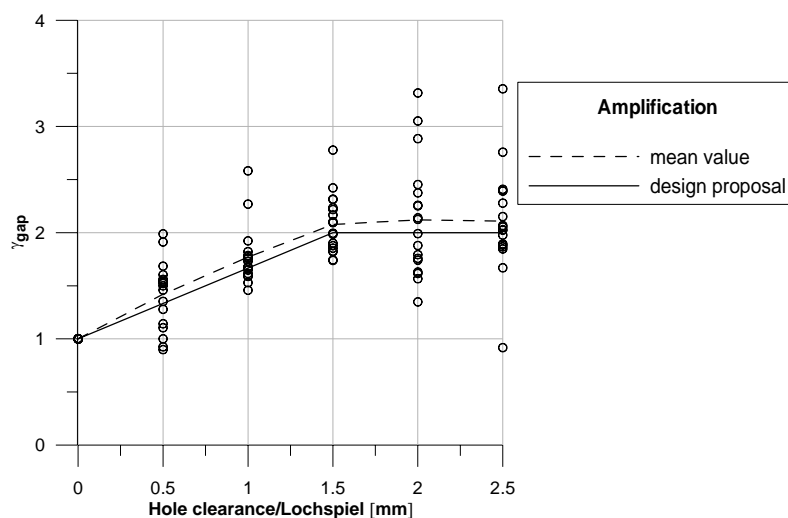


Figure 5.33: Gap dependent amplification

5.5.4 Design model for hammer effect

5.5.4.1 Single anchors

On the basis of the presented simulations and test results a proposal is presented to consider the hammer effect in case of a gap between anchor and base plate. This may be implemented in the *CEN/TS (2004)* by an additional factor γ_{gap} for the calculation of the seismic action

$$F_a = \frac{S_a \cdot W_a \cdot \gamma_a \cdot \gamma_{gap}}{q_a} [N] \quad (5.18)$$

With

$$\begin{aligned} \gamma_{gap} &= \frac{2}{3} \cdot \Delta + 1 && \text{for } 0 \leq \Delta \leq 1.5 \text{ mm} \\ &= 2 && \text{for } 1.5 < \Delta \leq 2.5 \text{ mm} \end{aligned} \quad (5.19)$$

and

$$\Delta = \frac{d_f - d_{nom}}{2} \quad (5.20)$$

Whereas

d_f diameter of clearance hole in the fixture [mm]

d_{nom} outside diameter of anchor in the fixture [mm]

5.5.4.2 Anchor groups

Since the presented design proposal is valid for single anchors the question arises how multiple connections might be affected in case of a gap between base plate and anchors. The positions of the anchors are distributed uniformly between zero and $2 \cdot \Delta$. On the base of a probabilistic approach the density function and the expected mean value for the minimum gap of a group consisting of N anchors can be calculated (*Tamparopoulos 2009*).

Let u_1, u_2, \dots, u_N be independent random variables, all have the same uniform distribution over the interval $[0, 2 \cdot \Delta]$. Let

$$m = \min(u_1, u_2, \dots, u_N) \quad (5.21)$$

Then the cumulative density function $F_m(x)$ is described by

$$F_m(x) = \begin{cases} 0 & x < 0 \\ 1 - \left(1 - \frac{x}{2\Delta}\right)^N & 0 \leq x \leq 2\Delta \\ 1 & x > 2\Delta \end{cases} \quad (5.22)$$

And the probability density function $f_m(x)$ by

$$f_m(x) = \frac{dF(x)}{dx} = \begin{cases} 0 & x < 0 \\ \frac{N}{2\Delta} \left(1 - \frac{x}{2\Delta}\right)^{N-1} & 0 \leq x \leq 2\Delta \\ 0 & x > 2\Delta \end{cases} \quad (5.23)$$

The mean value m is obtained through

$$m = \int_{\mathfrak{R}} x \cdot f_m(x) dx = \int_0^{2\Delta} \frac{N \cdot x}{2\Delta} \left(1 - \frac{x}{2\Delta}\right)^{N-1} dx \quad (5.24)$$

Substitution by $y = 1 - x/2\Delta$ yields

$$m = N \cdot 2\Delta \int_0^1 y^{N-1} (1 - y) dy \quad (5.25)$$

This integral can be solved analytically:

$$m = N \cdot 2\Delta \left(\frac{y^N}{N} - \frac{y^{N+1}}{N+1} \right) \Big|_0^1 \quad (5.26)$$

Finally, the mean value for the minimum gap of the group is reduced to the simple form

$$m = \frac{2\Delta}{N+1} \quad (5.27)$$

This calculation does not consider rotation of the base plate or a random position of an anchor perpendicular to the direction of loading. Therefore the result is on the safe side. In the following table the minimum gap of anchor groups and the corresponding amplification factor γ_{gap} are listed for practical combinations of N and Δ .

Table 5.2: Amplification factor for anchor groups

N	Δ [mm]	m [mm]	γ_{gap}
2	0.5	0.33	1.22
2	1	0.67	1.44
2	1.5	1.00	1.67
2	2	1.33	1.89
2	2.5	1.67	2.00
4	0.5	0.20	1.13
4	1	0.40	1.27
4	1.5	0.60	1.40
4	2	0.80	1.53
4	2.5	1.00	1.67
6	0.5	0.14	1.10
6	1	0.29	1.19
6	1.5	0.43	1.29
6	2	0.57	1.38
6	2.5	0.71	1.48
8	0.5	0.11	1.07
8	1	0.22	1.15
8	1.5	0.33	1.22
8	2	0.44	1.30
8	2.5	0.56	1.37

5.5.5 Conclusions for seismic tension loading

Although the analysis focuses on seismic shear loading the question arises how much the hammer effect influences the behaviour of anchors under tension loading. For this task it is necessary to estimate the maximum plastic deformation induced by seismic tension forces. Within this context it may be useful to have a look at the crack cycling test according to ETAG 001 (*EOTA 1997*) for non-seismic applications. In order to be qualified the maximum allowable displacement after 1000 crack openings is 3 mm. This displacement is composed by an elastic and a plastic part. Dependent on stiffness of the anchor the plastic part lies between 2 mm and 2.5 mm and thus corresponding to a gap $\Delta = 1$ mm. It should be mentioned that these values are limits for acceptance criteria and not for serviceability during life time.

A more realistic assessment could be achieved by analysis of seismic tests. The seismic qualification testing method according to *ACI (2004)* for tension loads yields (plastic) displacements in the range between 2 mm and 3 mm. Cracks are assumed to exhibit a width of 0.5 mm.

Seismic crack cycling tests in 0.8 mm wide cracks proposed by *Hoehler (2006)* with resulting displacements up to 15 mm for expansion anchors seem to be on the very safe side from the testing point of view. Nevertheless, time history analysis with a practically unrealistic gap $\Delta = 7.5$ mm show almost no hammer effect and therefore it does not seem to be critical.

The most realistic displacement under seismic tension loads may be deduced from the test results presented in chapter 4.4. According to these tests the interaction limit is reached at different seismic levels $\alpha/\alpha_{\text{nom}}$ dependent on the type of anchor. The corresponding displacements are taken from Figure 5.34 and on the base of equation (5.19) the amplification factors $\gamma_{\text{gap,calc}}$ can be calculated. The typical resonance frequency of an anchor in tension loaded with a mass of 300 kg as used in the shake table can be estimated on the base of anchor stiffness given in *Bergmeister (1998)*. Since the resulting

frequency exceeds 30 Hz the spectral amplification γ_{spec} is negligible according to Figure 4.59. This can also be seen in Figure 5.35 at low seismic levels where almost no displacement occurs. The (average and rounded) experimental results in the same figure show good agreement with the calculated values in Table 5.3 for the undercut and the expansion anchor, but the bonded anchor exhibits reduced amplification with respect to the predicted one. This may be due to the large plastic deformations and related energy dissipation which partially compensates the gap-induced amplification. These results are only valid for the investigated products and anchor sizes.

As already discussed in chapter 4.4 the crack width plays a significant role for the seismic performance of fasteners. This issue is evident in the figures below in terms of increased acceleration and plastic deformation of the undercut anchor in large cracks ($\Delta w = 1.5 \text{ mm}$).

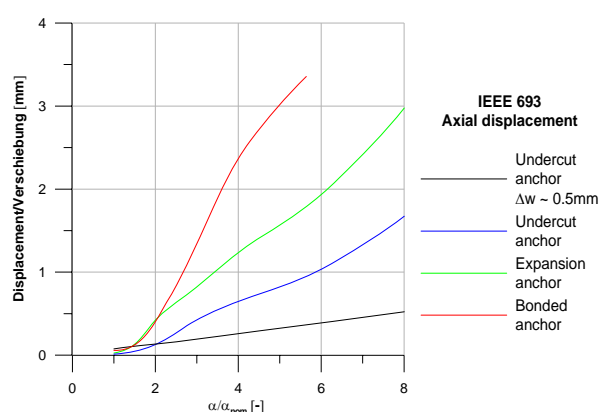


Figure 5.34: Axial displacements, shake table test according to IEEE 693

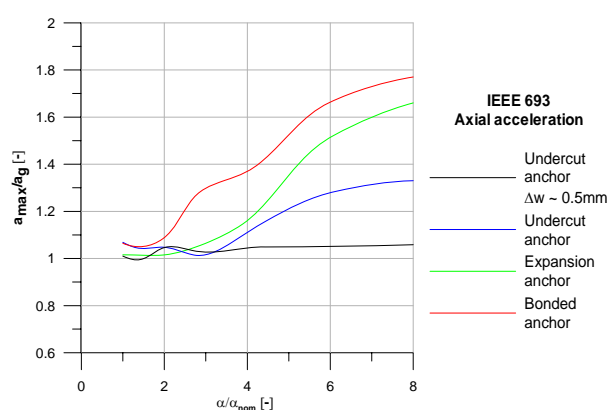


Figure 5.35: Axial accelerations, shake table test according to IEEE 693

Table 5.3: Anchor type dependent hammer effect (tension)

Anchor type	$\alpha/\alpha_{\text{nom}}$	s_{max} [mm]	Δ [mm]	$\gamma_{\text{gap,calc}}$	$\gamma_{\text{gap,test}}$
Undercut anchor	6	1	0.5	1.3	1.3
Expansion anchor	5	1.5	0.75	1.5	1.4
Bonded anchor	5	3	1.5	2.0	1.5

The increased displacement of expansion anchors (bolt and sleeve type) relative to undercut anchors is confirmed also by investigations of *Hoehler (2006)* with cycling cracks. However, the severe testing conditions do not seem to yield realistic displacements.

The proposed values for $\gamma_{\text{gap,calc}}$ of Table 5.3 are on the safe side for the following reasons:

1. The tests are performed in concrete with 1.5 mm wide cracks. Recent investigations of *Hoehler (2006)* suggest crack widths of 0.8 mm outside of plastic hinges at yielding of steel reinforcement. Therefore less displacement may be expected.
2. During the tests the seismic level is increased stepwise which leads to cumulative damage of the anchors resp. bonding and hence increased plastic axial deformation.
3. Potential energy dissipation due to friction and/or plastic deformation with resulting reduction of acceleration is not considered.

The proposed factor $\gamma_{\text{gap,calc}}$ may be interpreted as an anchor type dependent safety factor for seismic tension loading. It should be noted that this factor may vary between anchors from different producers. Especially in the case of bonded anchors many different anchor rod geometries and types of adhesives are available. Therefore the present investigations and conclusions represent a first step towards an anchor type specific seismic design of post-installed fasteners.

5.6 Real behaviour versus experimental and numerical studies

The seismic action on anchors in a real structure depends on several parameters and might be rather complex. Usually groups of anchors are used where one part may experience cracked concrete and the other part uncracked concrete (e.g. the probability that the anchors attaching the non-structural element in Figure 5.36 close to the beam-column joint are in cracked concrete is much higher than for those far away from the joint). Thus, different stiffness and load distribution on the different anchors occur. If the secondary structure itself is designed for yielding under seismic excitation the effective resonance frequency changes and may have an impact on the hole system consisting of fasteners, fixture and secondary structure.

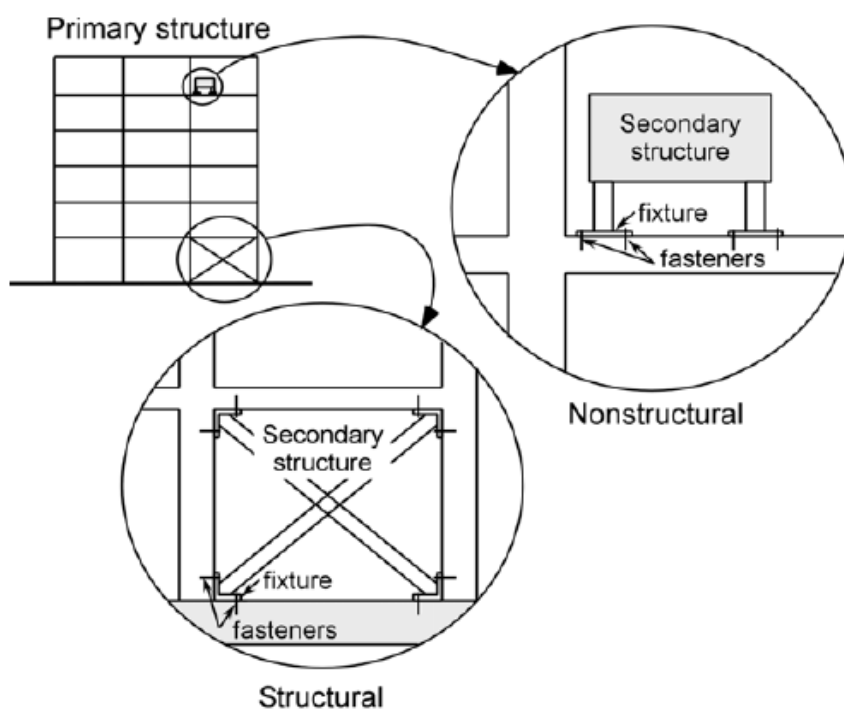


Figure 5.36: Anchors in a real structure (Hoehler 2006)

It is therefore evident that experimental testing (including quasi-static cycling, uniaxial and triaxial shake table testing) and numerical simulation represents a strong idealisation and simplification of the real situation. Nevertheless, a combination of experimental and numerical methods can give a decisive contribution in improving the knowledge and understanding of the response of post-installed anchors in concrete.

5.7 Summary

The “component” approach in terms of a semi-empirical model where concrete and steel are modelled separately is more efficient than the analytic model in simulating the hysteretic energy dissipation, strength and stiffness degradation of a fastener under shear loading. The various stiffness parameters are calibrated on static and cyclic tests with constant and variable amplitude. Peak load and displacement for cyclic loading at constant and increasing amplitude are captured with sufficient accuracy. The hysteretic damping is underestimated during the first cycles and especially in the case of decreasing load amplitudes due to the missing memory effect within the model. This leads to larger accelerations and hence more conservative results for seismic analysis.

The positive influence of plastic deformations in terms of micro-cracks in the concrete resulting in reduced amplification of the input signal is proven by experimental testing for various earthquake records and confirmed by simulated response on the base of the semi-empiric model.

The assumed effective damping in terms of 3% critical Rayleigh damping for time history analysis is consistent with the results obtained from quasi-static cyclic loading and uniaxial shake table testing. For seismic levels up to 0.25 g potential friction between concrete and base plate cannot be neglected although it is very low. Special effort is given in modelling the gap between anchor and base plate which has a significant influence on the amplification of the seismic input. On the base of a parametric study with a set of seismic records a design proposal for the modification of seismic shear action is presented which takes into account the gap dependent amplification of acceleration for practical hole clearances 2Δ between anchor and base plate. For single anchors the seismic action is increased by the factor $\gamma_{\text{gap}} = 2/3 \cdot \Delta + 1$ for Δ between zero and 1.5 mm and $\gamma_{\text{gap}} = 2$ for Δ between 1.5 mm and 2.5 mm. Additionally, a probabilistic based analytic approach for the calculation of amplification for anchor groups is presented which enables the determination of the minimum gap of the group dependent on hole clearance and number of anchors.

On the base of the numerical results and those of 3D shake table testing a proposal for an anchor type depending amplification factor in case of seismic axial loading is presented for undercut anchors, expansion anchors and a specific bonded expansion anchor. This factor may be interpreted as an anchor type dependent safety factor in seismic hazardous zones.

6 Mitigation of seismic induced shear loads

6.1 Introduction

The extent of damage on non-structural elements due to anchorage shear failure and/or excessive acceleration observed in previous earthquakes (*Silva 2001*) has confirmed the urgent need to develop more advanced fasteners capable of decreasing the expected damage to the attached element and fastener itself, without ideally requiring any repairing or substitution after a seismic event. Based on the model of a standard anchor in chapter 5.3 it is the aim to develop an innovative type of fastener or fastener component capable to mitigate accelerations on the fastened object (non-structural element) subjected to low-to-high levels of earthquake ground motions and consequently to reduce the resulting damage to fastener and/or concrete.

Basically, the ductility factor adopted in the codes for non-structural elements in compliance with *CEN/TS (2004)* intends to include all type of inelastic behaviour occurring during the vibration of the non-structural element itself. If the fastened element itself is considered as a rigid element, as it is often the case, the inelastic and dissipative mechanism should rely upon the inherent ductility and damping of the fastener itself. If the connection between a non-structural element and the supporting structure includes some form of additional damping, the acceleration in the mounted element can be reduced, furthermore reducing the force in fastener itself.

It is thus evident that the formula presented by code is not able to neither deal with nor quantify this phenomenon properly. More comprehensive studies are needed to investigate the behaviour of non-structural elements when the fastener behaves as a yielding element, which generates some hysteretic damping, or when some additional viscous or frictional damping is added to the fastener.

In order to meet this goal, among the various possibilities of damping devices available today only passive energy dissipation systems seem to be suitable due to the relatively low cost for implementation and operation. For seismic applications in engineering structures they are implemented since the mid-1990 (*Symans 2008*). The principle function of a passive energy dissipation system is to reduce the inelastic energy dissipation demand on the framing system of a structure and hence resulting in reduced damage to the framing system. Various passive energy dissipation devices are either commercially available or under development. The most commonly used devices include viscous fluid dampers, viscoelastic solid dampers, metallic dampers and friction dampers according to Figure 6.1 wherein the basic device construction, the idealized hysteretic response and associated physical model, and the major advantages and disadvantages are shown. Passive energy dissipation devices can be classified in three categories:

1. rate-dependent devices
2. rate-independent devices
3. others

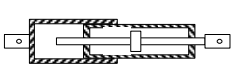
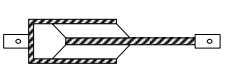
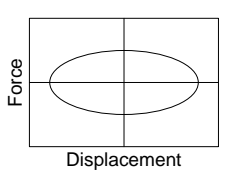
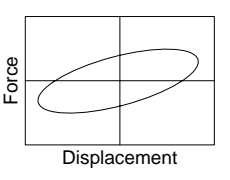
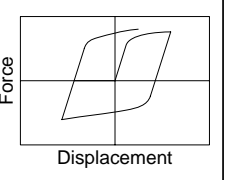
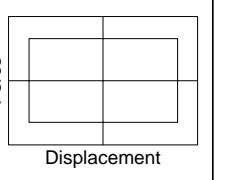
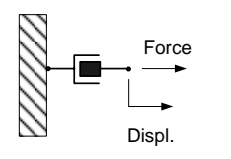
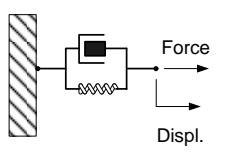
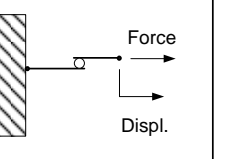
	Viscous fluid damper	Viscoelastic solid damper	Metallic damper	Friction damper
Basic construction				
Idealized hysteretic behavior				
Idealized physical model			Idealized model not available	
Advantages	<ul style="list-style-type: none"> - Activated at low displacements - Minimal restoring force - For linear damper, modeling is simplified - Properties largely frequency and temperature independent 	<ul style="list-style-type: none"> - Activated at low displacements - Provides restoring force - Linear behavior, modeling is simplified 	<ul style="list-style-type: none"> - Stable hysteretic behavior - Long term reliability - Insensitivity to ambient temperature - Materials and behavior familiar to practising engineers 	<ul style="list-style-type: none"> - Large energy dissipation per cycle - Insensitivity to ambient temperature
Dis-advantages	<ul style="list-style-type: none"> - Possible fluid seal leakage (reliability concern) 	<ul style="list-style-type: none"> - Limited deformation capacity - Properties are frequency and temperature dependent - possible debonding and tearing of viscoelastic material (reliability concern) 	<ul style="list-style-type: none"> - Device damaged after earthquake; may require replacement - Nonlinear behavior; may require nonlinear analysis 	<ul style="list-style-type: none"> - Sliding interface conditions may change with time (reliability concern) - Strongly nonlinear behavior; may excite higher modes and require nonlinear analysis - Permanent displacements if no restoring force mechanism is provided

Figure 6.1: Commonly used passive energy dissipation devices (after Symans 2008)

Rate-dependent devices provide a force output which is dependent on the rate of change of displacement and can be described using various models of linear viscoelasticity and realised by fluid dampers and solid dampers. Viscoelastic fluid dampers generally exhibit minimal stiffness and thus they have no significant influence on the fundamental natural frequency. Viscoelastic solid dampers, on the other hand, exhibit stiffness to the extent that the dampers will influence the natural frequencies of the system.

Rate-independent devices consist of dampers whose force output depends upon the magnitude of displacement. This behaviour is commonly described using various nonlinear hysteretic models that are implemented in commercially available software programs. Examples of such dampers include metallic

and friction dampers, whereas the first are characterized by smooth hysteretic behaviour associated with yielding of mild steel and the latter exhibit essentially bilinear hysteretic behaviour with very high initial stiffness.

The degree to which a certain device is able to meet this requirement depends on the inherent properties of the structure, the properties of the device and its connecting elements, the characteristics of the ground motion and the limit state being investigated. Due to the large variations in each of these parameters it is usually necessary to perform an extensive suite of nonlinear response-history analysis to determine which particular passive energy dissipation system is best suited for a given case.

The damage in a structural component or non-structural element can be quantified via a damage measure (DM) given by (*Symans 2008*)

$$DM = \frac{\mu_{Demand}}{\mu_{Capacity}} + 4\rho \frac{E_{Demand}}{E_{Capacity}} \quad (6.1)$$

where

μ_{Demand}	maximum displacement ductility demand
E_{Demand}	cumulative hysteretic energy dissipation demand
$\mu_{Capacity}$	ductility capacity
$E_{Capacity}$	hysteretic energy capacity for one full cycle of inelastic deformation
ρ	calibration factor (material dependent, selected to produce a damage measure value of 0.0 when the component is undamaged and 1.0 when the damage is severe, i.e. near or at anticipated collapse)

Damage measure values beyond 0.4 are generally considered unacceptable for structures or structural components (*Symans 2008*). Since fasteners are expected to behave linearly during the design earthquake, the concept of damage measure may only be adopted in case of overloading due to e.g. very near-fault events, general uncertainties on the action side (a_g is exceeded with 10% probability in 50 years), complex amplification between main structure and non-structural element), poor anchor design or unfavourable load redistribution. The latter may be expected in case of fastening of statically undetermined non-structural elements like pipes (*Hoehler 2007*).

The energy dissipation demand of a fastener subjected to seismic shear loads is equal to the cumulative hysteretic energy dissipated by the surrounding concrete and the steel rod in case of yielding. This energy represents one part of the total energy demand in the system, whereas the complete energy balance at time t is given by (*Uang 1990*)

$$E_I(t) = E_S + E_K + E_D + E_H \quad (6.2)$$

Where

E_I	cumulative input energy
E_S	instantaneous strain energy stored by the component

E_K	instantaneous kinetic energy of the moving mass
E_D	cumulative viscous damping energy
E_H	cumulative hysteretic energy

At the end of the earthquake ($t = t_f$) the kinetic energy is zero, the strain energy is zero for an elastic system (and zero or near zero for an inelastic system), and the cumulative hysteretic energy is equal to the energy demand, i.e. $E_H(t_f) = E_{\text{Demand}}$. The damage measure of equation (6.1) indicates that damage to the element can be reduced by decreasing the ductility or hysteretic energy demand or by increasing the ductility or hysteretic energy capacity. For a fastener it does not seem to be economically feasible to increase the ductility or hysteretic energy capacity (e.g. by using a hyper-elastic alloy, so-called shape memory alloy), therefore the performance may only be improved by reducing the ductility or hysteretic energy demand.

If a passive energy dissipation device in form of a viscous fluid damper is used, the reduction in ductility demand is facilitated through displacement reductions. In case of metallic yielding devices the reduction in ductility is provided by reduced displacements that arise from increased stiffness of the system and from hysteretic energy dissipation within the devices. Therefore the energy dissipation demand is partially transferred from the fastener to the passive energy dissipation devices which can be separated in a viscous damping energy and hysteretic energy term according to equation (6.2) as follows

$$E_D = E_{D, \text{Fastener}} + E_{D, \text{Devices}} \quad (6.3)$$

$$E_H = E_{H, \text{Fastener}} + E_{H, \text{Devices}} \quad (6.4)$$

with

$E_{D, \text{Fastener}}$	viscous damping energy that is inherent in the fastener
$E_{D, \text{Devices}}$	added damping from passive energy dissipation devices
$E_{H, \text{Fastener}}$	hysteretic energy dissipated by the fastener
$E_{H, \text{Devices}}$	energy dissipated by the added passive energy dissipation devices

The effect of additional damping applied on structures is discussed in *Symans (2008)* in detail and can be transferred easily to a fastening system. It is shown schematically in Figure 6.2a where two demand spectra are shown: one for the fastener with 3% nominal inherent damping (on the base of the results of chapter 4.2.2) and the other for a fastener with additional viscous damping from a damping system. If the fastener were assumed to remain elastic (which is the usual case), the performance point would lie along the line marked T_1 where T_1 represents the fundamental period of the non-structural element in the direction of consideration. Accounting for inelastic behaviour, the performance point lies along the line marked T_{1D} where T_{1D} represents the effective fundamental period based on the secant stiffness. In this case the effective damping coefficient B_{1D} has contributions from three components: (1) inherent damping β_i of the fastener at or just below yield; (2) hysteretic damping β_H at the amplitude of interest; and (3) added viscous damping β_V .

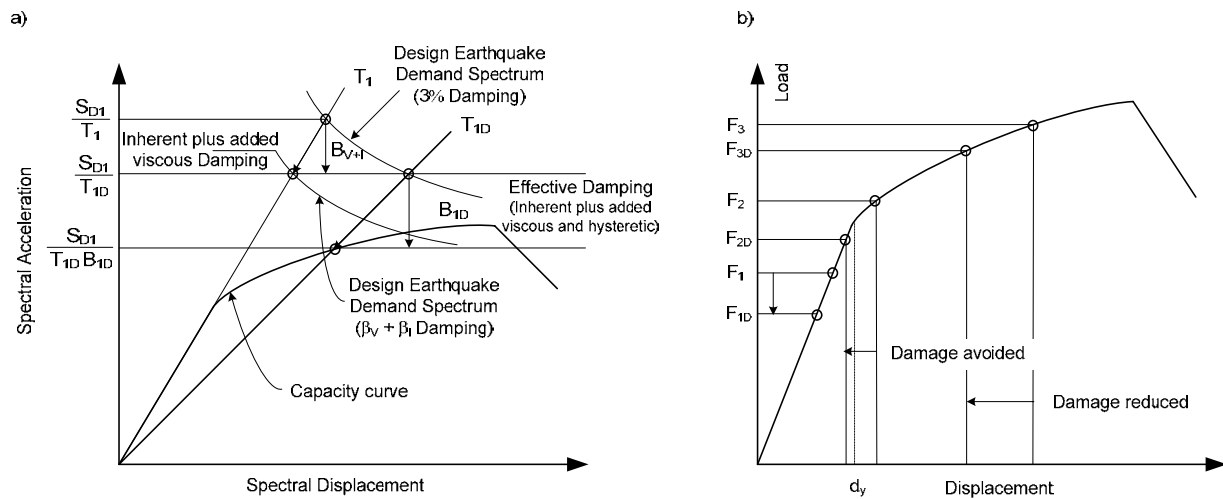


Figure 6.2: Effect of added damping: a) Reduction of design demand (after *Symans 2008*), b) Various load cases

Since design of fasteners usually is load based as already mentioned, i.e. a linear behaviour is expected, the main advantage of added damping consists in reducing the acceleration of the attached non-structural element. Additional advantage may be achieved in case of seismic overloads which can lead to plastic deformations in the anchor itself, in the concrete or in the attached element. This damage can be reduced or even prevented by use of a damping device. Therefore the effect of additional damping applied on a fastening system can be classified according to Figure 6.2b:

1. Reduction of force (acceleration) within the elastic range from F_1 to F_{1D}
2. Reduction of force from post-yield range F_2 to elastic range F_{2D} (damage is avoided)
3. Reduction of force from post-yield range F_3 to post-yield range F_{3D} (damage is reduced)

In the following chapter the effect of various damping devices added at specific positions within the fastening system is analysed for different accelerograms. On the basis of the results a feasibility study is presented.

6.2 Numerical feasibility study

Under the condition that the main engineering structure/frame does not collapse in case of strong ground motion, this chapter focuses on non-structural elements that are attached to the main structure by the use of fasteners presented in chapter 2.1 and a feasible solution incorporating a passive energy dissipation device is developed.

6.2.1 Viscous fluid damper

Viscous fluid dampers consist of a hollow cylinder filled with fluid which is forced to flow through orifices either around or through the piston head as the damper piston rod is stroked. The fluid flow at high velocities results in the development of friction between fluid particles and hence gives rise to energy

dissipation in the form of heat. A detailed discussion of viscous fluid dampers may be found in *Lee (2001)*.

Experimental testing (*Seleemah 1997*) has shown that a suitable mathematical model for describing the behaviour of viscous fluid dampers is given by the following non-linear force-velocity relation

$$P(t) = C|\dot{u}(t)|^\alpha \text{sgn}[\dot{u}(t)] \quad (6.5)$$

where

$P(t)$ force developed by the damper

$u(t)$ displacement across the damper

C damping coefficient

α exponent whose value is determined by the piston head orifice design

t time

Under steady-state harmonic motion, the hysteresis loops for the linear case ($\alpha = 1$) are elliptical and approach a rectangular shape as α tends to zero. The energy dissipated per cycle of steady state harmonic motion is obtained by integrating equation (6.5) over the displacement leading to the following expression (*Symans 1998*)

$$E_D = 4P_0u_0 2^\alpha \left(\frac{\Gamma^2(1 + \alpha/2)}{\Gamma(2 + \alpha)} \right) = \lambda P_0u_0 \quad (6.6)$$

where

P_0 peak force developed by the damper

u_0 peak displacement across the damper

Γ gamma function

λ parameter whose value depends exclusively on the velocity exponent α

In the case of a fastening system there are two possible positions where a viscous fluid damper could be applied: between anchor rod and base plate according to Figure 6.3a or between base plate and concrete as shown in Figure 6.3b. The first option has the advantage of relatively easy implementation. Potential slack behaviour between anchor rod and damper may be avoided by sufficient pre-stressing of the counter nut. The second option exhibits enhanced expenditure in connecting the damping device with the concrete and in dealing with the slack between damper and concrete for the case that anchors are used. Dependent on the expected force in the damper (see following results) a possible solution could consist in gluing the connecting element to the concrete by use of epoxy resin. This technique is investigated extensively by *Holzengkämpfer (1997)* and in the mean time various approved systems for the application of external additional reinforcement under predominantly static loading are available. The suitability for intended seismic use shall be proofed by experimental investigations.

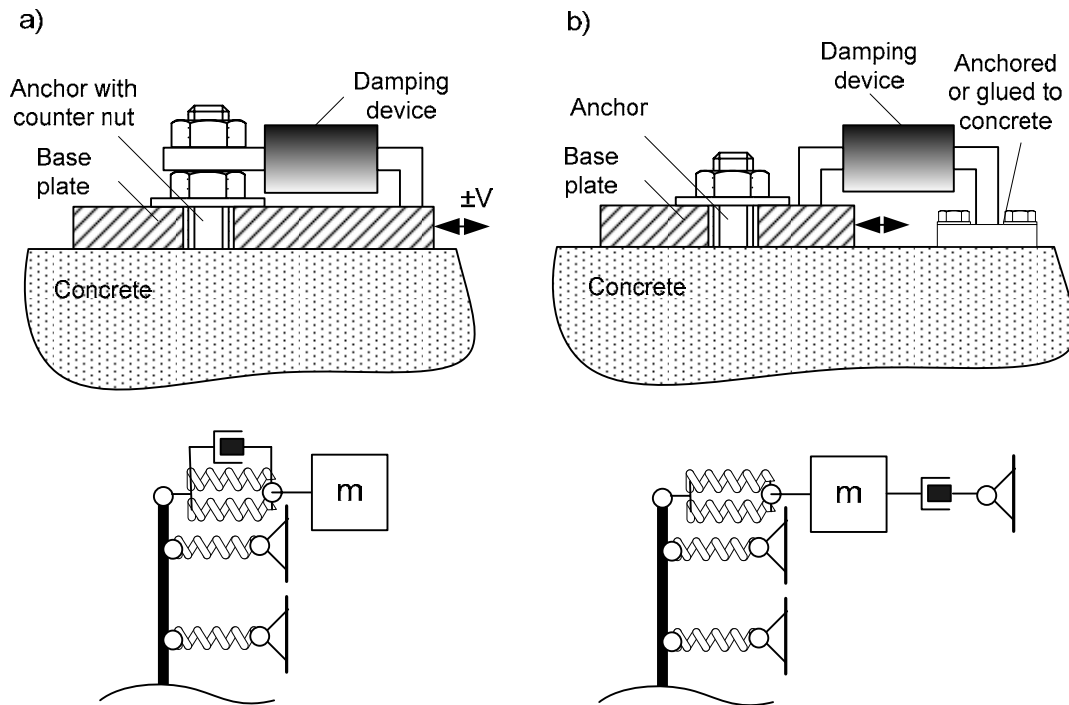


Figure 6.3: Possible application of viscous fluid damper and corresponding model: a) damper between anchor and base plate, b) damper between base plate and concrete

In order to evaluate the effect of both options time history analysis is performed with the same input accelerograms as used chapter 5.5 whereas in the model the mass is concentrated in the base plate without any friction to the concrete. The damper is assumed to behave linearly, i.e. $\alpha = 1$ and the damping coefficient C is obtained by the following formulas

$$C = \xi \cdot C_{crit} \quad (6.7)$$

$$C_{crit} = 2\sqrt{K \cdot m} \quad (6.8)$$

With

- ξ damping ratio
- K stiffness in N/m
= 5000000 N/m
- m mass
= 1800 kg

In Table 6.1 the damping coefficient is listed for different damping ratios. All simulations are based on a gap of 1 mm (which is the most probable case in practice) and a friction force of 200 N so that the results can be directly compared with those of the standard anchor from chapter 5.5. In the following diagrams the reduction of the maximum acceleration monitored on the base plate is plotted versus the seismic level for the different earthquakes and for the two options presented in Figure 6.3. In order to enhance the clearness only two damping ratios are shown for option b.

Table 6.1: Viscous damping parameters for time history analysis

ξ [%]	2.5	5.0	7.5	10
C [Ns/m]	5000	10000	15000	20000

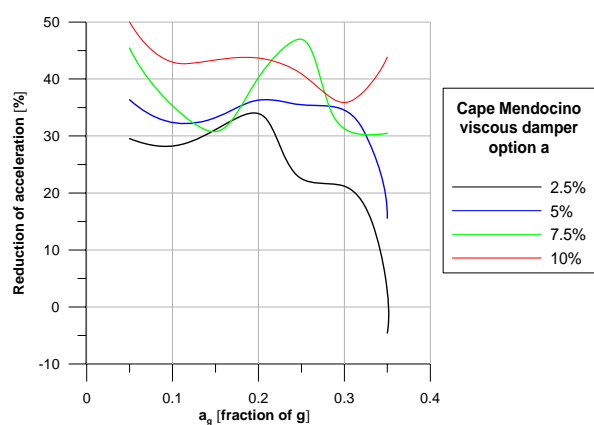


Figure 6.4: Viscous damper option a (Cape Mendocino)

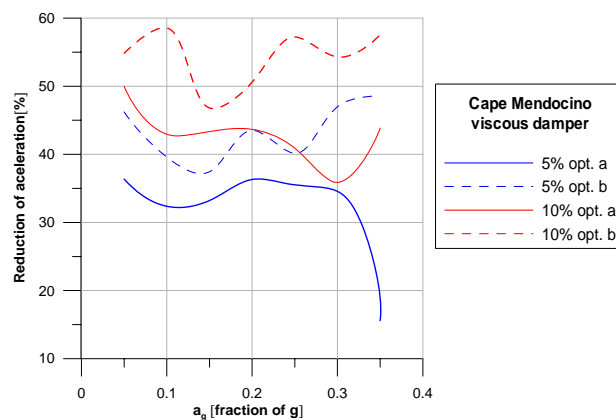


Figure 6.5: Viscous damper option a and b (Cape Mendocino)

All three cases presented in Figure 6.2b can be identified for the Cape Mendocino earthquake incorporating the damper option a. Up to a maximum ground acceleration $a_g = 0.3g$ no plastic deformation occurs and the acceleration on the base plate is reduced from 20% to 50% dependent on damping ratio (corresponding to case 1 in Figure 6.2b). For $a_g = 0.35g$ and additional 2.5% of viscous damping the ductility demand μ (of the concrete represented by the first spring) and hence the damage is reduced from 1.17 to 1.07 (case 2). On the other hand, the acceleration on the base is slightly amplified because the reduced energy dissipation due to reduced plastic deformation cannot be compensated by the energy dissipated by the damper. Finally, for $a_g = 0.35g$ and additional 5% of viscous damping plastic deformation is avoided and the complete loss of hysteretic energy dissipation is overcompensated by viscous energy dissipation resulting in reduce acceleration on the base plate. At even higher ground acceleration levels (which are not simulated) a significant mitigation of seismic induced damage to the concrete might be expected.

The benefit of positioning the damping device between concrete and base plate (option b) can be seen clearly in

Figure 6.5 for different damping ratios. Exemplarily for the Cape Mendocino earthquake the maximum force developed in the damper for a damping ratio of 10% is listed in Table 6.2 for both options.

Table 6.2: Maximum damper forces for $\xi = 10\%$

a_g [fraction of g]		0.05	0.1	0.15	0.2	0.25	0.3	0.35
Damper force [kN]	Option a	0.3	1.23	1.92	2.45	3.12	4.25	3.1
	Option b	0.18	0.37	0.53	0.76	0.93	1.05	1.13

The results show that the velocity between anchor and base plate is larger than between base plate and concrete and therefore the theory explaining the hammer effect is confirmed (see chapter 5.5.3). It is very interesting that option b with lower damping forces (only 35% compared to option a) exhibits higher

reduction of acceleration of the base plate. This issue can be explained by the fact that option a reduces only the relative acceleration between anchor and base plate and not the absolute value.

Due to the relatively low damper forces for option b the solution of gluing the connecting element to the concrete should be possible.

In the following diagrams the reduction of acceleration on the base plate for the Friulli earthquake and the artificial accelerogram in compliance with IEEE 693 are plotted.

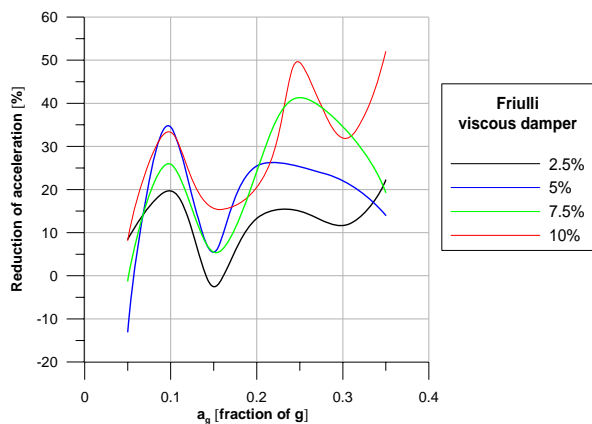


Figure 6.6: Viscous damper option a (Friulli)

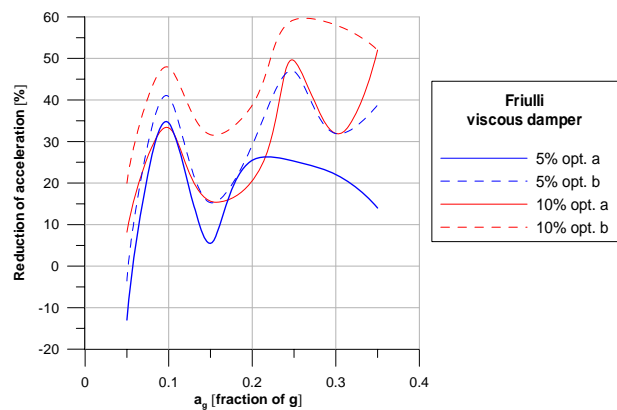


Figure 6.7: Viscous damper option a and b (Friulli)

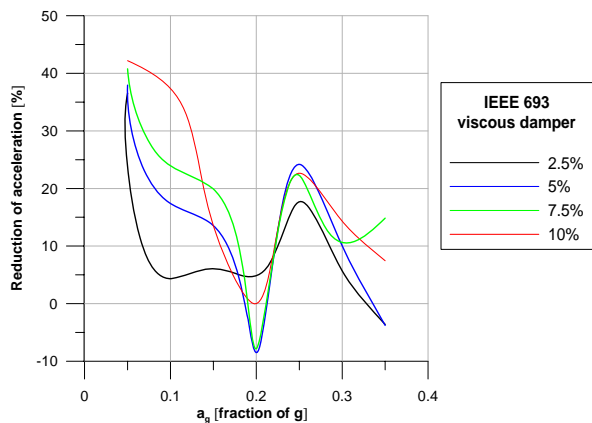


Figure 6.8: Viscous damper option a (IEEE 693)

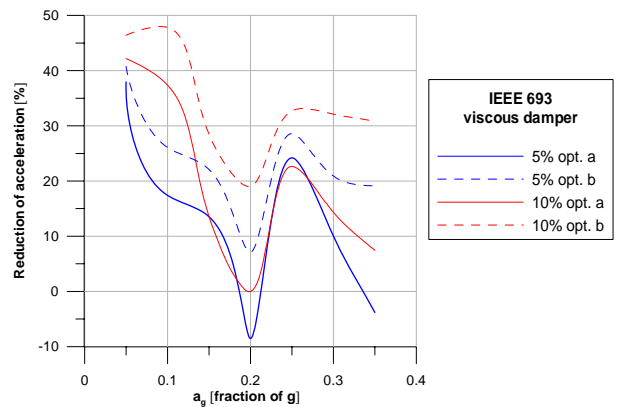


Figure 6.9: Viscous damper option a and b (IEEE 693)

The trend is similar as for the Cape Mendocino record, but the absolute values at specific peak ground accelerations differ quite strongly leading to a high degree of scatter. Therefore the average reduction and the average reduction minus standard deviation as an indicator for the scatter of the results are plotted in Figure 6.10 and Figure 6.11 respectively and summarized in Table 6.3. The reliability of the results could be enhanced by simulating additional earthquakes (real and/or synthetic). Nevertheless, for the investigated time histories the average reduction of acceleration on the base plate lies between 20% (5% damping option a) and 44% (10% damping option b). Thus option b seems to exhibit more advantages expressed in reduction of acceleration on base plate, mitigation of concrete damage and amount of forces developed within the damper. This system can be suggested for experimental validation and practical implementation.

Table 6.3: Reduction of acceleration for different viscous damper parameter

a_g [fraction of g]			0.05	0.1	0.15	0.2	0.25	0.3	0.35	mean
$\xi = 5\%$	Opt. a	Reduction of acceleration [%]	20.4	28.1	17.4	17.8	28.3	22.2	8.6	20.4
$\xi = 5\%$	Opt. b		33.5	37.9	24.2	21.4	37.7	27.4	34.4	30.9
$\xi = 10\%$	Opt. a		27.8	22.3	24.9	26.6	38.5	33.3	35.5	29.8
$\xi = 10\%$	Opt. b		40.4	51.4	35.6	36.2	49.8	48.2	46.8	44.0

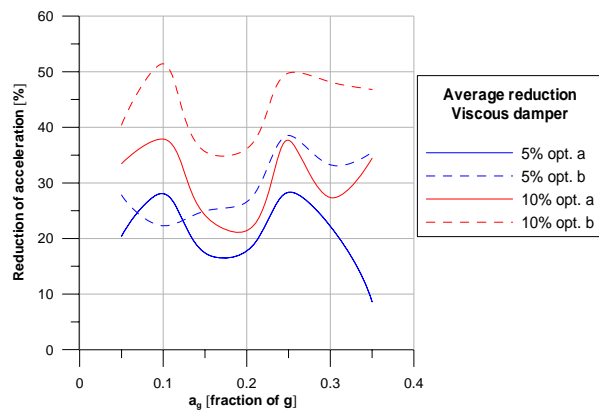


Figure 6.10: Viscous damper (average)

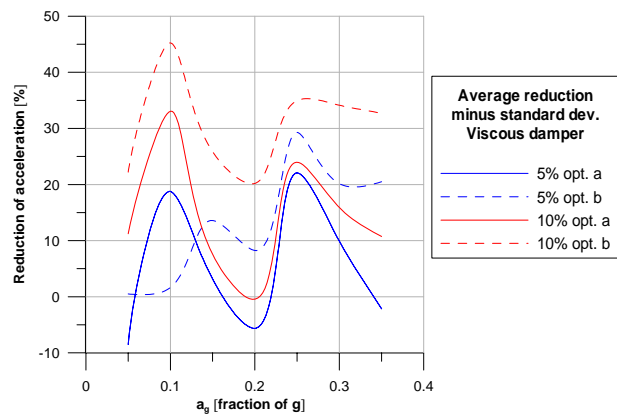


Figure 6.11: Viscous damper (average minus standard deviation)

As a concluding remark it should be noted that the application of a fluid viscous damper on a fastening system represents a quite sophisticated and time and price consuming solution, but it exhibits high efficiency in mitigating seismic induced acceleration. For sensitive essential non-structural equipment (e.g. medical devices, electric devices) the economic considerations might have a less significant impact on the decision whether to use such a damper or not.

6.2.2 Friction damper

Friction dampers dissipate energy via sliding friction across the interface between two solid bodies. A simple configuration includes slotted-bolted dampers (*Grigorian 1993*) wherein a series of steel plates are bolted together with a specific friction force.

Experimental testing (*Pall 1982*) has shown that a reasonable model to describe the behaviour of friction dampers is given by the idealized Coulomb model of friction

$$P = \mu \cdot N \cdot \text{sgn}(\dot{u}) \quad (6.9)$$

where

μ coefficient of dynamic friction

N normal force at the sliding interface

In practice it can be difficult to maintain a constant coefficient of friction and normal force over extended durations of time and therefore special materials may be utilized at the sliding interface. The rectangular hysteresis loops indicate that significant energy can be dissipated per cycle and that the cyclic

behaviour of friction dampers is strongly nonlinear. The deformations of the structural system are largely restricted until the friction force is overcome. Thus, the dampers add initial stiffness to the structural system.

Since a friction element described by equation (6.9) is not available within the used computer program, the friction damper is modelled by an elastic-plastic spring with high stiffness k (about two times of the overall anchor stiffness) and yielding at the friction force F_{fr} . It is placed between the base plate and concrete. A practical solution could consist of an elastic spring between nut and base plate which pushes the base plate against the concrete with the force F_{spring} and dependent on the friction coefficient μ a friction force $\mu \cdot F_{spring}$ is developed (Figure 6.12). Commercially available springs of suitable size exhibit forces up to 5 kN. Assuming a friction coefficient $\mu = 0.2$ between steel and concrete a maximum friction force of 1 kN may be obtained.

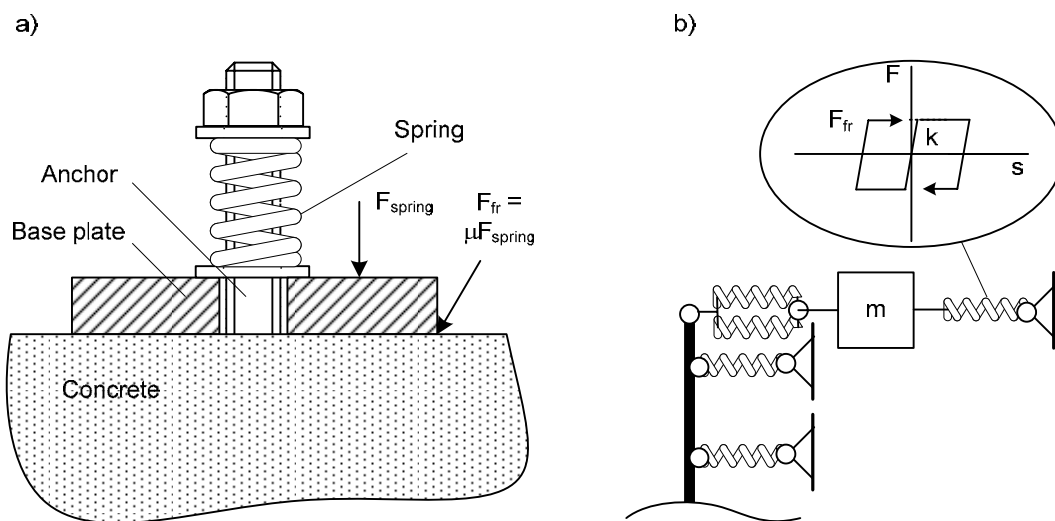


Figure 6.12: Possible application of friction damper (a) and corresponding model (b)

The proposed friction damper is restricted to applications with no or negligible axial tension forces on the anchor which may be assumed for the following cases:

1. The element is attached to the pavement
2. The centre of mass of the attached element is very close to the base plate
3. The maximum vertical acceleration a_v does not exceed gravity

The results of simulations with different friction forces and time histories are shown in the next figures. Herein the reduction of acceleration is referred to the system used for the simulations presented in chapter 5.5, i.e. the one with a friction force of 200 N.

Considerable scatter between the different accelerograms can be observed. For very low seismic level ($a_g = 0.05g$) the results seem to be contradictory because the system with the lowest friction force exhibits the largest reduction of acceleration. This phenomenon may be due to the fact that for this combination of parameters the spring representing the friction element undergoes very large plastic deformation ($\mu > 10$) but for higher friction forces the ductility demand and hence the dissipated energy is much lower ($1.5 < \mu < 3$). This problem could be solved by using an increased stiffness for larger

friction forces which should be calibrated by tests. But since the results are consistent at higher seismic levels, only $a_g = 0.05g$ is not considered for the average value in Figure 6.16, wherein the best performance of the friction damper is achieved for low seismic levels. A friction force $F_{fr} = 1$ kN leads to a mean reduction of almost 40% of the acceleration on the base plate as a mean value for all seismic levels and hence a similar average performance as for the viscous damper option b with 10% damping is yielded. However, the scatter for the friction damper is larger than for the viscous damping device, a fact that could be explained by the already discussed deficiency of the model used for the friction hysteresis loop.

Table 6.4: Reduction of acceleration for different friction damper parameter

a_g [fraction of g]			0.1	0.15	0.2	0.25	0.3	0.35	mean
F_{fr} [kN]	0.4	Reduction of acceleration [%]	27.3	12.2	10.5	24.2	19.1	8.5	17.0
	0.8		63.7	34.4	12.9	34.5	33.6	28.2	34.6
	1.0		55.7	47.9	30.5	26.5	32.6	35.3	38.1

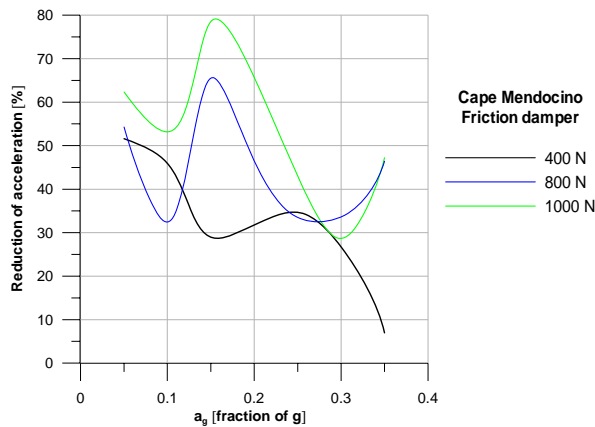


Figure 6.13: Friction damper (Cape Mendocino)

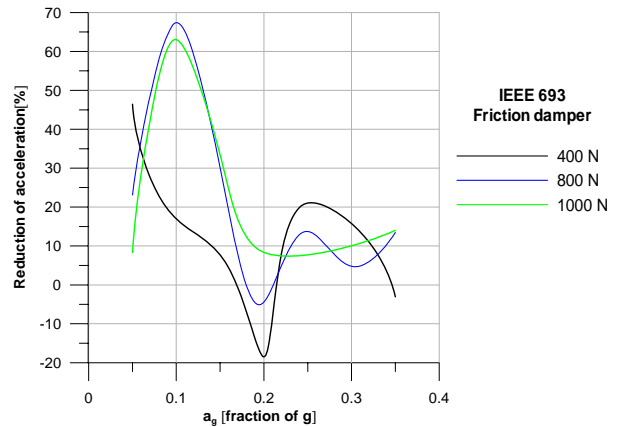


Figure 6.14: Friction damper (IEEE 693)

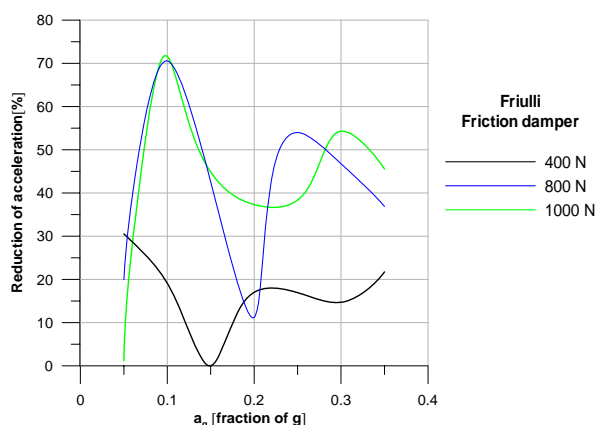


Figure 6.15: Friction damper (Friulli)

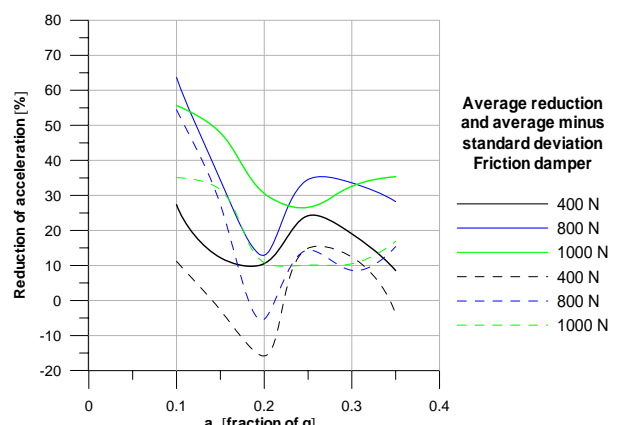


Figure 6.16: Friction damper (average and average minus standard deviation)

Thus, a friction damper can be realized with limited effort and it exhibits good performance especially at low seismic levels. The main disadvantage for practical applications consists in the restriction that only situations involving predominantly seismic shear loads are allowed.

6.2.3 Hysteretic damper

Hysteretic energy dissipation can be achieved by viscoelastic solid dampers, viscoplastic solid dampers or metallic dampers. The first generally consists of elastomeric pads bonded to steel plates that is sheared resulting in the development of heat which is dissipated to the environment. Viscoelastic solids are displacement and velocity dependent and can be modelled using the Kelvin model of viscoelasticity

$$P(t) = Ku(t) + C\dot{u}(t) \quad (6.10)$$

Where

K storage stiffness of the damper

C damping coefficient

After an earthquake a viscoelastic damper usually has not to be replaced. A viscoplastic material exhibits a displacement dependent stiffness that can be modelled by a nonlinear spring. Metallic dampers yield in tension and compression but don't show any velocity dependence. After a seismic event it is damaged and has to be replaced. The easiest way to apply a hysteretic damper on a fastening system and the corresponding model are shown in Figure 6.17.

Option a incorporates the damper with thickness t only between base plate and anchor. This can be a rubber ring with an inner diameter corresponding to the diameter of the anchor. It is modelled by a parallel arrangement of a nonlinear spring (representing the hysteretic behaviour of the damper) and a linear spring with a gap corresponding to the thickness of the damper. As a result, when the rubber is squeezed completely, direct contact between base plate and anchor is provided.

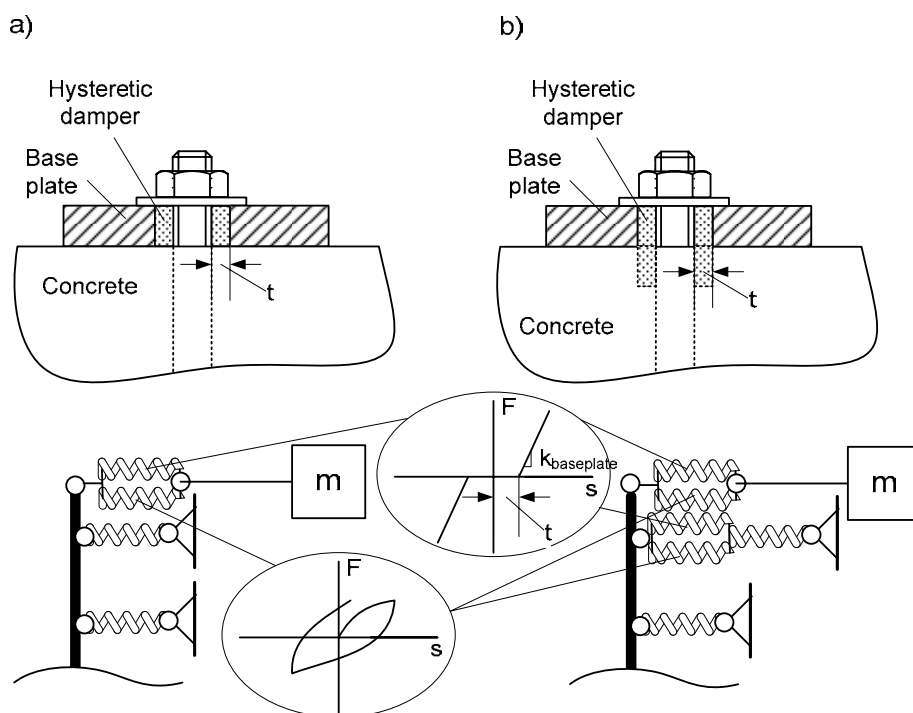


Figure 6.17: Possible application of hysteretic damper and corresponding model; (a) damper only on base plate, (b) damper on base plate and concrete

Option b consists of an extension of the rubber ring inside the concrete which is modelled by an additional set of springs as for option a but arranged in serial with the first concrete spring. In practise, after drilling the bore hole in accordance with the manufacturer's instructions, the upper part of the borehole has to be enlarged with a drill bit diameter equal to $d + 2t$, with d the nominal drill bit diameter and t the thickness of the rubber ring.

In order to simulate the rubber material properly, sophisticated models are available (e.g. *Wen 1976*). However, the numerous parameters have to be calibrated by experiments and therefore for the following simulations a very general hysteretic behaviour formulated by Ramberg and Osgood is used (s. Figure 6.18). Many rubber materials are not rate dependent (e.g. *Gerhaher 2009*) which is also proofed by the trial tests presented in chapter 6.3 and therefore no viscous damping is used. The three parameters are assumed with $K_0 = 1.5$ kN/mm, $F_y = 5$ kN and $r = 5$. Stiffness resp. strength degradation and pinching of the rubber is not considered.

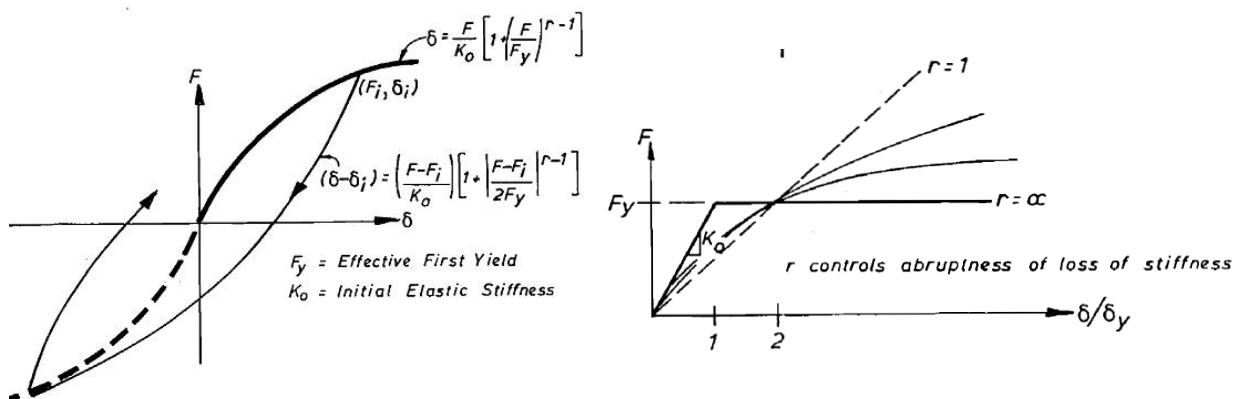


Figure 6.18: Ramberg-Osgood hysteresis (*Carr 2004*)

In Figure 6.19 it is shown that a trial parallel arrangement of the damper has no significant influence on the overall load-displacement behaviour of the anchor because the stiffness of the damper is too low compared to the stiffness of the anchor and hence the (plastic) deformation results too small. Serial positioning improves the overall hysteretic behaviour of the anchor especially at low load levels and describes also the experimental results in a proper way (s. chapter 6.3). Energy dissipation can be further increased by option b, i.e. by extension of the damper into the concrete and/or by increasing the thickness of the damper.

A disadvantage of adding a hysteretic damper consists in reducing the (static) load where yielding of the anchor steel takes place. This is due to increased anchor bending resulting from a softer base plate and foundation, respectively. Thus, according to the presented figures steel yielding decreases from 18 kN (standard anchor) to 17 kN (3 mm thick damper on base plate) and finally to approximately 13 kN in case of a 3 mm thick damper on base plate and concrete. This reduction of strength must be concerned in determining the static resistance of a fastener under shear loads. The basic challenge in adding a hysteretic damper to a fastening system consists in maximizing the damping properties and minimizing the reduction of static shear strength. Innovative materials (e.g. fiber reinforced rubber, composite plastics, self-adapting materials) could give a decisive contribution for solving this optimization problem.

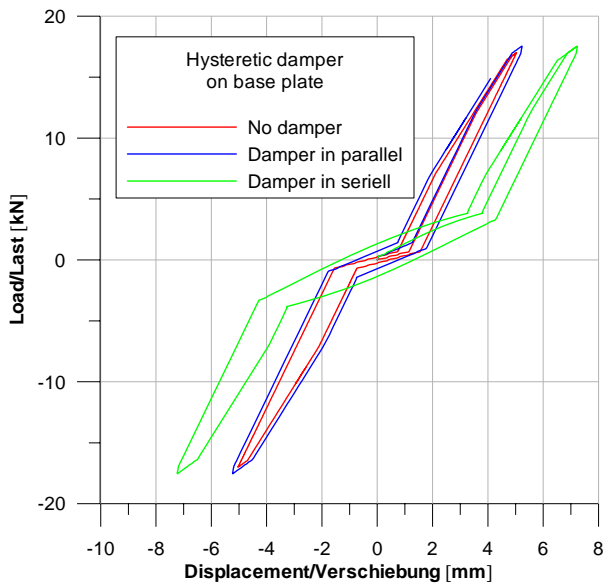
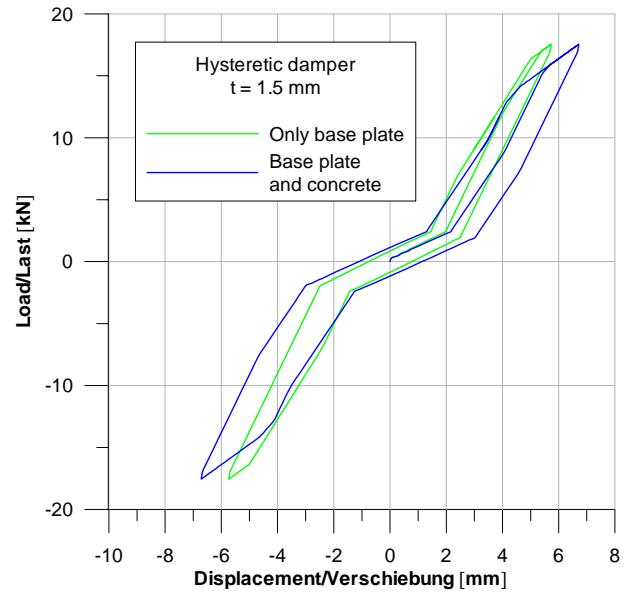
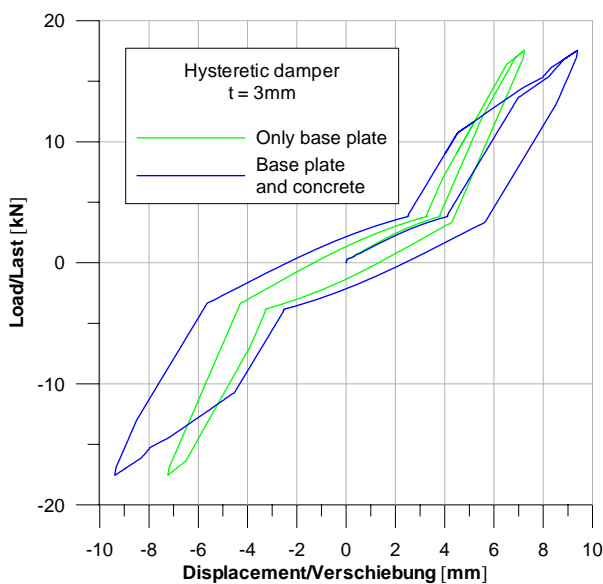
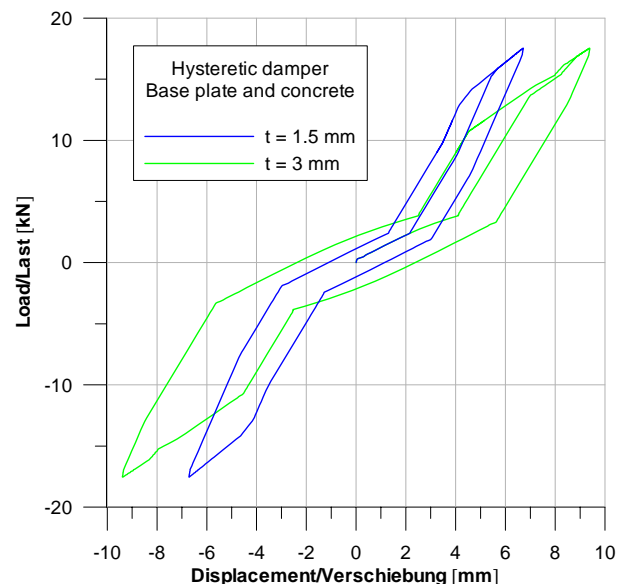
Figure 6.19: Hysteretic damper on base plate ($t = 3 \text{ mm}$)Figure 6.20: Serial hysteretic damper ($t = 1.5 \text{ mm}$)Figure 6.21: Serial hysteretic damper ($t = 3 \text{ mm}$)

Figure 6.22: Hysteretic damper (different thickness)

In the following figures the reduction of acceleration on the base plate is plotted for the same accelerograms used already before dependent on arrangement and thickness of hysteretic damper. The scatter between the various earthquakes is considerably. The average reduction of acceleration decreases with increasing seismic level which may be due to complete squeeze of the rubber element and resulting hammer effect induced by contact with the stiff base plate. Interestingly, there is no significant difference between option a and option b although the dissipated energy for the arrangement with damper on base plate and concrete is larger at least for the first cycle. This issue could also be explained by the hammer effect which occurs at very similar load levels for both options. Thus, the results seem to be on the safe side.

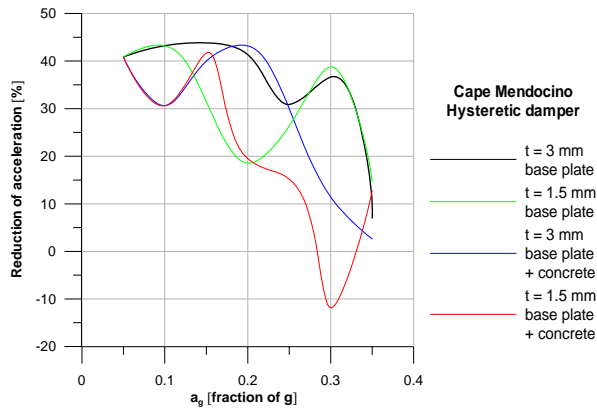


Figure 6.23: Hysteretic damper (Cape Mend.)

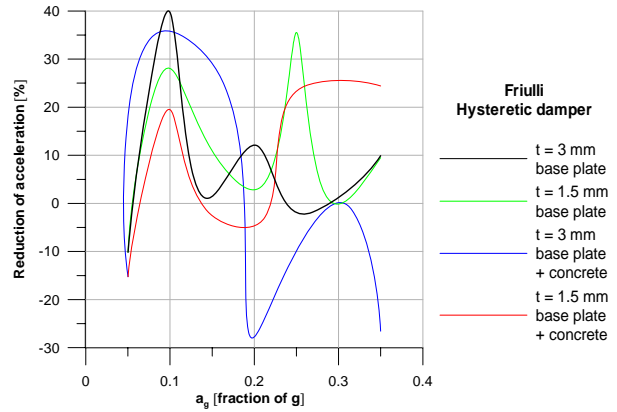


Figure 6.24: Hysteretic damper (Friulli)

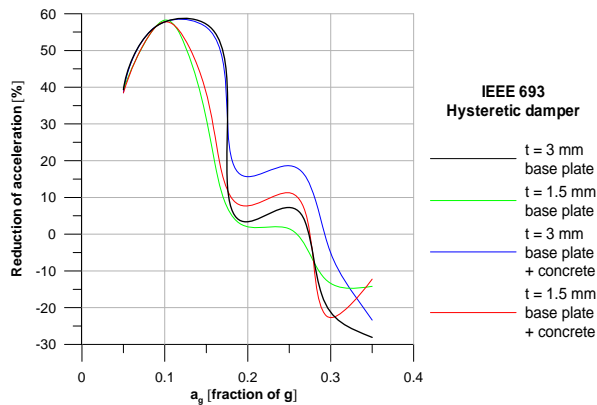


Figure 6.25: Hysteretic damper (IEEE 693)

Table 6.5: Reduction of acceleration for different hysteretic damper parameter

a_g [fraction of g]			0.05	0.1	0.15	0.2	0.25	0.3	0.35	ave.
t = 1.5 mm	Base pl.	Reduction of acceleration [%]	23.3	43.2	24.6	7.8	21.1	8.4	3.3	18.8
t = 1.5 mm	Base pl./concr.		21.4	36.0	25.9	7.5	16.6	-3.0	8.3	16.1
t = 3 mm	Base pl.		23.3	46.9	34.2	19.0	12.1	5.5	-3.7	19.6
t = 3 mm	Base pl./concr.		21.4	41.4	41.8	10.3	12.9	2.2	-15.8	16.3

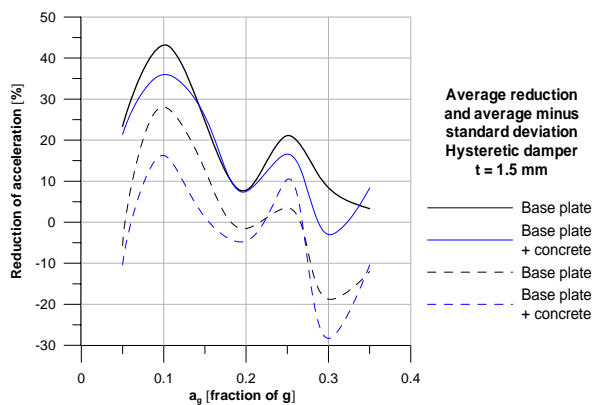


Figure 6.26: Hysteretic damper t = 1.5 mm (solid line average and dashed line average minus standard dev.)

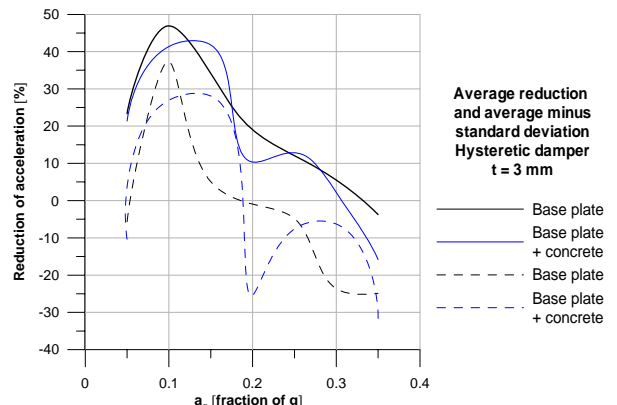


Figure 6.27: Hysteretic damper t = 3 mm (solid line average and dashed line average minus standard dev.)

According to Table 6.5 the reduction of acceleration on the base plate lies between 25% at low levels and zero at high seismic levels. Note that in some cases a slight amplification takes place. More realistic results could be obtained with a rubber model incorporating strain hardening (e.g. *Wen 1976*) so that the transition zone preceding contact between base plate and concrete becomes smoother.

The reduction of concrete stress has already been discussed for the viscous damper. In the following figures the reduction of maximum concrete stress (expressed in terms of force in the first concrete spring) of option b referred to option a is plotted for each earthquake and both damper thicknesses. The advantage of an extension of the damper inside the concrete can be seen very clearly. Up to $a_g = 0.25g$ a mean reduction of 45% is achieved independent on the thickness of the damper. At higher levels the hysteretic damper with enhanced thickness exhibits a better performance. Scatter of concrete stress is much lower compared with the scatter of acceleration on the base plate presented in the previous figures.

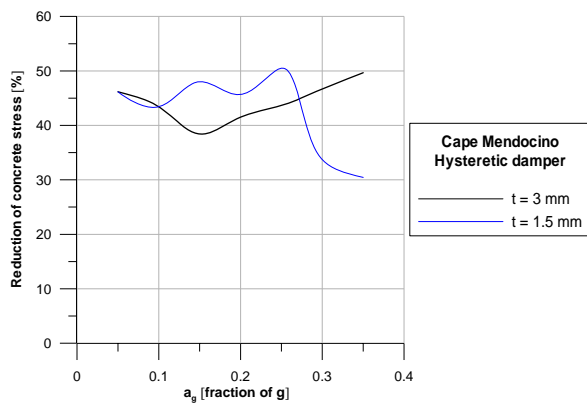


Figure 6.28: Reduced concrete stress for option b (Cape Mendocino)

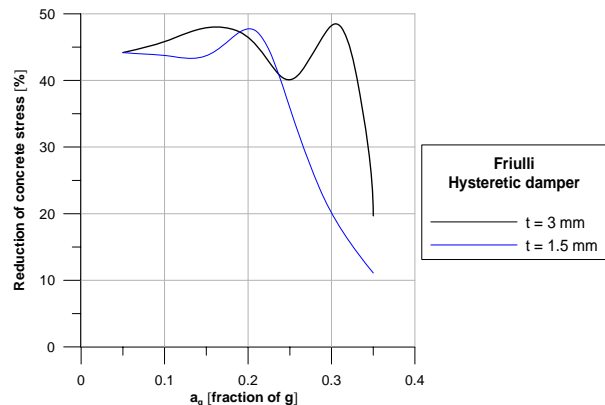


Figure 6.29: Reduced concrete stress for option b (Friulli)

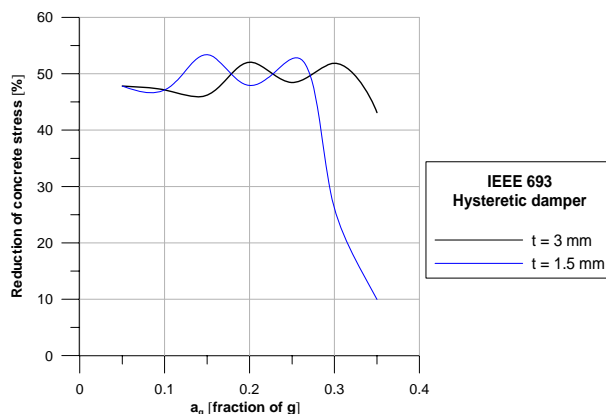


Figure 6.30: Reduced concrete stress for option b (IEEE 693)

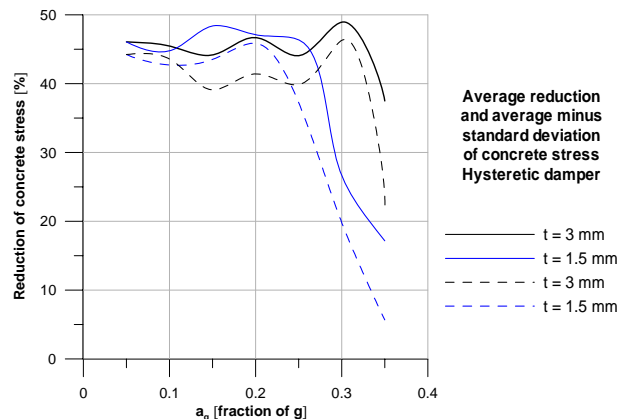


Figure 6.31: Reduced concrete stress for option b (average and average minus standard deviation)

Thus, by extension of the hysteretic damper inside the concrete the maximum concrete stress and therefore damage of concrete can be reduced considerably on one hand. On the other hand, this solution promotes yielding of anchor steel with resulting reduced static shear strength and hence the validity of existing approvals has to be checked. Thus the question, whether the first effect overcompensates the second one can be answered only by future experimental verification.

6.2.4 Comparison of different dampers

The most efficient and reliable (in terms of scatter of simulated response for different earthquakes) solutions is represented by a viscous fluid damper applied between base plate and concrete. The acceleration on the base plate can be reduced up to 50%, concrete damage is either mitigated or prevented and anchor forces decrease. The main disadvantage of the damping system consists in considerable effort and costs for implementation, especially in connecting the damper with the concrete. Thus, optimizing economical and safety concerns a viscous fluid damper seems to be applicable only for very special cases (e.g. electrical equipment prone to vibrations).

The friction damper presented in chapter 6.2.2 exhibits a good performance especially at low seismic levels. However, numerical modelling involves strong nonlinear behaviour and enhanced sensitivity with regard to type of earthquake leading to large scatter of simulated response. Seismic axial loads shall be excluded. A potential change over time of the friction coefficient between base plate and concrete has to be guaranteed by special measures.

From the numerical point of view a hysteretic damper needs the most sophisticated model in order to be able to capture the damping behaviour of the fastening system with sufficient accuracy. The used simplified model suggests that the acceleration on the base plate can be reduced more efficient at low seismic levels. Quite high values are obtained for the general scatter of the simulated response. Dependent on the geometry of the hysteretic damping element (thickness and extension) the damage to the concrete can be mitigated. All the positive and negative features of the various dampers are summarized in Table 6.6 and the quantitative reduction of acceleration is listed in Table 6.7 for the most effective design indicated in the second column. Herein the mean resp. the maximum and minimum values are related to the seismic levels between 0.05g and 0.35g.

Table 6.6: Summary of qualitative damping features

damper	advantage	disadvantage
Viscous	Efficient reduction of acceleration for all seismic levels Low scatter Easy modelling	Large effort and costs for implementation Possible fluid seal leakage
Friction	Easy implementation Good performance at low seismic levels	Restricted to seismic shear forces Poor performance at higher seismic levels Large scatter Possible change of friction conditions with time
Hysteretic	Very easy implementation Good performance at low seismic levels Large scatter	Sophisticated modelling Reduction of static strength Possible change of material properties with time

Table 6.7: Summary of quantitative damping features

damper	Design	Reduction of acceleration [%]		
		mean	max	min
Viscous	$\xi = 10\%$, damper between base plate and concrete	44	51	36
Friction	$F_{fr} = 1 \text{ kN}$	38	56	26
Hysteretic	$t = 1.5 \text{ mm}$, damper between base plate and anchor	19	43	3

6.3 Experimental validation

6.3.1 General

On the base of the numerical feasibility study presented in chapter 6.2 it can be concluded, that although the hysteretic damper exhibits the lowest mean reduction of acceleration, it may be transferred into practice in the easiest way. For this purpose the damper has to be validated by experiments which can be performed according to the flow chart presented in Figure 6.32. Herein two complementary testing methods are proposed: cost consuming quasi-static cycling and uniaxial shake table testing. The evaluation of the results of the first method yields information about the validity of potential existing approvals and at the same time a first assessment of the hysteretic damping behaviour of the prototype proposed by numerical simulations can be undertaken. Shake table testing is necessary for the final verification of the damping properties of the fastening system under real seismic excitations.

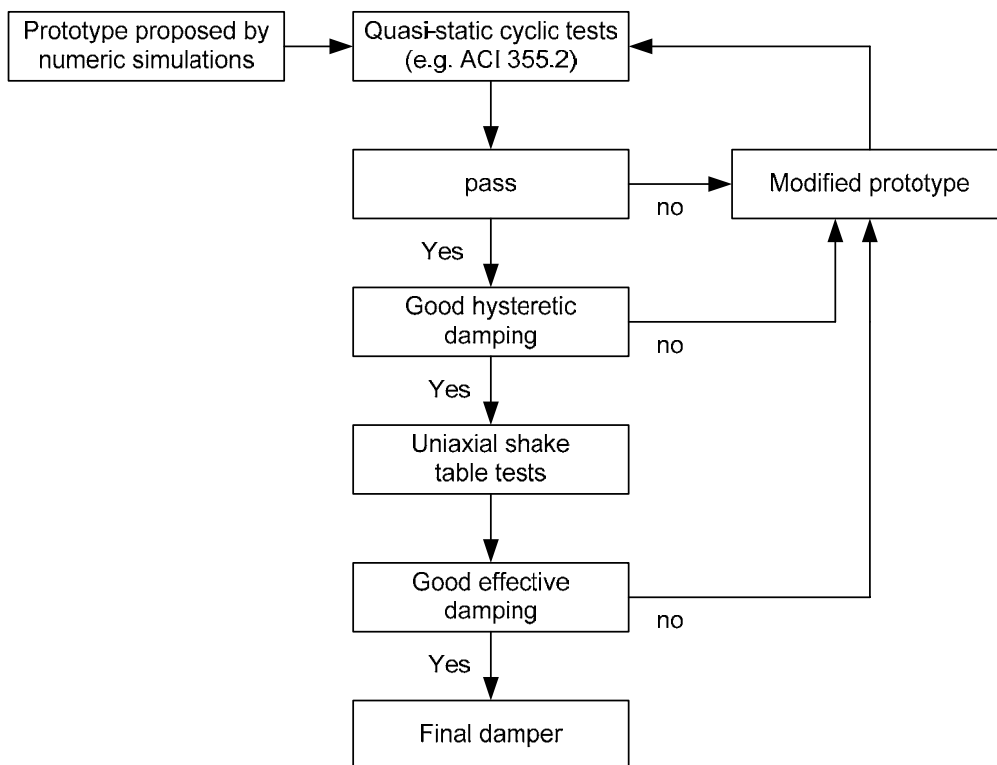


Figure 6.32: Flow chart for the development of a seismic damper

6.3.2 Quasi-static cycling pre-tests

Cyclic alternating shear tests are performed in non-cracked concrete of the strength class C20/25 with various anchors and damping elements. After installing the anchor the prescribed torque is applied and reduced to zero afterwards in order to avoid friction between concrete and fixing element. This measure simulates the opening of cracks during seismic events with resulting complete loss of pre-stressing force in the anchor. Tests are performed with a servo-hydraulic testing equipment yielding a maximum velocity of 90 mm/s which is far below of typical velocities resulting from seismic action. Therefore the sinusoidal load controlled quasi-static cycling tests are not suitable to capture rate dependent seismic

damping effects, but the trend for different damper arrangements should be clearly visible with the used testing equipment.

In order to eliminate possible rate dependent damping effects the maximum velocity is kept constant for all the tests by reducing the frequency at larger amplitudes. Thus, the frequency is varied between 0.5 Hz for anchors with damper and 2 Hz for anchors without damper. Service load is defined as V_{Rd}/γ_F with V_{Rd} as static shear resistance from the relevant ETA (*DIBt 2007*) and $\gamma_F = 1.4$. Details of the test set-up can be found in *Rieder (2008a)*. The equivalent viscous damping is calculated according to equation (4.1).

In the following figure the hysteresis of a standard expansion anchor (sleeve type) and an anchor with damper are shown. The damping element consists of a sleeve made of polyamide with a thickness of 2 mm which exchanges the original metallic sleeve in the upper part of the anchor. This arrangement corresponds to option b in Figure 6.17 (damper on base plate and inside the concrete). Unfortunately, load control is not symmetric but the difference between maximum and minimum load is comparable for standard anchor and modified one. The significant increased hysteretic damping at service load and the reduced stiffness is evident from the load-displacement plots; the values listed in Table 6.8 represent the average equivalent viscous damping calculated for the 5th, 10th and 20th cycle. Hysteresis is stable also at larger number of cycles so that in equation (4.4) $\lambda = 1.0$ applies. Thus, the trend of the numerical results from the previous chapter is verified by the quasi-static cycling tests. The advantage of increased hysteretic damping however is accompanied by the disadvantage of changing details of the anchor design. The ramification on the (static) performance given in existing approvals has to be checked.

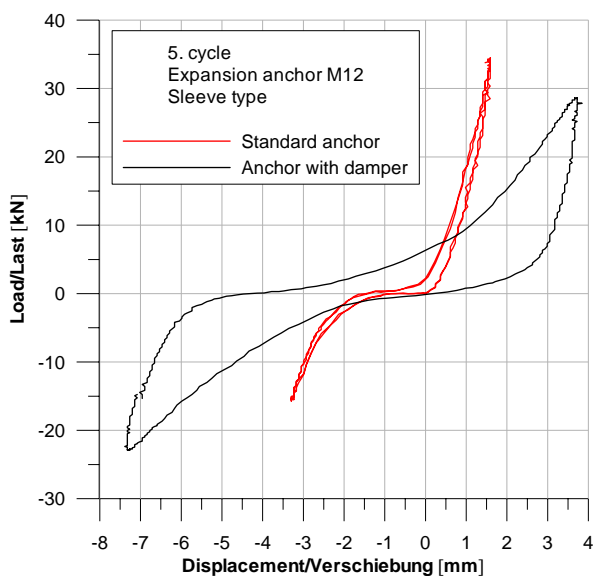


Figure 6.33: Hysteretic damper for sleeve type expansion anchor (service load)



Figure 6.34: Standard anchor (bottom) and anchor with damper (top)

The results of an arrangement according to option a in Figure 6.17 is presented in Figure 6.35 for an expansion anchor of the bolt type M10. In this case a low damping rubber ring exhibiting a shore hardness of 90 is placed between base plate and anchor (Figure 6.37). No significant increase of hysteretic damping can be achieved at service load and stiffness is reduced slightly. At 140 % of service

load damping is approximately doubled from 5% to 10% and stiffness is strongly reduced (see Figure 6.36, note the different scale of displacement axis). The use of a high damping rubber material could enable good results also at lower load levels. In Table 6.8 the equivalent viscous damping as a fraction of critical damping is listed for all tests.

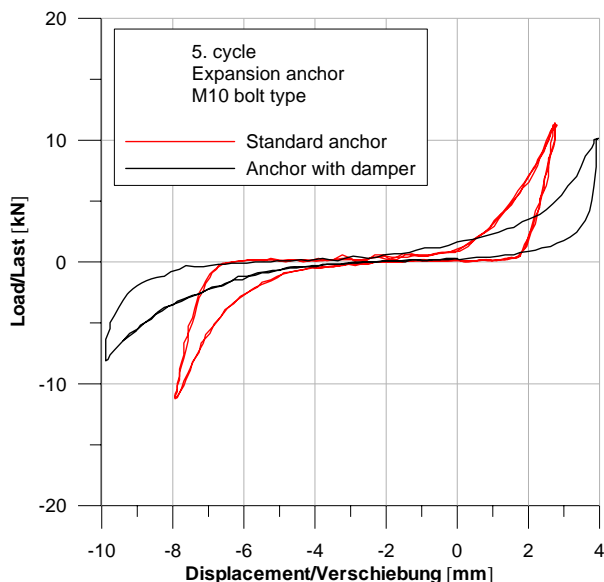


Figure 6.35: Hysteretic damper on base plate for bolt type expansion anchor (service load)

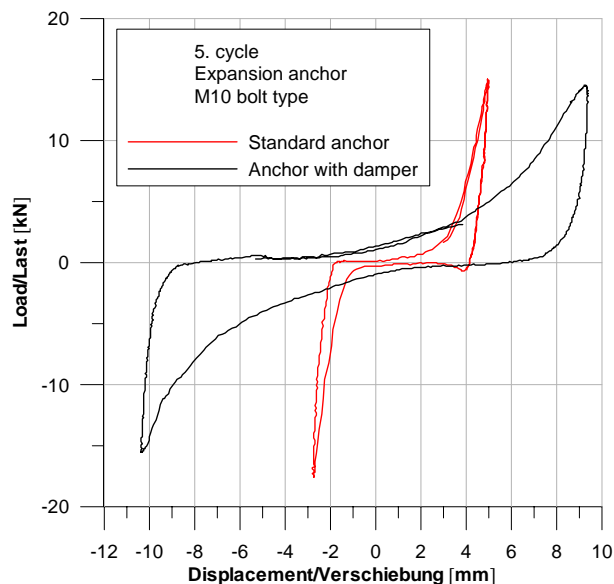


Figure 6.36: Hysteretic damper on base plate for bolt type expansion anchor (140% service load)

Table 6.8: Hysteretic damping properties

Anchor type	damper	Hole clearance [mm]	Load ampl.	Eq. visc. damping [%]
Sleeve M12	No	0	V_{Rd}/γ_F	3.0
Sleeve M12	Yes	2	V_{Rd}/γ_F	9.8
Bolt M10	No	2	V_{Rd}/γ_F	4.7
Bolt M10	Yes	2	V_{Rd}/γ_F	5.7
Bolt M10	No	2	V_{Rd}	4.9
Bolt M10	Yes	2	V_{Rd}	10.7

6.3.3 Uniaxial shake table tests

On the basis of the encouraging results of the numerical simulations and the pseudo-dynamic pre-tests shake table tests with sinusoidal and seismic input are performed. Since the same test-setup is used as in chapter 4.3 only the inner diameter of the adapter simulating the base plate has to be changed. Decisive for the selection of the prototype is the condition that the anchor itself must not be changed. Therefore an expansion anchor of the bolt type is used and the option of a hysteretic damper between anchor and base plate according to Figure 6.37 is chosen. In the following sections a summary of the test reports of *Pampanin (2008)* and *Rieder (2008b)* is given.

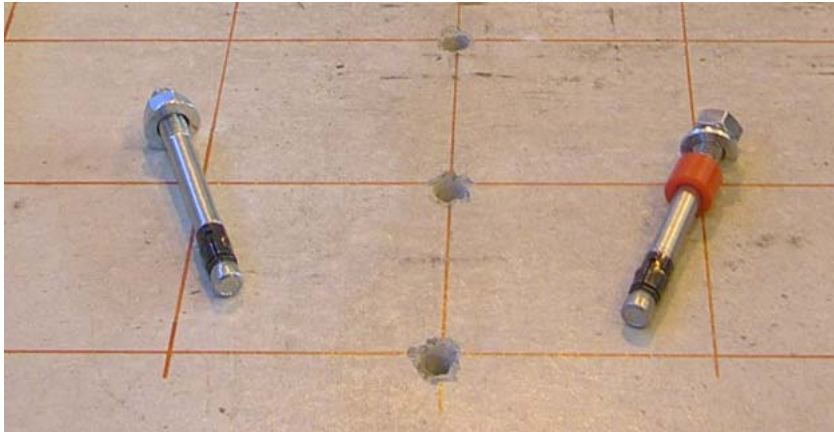


Figure 6.37: Standard anchor (left) and anchor with damper (right)

6.3.3.1 Sinusoidal input

Shake table tests with sinusoidal input constitute a helpful tool in studying the stability of the hysteresis and potential resonance effects. In Figure 6.38 and Figure 6.39 the load-displacement plots of the anchor with hysteretic damper is compared with the standard anchor for two different amplitudes at 1 Hz sinusoidal shake table input.

It is evident that the anchor with hysteretic damper exhibits reduced peak load, less stiffness and slightly reduced pinching. It is also characterized by a stable hysteresis. According to the load spectrum in Figure 6.40 resp. Figure 6.41 higher frequencies are more suppressed in case of presence of a hysteretic damper. This effect may be interpreted in the way that higher frequencies induced by the hammering of the anchor against the base plate are cut off by the damping element. As a main result the acceleration on the base respectively the anchor load are reduced by approximately 20% as an average value taken from positive and negative acceleration.

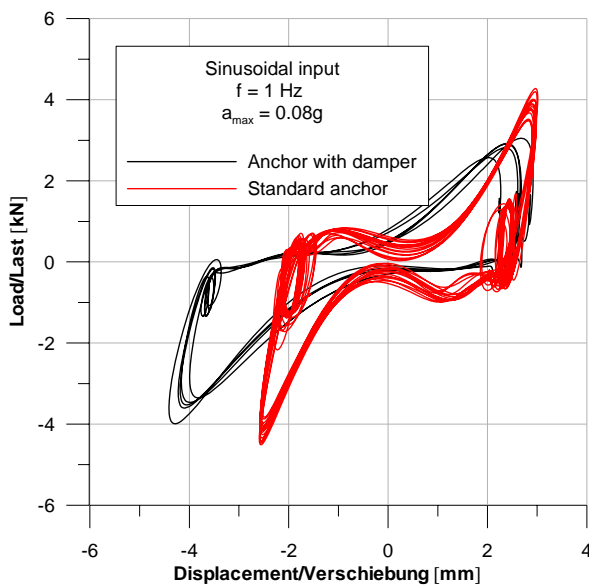


Figure 6.38: Sinusoidal input 1 Hz, $a_{\max} = 0.08g$

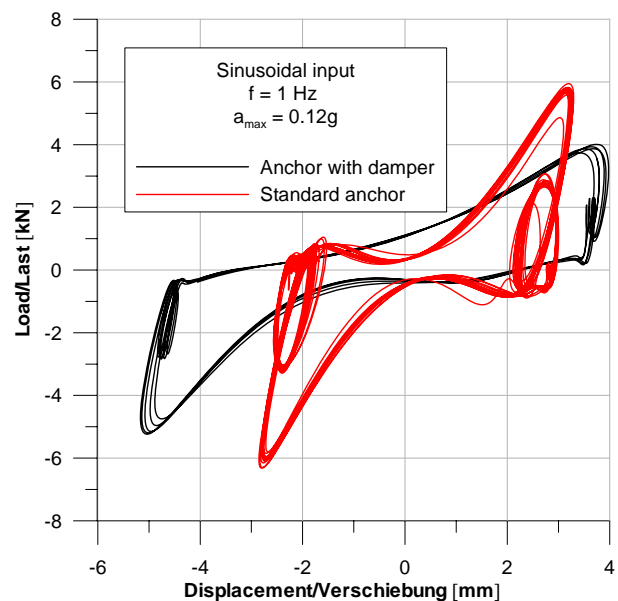


Figure 6.39: Sinusoidal input 1 Hz, $a_{\max} = 0.12g$

Table 6.9: Acceleration on attached mass for various dampers

		Standard anchor		Hysteretic damper		Friction damper	
f [Hz]	a_g [g]	min [g]	max [g]	min [g]	max [g]	min [g]	max [g]
1	0.08	-0.26	0.25	-0.24	0.19	-0.13	0.12
1	0.1	-0.3	0.29	-0.26	0.2	-0.13	0.13
1	0.12	-0.36	0.35	-0.32	0.25	-0.19	0.19
3	0.18	-0.52	0.49	-0.61	0.59	-0.47	0.44
3	0.27	-0.88	0.65	-0.79	0.80	-	-

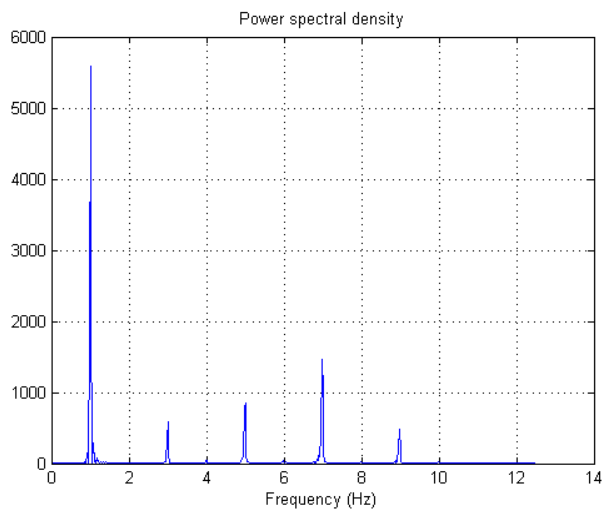


Figure 6.40: Load spectrum for standard anchor at 1 Hz input

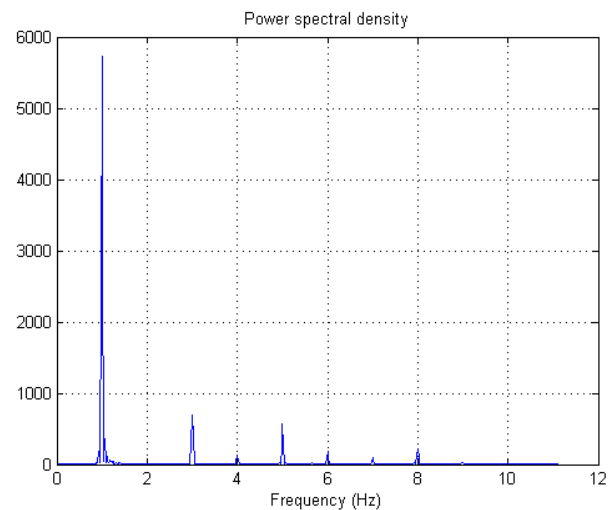


Figure 6.41: Load spectrum for anchor with hysteretic damper at 1 Hz input

An easy way to realize a friction damper is represented by pre-stressing the anchor with a specific torque. In a trial test, after installation of the anchor in compliance with the manufacturer's instruction the torque is not reduced to zero (like in the previous experiments) but to 50% of the nominal value and hence to 30 Nm. From approval tests (*Bergmeister 2005*) the prestressing force at 30 Nm results in approximately 10 kN. As shown in Figure 6.43 notable relative anchor displacement occurs at $a_g > 0.1g$ where a mass acceleration of 0.13g is measured. This corresponds to an anchor shear load of 2.3 kN and a (dynamic) friction coefficient $\mu = 0.23$ can be deduced, a value which meets the assumed one in chapter 6.2.2 quite well.

It should be noted that in case of an earthquake cracks are formed with high probability at the position of the anchors or close to them resulting in complete loss of prestressing force. Thus, the presented solution is suitable only to demonstrate the effect of a friction damper under laboratory condition.

The maximum acceleration of the attached mass is reduced considerably by approximately 50% for 1 Hz sinusoidal input within the limit of the shake table. Larger ground acceleration is possible only by increasing the frequency to 3 Hz where the reduction is expected to be lower because of increasing relative anchor displacement and resulting hammer effect between anchor and base plate. According to Table 6.9 this assumption is confirmed by the fact that the acceleration on the attached mass is reduced only by 10% at $a_g = 0.18g$. It is also worth to mention that the friction damper exhibits much more symmetric reduction of acceleration (i.e. positive/negative) compared to the hysteretic damper.

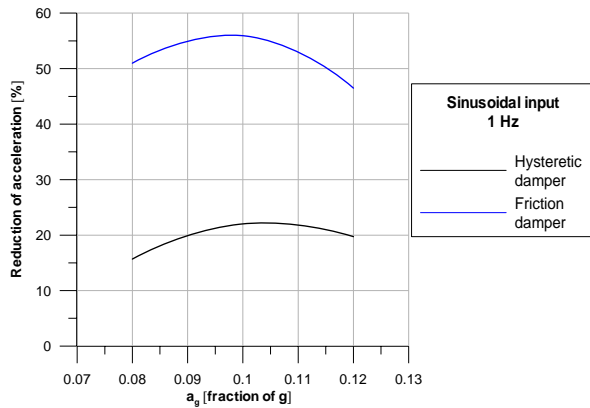


Figure 6.42: Effect of hysteretic and friction damper

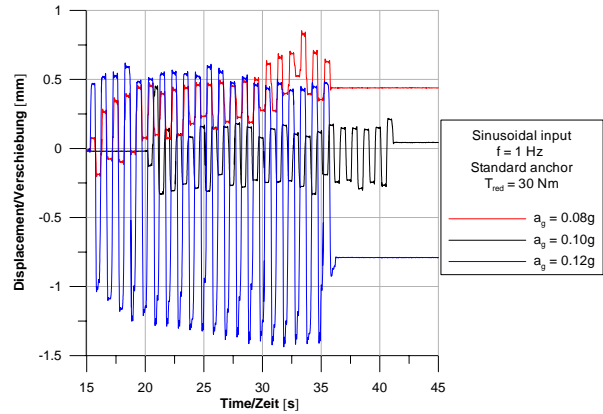


Figure 6.43: Relative anchor displacement for friction damper

The sinusoidal shake table tests confirm the effectiveness at low seismic levels of the simulated friction damper presented in chapter 6.2.2, but for the final proof shake table tests with various seismic inputs have to be performed. Before that a resonance check is made through a sinusoidal test at 3 Hz and different amplitudes. From the 1 Hz sinusoidal tests an effective stiffness and the corresponding resonance frequency can be determined. With the applied mass of 1800 kg a resonance frequency of 5.4 Hz and 4.4 Hz for the standard anchor respectively the anchor with hysteretic damper s calculated. Since the maximum amplitude of the shake table at these frequencies is limited to 2 mm and hence to the effective gap between anchor and base plate no significant load might be expected. This is also proven by experiments in *Rieder (2008b)*.

Thus, a frequency of 3 Hz is chosen where the shake table displacement limit is far beyond the hole clearance between anchor and base plate. Considerable resonance effects can be observed at this frequency according to Figure 6.44 and Figure 6.45, i. e. the load of the anchor with hysteretic damper is increased with respect to the standard anchor.

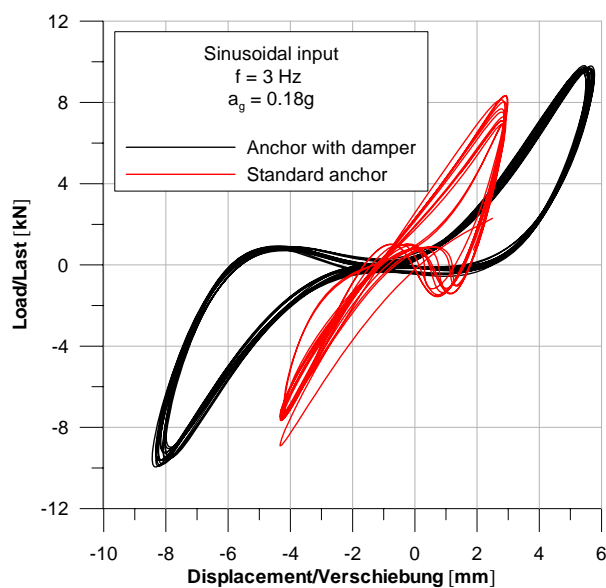


Figure 6.44: Sinusoidal input 3 Hz $a_g = 0.18g$

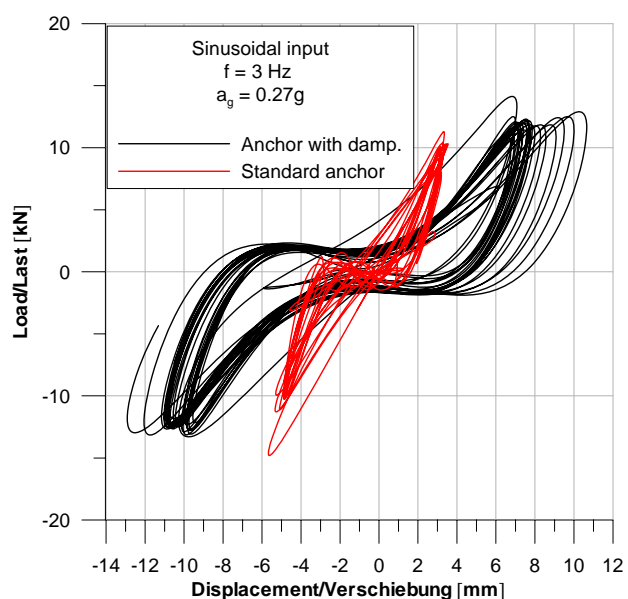


Figure 6.45: Sinusoidal input 3 Hz $a_g = 0.27g$

At higher amplitude the resonance is more pronounced leading to instable hysteresis in terms of stiffness degradation and finally to steel failure of the anchor. The rubber element is strongly squeezed and deformed and the damage pattern of the concrete shown in Figure 6.46 resembles the damage observed during quasi-static cycling shear tests presented in chapter 4.2.2. Steel rupture takes place at approximately $2 \cdot d_s$ below the concrete surface with d_s the bolt diameter. A considerable increase of temperature of the steel bolt is registered after failure, a phenomenon which might have an impact also on the damping properties of the rubber material and which should be investigated in specific experiments.



Figure 6.46: Anchor failure at sinusoidal input 3 Hz and $a_g = 0.27g$

As an important result it can be concluded that the investigated prototype hysteretic damper influences the static and dynamic behaviour of a fastening system. The first is manifested by reduced shear strength and stiffness compared to the standard anchor and the latter by decreased shear forces outside of resonance and increased shear forces close to resonance.

6.3.3.2 Seismic input

For the seismic input the same earthquake records from chapter 4.3 are used. All the hysteretic dampers are placed between anchor and base plate, whereas version 1 consists of a low damping rubber, version 2 of a high damping rubber and version 3 of the same material as version 1 but in addition a torque moment of 20 Nm is applied. Therefore the last version can be regarded as a combination of a hysteretic damper with a friction damper.

As shown exemplarily in Figure 6.47, it can happen that the response is amplified in one direction and de-amplified in the other one. In order to determine the mitigation of seismic induced accelerations the reduction of the maximum absolute value is considered (real maximum acceleration felt by the fastened object). Thus, a negative value means an amplification of the acceleration.

The experimental results confirm the main findings of the numerical simulations. Thus, the mitigation of acceleration depends strongly on type of earthquake record, peak ground acceleration and type of damper. For the first two parameters (i.e. type and intensity of earthquake) no general trend can be

established. Large scatter between amplification up to 45% and mitigation up to 55% for version 1 can be observed. Although version 2 consists of a high damping rubber it exhibits no significant difference. It seems that for the hysteretic damper (version 1 and 2) the change of acceleration describes a stochastic process resulting in no reliable decrease of seismic action.

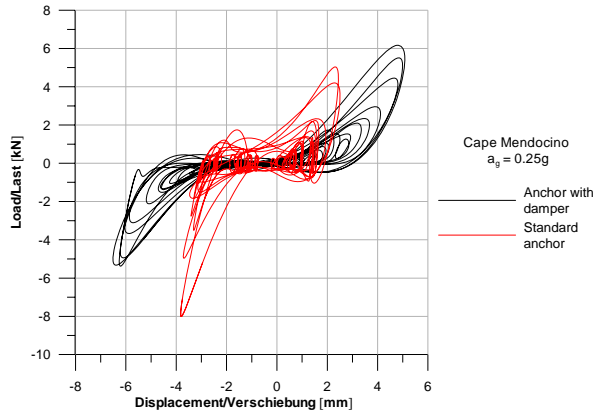


Figure 6.47: Load-displ., Cape Mendocino

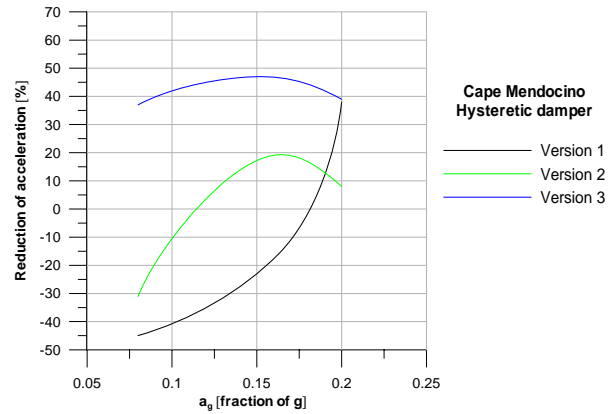


Figure 6.48: Various dampers, Cape Mendocino

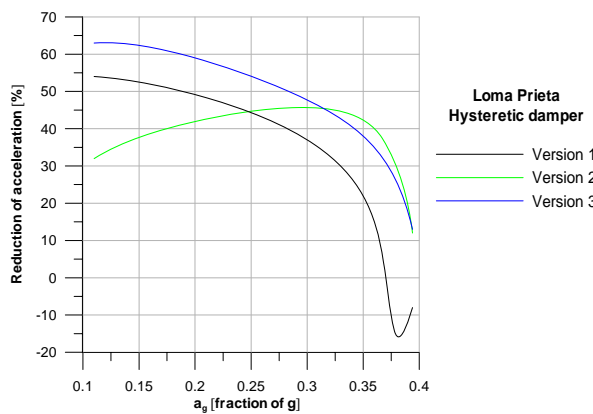


Figure 6.49: Various dampers, Loma Prieta

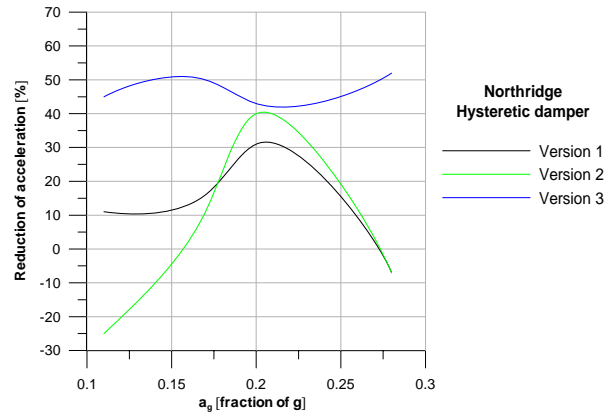


Figure 6.50: Various dampers, Northridge

A significant influence of the type of damper and a clear trend is evident from the experimental results achieved with version 3. Independent of type of earthquake record, the combination of a hysteretic damper with a friction damper yields a reduction of the acceleration on the attached element by at least 40% up to a peak ground acceleration of 0.35 g. At higher seismic levels the friction is overcome resulting in reduced damping efficiency. This solution utilizes the high friction coefficient between concrete and rubber. All results for the various damper versions and corresponding seismic inputs are listed in Table 6.10.

However, the material properties (creeping behaviour, temperature dependence, etc.) have to be checked and verified for a practical implementation in order to guarantee the reliability of the friction conditions for the intended time of use.

Table 6.10: Reduction of acceleration compared to standard anchor

PGA [g]	Earthquake	Reduction of acceleration [%]		
		Version 1	Version 2	Version 3
0.08	Cape Mendocino	-45	-31	37
0.17		-11	19	46
0.2		38	8	39
0.11	Loma Prieta	54	32	63
0.36		15	40	35
0.385		-15	25	22
0.394		-8	12	13
0.11	Northridge	11	-25	45
0.17		16	11	50
0.2		31	40	43
0.28		-7	-7	52

6.4 Summary

The ability of simulating additional damping elements at specific locations of a fastener under shear loads is proven with the semi-empiric model for various earthquake records. Both advantages and disadvantages of a fluid viscous damper, a friction damper and a hysteretic damper are examined for the basic criteria performance, reliability and costs.

The most efficient and reliable solutions for low and high seismic levels is represented by a viscous fluid damper applied between base plate and concrete. The acceleration on the base plate can be reduced up to 50%, concrete damage is either mitigated or prevented and anchor forces decrease. The main disadvantage of the damping system consists in considerable effort and costs for implementation.

A friction damper consumes limited expenditure and exhibits good performance especially at low seismic levels. However, numerical modelling involves strong nonlinear behaviour and large scatter of simulated response. The main disadvantage consists in the restriction of the system to pure shear loading.

From the numerical point of view a hysteretic damper in terms of a rubber element needs the most sophisticated material model. The used simplified model suggests that the acceleration on the base plate can be reduced more efficient at low seismic levels. Quite high values are obtained for the general scatter of the simulated response which is also confirmed by shake table tests. Dependent on the geometry of the hysteretic damping element in terms of thickness and extension inside the borehole the damage to the concrete can be mitigated considerably on cost of increased anchor bending.

Sinusoidal tests show that the resonance frequency of the fastener under shear load decreases when a hysteretic damper consisting of pure elastomeric material is applied. For seismic design this fact might be taken into account.

Independent of type of earthquake record, the combination of a hysteretic damper with a friction damper yields a reduction of the acceleration on the attached element by at least 40% up to a peak ground acceleration of 0.35 g. This solution utilizes the high friction coefficient between concrete and rubber which is activated by pre-stressing of the anchor. For future research a combination of a modified hysteretic and a friction damper is recommended.

7 Summary and outlook

When dealing with seismic risk the effect of failure of non-structural elements or secondary structures and other equipment is often neglected or underestimated. Since these elements are fixed to the main structure usually by means of post-installed anchors, failure of the anchor leads to failure of the attached element with huge potential of secondary damage. Inadequately tested or inappropriately used fasteners increase the risk of unanticipated behavior and hence impose a considerable threat to human life. Relatively little information exists about the behaviour of fasteners under earthquake conditions in general. No specific provisions are available concerning the response to seismic shear loading for the case that a hole clearance between base plate and anchor exists. Additionally, most design codes do not take into account the mitigating effect of damping devices applied on a post-installed anchor connection.

A brief literature review of the behaviour and testing of post-installed anchors under earthquake conditions is given with special emphasize on monotonic and cyclic shear loading. Various models attempting to predict the shear load where concrete damage occurs are presented. By evaluation of test results from the literature it is shown that the main source for plastic deformations stems from the concrete where a much larger volume compared to the steel bolt is activated for the formation of micro- and macro-cracks. Since the plastic deformation capacity depends upon type (sleeve or bolt) and diameter of anchor, it is proposed to relate the behaviour factor q_a to the type of fastener and not to the type of non-structural element as recommended in *CEN/TS (2004)*. Further tests and evaluations are necessary to establish an anchor type dependent behaviour factor for seismic tension loads.

Cyclic shear loading with increasing amplitude show that the cyclic ultimate load and hysteretic damping depend on anchor type. Sleeve type anchors exhibit 82% of the static capacity and bolt-type anchors 54% of the ultimate load determined in monotonic tests. Larger concrete stresses in front of the bolt-type anchor lead to enhanced cumulative damage of the concrete. Consequently, the superposition of shear and bending stresses in the anchor result in reduced cyclic ultimate load. Additional tests with groups of anchors are necessary to study the influence of premature failure of single anchors within the group.

Friction between base plate and concrete achieved by pre-stressing forces increases the average hysteretic damping in terms of equivalent viscous damping in uncracked concrete. In cracked concrete the loss of pre-stressing force is compensated by enhanced probability of micro-cracks resulting in similar hysteretic damping as in uncracked concrete. The investigated undercut anchor exhibits approximately the double average hysteretic damping ratio in uncracked concrete when compared to the expansion anchor. Since the influence of a more ductile anchor material (e.g. stainless steel) is negligible, it can be concluded that the main source for hysteretic damping is provided by friction between base plate and concrete for low and medium amplitudes and by damage of concrete at high amplitudes.

Due to irreversible mechanisms, at decreasing amplitudes the memory effect causes slightly enhanced energy dissipation and reduced stiffness. For seismic shear loading an effective stiffness equal to 60% of the stiffness determined in monotonic tests is proposed. The smooth fracture surface indicating low-

cycle fatigue failure legitimates a critical review of current seismic testing protocols where decreasing amplitude is prescribed.

Uniaxial shake table tests with sinusoidal and various seismic inputs yield a first basis for the assessment of the amplification of acceleration in case of a gap between anchor and base plate under shear loading. With increasing peak ground acceleration the amplification increases up to an average factor of 2.5 and then a slight decrease occurs which may be due to the first micro-cracks in the concrete leading to plastic deformations and energy dissipation. In order to get a comprehensive understanding of the gap-induced amplification effect, additional tests are necessary.

Triaxial shake table tests with increasing amplitude show that the failure mode of post-installed metal anchors depends on the anchor type. Undercut and expansion anchors fail by excessive axial and shear deformations resulting in steel bolt bending and concrete crushing, whereas the investigated bonded expansion anchor exhibits complete pullout failure. A safety margin for each anchor type can be defined for various design models for interaction.

The undercut anchor shows the smallest deformations for all seismic levels which can be attributed to the working principle in case of axial loads and to the monolithic design of the sleeve in case of shear loads. A positive influence of small axial displacements can be observed in terms of reduced amplification of acceleration. Seismic anchor performance is strongly influenced by damage of the concrete in terms of large cracks. Triaxial shake table testing may serve for the identification of anchors which are sensitive to combined axial and shear loading under seismic excitation.

The “component” approach in terms of a semi-empirical model where concrete and steel are modelled separately and calibrated on monotonic and cyclic tests is proven to be suitable in simulating the hysteretic energy dissipation, strength and stiffness degradation of a fastener under shear loading. Special effort is given in modelling the gap between anchor and base plate which has a significant influence on the amplification of the seismic input. The assumed effective damping in terms of 3% critical Rayleigh damping for time history analysis is consistent with the results obtained from quasi-static cyclic loading and uniaxial shake table testing.

On the base of a parametric study with a set of seismic records a design model for single anchors is presented which takes into account the gap dependent amplification of acceleration for practical hole clearances up to 5 mm. Additionally, a probabilistic based analytic approach for the calculation of the amplification for anchor groups dependent on hole clearance and number of anchors is presented. In order to obtain enhanced safety of non-structural elements in seismic regions, an integration of the presented models in current design codes is recommended.

On the base of the numerical results and those of 3D shake table testing a proposal for an anchor type dependent amplification factor in case of seismic axial loading is presented for undercut anchors, expansion anchors and a specific bonded expansion anchor. This factor is valid only for the investigated products and may be interpreted as an anchor type dependent safety factor in seismic hazardous zones.

In a second step, the ability of simulating additional damping elements at specific locations of a fastener under shear loads is proven with the semi-empiric model for various earthquake records. Both advantages and disadvantages of a fluid viscous damper, a friction damper and a hysteretic damper are examined for the basic criteria performance, reliability and costs. The numerical feasibility study is completed by uniaxial shake table tests.

The most efficient and reliable solutions for low and high seismic levels is represented by a viscous fluid damper applied between base plate and concrete. The acceleration on the base plate can be reduced up to 50%, concrete damage is either mitigated or prevented and anchor forces decrease. The main disadvantage of the damping system consists in considerable effort and costs for implementation.

A friction damper consumes limited expenditure and exhibits good performance especially at low seismic levels. However, numerical modelling involves strong nonlinear behaviour and large scatter of simulated response. The main disadvantage consists in the restriction of the system to pure shear loading.

From the numerical point of view a hysteretic damper in terms of a rubber element needs the most sophisticated material model. The used simplified model suggests that the acceleration on the base plate can be reduced more efficient at low seismic levels. The high degree of scatter of the simulated response is also confirmed by shake table tests. Dependent on the geometry of the hysteretic damping element in terms of thickness and extension inside the borehole the damage to the concrete can be mitigated considerably on cost of increased anchor bending.

Shake table tests with sinusoidal input show that the resonance frequency of the fastener under shear load decreases when a hysteretic damper consisting of pure elastomeric material is applied. For seismic design this fact might be taken into account.

Uniaxial shake table tests show that the combination of a hysteretic damper with a friction damper yields a reduction of the acceleration on the attached element by at least 40% up to a peak ground acceleration of 0.35 g. This solution utilizes the high friction coefficient between concrete and rubber which is activated by pre-stressing of the anchor. For future research a combination of a modified hysteretic damper with enhanced stiffness (e.g. fibre reinforced elastomeric material) and a friction damper is recommended. For a comprehensive mitigation of earthquake induced accelerations similar procedures and methods might be applicable for seismic tension loads acting on post-installed anchors.

Zusammenfassung

Bei der Betrachtung von Erdbebenrisiken wird Versagen von nichttragenden Bauteilen oder Geräten oft vernachlässigt oder unterschätzt. Da solche Elemente mit der Tragstruktur üblicherweise mit nachträglich installierten Dübeln verbunden werden, bedeutet ein Versagen des Dübels gleichzeitig auch Versagen des befestigten Elementes mit hohem sekundärem Schadenspotential. Unzureichend geprüfte oder ungeeignet eingesetzte Dübel erhöhen das Risiko eines unerwarteten Versagens und stellen somit eine beträchtliche Bedrohung für Leib und Leben dar. Es gibt relativ wenige Informationen über das Verhalten von Befestigungselementen unter Erdbebenbelastung. Die Ein- und Auswirkung von seismischen Querlasten im Fall eines in der Praxis häufig auftretenden Lochspiels zwischen Dübel und Ankerplatte wird in Leitlinien nicht behandelt. Außerdem berücksichtigen die meisten Vorschriften keine mögliche Reduktion der seismischen Lasten falls Isolations- oder Dämpfersysteme in die Dübelverbindung eingebaut werden.

Eine kurze Literaturübersicht betreffend die Prüfung und das Verhalten von nachträglich installierten Dübeln unter besonderer Berücksichtigung von monotoner und alternierender Querkzugbeanspruchung leitet in die Thematik ein. Verschiedene Modelle zur Bestimmung der Querlast, die zu muschelförmigen Betonabplatzen führt werden vorgestellt. Durch Auswertung von Ergebnissen aus der Literatur kann gezeigt werden, dass der Beton als Hauptquelle für plastische Verformung in Frage kommt. Im Untergrund kann ein viel größeres Volumen zur Bildung von Mikro- und Makrorissen aktiviert werden als im Dübelbolzen. Da das plastische Verformungsvermögen für Stahlversagen unter Querlast vom Dübeltyp (Hülsen- oder Bolzendübel) und vom Durchmesser abhängt, wird empfohlen, den Verhaltensfaktor q_a auf diese zwei Parameter zu beziehen anstatt auf den Typ des zu befestigenden nichttragenden Bauteils wie in *CEN/TS (2004)* gefordert. Weitere Versuche und Auswertungen sind notwendig, um in analoger Weise einen dübelabhängigen Verhaltensfaktor unter seismischer Zuglast für unterschiedliche Versagensursachen abzuleiten.

Quasi-statische zyklische Querkraftversuche mit zunehmender Amplitude zeigen, dass Bruchlast und hysteretische Dämpfung vom Dübeltyp abhängen. Die untersuchten Befestigungselemente vom Hülsentyp erreichen 82% und jene vom Bolzentyp 54% der aus monotonen Versuchen abgeleiteten Bruchlast. Bolzendübel erzeugen höhere Betonpressungen und damit eine stärkere kumulative Schädigung des Betons. Infolgedessen wird der Bolzen zusätzlich auf Biegung beansprucht und eine geringere Bruchlast erreicht.

Reibung zwischen Ankerplatte und Beton aufgrund der Vorspannkraft im untersuchten kraftkontrolliert spreizenden Dübel erhöht die durchschnittliche äquivalente viskose Dämpfung von 2,5% (keine Vorspannung) auf 5% (halbe Vorspannung) in ungerissenem Beton. Etwa 5% Dämpfung werden auch in gerissenem Beton erreicht, obwohl die Vorspannung infolge der Rissöffnung auf Null sinkt. Der untersuchte Hinterschnittdübel weist eine doppelt so hohe Dämpfung wie der Spreizdübel in ungerissenem Beton auf. Der Einfluss eines duktileren Dübelmaterials (Edelstahl) auf die Dämpfung kann vernachlässigt werden. Dies legt die Schlussfolgerung nahe, dass bei kleinen und mittleren Lastamplituden die Reibung zwischen Beton und Ankerplatte und bei hohen Amplituden die Betonschädigung für die hysteretische Dämpfung verantwortlich ist.

Irreversible Mechanismen bewirken bei abnehmender Lastamplitude einen Erinnerungseffekt, der zu reduzierter Steifigkeit führt. Für seismische Querbelastung wird eine effektive Steifigkeit entsprechend 60% von der in monotonen Versuchen ermittelten Steifigkeit empfohlen. Wenn in Versuchen nach gängigen seismischen Prüfmethode Stahlbruch auftritt, ist die glatte Bruchoberfläche ein Hinweis auf Ermüdungsversagen. Da Erdbebenlasten normalerweise nicht ermüdungsrelevant sind, ist eine kritische Beurteilung bestehender seismischer Prüfrichtlinien gerechtfertigt.

Einaxiale Rütteltischversuche in ungerissenem Beton mit unterschiedlichen Erdbebenerregungen ergeben eine erste Basis für die Beurteilung der lochspielinduzierten Verstärkung des Eingangssignals unter Querlast. Mit zunehmender maximaler Bodenbeschleunigung steigt die mittlere Verstärkung bis zu einem Faktor von 2,5 an. Die anschließende leichte Abnahme ist auf die energiedissipierende Wirkung der ersten Mikrorisse im Beton zurückzuführen. Für ein umfassendes Verständnis der lochspielinduzierten seismischen Verstärkung sind weiterführende Versuche notwendig.

Dreiaxiale Rütteltischversuche in gerissenem Beton ($\Delta w = 1,5 \text{ mm}$) mit zunehmender Amplitude zeigen, dass der Versagensmodus von nachträglich installierten Dübeln vom Ankertyp abhängt. Die untersuchten Hinterschnitt- und Spreizdübel versagen aufgrund übermäßiger Axial- und Querverformung sowie Biegung und oberflächlichem Betonausbruch, während der Verbund(spreiz)dübel komplett aus dem Bohrloch herausgezogen wird. Für die untersuchten Dübeltypen kann entsprechend unterschiedlicher Interaktionsmodelle ein Sicherheitsabstand angegeben werden.

Der betreffende Hinterschnittdübel weist die geringsten plastischen Verformungen bei allen seismischen Stufen auf. Dies kann mit dem Funktionsprinzip (steifer Formschluss in axialer Richtung) sowie mit der monolithischen Bauweise der Hülse erklärt werden. Für ein besseres Erdbebenverhalten wird für den Spreizdübel eine ähnliche Hülsegeometrie empfohlen. Eine geringere Axialverformung bewirkt eine weniger stark ausgeprägte Verstärkung der Bodenbeschleunigung. Breite Risse im Beton ($\Delta w > 0,5 \text{ mm}$) haben einen entscheidenden Einfluss auf das Trag- und Verformungsverhalten unter seismischer Beanspruchung.

Zur Entwicklung und Kalibrierung eines semi-empirischen Feder-Masse Modells werden monotone und zyklische Querkraftversuche herangezogen. Die getrennte Modellierung von Beton und Stahl unter Berücksichtigung des Lochspiels ermöglicht eine ausreichend genaue Simulation des Hystereseverhaltens sowie der Steifigkeitsdegradation unter seismischer Querbelastung. Die angenommene 3%ige Rayleigh-Dämpfung ist konsistent mit den Ergebnissen der quasi-statischen zyklischen Querkraftversuche und der einaxialen Rütteltischversuche.

Auf der Grundlage einer Parameterstudie mit unterschiedlichen Erdbebenerregungen und verschiedener maximaler Beschleunigung wird ein Bemessungsmodell für Einzeldübel vorgeschlagen, das die lochspielabhängige Verstärkung der Beschleunigung für praxisübliche Lochspiele berücksichtigt. Außerdem ermöglicht ein probabilistischer Ansatz die Berechnung der lochspielabhängigen Verstärkung für Dübelgruppen mit beliebig vielen Dübeln.

Die in den dreiaxialen Rütteltischversuchen gemessenen (plastischen) Axialverschiebungen in Kombination mit den numerischen Resultaten ergeben einen dübeltypabhängigen Verstärkungsfaktor für seismische Axialbelastung, der allerdings nur für die untersuchten Produkte gültig ist.

In einem zweiten Schritt werden mithilfe des Modells die Vor- und Nachteile eines viskosen Flüssigkeitsdämpfers, eines Reibungsdämpfers sowie eines Hysteresedämpfers untersucht, wobei die Kriterien Effizienz, Zuverlässigkeit und Kosten berücksichtigt werden. Einaxiale Rütteltischversuche ergänzen die numerische Machbarkeitsstudie.

Ein viskoser Flüssigkeitsdämpfer eingebaut zwischen Beton und Ankerplatte reduziert die auftretenden Beschleunigungen um bis zu 50%, wobei die Schädigung des Betons entweder verhindert oder abgemildert und die Kraft auf den Dübel abgeschwächt wird. Als Nachteile dieser Variante sind die relativ hohen Kosten und der beträchtliche Aufwand beim Einbau zu werten.

Ein Reibungsdämpfer kann relativ günstig realisiert werden und weist eine hohe Effizienz vor allem bei niedrigen Beschleunigungen auf. Er ist charakterisiert durch stark nichtlineares Verhalten und hohe Streuung der Antwortbeschleunigung. Der Hauptnachteil besteht in der Beschränkung auf reine seismische Querbelastung.

Vom numerischen Gesichtspunkt aus benötigt ein Hysteresedämpfer bestehend aus einem Elastomer ein relativ komplexes Materialmodell. Das benutzte vereinfachte Modell ergibt eine effiziente Reduktion der Beschleunigung vor allem bei niedrigen seismischen Stufen. Die hohe Streuung der Ergebnisse und die teilweise Verstärkung des Eingangssignals werden auch durch einaxiale Rütteltischversuche bestätigt. Durch Variation der Geometrie des Dämpfungselementes kann die Schädigung des Betons erheblich reduziert werden, wobei jedoch die Biegung des Ankerbolzens zunimmt.

Einaxiale Rütteltischversuche mit sinusförmigem Eingangssignal zeigen, dass die Resonanzfrequenz eines Dübels mit Hysteresedämpfer abnimmt. Bei detaillierten Berechnungen der seismischen Einwirkung muss dies berücksichtigt werden.

Die Kombination eines Hysteresedämpfers (Elastomer) mit einem Reibungsdämpfer ergibt in Rütteltischversuchen eine Reduktion der an der Ankerplatte auftretenden Beschleunigung von mindestens 40%. Dies wird durch den hohen Reibungskoeffizienten zwischen Beton und Elastomer ermöglicht. Für weiterführende Forschung scheint eine optimierte Variante dieser Kombination zielführend zu sein, wobei für das Elastomer eine erhöhte Steifigkeit und Festigkeit erstrebenswert ist. Eine mögliche Lösung hierfür könnte der Einsatz von faserverstärktem Elastomer bieten. Für eine umfassende Reduzierung von seismisch induzierten Lasten ist es notwendig, ähnliche Verfahren und Methoden in axialer Richtung von nachträglich installierten Dübeln zu entwickeln und zu prüfen.

8 Literature

- ACI 318 (2005) American Concrete Institute (ACI), Building Code Requirements for Structural Concrete (ACI 318-05). Farmington Hills, Michigan, 2005
- ACI 355.2 (2004) ACI 355.2-04 (2004). Evaluating the Performance of Post-Installed Mechanical Anchors in Concrete. Farmington Hills, Michigan, 2004
- Bachmann (1993) Bachmann, H (1993). Earthquake Actions on Structures. Institut für Baustatik und Konstruktion. ETH Zürich, Bericht Nr. 115.
- Bachmann (1995) Bachmann, H. (1995). Erdbebensicherung von Bauwerken. Birkhäuser Verlag, Basel
- Basler (1967) Basler, E., Witta, E. (1967). Grundlagen für kraftschlüssige Verbindungen in der Vorfabrikation. Beton-Verlag GmbH
- Bažant (1990) Bažant, Z. P., Ožbolt, J. (1990). Nonlocal Microplane Model for Fracture, Damage and Size Effect in Structures. Journal of Engineering Mechanics, ASCE, Vol. 116, No. 11
- Bergmeister (1988) Bergmeister, K. (1988). Stochastik in der Befestigungstechnik mit realistischen Einflussgrößen. Dissertation, Universität Innsbruck
- Bergmeister (1998) Bergmeister, K. (1998). Evaluation Report for Undercut Anchor FZA. Institut für Konstruktiven Ingenieurbau, Universität für Bodenkultur Wien
- Bergmeister (2000) Bergmeister, K. (2000). Structural Detailing in Seismic Zones. In: Berichte aus dem konstruktiven Ingenieurbau, Veröffentlichung des Institutes, Heft Nr. 45, ISSN 1028-5334, Institut für Konstruktiven Ingenieurbau, Universität für Bodenkultur Wien
- Bergmeister (2004) Bergmeister, K., Strauss, A., Rieder, A. (2004). Bemessung durch Versuche. ISSN 1811-8747, Institut für Konstruktiven Ingenieurbau, Universität für Bodenkultur Wien
- Bergmeister (2005) Bergmeister, K. (2005). Evaluation Report for Torque-Controlled Anchor bolt FAZ II. Institut für Konstruktiven Ingenieurbau, Universität für Bodenkultur Wien
- Carr (2004) Carr, A. J.: (2004) Ruaumoko: Program for Inelastic Dynamic Analysis, User's Manual, Department of Civil Engineering, University of Canterbury, Christchurch, NZ
- CEB (1995) Comite Euro-International du Beton (CEB) (1995). Fastenings for Seismic Retrofitting. Thomas Telford Ltd., London
- CEN/TS (2004) European Organization for Standardization CEN TC 250 (2004., Design of Fastenings for Use in Concrete. Draft 9 – Part 1
- Chase (2005) Chase, J. G., Hudson, N. H., Lin, J., Elliot, R., Sim, A. (2005). Nonlinear shake table identification and control for near field earthquake testing. Journal of Earthquake Engineering, Vol. 9, No. 4 pp. 461–482
- Clough (1993) Clough, R.W. and Penzien, J. (1993). Dynamics of Structures (second ed.), McGraw Hill Inc., New York, NY pp. 635.

- Cook (1998) Cook, R. A., Kunz, J., Fuchs, W. and Konz, R. C. (1998). Behavior and design of single adhesive anchors under tensile load in uncracked concrete. *ACI Structural Journal*, Vol. 95, No. 1, 9-26.
- CSA-N287.2 (2003) Canadian Standards Association (CSA) (reaffirmed 2003). Material requirements for concrete containment structures for CANDU nuclear power plants. CSA, Toronto, Canada.
- Cziesielski (1983) Cziesielski, E., Friedmann, M. (1983). Tragfähigkeit geschweißter Verbindungen im Betonfertigteiltbau. Schriftenreihe des Deutschen Ausschusses für Stahlbetonbau, Heft 346, Verlag Ernst & Sohn, Berlin
- Dei Poli (1987) Dei Poli, S., Di Prisco, M., Gambarova, P. (1987). In tema di trasmissione del taglio negli elementi di calcestruzzo armato alcuni risultati sperimenti attinenti alla cosiddetta azione di spinotto. *Studi e ricerche*, Vol. 9, Politecnico di Milano
- DIBt (1998a) Deutsches Institut für Bautechnik (DIBt) (1998). Verwendung von Dübeln in Kernkraftwerken und kerntechnischen Anlagen. Ausgabe 9/98, Berlin
- DIBt (1998b) Deutsches Institut für Bautechnik (DIBt) (1998): European Technical Approval for fischer Zykon Anker FZA. ETA 98/0004
- DIBt (2003) Deutsches Institut für Bautechnik (DIBt) (2003). Concrete screw for anchorage in normal weight concrete. (Draft). ETA request No. 06.01/20, Common Understanding of Assessment Procedure, Berlin
- DIBt (2005) Deutsches Institut für Bautechnik (DIBt) (2005). European Technical Approval for fischer Highbond Anker FHB II. ETA 05/0164
- DIBt (2007a) Deutsches Institut für Bautechnik (DIBt) (2007). European Technical Approval for torque-controlled Expansion Anchor FH II. ETA 07/0025
- DIBt (2007b) Deutsches Institut für Bautechnik (DIBt) (2007). European Technical Approval for torque-controlled Expansion Anchor FAZ II. ETA 05/0069
- Eibl (1989a) Eibl, J. and Keintzel, E. (1989). Zur Beanspruchung von Befestigungsmitteln bei dynamischen Lasten (On the dynamic loading of fastenings). Institut für Massivbau und Baustofftechnologie, Universität Karlsruhe.
- Eibl (1989b) Eibl, J. and Keintzel, E. (1989). Verhalten von Dübeln unter hoher Stoßund Wechselbeanspruchung (Behavior of anchors under high speed impact and reversed cyclic loads). Institut für Massivbau und Baustofftechnologie, Universität Karlsruhe.
- Eligehausen (1995) Eligehausen, R., Balogh, T. (1995). Behavior of fasteners loaded in tension in cracked reinforced concrete. *ACI Structural Journal*, Vol. 92, No. 3, 365-379.
- Eligehausen (2000) Eligehausen, R.; Mallee, R.: Befestigungstechnik im Beton- und Mauerwerksbau. Bauingenieur-Praxis. Ernst & Sohn Verlag. Berlin, 2000
- EOTA (1997) European Organisation for Technical Approvals (1997). Guideline for European Technical Approval of Metal Anchors for Use in Concrete (ETAG 001). Bruxelles
- Eurocode 2 (2005) Österreichisches Normungsinstitut (2005). Design of concrete structures. Part 1-1: General rules and rules for buildings., Wien

- Eurocode 8 (2003) European Committee for Standardization (CEN) (2003). Eurocode 8: Design of structures for earthquake resistance Part 1: General rules, seismic actions and rules for buildings. prEN 1998-1 : 2003, Stage 49, version: September, 2003.
- Fardis (2008) Fardis, M. N. (2008). Ertüchtigung von seismisch beanspruchten Betonbauwerken. Betonkalender 2008 (Hrsg.: Bergmeister, Wörner), Band 2, 277 – 307, Ernst&Sohn, Berlin
- fib (2003) Fédération Internationale du Béton (fib) (2003). Displacement-based seismic design of reinforced concrete buildings. State-of-art report, Lausanne
- fib (2008) Fédération Internationale du Béton (fib) (2008) Design Guide for Anchorages to Concrete. fib-draft 2008, Lausanne.
- fischer (2007) fischer handbook (2007). Systems and solutions for building in a seismic zone. Artur Fischer GmbH & Co. KG
- Foschi (1974) Foschi, R. O. (1974). Load-slip characteristics of nails. Wood science, Vol. 7 (1), pp. 69 - 76
- Franchi (2009) Franchi, A. (2009). Personal Communications on 30th of June 2009, Milan
- Friberg (1940) Friberg, F. (1940). Load and Deflection Characteristics of Dowels in Transverse Joints of Concrete Pavements. Proceedings of the Highway Research Board, 20th annual Meeting, pp. 481 - 493
- Fuchs (1992) Fuchs, W. (1992). Tragverhalten von Befestigungen unter Querlasten in ungerissenem Beton. Deutscher Ausschuss für Stahlbeton, Beuth Verlag, Berlin
- Fuchs (1995) Fuchs, W., Eligehausen, R., Breen, J.E. (1995) Concrete Capacity Design (CCD) Approach for fastening to concrete. ACI Structural Journal, 92(S9).
- Fujikake (2003) Fujikake, K., Nakayama, J., Sato, H., Mindess, S. and Ishibashi, T. (2003). Chemically bonded anchors subjected to rapid pullout loading. ACI Materials Journal, Vol. 100, No. 3, 246-252.
- Gerhaher (2009) Gerhaher, U., Strauss, A., Bergmeister, K. (2009) Effectiveness of Fiber Reinforced Elastomeric Bearings as Anti-Seismic Devices. Paper submitted for the 33rd IABSE Symposium Sustainable Infrastructure Environment Friendly, Safe and Resource Efficient. September 9-11, Bangkok, Thailand
- Grigorian (1993) Grigorian, C. E., Yang, T. S., and Popov, E. P. (1993). Slotted bolted connection energy dissipators. Earthquake Spectra, 9(3), pp. 491–504.
- Gutenberg (1944) Gutenberg, B., Richter, C. (1944). Frequencies of Earthquakes in California, Bul. Seism. Soc. Amer., 34, 185 - 188
- Heine (2001) Heine, C. P. (2001). Simulated Response of Degrading Hysteretic Joints With Slack Behavior, PhD thesis, Virginia Polytechnic Institute, Blacksburg, Virginia
- Hetényi (1946) Hetényi, M. (1946). Beams on Elastic foundation. University of Michigan Press, Ann Arbor
- Hoehler (2006) Hoehler, M. S. (2006) Behavior and Testing of Fastenings to concrete for use in seismic Applications. PhD-Dissertation, Universität Stuttgart, 2006
- Hoehler (2007) Hoehler, M. S., Silva, J. F., Floriani, L., Bourgund, U., Gassner, H., Restrepo, J. I., Panagiotou, M. (2007). Full-shake Table Test of Pipes anchored in a 7-

- Storey RC Building. 2nd International Symposium on Connections between Steel and Concrete (Ed.: Eligehausen, Fuchs, Genesio, Grosser), ibidem-Verlag, Stuttgart, pp. 747 – 757
- Hofmann (2004) Hofmann, J. E. (2004). Tragverhalten und Bemessung von Befestigungen unter beliebiger Querbelastung in ungerissenem Beton, Dissertation, Universität Stuttgart
- Holzenkämpfer (1997) Holzenkämpfer, P. (1997). Ingenieurmodelle des Verbunds geklebter Bewehrung für Betonbauteile. Deutscher Ausschuss für Stahlbetonbau, Heft 473, Beuth Verlag, Berlin
- ICBO (2000) International Conference of Building Officials (ICBO) (2000). Acceptance Criteria for Seismic Qualification Testing of Nonstructural Components. ICBO Evaluation Service Inc., Whittier, California
- ICC-ES (2009) Acceptance Criteria for Post-installed Adhesive Anchors in Concrete Elements, AC308 (2009). ICC Evaluation Service, Inc.
- IEEE (1997) IEEE Standard 693 (1997). IEEE Recommended Practice for Seismic Design of Substation. The Institute of Electrical and Electronics Engineers, Inc.
- JCSS (2001) JCSS Probabilistic Model Code; part 2.17: earthquake, <<http://www.jcss.ethz.ch/>> (accessed February, 26 2007)
- Klingner (1982) Klingner, R.E., Mendonca, J.A. and Malik J.B. (1982). Effect of reinforcing details on the shear resistance of anchor bolts under reversed cyclic loading. ACI Journal, Vol. 79, No. 1, 471-479.
- Klingner (1998) Klingner, R. E., Hallowell, J. M., Lotze, D., Park, H-G., Rodriguez, M. and Zhang, Y-G. (1998). Anchor bolt behavior and strength during earthquakes. U.S. Nuclear Regulatory Commission, NUREG/CR-5434.
- Lee (2001) Lee, D., and Taylor, D. P. (2001). Viscous damper development and future trends. Struct. Des. Tall Build., 10(5), pp. 311–320
- Mesureur (2004) Measureur, B., Guillet, T, David, E. (2004). Seismic Behavior of Metal Anchors in Concrete. fib SAG “fastening” Lisbon
- Meszaros (1994) Meszaros, J. and Eligehausen, R. (1994). Tragverhalten von nicht generell zugzonetauglichen Dübeln – Teil 5: Verhalten bei Belastung mit konstanter Axiallast und gleichzeitig wirkender Querkraft mit wechselndem Vorzeichen (Load-bearing behavior of anchors not suitable for use in cracked concrete. Part 5: Behavior under constant axial load and simultaneous reversed cyclic shear load), Report No. 1/63-94/9, Institut für Werkstoffe im Bauwesen, Universität Stuttgart.
- Momtahan (2009) Momtahan, A., Rieder, A. (2009). Evaluating the effects of strain aging on New Zealand reinforcing steel bars. Bulletin of the New Zealand society for earthquake engineering, submitted for publication
- Owen (1963) Owen, D. (1963). Handbook of Statistical Tables, Addison/Wesley Publishing Company Inc.

- Ozbolt (2005) Ožbolt, J., Periškić, G., Eligehausen, R. (2005). Ersatz von Zulassungsversuchen für Befestigungselemente durch numerische Untersuchungen, Bericht Nr. AF 05/01 – DIBt 0105, Fraunhofer IRB Verlag
- Pall (1982) Pall, A. S., and Marsh, C. (1982). Seismic response of friction damped braced frames. *J. Struct. Div.*, 108(6), pp. 1313–1323.
- Pampanin (2008) Pampanin, S., Quintanagallo, P., Moghaddasi, M., Rieder, A. (2008). EQ-rod: New Generation of Earthquake-Resistant Fastener, Internal Test Report, Department of Civil Engineering, University of Canterbury, Christchurch, New Zealand
- Paschen (1983) Paschen, H., Schönhoff, T. (1983). Untersuchungen über in Beton eingelassene Scherbolzen aus Betonstahl. Schriftenreihe des Deutschen Ausschusses für Stahlbeton, Heft 346, Verlag Ernst & Sohn, Berlin
- Rasmussen (1963) Rasmussen, B. H. (1963). The Carrying Capacity of Transversely Loaded Bolts and Dowels Embedded in Concrete. *Bygningsttske Meddelelser*, Kopenhagen
- Rieder (2001) Rieder, A. (2001). Dübel unter Erdbebenbeanspruchung. Dissertandenseminar, Institut für Konstruktiven Ingenieurbau, Universität für Bodenkultur Wien
- Rieder (2003) Rieder, A. (2003). Dübel unter statischer und wechselnder Querkraftbeanspruchung. Festschrift Konrad Bergmeister. 10jähriges Wirken am Institut, 1993 - 2003. Veröffentlichung des Instituts für Konstruktiven Ingenieurbau, Heft 55, S.10.1 - 10.6, ISBN 3-900962-49-9, Wien.
- Rieder (2004) Rieder, A. (2004). Anchoring to concrete under seismic conditions. In: 5th International PhD Symposium in Civil Engineering, Ed: Walraven, Scarpas & Snijder; ISBN 90 5809 676 9, Delft.
- Rieder (2005a) Rieder, A. (2005). Rütteltischversuche mit Hinterschnittdübel FZA, Spreizdübel FH und Injektionsdübel OZV. Forschungsbericht Nr. 875-05-009, Institut für Konstruktiven Ingenieurbau, Universität für Bodenkultur Wien
- Rieder (2005b) Rieder, A., Bergmeister, K. (2005). Seismic Behaviour of Concrete Anchors. *fib Symposium "Keep Concrete Attractive"*, p. 989 – p. 994, Ed.: Balázs & Borosnyói, ISBN 963 420 839 8. Budapest.
- Rieder (2007) Rieder, A., Bergmeister, K. (2007). Experimental and numerical investigation of the seismic behavior of concrete anchors. In: Eligehausen, R.; Fuchs, W.; Genesio, G.; Grosser, P. (Eds.), 2nd International Symposium on Connections between Steel and Concrete. *Proceedings Vol. 1*, ibidem Verlag, Stuttgart
- Rieder (2008a) Rieder, A. (2008). Hysteretic Damping of Anchors for Seismic Applications. Internal Test Report, Institut für Konstruktiven Ingenieurbau, Universität für Bodenkultur Wien
- Rieder (2008b) Rieder, A. (2008). Shake Table Tests with traditional anchor and EQ-rod under shear loads. Internal Test Report. Institut für Konstruktiven Ingenieurbau, Universität für Bodenkultur Wien

- Rieder (2008c) Rieder, A., Spyridis, P., Bergmeister, K. (2008). Seismic behaviour of post-installed anchors in concrete - A case study. In: G. Gazetas, 3rd Panhellenic Congress of Earthquake Engineering and Engineering Seismology
- SEAOSC (1997) SEAOSC (1997). Standard Method for Cyclic Load Test for Anchors in Concrete or Grouted Masonry. Structural Engineers Association of Southern California, Whittier, California
- Seleemah (1997) Seleemah, A., and Constantinou, M. C. (1997). Investigation of seismic response of buildings with linear and nonlinear fluid viscous dampers. Report No. NCEER 97-0004, National Center for Earthquake Engineering Research, State Univ. of New York at Buffalo, Buffalo, N.Y.
- Silva (2001) Silva, J. F. (2001). Test Methods for Seismic Qualification of Post-Installed Anchors, in: Proceedings of the International Symposium on Connections between Steel and Concrete, RILEM proceedings PRO 21, Vol. 1, Ed.: R. Eligehausen, Stuttgart
- Silva (2007) Silva, J. F., Hoehler, M. S. (2007). Seismic Design Provisions for Anchors in the U.S. In: Eligehausen, R.; Fuchs, W.; Genesio, G.; Grosser, P. (Eds.), 2nd International Symposium on Connections between Steel and Concrete. Proceedings Vol. 1, pp.667 – 676, ibidem Verlag, Stuttgart
- Simons (2008) Simons, I., Eligehausen, R. (2008). Tragverhalten und Bemessung von eingemörtelten Bewehrungsstäben unter zyklischer Beanspruchung im ungerissenen und gerissenen Beton. Beton- und Stahlbetonbau 103, Heft 9, pp. 598 – 608
- Sippel (2007) Sippel, T., Rieder, A. (2007). Behavior of fastenings under realistic earthquake excitations. In: Eligehausen, R.; Fuchs, W.; Genesio, G.; Grosser, P., 2nd International Symposium on Connections between Steel and Concrete. Proceedings Vol. 1, Universität Stuttgart, 2nd International Symposium on Connections between Steel and Concrete, 4th - 7th September 2007, Stuttgart, 693-702; ISBN: 3-89821-807-4
- Spieth (2009) Spieth, H., Bergmeister, K., Stein, A., Lehmann, D., Hilber, R., Unterweger, R., Lehmann, J., Schmieder, P. (2009). Verankerungs- und Befestigungstechnik für Fassaden. Betonkalender 2009 (Hrsg.: Bergmeister, Fingerloos, Wörner), 98. Jahrgang, Band 2, 373 – 446, Ernst&Sohn, Berlin
- Spyridis (2008) Spyridis, P., Unterweger, A., Bergmeister, K. (2008). Querbeanspruchung von Ankergruppen in Randnähe - Stochastische Studien. Beton- und Stahlbetonbau, 103, Heft 9, pp. 617-624;
- Stewart (1987) Stewart, W. G. (1987). The seismic Design of Plywood-Sheathed Shearwalls. Ph.D. dissertation, University of Canterbury, Christchurch, New Zealand
- Symans (1998) Symans, M. D., and Constantinou, M. C.: Passive fluid viscous damping systems for seismic energy dissipation. J. of Earthquake Technology, 35(4), pp. 185–206, 1998

- Symans (2008) Symans, M. D., Charney, F. A., Whittaker, A. S., Constantinou, M. C., Kirchner, C. A., Johnson, M. W. McNamara, R. J. (2008). Energy Dissipation Systems for Seismic Applications: Current Practice and Recent Developments, *Journal of Structural Engineering*, Vol. 134, No.1
- Tamparopoulos (2009) Tamparopoulos, A. (2009). Personal communications on 3rd of July 2009, Vienna
- Timoshenko (1951) Timoshenko, S., Goodier, N. (1951). *Theory of Elasticity*. Mc Graw Hill Book Company
- Uang (1990) Uang, C., Bertero, V. V. (1990). Evaluation of seismic energy in structures. *Earthquake Eng. Struct. Dyn.*, 19(1), pp. 77–90
- UBC (1997) International Code Council (ICC) (1997). *Uniform Building Code*, 1997 Edition. ICC, Whittier, California.
- Unterweger (2008) Unterweger, A. (2008). *Randnahe Anker unter Querlast – Mechanische Modellierung und Bemessung*, Dissertation, Institut für Konstruktiven Ingenieurbau, Universität für Bodenkultur Wien
- Usami (1980) Usami, S., Abe, U. and Matsuzaki, Y. (1980). “Experimental study on the strength of headed anchor bolts under alternate shear load and combined load (shear and axial).” *Proceedings of the Annual Meeting of the Kantou Branch of the Architectural Institute of Japan*.
- Vintzéleou (1987) Vintzéleou, E., Tassios, T. P. (1987). Behavior of dowels under Cyclic Deformations. *ACI Journal* January/February 1987, pp. 18 – 30
- Vintzéleou (1991) Vintzéleou, E. and Eligehausen, R. (1991). “Behavior of fasteners under monotonic or cyclic displacements.” *Anchors in Concrete – Design and Behavior*, Special Publication SP 130, American Concrete Institute, Detroit, 181-204.
- Wen (1976) Wen, Y. K. (1976). Method for random vibration of hysteretic systems. *J. Engrg. Mech. Div.*, 102(2), pp. 249–263.
- Zhang (2001) Zhang, Y.G., Klingner, R. E., Graves, H. L. (2001). Seismic Response of Multiple-Anchor Connections to Concrete, *ACI Structural Journal*, V. 98, No. 6, pp. 811 - 822,

Curriculum Vitae

Persönliche Daten

Name: Anton Rieder
Geboren am: 30.12.1974 in Brixen, Südtirol
Familienstand: Ledig

Ausbildung

1988 – 1993: Realgymnasium in Brixen, Südtirol
10/93 – 03/00 Diplomstudium der Technischen Physik
Technische Universität Wien
Schwerpunkt: Methoden und Technologie der Technischen Physik
10/03 – 09/09 Doktorstudium der Kulturtechnik und Wasserwirtschaft
Universität für Bodenkultur Wien
Thema: Befestigungen unter Erdbebenbeanspruchung
5 Monate Forschungsaufenthalt am Department of Civil Engineering, University of Canterbury, Christchurch, Neuseeland

Praktika und Beruf

Sommer 94 Ferialpraxis beim Bauunternehmen J. Amort, Rodeneck
Sommer 95, 96 Ferialpraxis bei Holzleimbau A. Lanz, Mühlbach,
Juli 1997 Ferialpraxis am Institut für Meteorologie und Physik, Universität für Bodenkultur Wien
10/97 – 06/98 Studienassistent am Inst. für Meteorologie und Physik, Universität für Bodenkultur Wien
04/99 – 03/00 Technischer Mitarbeiter am Institut für Konstruktiven Ingenieurbau, Universität für Bodenkultur Wien
04/00–12/06 Leitung des Prüflabors am Institut für Konstruktiven Ingenieurbau, Universität für Bodenkultur Wien
Seit 2003 Lehre im Bereich Werkstoffkunde und Bauerhaltung, Universität für Bodenkultur Wien
11/06 – dato Wissenschaftlicher Mitarbeiter am Institut für Konstruktiven Ingenieurbau, Universität für Bodenkultur Wien